Copyright Warning & Restrictions

The copyright law of the United States (Title 17, United States Code) governs the making of photocopies or other reproductions of copyrighted material.

Under certain conditions specified in the law, libraries and archives are authorized to furnish a photocopy or other reproduction. One of these specified conditions is that the photocopy or reproduction is not to be "used for any purpose other than private study, scholarship, or research." If a, user makes a request for, or later uses, a photocopy or reproduction for purposes in excess of "fair use" that user may be liable for copyright infringement,

This institution reserves the right to refuse to accept a copying order if, in its judgment, fulfillment of the order would involve violation of copyright law.

Please Note: The author retains the copyright while the New Jersey Institute of Technology reserves the right to distribute this thesis or dissertation

Printing note: If you do not wish to print this page, then select "Pages from: first page # to: last page #" on the print dialog screen

ABSTRACT

ASSESSMENT OF NANOCOMPOSITES VS. AMORPHOUS SOLID DISPERSIONS FOR DISSOLUTION ENHANCEMENT OF BCS CLASS II DRUGS

by
Meng Li

Nanoparticle-based formulations (nanocomposites) and amorphous solid dispersions, shortly ASDs, are two major pharmaceutical formulation platforms used for the bioavailability enhancement of poorly water-soluble drugs. While they both have several advantages–disadvantages, a scientific comparative assessment of their drug release performance and dissolution mechanisms at different drug doses is not available. With the goal of addressing this issue, the dissertation aims to achieve three major objectives: (1) develop a processing–formulation understanding of wet media milling process for fast–efficient production of drug nanoparticles in stable nanosuspension form, (2) elucidate the impact of various classes dispersants on drug release rate and mechanisms during the redispersion–dissolution of nanocomposites prepared via dying of the drug nanosuspensions, and (3) assess the dissolution enhancement imparted by drug nanocomposites vs. ASDs prepared via drying of drug nanosuspensions by a novel nanoextrusion process, which allows for a scientific, head-to-head assessment of the two formulation platforms at various drug doses.

In achieving the first objective, this dissertation work firstly establishes a general stabilization strategy for ensuring the physical stability of five different wet-milled drug nanosuspensions via combined use of a polymer (HPC: hydroxypropyl cellulose)–anionic surfactant (SDS: sodium dodecyl sulfate). A microhydrodynamic model is used for enhanced process understanding of the wet media milling process and rational selection

of bead sizes. Then, the media milling process is intensified with the guidance of the microhydrodynamic model for fast production of sub-100 nm drug particles with reduced specific energy consumption and low bead wear. In achieving the aforementioned second objective, drug nanosuspensions prepared by the media milling are processed into nanocomposite microparticles with various classes of dispersants via either fluidized bed coating/drying or spray drying process. The drug nanosuspensions stabilized by HPC–SDS or HPC alone are coated on Pharmatose® carrier particles, which allows us to elucidate the impact of the physical stability of drug nanosuspensions and different dispersants on drug dissolution from the nanocomposites. It is found that good physical stability of a drug nanosuspension is a necessary condition for fast nanoparticle recovery and drug dissolution, but it is insufficient; dispersant concentration/type plays a critical role for fast drug release. Fast drug dissolution from the nanocomposites is also attained by high drug-loaded, surfactant-free nanocomposites with a co-milled superdisintegrant–HPC prepared via spray drying. The drug release rate is found to correlate positively with the dispersant concentration and the swelling capacity of the superdisintegrant. In achieving the last objective, drug nanosuspensions are dried in an identical nanoextrusion process with two polymers, which enables to produce both a nanocomposite (poor polymer–drug miscibility) and an ASD of the same drug (good polymer–drug miscibility). Nanocomposites outperforms the ASDs at low drug dose, whereas ASDs exhibits much higher supersaturation, outperforming the nanocomposites at high dose. Overall, this dissertation has established a platform approach (nanoextrusion) for a scientific comparison of drug nanocomposites vs. ASDs and the prerequisite processing–materials knowledge and methodology needed for such scientific comparison.

ASSESSMENT OF NANOCOMPOSITES VS. AMORPHOUS SOLID DISPERSIONS FOR DISSOLUTION ENHANCEMENT OF BCS CLASS II DRUGS

by
Meng Li

A Dissertation
Submitted to the Faculty of
New Jersey Institute of Technology
in Partial Fulfillment of the Requirements for the Degree of
Doctor of Philosophy in Chemical Engineering

Otto H. York Department of
Chemical, Biological and Pharmaceutical Engineering

December 2017

.

APPROVAL PAGE

ASSESSMENT OF NANOCOMPOSITES VS. AMORPHOUS SOLID DISPERSIONS FOR DISSOLUTION ENHANCEMENT OF BCS CLASS II DRUGS

Meng Li

Dr. Ecevit A. Bilgili, Dissertation Advisor Date
Associate Professor of Chemical, Biological, and Pharmaceutical Engineering, NJIT

Dr. Rajesh N. Davé, Committee Member Date
Distinguished Professor of Chemical, Biological, and Pharmaceutical Engineering, NJIT

Dr. Robert B. Barat, Committee Member Date
Professor of Chemical, Biological, and Pharmaceutical Engineering, NJIT

Dr. Piero M. Armenante, Committee Member Date
Distinguished Professor of Chemical, Biological, and Pharmaceutical Engineering, NJIT

Dr. Dan Zhang, Committee Member Date
Senior Research Fellow of Merck Co. Inc.

BIOGRAPHICAL SKETCH

Author: Meng Li

Degree: Doctor of Philosophy

Date: December 2017

Undergraduate and Graduate Education:

- Doctor of Philosophy in Chemical Engineering,
  New Jersey Institute of Technology, Newark, NJ, 2017
- Master of Science in Chemical Engineering,
  New Jersey Institute of Technology, Newark, NJ, 2013
- Bachelor of Science in Polymer Materials and Engineering,
  Shanghai University, Shanghai, P. R. China, 2011

Major: Chemical Engineering

Publications:

M. Li, N. Ioannidis, C. Gogos, E. Bilgili, A comparative assessment of nanocomposites vs. amorphous solid dispersions prepared via nanoextrusion for drug dissolution enhancement. Eur J Pharm Biopharm 119 (2017) 68–80.

M. Li, P. Alvarez, E. Bilgili, A microhydrodynamic rationale for selection of bead size in preparation of drug nanosuspensions via wet stirred media milling. Int J Pharm 524 (2017) 178–192.

S. Krull, J. Moreno, M. Li, E. Bilgili, R.N. Davé, Critical material attributes (CMAs) of strip films loaded with poorly water-soluble drug nanoparticles: III. Impact of drug nanoparticle loading, Int J Pharm, 523 (2017) 33–41.

S. Krull, J. Ammirata, S. Bawa, M. Li, E. Bilgili, R. Dave, Critical material attributes of strip films loaded with poorly water-soluble drug nanoparticles: II. Impact of polymer molecular weight. J Pharm Sci 106(2017) 619–628.

M. Li, M. Azad, R. Dave, E. Bilgili, Nanomilling of drugs for bioavailability enhancement: A holistic formulation–process perspective. Pharmaceutics, 8(2016) 17.

S. Krull, H. Patel, M. Li, E. Bilgili, R. Davé, Critical material attributes (CMAs) of strip films loaded with poorly water-soluble drug nanoparticles: I. Impact of plasticizer on film properties and dissolution. Eur J Pharm Sci 92(2016) 146–155.

M. Li, N. Lopez, E. Bilgili, A study of the impact of polymer-surfactant in drug nanoparticle coated pharmatose composites on dissolution performance. Adv Powder Technol 27(2016) 1625–1636.

S. Krull, Z. Ma, M. Li, R. Davé, E. Bilgili, Preparation and characterization of fast dissolving pullulan films containing BCS Class II drug nanoparticles for bioavailability enhancement. Drug Dev Ind Pharm 42(2016) 1073–1085.

A. Bhakay, E. Vizzotti, M. Li, R. Dave, E. Bilgili, Incorporation of fenofibrate nanoparticles prepared by melt emulsification into polymeric strip films. J Pharm Innov 11(2016) 52–63.

M. Li, L. Zhang, R. Dave, E. Bilgili, An intensified vibratory milling process for enhancing the breakage kinetics during the preparation of drug nanosuspensions. AAPS PharmSciTech 17(2016) 389–399.

S.M. Krull, M. Li, E. Bilgili, R.N. Davé, Polymer strip films for delivery of poorly water-soluble drugs, Am Pharm Rev 18(2015) 48–52.

M. Li, N. Yaragudi, A. Afolabi, R. Dave, E. Bilgili, Sub-100 nm drug particle suspensions prepared via wet milling with low bead contamination through novel process intensification. Chem Eng Sci 130 (2015) 207–220.

S.M. Krull, R. Susarla, A. Afolabi, M. Li, Y. Ying, Z. Iqbal, E. Bilgili, R.N. Davé, Polymer strip films as a robust, surfactant-free platform for delivery of BCS Class II drug nanoparticles, Int J Pharm 489 (2015) 45–57.

E. Bilgili, M. Li, A. Afolabi, Is the combination of cellulosic polymers and anionic surfactants a good strategy for ensuring physical stability of BCS Class II drug nanosuspensions? Pharm Dev Technol 21 (2016) 499–510.

M. Li, C. Gogos, N. Ioannidis, Improving the API dissolution rate during pharmaceutical hot-melt extrusion I: Effect of the API particle size, and the co-rotating, twin-screw extruder screw configuration on the API dissolution rate. Int J Pharm 478 (2015) 103–112.

To my beloved parents,
my brother, and my lifelong partner.

ACKNOWLEDGMENT

I would like to express my sincere gratitude to my dissertation advisor, Dr. Ecevit A. Bilgili, who is knowledgeable, stringent, perfectionist, considerate, and always supportive. He pushes and guides me to reach my personal best. At the same time, he is always there supporting me, defending me, encouraging me, and spending time with me throughout my Ph.D. program. He is not only an advisor in my research, but also the one doing everything in his power to guide me towards a successful future career. I am truly blessed having him as my dissertation advisor.

I would like to also express my appreciation to all my Ph.D. dissertation committee members. I especially thank Dr. Rajesh N. Dave for his support, constructive comments and feedback, and intellectual discussions throughout my research experience as well as the opportunity to collaborate with his group besides his allowing me to use his laboratories and instruments without which I would not be able to generate some significant data presented here. I would like to extend my thanks to other committee members, Dr. Robert B. Barat, Dr. Piero M. Armenante, and Dr. Dan (Dina) Zhang, whose guidance, constructive feedback, and suggestions significantly helped me to reach excellence in research.

I am grateful for financial support from the National Science Foundation in part through the ERC (EEC-0540855) award.

I would like to recognize all the co-workers for their direct involvement in my research, either spiritually or physically: Dr. Scott Krull, Dr. Zhonghui Huang, Lu Zhang, Kai Zheng, Liang Chen, Mahbubur Raman, Paulina Alvarez, Nicole Lopez, Kihyun Kim,

Gregory Nistal, Casey Furey, Jeffery Skros, Jay Vekaria, James Proske, Indiana Suriel, Mina Armani, Paul Orbe. I am especially grateful to Dr. Afolawemi Afolabi, Dr. Anagha Bhakay, and Dr. Mohammad Azad for helping me develop the skills necessary to succeed in my research. I also offer special thanks to Dr. Costas Gogos and Dr. Nicolas Ioannidis for the opportunity of collaboration.

Finally, I would like to express my deepest gratitude to my family. To my mother, Li (莉), and my father, Qinghai (庆海), for their endless love and support at every stage of my life, my brother, He (鹤), the most wonderful gift in my life, and most importantly, my husband and lifelong best friend since high school, Zhaokai (兆凯). I would not have been able to accomplish what I have without you, and I promise to continue to make you proud!

TABLE OF CONTENTS

TABLE OF CONTENTS
(Continued)

Chapter **Page**

TABLE OF CONTENTS
(Continued)

Chapter **Page**

TABLE OF CONTENTS
(Continued)

Chapter **Page**

TABLE OF CONTENTS
(Continued)

TABLE OF CONTENTS
(Continued)

TABLE OF CONTENTS
(Continued)

TABLE OF CONTENTS
(Continued)

Chapter **Page**

TABLE OF CONTENTS
(Continued)

Chapter **Page**

LIST OF TABLES

LIST OF TABLES
(Continued)

LIST OF FIGURES

LIST OF FIGURES
(Continued)

LIST OF FIGURES
(Continued)

LIST OF FIGURES
(Continued)

LIST OF FIGURES
(Continued)

LIST OF FIGURES
(Continued)

LIST OF FIGURES
(Continued)

LIST OF FIGURES
(Continued)

LIST OF SYMBOLS

Nomenclature

a	average frequency of drug particle compressions, Hz
c	volumetric concentration of the beads, –
d	particle diameter (size), m
D	rotor tip diameter, m
E	cumulative energy consumption by the slurry, J
E^*	specific energy consumption per unit mass of drug suspension, J/kg
F	milling intensity factor, $m^{0.6}/s^{2.6}$
F_b^n	average maximum normal force during collision of two identical elastic beads, N
k	restitution coefficient for bead–bead collisions, –
K	coefficient obtained from an empirical correlation, –
m_{sus}	total mass of drug suspension, kg
N	angular speed of the rotor, 1/s
p	probability to be caught between the beads for a single drug particle, –
P	Power applied by the mill stirrer (rotor), W
P_w	power applied by the mill rotor per unit volume, W/m^3
Q	volumetric flow rate of the drug suspension, m^3/s
R	radius, m
R_{diss}	dissipation (effective drag) coefficient of the bead, –
R_{diss0}	dissipation coefficient when relative motion of the bead–liquid is absent, –
Re	stirrer (rotor) Reynolds number, –
t	milling time, s

t_{d50}	milling time required to attain a median drug particle size d_{50} of 0.5 μm, s
t_{d90}	milling time required to attain a median drug particle size d_{90} of 1 μm, s
u	rotor/stirrer tip speed, m/s
u_b	average bead oscillation velocity, m/s
V_m	volume of the milling chamber, m^3
Y	Young modulus, Pa
Y^*	reduced elastic modulus for the bead–drug contact, Pa
Greek letters	
α	radius of the contact circle formed at the contact of two beads, m
ε	volumetric fraction of drug particles in the drug suspension, –
ε_{coll}	energy dissipation rate due to partially inelastic bead–bead collisions, W/m^3
ε_{ht}	power spent on shear of equivalent liquid of the slurry at the same shear rate but calculated (measured) as if no beads were present in the flow, W/m^3
ε_m	non-dimensional bead–bead gap thickness at which the lubrication force stops increasing and becomes a constant, –
ε_{tot}	total energy dissipation rate, W/m^3
ε_{visc}	energy dissipation rate due to both the liquid–beads viscous friction and lubrication, W/m^3
η	Poisson's ratio, –
λ	material-dependent factor, $kg/m^{1.6}\cdot s^{0.4}$
μ_L	apparent shear viscosity of the equivalent fluid, Pa·s
ν	frequency of single-bead oscillations, Hz
Π	energy dissipation rate attributed to the deformation of drug particles per unit volume, W/m^3
θ	granular temperature, m^2/s^2
ρ	density, kg/m^3

σ_b^{max}	maximum bead contact pressure at the center of the contact circle, Pa
σ_y	contact pressure in a drug particle when the fully plastic condition is obtained, Pa
τ_p	characteristic time constant of the milling process, s
ω	stirrer (rotational) speed, rpm
Indices	
b	beads
L	equivalent liquid (milled drug suspension)
p	drug particle
y	yield
T	total
50, 90	50% passing size and 90% passing size of the cumulative PSD

CHAPTER 1

INTRODUCTION

1.1 Motivation

It is estimated that between 40% and 70% of all new chemical entities identified in drug discovery programs have very low solubility in aqueous media (Kipp, 2004; Lipinski, 2002). Such drugs are difficult to formulate due to their low bioavailability, which can be improved, in general, by either increasing the drug surface area via size reduction or increasing the saturation solubility of the drug through the formation of an amorphous solid dispersion.

Size reduction of drug crystals increases the specific surface area, which can improve their dissolution rate (Singh et al., 2011; Tanaka et al., 2012) according to the Noyes–Whitney equation (Noyes and Whitney, 1897). Nanoparticles have larger surface area; they may exhibit higher saturation solubility owing to their increased curvature especially when their size is in the sub-100 nm domain (Müller and Peters, 1998), and therefore dissolve faster than micron-sized particles (Hall, 2010). In pharmaceutics literature, particles of sizes up to 1000 nm have been referred to as "nanoparticles" and used for enhancing the bioavailability of BCS Class II (poorly water-soluble) drugs (Keck and Müller, 2006).

Among various methods used for the production of drug nanoparticles, wet stirred media milling (WSMM) has been commonly used in the pharmaceutical industry as it is continuous, scalable, solvent-free and environmentally benign (Afolabi et al., 2014; Kesisoglou et al., 2007; Merisko-Liversidge and Liversidge,

2008; Monteiro et al., 2013). Moreover, nanosuspensions prepared via wet media milling have the distinct advantages of high drug loading, low excipient side effects, and can be generally formulated for most drug candidates (Müller et al., 2001), while also offering the advantage of higher mass packing (and thus higher dose) per injection volume and improved physical stability through the use of stabilizers such as polymers and/or surfactants (Müller and Peters, 1998; Rabinow, 2004). Several marketed products such as Rapamune® (Pfizer (Wyeth), New York City, NY, USA), Emend® (Merck, Kenilworth, NJ, USA), Tricor® (AbbVie, North Chicago, IL, USA), Megace® ES (PAR Pharmaceuticals, Woodcliff Lake, NJ, USA), and Invega® SustennaTM (Janssen, Beerse, Belgium) made use of wet media milling.

In wet stirred media milling, micron-sized drug particles in an aqueous solution of stabilizers, usually polymers and/or surfactants, pass through a milling chamber, while the milling media (beads) are retained inside the milling chamber by a screen. High-speed rotation of the mill stirrer induces turbulent motion in the suspension, which leads to frequent bead–bead collisions (Eskin et al., 2005b). The particles captured by the colliding beads are subjected to stress and broken down to smaller particles, eventually forming nanoparticles. Since the particle size reduction via wet media milling increases the surface energy of particles and there are significant interparticle interactions via Van der Waals forces and hydrophobic interactions among the particles, adequate stabilization is required by various stabilizers (Cerdeira et al., 2010; Wu et al., 2011), also known as dispersants. The selection of proper type and concentration of stabilizers plays a major role in formulating drug nanosuspensions. Although wet media milling has been used for

about two decades to produce drug nanoparticles (see e.g., Elan's Nanocrystal Technology (Bruno et al., 1996)), it is still not possible to predict, based solely on first principles and mechanistic understanding, the optimal stabilizer type and concentration for a given drug to ensure a feasible wet media milling process and adequate short- and long-term physical stability. In addition, while polymers and surfactants alone can be effective for some drugs, there is a great need for (i) new combinative use of polymer–surfactant pairs, (ii) development of a general stabilization strategy for multitude of drug nanosuspensions, and (iii) development of novel stabilizers/dispersants besides polymers–surfactants.

Another major issue in production of drug nanoparticles via media milling is that most wet media milling studies have focused mainly on optimization of various stabilizers and physical stability of the milled drug suspensions via trial-and-error approach (Kesisoglou et al., 2007; Peltonen and Hirvonen, 2010; Van Eerdenbrugh et al., 2008b), largely ignoring process development and optimization. Furthermore, WSMM process is considered time-consuming, costly, and energy-intensive (Kawatra, 2006; Li et al., 2016a), which limits its potential use as a platform technology in the pharmaceutical industry for bioavailability enhancement of BCS Class II drugs. Process parameters such as stirrer speed, bead loading, and suspension flow rate can significantly affect the breakage kinetics and milling time required for desired product fineness (Afolabi et al., 2014; Ghosh et al., 2012). In addition, proper selection of bead size along with processing conditions can reduce the energy consumption, cycle time, and operational costs for a desired drug particle size (Kawatra, 2006; Li et al., 2015b). To the author's best knowledge, there is no

fundamental, scientific rationale that guides the selection of bead sizes as a function of specific energy consumption or fundamental microhydrodynamic parameters.

Wet media milling was typically used to prepare 150–300 nm particles (Sinha et al., 2013) or larger in the pharmaceutical industry. The preparation of "true drug nanoparticles," i.e., particles with sub-100 nm sizes, has been another great challenge in pharmaceutical literature. Drug particles with sub-100 nm sizes offer improved permeation through various biological barriers and rapid onset of therapeutic action (Merisko-Liversidge and Liversidge, 2011; Shegokar and Müller, 2010). Moreover, sub-100 nm particles could render sterile filtration of drug suspensions feasible and allow higher drug loading for reduced injection volume in parenteral dosage forms (Baert et al., 2009; Xiong et al., 2008). Lack of mechanistic, first-principle-based understanding of the impact of process parameters and/or heavy reliance on purely empirical approaches has been a barrier to process improvement (Afolabi et al., 2014) for effective production of sub-100 nm drug particles.

As solid dosage forms are preferred over suspensions due to convenience and easiness of their use, nanosuspensions prepared via wet stirred media milling are usually converted via drying into nanocomposite microparticles, which will be synonymously referred to as the drug nanocomposites (or simply nanocomposites) throughout the dissertation, and incorporated into standard solid dosage forms such as capsules, tablets, and sachets (Basa et al., 2008; Bhakay et al., 2014a; Van Eerdenbrugh et al., 2008a). Drying of nanosuspensions can be achieved via spray drying (Azad et al., 2014a; Lee, 2003), spray-freeze drying (Cheow et al., 2011; Wang et al., 2012), freeze drying (de Waard et al., 2008; Layre et al., 2006), vacuum

drying (Choi et al., 2008; Kim and Lee, 2010), as well as granulation with, or coating onto, inert excipient particles (Basa et al., 2008; Bhakay et al., 2014b). Unfortunately, drug nanoparticles tend to form aggregates during both milling and drying of the drug suspensions (Bhakay et al., 2013; Lee, 2003), leading to the loss of their large surface area. Soluble polymers and surfactants can be used as dispersants to impart physical stability and retain the large surface area of the nanoparticles during the redispersion and dissolution (Bhakay et al., 2011; Bilgili and Afolabi, 2012; Kesisoglou et al., 2007). However, depending on the formulation, drug nanoparticles may not be fully recovered from the dried composites during redispersion and dissolution, which will cause unexpectedly low dissolution rate and poor bioavailability from such nanoparticle-based formulations (Bhakay et al., 2013; Chaubal and Popescu, 2008). Hence, elucidation of the roles and impact of type/concentration of various classes of both traditional dispersants such as polymers and surfactants as well as relatively novel dispersants such as superdisintegrants on drug release from drug nanocomposites is warranted.

Despite their effectiveness as dispersants, surfactants may pose several challenges such as aggregation of the drug nanoparticles in suspensions during milling/storage (Cerdeira et al., 2010; Knieke et al., 2013), micellar solubilization of the drug (Yalkowsky, 1981) and particle growth via Ostwald ripening during milling and/or storage (Ghosh et al., 2011; Knieke et al., 2013; Verma et al., 2011). Additional challenges associated with the use of anionic surfactants include incompatibilities with other ionic molecules, sensitivity to pH, salt or temperature changes, GIT irritation (Gupta and Kompella, 2006; Liversidge and Cundy, 1995),

and even toxicity when used in excess (Liversidge and Cundy, 1995), especially for inhalation applications (Lebhardt et al., 2011; Suzuki et al., 2000). In view of all the aforementioned issues, surfactant usage should be minimized to mitigate all potential negative impact during formulation development. Alternative surfactant-free formulations with novel dispersants that allow for high drug loading should be developed in comparison to conventional dispersants used in nanoformulations.

Enhanced dissolution rate, improved bioavailability, safe dose escalation, elimination of food effects, and enhanced safety, efficacy and tolerability profiles are some of the numerous advantages of crystalline drug nanoparticles (Junghanns and Müller, 2008). However, with all the above-mentioned nanoparticle delivery techniques and advantages, the limitation is still the limited improvement on drug solubility. Often for drugs with very low aqueous solubility, the achieved increase in dissolution rate via size reduction is limited and insufficient to provide significant enhancement of bioavailability (Müller et al., 2001). Another platform approach is to produce amorphous solid dispersion (ASD) of poorly water-soluble drugs. ASDs tend to exhibit high levels of supersaturation in aqueous media relative to the crystal, and thus higher apparent solubility (Newman et al., 2012). The strategy is to combine a drug with a water-soluble polymer to produce a single-phase amorphous mixture of the drug and the polymer. It is well-known that utilizing the amorphous form of a drug can be a useful approach to improve the dissolution performance and bioavailability of poorly water-soluble drugs, as a result of supersaturation (Chiou and Riegelman, 1970; Goldberg et al., 1966; Hancock and Parks, 2000). Overall, both nanoparticle-based formulations (nanocomposites) and ASDs are two major

pharmaceutical formulation platforms used for the bioavailability enhancement of poorly water-soluble drugs. While they both have several advantages–disadvantages, a scientific comparative assessment of their drug release performance and dissolution mechanisms at different drug doses is not available. A major challenge is to develop a common processing approach which allows for production of both nanocomposites and ASDs and thus their scientific, head-to-head comparison. Recently, a novel nanoextrusion process has been developed to disperse drug nanoparticles in a polymeric matrix using a modified version of the standard hot melt extrusion process (Baumgartner et al., 2014; Khinast et al., 2013), which produced solid nanoparticle-based formulations (nanocomposites), thereby improving the dissolution rate and thus the bioavailability of the drug as well as enhancing patient compliance. However, nanoextrusion has not been used for producing ASDs despite the fact that it poses a great potential to produce both forms of a drug, thus allowing a comparative assessment of the dissolution performance from both nanoparticle-based formulations and ASDs.

In the rest of Chapter 1, the current state-of-art regarding stabilization of nanosuspensions, process intensification/optimization of wet media milling with the guidance of microhydrodynamic model, and production of nanocomposites and ASDs for drug dissolution enhancement via fluidized bed coating/drying, spray drying, and nanoextrusion will be discussed in greater detail. Also, how each chapter of this dissertation will address the existing gaps, issues, and challenges will be indicated.

1.2 Background

1.2.1 Stabilization of Drug Nanosuspensions

Drug nanosuspensions produced by wet media milling must be physically stable during milling and storage for proper downstream processing or adequate shelf-life depending on the intended final dosage form (Kesisoglou et al., 2007). Moreover, the dissolution performance of dried nanocomposites may be affected by the presence/absence of drug aggregates, i.e., clusters of primary nanoparticles. In this dissertation, physical stability of the suspensions is broadly defined in terms of the extent of particle aggregation in the milled suspensions and prevention of size increase during short-term storage following wet media milling. Particle size reduction via wet media milling increases the surface energy of particles and there are significant interparticle interactions via Van der Waals forces and hydrophobic interactions among the particles. Therefore, nanoparticles tend to aggregate (Cerdeira et al., 2010; Wu et al., 2011). Polymers and surfactants are generally used to protect drug particles against aggregation via electrostatic, steric, and electrosteric interactions (Napper, 1970; Wu et al., 2011). In electrostatic stabilization, the surfaces of the particles are charged so that repulsion forces are created, which can overcome the attractive Van der Waals forces between the particles. However, particles of most drugs are not inherently charged (Meng et al., 2012); hence, surface charges typically originate from adsorbed anionic surfactants and/or ionic polymers (Figure 1.1). Steric stabilization results from the adsorption of polymers onto the surface of the particles. If either the adsorbed polymer contains charged functional groups or non-ionic polymers and anionic surfactants are used in combination, steric and electrostatic

mechanisms act simultaneously, which is typically described as electrosteric stabilization.

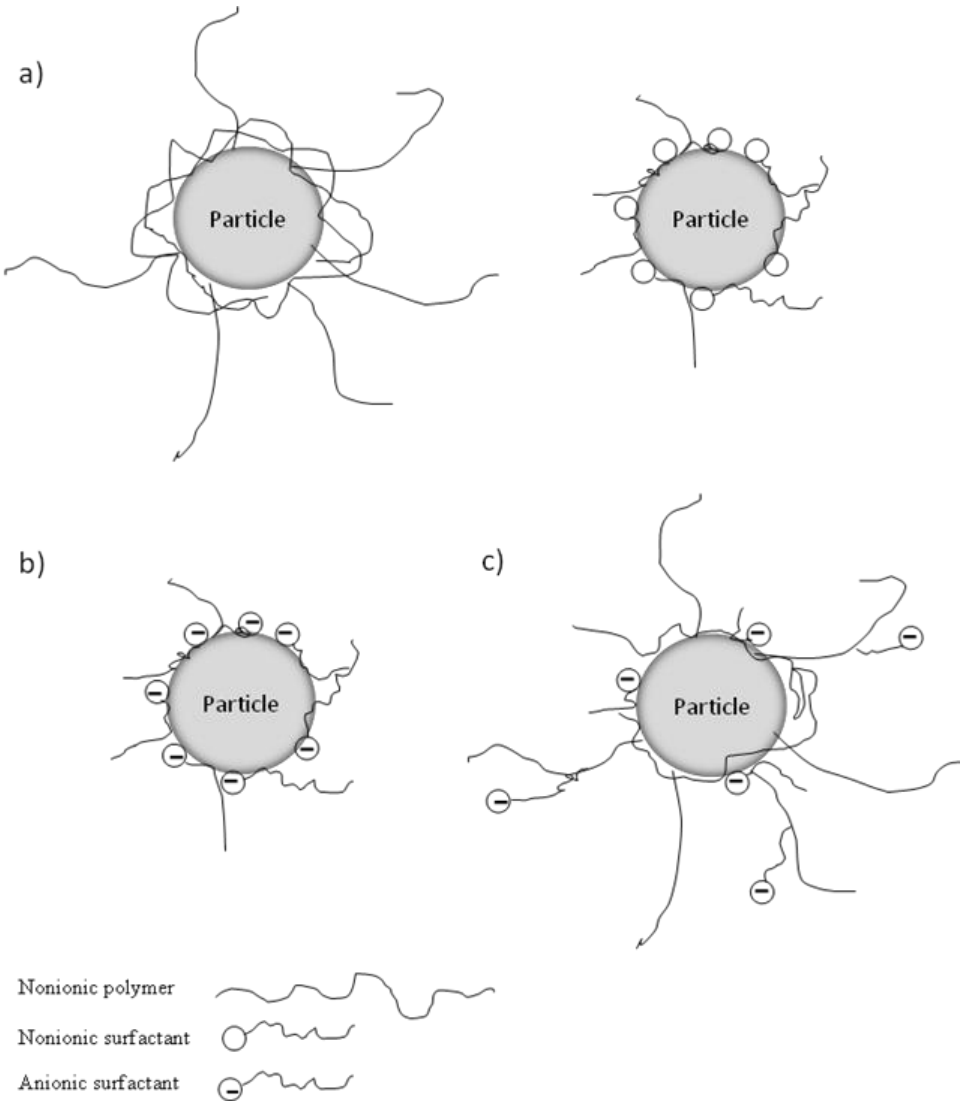

Figure 1.1 Schematic of physical stabilization mechanisms in drug nanosuspensions: (a) steric stabilization imparted by nonionic polymers or nonionic surfactants, (b) electrostatic stabilization imparted by anionic surfactants, and (c) electrosteric stabilization imparted by both nonionic polymers and anionic surfactants. The schematic assumes near neutral surface charge of drug nanoparticles before adsorption of the stabilizers. Figure is not drawn to scale.

The selection of proper type and concentration of stabilizers plays a major role in formulating drug nanosuspensions. If used at insufficiently low concentrations,

stabilizers in drug nanosuspensions usually cannot prevent aggregation, while their excessive use, especially for surfactants, can promote Ostwald ripening (Knieke et al., 2013; Verma et al., 2011) or raise the viscosity so much that downstream processing may be negatively affected. The first systematic investigations of the stabilizing capability of adsorbed polymers were carried out by Lee and Choi (Lee et al., 2008; Lee et al., 2005). A connection between the hydrophobicity of the polymer and the ability to stabilize drug nanocrystals was indicated (Lee et al., 2005). In addition, differences in the surface energy between the particle and the polymer were found to play a role in the stabilization process (Lee et al., 2008). Choi et al. (2005) concluded that not only the surface energy, but also the specific interaction between the stabilizer and the drug appears to play important role. George and Ghosh (2013) investigated the correlation between drug–stabilizer properties and critical quality attributes (CQAs) of drug nanosuspension formulations. Their study suggested that log*P* and fusion enthalpy of the drugs had direct impact on the feasibility of a stable nanosuspension and that the most likely candidate for wet media milling was a drug with high enthalpy and hydrophobicity. In contrast, a more comprehensive study (Van Eerdenbrugh et al., 2009) using 13 stabilizers at three different concentrations to stabilize nine drug compounds concluded that no correlation between physicochemical drug properties (molecular weight, melting point, log*P*, solubility, and density) and stable nanosuspension formation exists. In view of the contradictory results from the aforementioned studies, it is fair to assert that although WSMM has been used for about two decades to produce drug nanoparticles (see e.g., Elan's Nanocrystal Technology (Bruno et al., 1996)), it is still not possible to predict, based

solely on first principles and mechanistic understanding, the optimal stabilizer type and concentration for a given drug to ensure a feasible WSMM process and adequate short- and long-term physical stability. Other researchers have focused on development of complementary characterization methods that help to screen stabilizer(s) and determine their optimal concentrations in a streamlined fashion. Verma et al. (2009) demonstrated that the use of atomic force microscopy (AFM) in visualizing the morphology of various adsorbed polymers/surfactants on ibuprofen to gain surface coverage and adhesion information, and used this information as a means of selecting suitable stabilizers for the production of a stable drug nanosuspension. Knieke et al. (2013) developed a streamlined stabilizer optimization method based on step-wise addition of stabilizers at the end of milling (Bhakay et al., 2011) and the concept of dynamic equilibrium (Opoczky and Farnady, 1984). Lee (2003), Bilgili and Afolabi (2012), Knieke et al. (2013), and Panmai and Deshpande (2003) constructed polymer adsorption isotherms to help the selection of polymer type and concentration.

Recent modeling and experimental investigations (Bhakay et al., 2014b; Bhakay et al., 2013; Bilgili and Afolabi, 2012; Gupta and Kompella, 2006; Knieke et al., 2013; Ryde and Ruddy, 2002; Zhu et al., 2012) have suggested that the combined use of non-ionic cellulosic polymers such as hydroxypropyl cellulose (HPC), hydroxypropyl methyl cellulose (HPMC), etc. and surfactants, especially anionic surfactants such as sodium dodecyl sulfate (SDS), dioctyl sodium sulfosuccinate (DOSS), etc., can have synergistic stabilization effects on some drug nanosuspensions. However, whether such a strategy is general enough to be applied

to multiple drugs is unknown and its advantages and disadvantages have not been thoroughly investigated in a comparative study. Moreover, whether the interactions between non-ionic cellulosic polymers and anionic surfactants significantly affect apparent breakage kinetics, zeta potential and/or polymer adsorption for multiple drug suspensions needs exploration. Thus, the combined use of a non-ionic cellulosic polymer, HPC and an anionic surfactant, SDS, as a general strategy to stabilize nanosuspensions of multiple drugs with different physicochemical properties is investigated in Chapter 2.

1.2.2 Rationale for Selection of Bead Size in Wet Stirred Media Milling

Wet stirred media milling (WSMM) process is considered time-consuming, costly, and energy-intensive, which limits its potential use as a platform technology in pharmaceutical industry for bioavailability enhancement of BCS Class II drugs. Proper selection of bead size along with processing conditions can reduce the energy consumption, cycle time, and operational costs for a desired drug particle size (Kawatra, 2006; Li et al., 2015b). Although selection of bead size is of utmost importance in wet media milling (Li et al., 2016d), this has been largely performed as an empirical exercise throughout the literature, based on trial-and-error, which is usually costly and labor/material intensive. A cursory review of recent literature, which is not intended to be comprehensive, on bead sizes used in pharmaceutical wet media milling is presented in Table 1.1. For each study in Table 1.1, the optimal bead size, among several bead sizes used, was indicated based on the smallest final particle size after the same duration of milling (fastest overall breakage). Table 1.1 illustrates that zirconium dioxide beads with wide range of sizes (e.g., 50–15,000 μm) have

been used for the production of drug nanoparticles. The investigations cited were mostly empirical, providing little to no first-principle mechanistic understanding of the impact of bead size. Moreover, they did not provide any fundamental rationale behind the selection of specific bead sizes. Another important consideration is that wet media mills of different energetic levels (specific energy consumption), ranging from low-energy mills such as ball mills to high-energy mills such as WSMM, were used from small-scale to large-scale manufacture of drug nanosuspensions. Unfortunately, the studies in Table 1.1 did not offer any fundamental, scientific rationale that guides the selection of bead sizes as a function of specific energy consumption or fundamental microhydrodynamic parameters. Overall assessment of the studies in Table 1.1 also reveals that large beads in the range of 400–15,000 μm appear to be used at low stirrer speeds or in low-energy mills (Ain-Ai and Gupta, 2008; Bitterlich et al., 2015; Branham et al., 2012; Choi et al., 2008; Ghosh et al., 2012; Sarnes et al., 2014; Tuomela et al., 2015), whereas small beads in the range of 50–400 μm appear to be preferably used at high stirrer speeds or in high-energy mills (Cerdeira et al., 2011; Ghosh et al., 2011; Ghosh et al., 2012; Juhnke et al., 2012; Konnerth et al., 2016; Li et al., 2015a; Niwa et al., 2011; Shah et al., 2014; Singare et al., 2010). When relatively small beads (e.g., 200 and 400 μm) were used in medium/low-energy ball mills, the production of fine drug nanoparticles took days (Salazar et al., 2014; Sepassi et al., 2007), which was inefficient. It is obvious that the selection of bead size could significantly affect the cycle time, operational efficiency, and/or final drug particle size during wet media milling, which are important to process economics as well as the dissolution enhancement provided by the drug

nanoparticles. Hence, a fundamental understanding of the impact of bead size on breakage kinetics and particle size could help one to develop guidance and rationale for optimal bead size selection for wet media milling processes.

Table 1.1 Recent Literature on Bead Sizes used in Pharmaceutical Wet Media Milling

References (Year)	Mill Type	Stirrer/ Circumference Speed (rpm)	Nominal Bead Size Investigated[a] (μm)	Optimal Bead Size[b] (μm)	Drug Particle Size Produced[d] (μm)
Konnerth et al. (2016)	Wet stirred media mill	2.9–6.4[c]	100–2,000	100	0.179[e]
Bitterlich et al. (2015)	Planetary ball mill	6.3[c]	100–500	500	~0.100[f]
Li et al. (2015)	Wet stirred media mill	11.7–14.7[c]	50–800	50	0.088[f]
Tuomela et al. (2015)	Planetary ball mill	600	5,000	5,000	0.550, 0.970[f]
Sarnes et al. (2014)	Planetary ball mill	1100	1,000	1,000	0.315[f]
Shah et al. (2014)	Wet media mill	400–1100	100 and 1,000	100	0.329[f]
Branham et al. (2012)	Planetary ball mill	200	15,000	15,000	0.355[g]
Ghosh et al. (2012)	Planetary ball mill	150	100–500	500	~0.600[f]
		400	100–500	100	~0.250[f]
Juhnke et al. (2012)	Wet stirred media mill	6–12[c]	100 and 200	100	~0.150[e]
Cerdeira et al. (2011)	Agitator media mill	2400–3600	400–800	400	~0.130[e]
Ghosh et al. (2011)	Wet stirred media mill	2500	100–500	200	0.230[f]
Niwa et al. (2011)	Oscillating beads-milling apparatus	2700	100–1,000	300	~0.250[e]
Singare et al. (2010)	Wet stirred media mill	2500–3400	200	200	0.211[i]
Ain-Ai and Gupta (2008)	Centrifugal ball mill	400	800	800	0.536[h]
Choi et al. (2008)	Ball mill	100	1,000	1,000	0.100[h]

[a]Bead made up of zirconium dioxide; [b]Bead size which led to the smallest final drug particle size or the only bead size chosen for the particular study; [c] m/s; [d]The smallest drug particle size produced using the optimal bead size; [e]d_{50}; [f] Z-average; [g]Sauter mean diameter; [h]Mean size; [i]d_{90}

Only very recently, various microhydrodynamic models (Eskin et al., 2005a, b) have been adopted by Afolabi et al. (2014) to describe the fluctuating motion of the beads during WSMM and elucidate the impact of process parameters with the goal of developing a fundamental understanding of the WSMM process. The important findings can be summarized as follows: upon an increase in stirrer speed, more mechanical energy was imparted and all microhydrodynamic parameters increased monotonically. This suggests that more frequent and energetic/forceful bead–bead collisions and more frequent drug particle compressions occurred during WSMM, thus explaining the faster drug particle breakage at higher stirred speed. An increase in volumetric bead concentration led to more bead–bead collisions and drug particle compressions, which favored faster breakage; yet, such collisions were less energetic/forceful, which could slow down the breakage. Overall, despite these two counteracting effects of bead concentration, the overall impact was favorable in terms of enhanced breakage kinetics. An increase in drug loading led to a slight, almost linear decrease in all microhydrodynamic parameters, thus explaining the reduced breakage rate. However, a comprehensive study has not been conducted to determine the impact of bead size at different stirrer speeds and elucidate any optimal bead size, with the ultimate goal of developing a fundamental rationale for bead size selection.

Proper stabilizer formulation is selected based on the investigation presented in Chapter 2. Chapter 3 in this dissertation aims to elucidate the impact of bead size on the breakage kinetics at different stirrer speeds and rationalize the selection of bead size for the optimal performance of WSMM. The experimental observations were explained within the context of a microhydrodynamic model. Furthermore, the

implications of the findings were indicated so as to develop a rationale for bead size selection in WSMM process and offer an overarching explanation about the typical bead sizes used for all wet media milling processes with low–medium vs. high-energy levels.

1.2.3 Preparation of Sub-100 nm Drug Particles

Preparation of "true drug nanoparticles," i.e., particles with sub-100 nm sizes, has been a great challenge in pharmaceutical literature. Despite the use of various top-down and bottom-up approaches in the last few decades, only a few examples of nanosized drugs having a median particle size below 100 nm are available in the literature (refer to Sinha et al. (2013)). Among the bottom-up approaches such as liquid anti-solvent precipitation, melt emulsification, precipitation using supercritical fluids, evaporative precipitation, and micro-emulsions, only the micro-emulsion approach appears to be capable of producing sub-100 nm particles for multiple drugs. For example, about 85 nm griseofulvin particles were prepared with use of lecithin and water–butyl lactate/1,2-propanediol system (Trotta et al., 2003), and simvastatin particles of 50–70 nm were prepared with use of lecithin/polysorbate 80 and water–ethanol/butylacetate system (Margulis-Goshen and Magdassi, 2009). Although this technique demonstrates the feasibility of preparing sub-100 nm particles, like other bottom-up approaches, it suffers from various limitations such as low drug loading, the presence of organic solvents, and thermodynamically unstable particles. Contrary to bottom-up approaches, WSMM, a top-down approach, is considered more universal and promising for the large-scale production of poorly water-soluble drug

nanoparticles as mentioned before. A cursory review of recent literature, which is not intended to be comprehensive, on finely milled BCS Class II drugs via WSMM is presented in Table 1.2. The data support the commonly held notion that preparation of drug suspensions with a sub-100 nm particle size via WSMM is extremely challenging. Since the use of sub-100 nm drug nanoparticles can have a positive impact on bioavailability enhancement through solid and parenteral dosage forms while potentially enabling sterile filtration, development of an improved WSMM process with sub-100 nm particle formation capability is highly desirable.

Table 1.2 Recent Literature on Drug Nanosuspensions with Median Particle Size < 200 nm Prepared via Wet Stirred Media Milling

Drug	Initial Median Size (μm)	Drug Loading (% w/w)	Batch Size	Milling Time (min)	Final Median Size (nm)	Reference
Arsenic sulfide	NR[a]	~1.7	300[b]	120	115	(Bujňáková et al., 2015)
Bifendate	8	20	NR[a]	45	120	(Yao et al., 2014)
Etravirine	11	20	NR[a]	60	140	(Cerdeira et al., 2011)
Fenofibrate	16	10	200[b]	120	150	(Knieke et al., 2013)
Griseofulvin	20	10	200[b]	96	132	(Afolabi et al., 2014)
Itraconazole	20	20	300[c]	60	136	(Cerdeira et al., 2013a)
Miconazole	20	20	300[c]	60	140	(Cerdeira et al., 2013a)
Naproxen	NR[a]	1	NR[a]	240	196	(Kumar and Burgess, 2014)
Undisclosed	15–20	5	NR[a]	360	200	(Bose et al., 2012)

[a]Not reported.
[b]Volume of water used in the suspension.
[c]Mass (g) of the suspension.

It is arguable that one can prepare sub-100 nm drug particles with the currently existing WSMM processes by simply prolonging the milling. WSMM process is generally regarded as time-consuming, costly, and energy-intensive (Kawatra, 2006). Contamination of the milled product due to bead wear and possible changes in the crystalline state of the drugs are some other concerns (Kesisoglou et al., 2007). Although drug product contamination introduced by typical ceramic and polymeric milling beads are mostly not regulated by health authorities, they should be quantified in the lower ppm range, according to the current regulatory concepts and permitted daily exposures for oral, parenteral, pulmonary and topical administration (Juhnke et al., 2012). Besides these issues and concerns, most suspensions approach a well-known grinding limit or dynamic equilibrium after a certain milling time (Knieke et al., 2009; 2013). Hence, simply prolonging the milling process would make the aforementioned issues worse without necessarily reducing the particle size below 100 nm.

A more feasible approach for the preparation of sub-100 nm particles can be process improvement/optimization that ensures faster particle breakage. However, lack of mechanistic, first-principle-based understanding of the impact of process parameters and/or heavy reliance on purely empirical approaches has been a barrier to process improvement (Afolabi et al., 2014). In fact, most wet media milling studies have focused mainly on optimization of various stabilizers and physical stability of the milled drug suspensions (Kesisoglou et al., 2007; Peltonen and Hirvonen, 2010; Van Eerdenbrugh et al., 2008b). While ensuring the physical stability of the nanosuspensions is important, so are other aspects such as breakage kinetics, energy

consumption, and bead wear; however, such aspects have not been thoroughly examined in a holistic approach, especially with the ultimate goal of preparing sub-100 nm particles. Enhanced breakage kinetics can reduce milling time required, energy consumption, and even bead wear, which can be achieved by proper selection of the milling parameters such as bead size, bead loading, drug loading, rotor speed, and suspension flow rate. Influence of these parameters on the final drug particle size has been studied previously through experiments (Afolabi et al., 2014; Cerdeira et al., 2011; Ghosh et al., 2011; Ghosh et al., 2013; Ghosh et al., 2012; Monteiro et al., 2013; Singare et al., 2010; Singh et al., 2011). However, the influence of these parameters on breakage kinetics leading to sub-100 nm drug particles with reduced energy consumption and low bead wear has not been addressed. Moreover, no first-principle mechanistic understanding of the breakage kinetics has emerged, except that presented in Afolabi et al. (2014), and conflicting results about the optimal bead size have been reported. Moreover, Cerdeira et al. (2011), Ghosh et al. (2011; 2012; 2013), and Juhnke et al. (2012) used only two-three different bead sizes while investigating the impact of bead size without considering the microhydrodynamics inside the mills. Nonetheless, the studies above overall suggest that sub-100 nm drug nanoparticles may be produced by increasing rotor speed, bead loading, and suspension flow rate. On the other hand, the ever-present concerns about bead contamination along with high energy consumption and the need for selecting an optimal bead size may have prevented or delayed such attempts. In addition, some drugs can be so hard that it may not be feasible to produce sub-100 nm drug particles with low bead contamination in a reasonable time. While developing a particle-scale

understanding of breakage in view of the mechanical properties of drug particles is important, this aspect is beyond the scope of the current work.

A brute-force approach that uses a more energetic milling process without any consideration of the impact of bead size could actually lead to excessively high bead wear and high energy consumption. Hence, fast preparation of sub-100 nm drug particles with reduced energy consumption and acceptable media contamination entails a thorough mechanistic understanding of the impact of the bead size and process parameters. This objective can be achieved by analyzing the fluctuating motion of beads in sheared suspensions, i.e., microhydrodynamics of beads and capture/deformation of the drug particles. To this end, Eskin et al. (2005a, b) developed a microhydrodynamic model for a dense slurry flow of beads and particles. Bilgili and Afolabi (2012) applied it to WSMM of drugs in order to elucidate the viscous dampening caused by various stabilizers. Recently, Afolabi et al. (2014) has elucidated the impact of stirrer speed and bead–drug loading on the breakage kinetics using this microhydrodynamic model; however, preparation of sub-100 nm particles, the impact of bead size, and reduction of wear and energy consumption have not been addressed.

Chapter 4 presents an intensified WSMM process for the faster production of sub-100 nm BCS Class II drug particles with reduced specific energy consumption and low bead wear. Since stabilization plays a significant role in preparing drug nanosuspensions, an aggressive baseline WSMM process along with proper stabilizer formulation was selected based on the investigations presented in Chapters 2 and 3. In Chapter 4, the impact of bead size on the drug particle size, breakage kinetics, energy

consumption, and bead wear was investigated for griseofulvin and indomethacin, two poorly water-soluble drugs, under highly energetic milling conditions in the turbulent flow regime. The microhydrodynamic model of the process was used to gain insight into the impact of bead size. Then, the baseline process with the optimal beads was intensified stepwise by increasing the rotor tip speed, bead loading, and suspension flow rate, as guided by the microhydrodynamic model. In pursuit of the goal of preparing sub-100 nm drug particles fast, this study contributes to a fundamental understanding of the impact of bead size and process intensification while addressing all major issues associated with the WSMM process, i.e., excessively long processing time, high energy consumption, and potentially high media contamination in a holistic, model-guided approach.

1.2.4 Impact of Polymer–Surfactant on Dissolution Performance of Drug Nanocomposites

The studies in Chapters 2–4 enable to develop fundamental process–formulation understanding for the effective production and stabilization of drug nanosuspensions. Interestingly, except for parenteral formulations, drug nanosuspensions were not directly applied to patients. Depending on the route of administration intended, drug nanosuspensions are usually converted via drying into drug composites, and incorporated into standard solid dosage forms such as capsules, tablets, and sachets (Basa et al., 2008; Bhakay et al., 2014a; Van Eerdenbrugh et al., 2008a) to meet the high patient/clinical demand for solid dosage forms. Drying of nanosuspensions can be achieved via spray drying (Azad et al., 2014a; Lee, 2003), spray-freeze drying (Cheow et al., 2011; Wang et al., 2012), freeze drying (de Waard et al., 2008; Layre

et al., 2006), vacuum drying (Choi et al., 2008; Kim and Lee, 2010), as well as granulation with, or coating onto, inert excipient particles (Basa et al., 2008; Bhakay et al., 2014b).

Unfortunately, drug nanoparticles tend to form aggregates during both milling and drying of the drug suspensions (Bhakay et al., 2013; Lee, 2003), leading to the loss of their large surface area. Soluble polymers and surfactants can be used to impart physical stability and retain the large surface area of the nanoparticles (Bhakay et al., 2011; Bilgili and Afolabi, 2012; Kesisoglou et al., 2007). However, depending on the formulation, drug nanoparticles may not be fully recovered from the dried composites during redispersion and dissolution, which will slow down the drug dissolution and reduce the bioavailability (Bhakay et al., 2013; Chaubal and Popescu, 2008). Here, redispersion testing entails dispersing the drug composites in various physiologically relevant fluids like water, and comparing the particle size of the resulting suspension with that of the precursor suspension used in drying. Various redispersion methods were studied extensively by Bhakay et al. (2013). Slow/incomplete recovery of drug nanoparticles from the composites was observed when a steric stabilizer or ionic stabilizer was used alone in the precursor drug suspension (e.g., (Bhakay et al., 2013; Lee, 2003). Drug nanoparticles were fully recovered only when steric stabilizer and ionic stabilizer were used in combination (e.g., (Basa et al., 2008; Bhakay et al., 2013) or when swellable dispersants were co-milled along with the drug (Azad et al., 2014a; Bhakay et al., 2014b). However, in all these studies, either single grade (molecular weight) of polymer and/or single polymer concentration was investigated. Molecular weight (MW), a critical property

of the polymer, determines both the solution properties of polymer chains and the capability for steric stabilization (Adamson and Gast, 1997; Ploehn and Russel, 1990), mechanical properties of films (Rowe, 1986), and the release of drug particles for oral administration (Mittal et al., 2007). Therefore, MW of polymers may be tailored to achieve the best stabilization performance in milling and fast drug release from the composites. Choi et al. (2008) investigated the impact of hydroxypropyl cellulose (HPC) MW on itraconazole nanoparticle production and their recovery from the drug composites. In that paper, HPC was used as a sole stabilizer at a single concentration, and dissolution performance was not investigated. Sepassi et al. (2007) investigated the impact of hydroxypropylmethyl cellulose (HPMC) and polyvinylpyrrolidone (PVP) MW on the particle size of milled nabumetone and halofantrine suspensions; however, drying, redispersion, and drug dissolution were not studied. In addition, in the previous works mentioned above, an optimal polymer concentration that ensures full recovery of drug nanoparticles from the composites with minimal usage has not been identified.

The literature review suggests that there is no systematical and comprehensive study about the impact of polymer concentration and molecular weight in the presence/absence of an ionic surfactant on the redispersion and drug dissolution from the nanoparticle-laden composites. Chapter 5 aims to fill this gap and develop an understanding of the relationships between the physical stability of drug nanosuspension, redispersion, and drug dissolution from the composites prepared via fluidized bed coating/drying. The role of nanoparticle stabilization and drug particle size in drug dissolution performance was also investigated. Moreover, Chapter 5 also

attempts to test the validity of the commonly-held notion that the use of stable wet-milled drug nanosuspensions ensures fast redispersion and drug dissolution from the dried composites.

1.2.5 Impact of Various Dispersants on the Dissolution Performance of Nanocomposites

Among various dispersants used in nanocomposite formulations, a soluble polymer, typically cellulosic ones, and an anionic surfactant in combination has been shown to be very effective in stabilizing drug nanosuspensions (Bilgili and Afolabi, 2012; Bilgili et al., 2016d; Cerdeira et al., 2010) and allowed for complete recovery of drug nanoparticles from the nanocomposites during redispersion/dissolutions tests, thus, enabling enhanced drug dissolution performance (Basa et al., 2008; Li et al., 2016c; Niwa et al., 2011). However, despite their effectiveness as dispersants, surfactants may pose several challenges such as aggregation of the drug nanoparticles in suspensions during milling/storage (Cerdeira et al., 2010; Knieke et al., 2013), micellar solubilization of the drug (Yalkowsky, 1981) and particle growth via Ostwald ripening during milling and/or storage (Ghosh et al., 2011; Knieke et al., 2013; Verma et al., 2011). Additional challenges associated with the use of anionic surfactants include incompatibilities with other ionic molecules, sensitivity to pH, salt or temperature changes, GIT irritation (Gupta and Kompella, 2006; Liversidge and Cundy, 1995), and even toxicity when used in excess (Liversidge and Cundy, 1995), especially for inhalation applications (Lebhardt et al., 2011; Suzuki et al., 2000).

In view of all the aforementioned issues, surfactant usage should be minimized to mitigate all potential negative impact during formulation development.

Sugars (e.g., Sucrose, Lactose), sugar alcohols (e.g., Mannitol, Sorbitol), and water-soluble polymers (e.g., HPC, HPMC, PVP, and PEG) are commonly used in nanocomposite formulations as dispersants. However, in the absence of surfactants, sugars and sugar alcohols must be added in high concentrations up to 1000% w/w w.r.t. (with respect to) the drug nanoparticles to ensure fast nanoparticle release from the nanocomposites (Hu et al., 2011; Kho and Hadinoto, 2010; Kim and Lee, 2010). Such high dispersant concentrations render drug concentration in the composite particles relatively low, minimizing the drug carrying capacity of the nanocomposites. Besides, when used alone, water-soluble polymers may not guarantee fast drug dissolution from drug nanocomposites (Choi et al., 2008; Li et al., 2016c), and their overuse may potentially slow down dissolution (Jagtap et al., 2012; Knieke et al., 2015a; Möckel and Lippold, 1993; Shah and Sheth, 1976). Alternative surfactant-free formulations with novel dispersants that allow for high drug loading should be developed in comparison to conventional dispersants used in nanoformulations.

Bilgili et al. (2016b) and Azad et al. (2015a) wet co-milled superdisintegrants and BCS Class II drugs in the presence of an adsorbing neutral polymer, thus, providing a novel method for formulating surfactant-free drug nanosuspensions. While large superdisintegrant particles with high swelling capacities are typically used for fast disintegration of tablets in the pharmaceutical industry (Omidian and Park, 2008), the use of colloidal or wet-milled superdisintegrants for enhancing drug nanoparticle release/dissolution from nanocomposites is relatively novel. A recent study by Bhakay et al. (2014b) explored the use of wet-milled superdisintegrants as a novel class of dispersants that improve the recovery/dissolution of drug nanoparticles

from nanocomposites in the absence of surfactants. Bhakay et al. (2014b) coated wet co-milled griseofulvin (GF)–croscarmellose sodium (CCS) suspensions on Pharmatose® via a fluidized bed processor, which yielded core–shell type GF nanocomposites with a relatively low drug loading: <13% w/w. The major focus there was to optimize the co-milling time of the superdisintegrant for the best dissolution improvement. In a separate study, Azad et al. (2015b) demonstrated the positive impact of CCS and SSG on the dissolution performance of GF nanocomposites and the feasibility of spray drying to prepare high-loaded, surfactant-free GF nanocomposites. GF was used as the model drug in both studies (Azad et al., 2015b; Bhakay et al., 2014b) and superdisintegrants were used at one concentration. While the aforementioned studies provided the proof-of-concept for surfactant-free nanocomposites with colloidal superdisintegrants in dissolution enhancement, the positive correlation with their swelling capacity was not established. Besides, no head-to-head comparison between colloidal superdisintegrants and conventionally used dispersants, e.g., sugar, sugar alcohol, and soluble polymers, at various concentrations has been conducted previously. More importantly, the mechanisms associated with the dissolution enhancement provided by wet-milled superdisintegrants have not been fully elucidated.

In Chapter 6, nanocomposites of itraconazole (a BCS Class II drug) was prepared by spray-drying precursor wet media milled drug suspensions with various classes of dispersants with the goal of elucidating their roles in drug release from the nanocomposites during dissolution. Itraconazole (ITZ) is an antifungal drug for the treatment of local and systemic mycoses, which belongs to BCS Class II, having high

permeability, but a very poor water solubility (< 1 ng/mL) (Peeters et al., 2002). The impact of Sucrose vs. microcrystalline cellulose (MCC) on the dissolution of freeze-dried ITZ nanocomposites was assessed by Bernard et al. (2008) in the presence of D-α-tocopherol polyethylene glycol 1000 succinate (TPGS), where Sucrose and MCC as extra dispersants had to be used at 50% and 200%, respectively, w.r.t ITZ to achieve 80% ITZ dissolution in 20 min. Similarly, Mannitol and MCC were studied as extra dispersants in the presence of HPC and SDS by Cerdeira et al. (2013b), where Mannitol and MCC were used at 100% w.r.t ITZ for effective dissolution improvement of spray-dried ITZ nanocomposites. Other literature on ITZ nanocomposite did not investigate different dispersants on ITZ dissolution. For example, Parmaentier et al. (2017) and Azad et al. (2016) used the HPMC–SDS combination to achieve fast dissolution of ITZ nanocomposites produced by fluid bed coating; Sarnes et al. (2014) produced fast-dissolving ITZ nanocomposite with Poloxamer P407 via freeze drying; De Smet et al. (2014) spray-dried ITZ nanocomposite in the presence of adipic acid and Tween 80. Interestingly, all of the work mentioned above relied upon the use of certain surfactant, e.g., TPGS, sodium dodecyl sulfate (SDS), Tween, Poloxamer, etc., and thus none of them produced fast dissolving surfactant-free ITZ nanocomposites. More importantly, wet co-milled superdisintegrants and polymer alone at high concentration were not considered for the dissolution improvement of ITZ nanocomposites. The comparison between co-milled superdisintegrants and conventionally used dispersants was completely missing. All these gaps and issues will be addressed in Chapter 6.

1.2.6 Comparative Assessment of the Dissolution Performance of Nanocomposites and Amorphous Solid Dispersions: Matrix Size Effect

Chapters 2–6 deal with the production, stabilization, and dissolution of the drug nanoparticle-based formulations, i.e., drug nanosuspensions and nanocomposite microparticles. Nanoparticle delivery relies on reduced particle size for increased dissolution rate (Möschwitzer et al., 2011), according to the Noyes–Whitney equation (Noyes and Whitney, 1897). Enhanced dissolution rate, improved bioavailability, safe dose escalation, elimination of food effects, and enhanced safety, efficacy and tolerability profiles are some of the numerous advantages of crystalline drug nanoparticles (Junghanns and Müller, 2008). Despite all the above-mentioned advantages, nanoparticle formulations have a serious drawback: the limited improvement on drug solubility. Often for drugs with very low aqueous solubility, the achieved increase in dissolution rate via size reduction is limited and insufficient to provide significant enhancement of bioavailability (Müller et al., 2001).

Another approach to enhance the bioavailability of poorly water-soluble drugs is to produce amorphous solid dispersions (ASDs). ASDs tend to exhibit high levels of supersaturation in aqueous media relative to the crystal form of the drug, and thus higher apparent solubility (Newman et al., 2012). The preparation involves combining a drug with a water-soluble polymer to produce a single-phase amorphous mixture of the drug and the polymer. Once the solid dispersion encounters dissolution media, supersaturation in solution must be maintained over a period of time that will ensure complete dissolution and potential enhancement in bioavailability (Alonzo et al., 2010; Brouwers et al., 2009). Processes for the preparation of amorphous solid dispersions can be categorized into two general types: solvent methods and fusion–

melting methods (Brough and Williams III, 2013). With solvent methods, solid dispersions are obtained by evaporating solvent from a drug and carrier solution. Practical applications of the solvent method are spray drying (Langham et al., 2012; Paradkar et al., 2004) and freeze drying (Kagotani et al., 2013; Schersch et al., 2010). On the other hand, pharmaceutical hot-melt extrusion (HME), is an evolving, solvent-less fusion technique, currently being investigated by both industry and academia as a means to produce amorphous solid oral dosages, with improved bioavailability of the poorly water-soluble drugs (Gogos et al., 2012).

It is well known that utilizing the amorphous form of a drug can be a useful approach to improve the dissolution behavior and bioavailability of poorly water-soluble drugs, as a result of supersaturation (Chiou and Riegelman, 1970; Goldberg et al., 1966; Hancock and Parks, 2000). However, the dissolution advantage of amorphous solids can be negated either by crystallization of the amorphous solid on contact with the dissolution medium or through rapid crystallization of the supersaturated solution (Alonzo et al., 2010). The majority of research work on amorphous dispersions focused on the drugs at a relatively high dose, which led to supersaturation in the dissolution media (Konno et al., 2008; Langham et al., 2012; Yang et al., 2010), where the major research focus was to retard the recrystallization and maintain the highest level of supersaturation during dissolution (Konno et al., 2008). It is interesting to note that a head-to-head comparison of the dissolution performance between nanoparticle-based formulations and amorphous solid dispersion of poorly water-soluble drugs is not available in the open literature. Yang et al. (2010) investigated the bioavailability enhancement induced by amorphous

versus crystalline itraconazole nanoparticles. It was found that amorphous itraconazole had higher supersaturation that increased the permeation, but dissolution performance was not investigated. Six et al. (2004) investigated the relative dissolution improvement achieved by ASD with respect to as-received itraconazole microparticles. It was found that the dissolution of itraconazole was significantly improved by producing ASD compared to the microparticles. However, it is still unknown if nanoparticles of itraconazole can also achieve similar or better dissolution improvement. Similar to Six et al. (2004), Jung et al. (1999) conducted a comparison between amorphous solid dispersion of itraconazole to commercial products as well as as-received itraconazole microparticles in tablet form. By changing different polymers during spray drying process, fast dissolution of itraconazole amorphous solid dispersion can be achieved. A comparison of the dissolution performance of nanoparticles vs. ASD does not exist. Furthermore, the drug doses in the above-mentioned dissolution studies were all above 100 mg up to 200 mg. For drugs with high potency, low dose (typically <<10 mg), is preferred to mitigate the potential side effects (Branchey et al., 1978; Law et al., 2003). Hence, a direct comparison of the dissolution enhancement imparted by nanocomposites versus ASDs for low drug dose can be of special interest for formulating high potency drugs. A commonly-held notion in pharmaceutical literature is that nanocrystals of a drug formulated in nanocomposites are not as effective as the amorphous form of the drug formulated in the form of ASDs because the latter offers significant supersaturation advantage. Chapters 7 and 8 of this dissertation will challenge this commonly-held notion and test its limits in terms of drug dose and particle size of the nanocomposites vs. ASDs.

Recently, a nanoextrusion process has been developed to disperse drug nanoparticles in a polymeric matrix using a modified version of the standard hot melt extrusion process (Baumgartner et al., 2014; Khinast et al., 2013). Nanoextrusion appears to be a new promising platform technology to make solid nanoparticle-based formulations (nanocomposites), thereby improving the dissolution rate and thus the bioavailability of the drug as well as enhancing patient compliance. This technique was first presented by Khinast et al. (2013) as a one-step process for drying a stabilized nanosuspension of crystalline titanium oxide. In a followed-up study by Baumgartner et al. (2014), drug nanoparticles were used to demonstrate applicability to pharmaceutical products. However, the dissolution rate of the produced nanocomposite was very low, which casts doubt about the use of the technology for immediate-release drug products. In a separate study conducted by Park et al. (2013), the same technique was explored with an emphasis on the preparation of content-wise uniform solid dosage forms with very low dose drugs. In that study, the dissolution performance of the produced nanocomposites was not studied. Ye et al. (2015) combined the use of high-pressure homogenization and extrusion for the production of nanocomposites with low drug concentration, i.e., 1–2%. Throughout the literature, no study has been conducted on the dissolution performance comparison between drug nanocomposites and ASDs that are prepared via the same nanoextrusion process.

Extrusion processes of manufacturing drug solid dosages, including traditional hot melt extrusion and nanoextrusion, usually involve downstream processes such as milling of the extrudates, sieving, compression, and coating. Milling of extrudates into various particle (matrix) sizes opens the possibility of manipulating the drug

dissolution performance. The majority of the literature on extrusion process ignored the matrix size effect of the milled extrudates on the dissolution performance. For examples, Fule et al. (2016) used hot melt extrusion process to produce ASD of artesunate in the matrices of Soluplus® and Kollidon® VA64. The produced extrudates were milled and passed through a 200 μm for various characterizations. Similar to Fule et al. (2016), most literature simply passed the milled extrudate powder through a sieve without reporting the actual particle sizes and their distribution, e.g., (Ghebremeskel et al., 2006; Juluri et al., 2016; Perissutti et al., 2002; Pudlas et al., 2015). Most importantly, all the reported literature focused on only one particle size of the extrudates. Even when nanocomposites were produced by an extrusion process, i.e., nanoextrusion (Baumgartner et al., 2014; Ye et al., 2015), the impact of matrix size was not thoroughly investigated. Hence, it is not unfair to assert that the impact of particle (matrix) size of the milled extrudate powders on drug dissolution has been extensively studied neither for nanocomposites nor for ASDs produced by an extrusion process.

To address the aforementioned issues and challenges, Chapter 7 presents a first attempt to prepare both a drug nanocomposite and a drug ASD using the same nanoextrusion process by using two different extrusion polymers with different polymer–drug miscibility. As the nanoextrusion process is a newly developed process to create a dispersion of drug nanoparticles while drying the drug nanosuspensions, its comparison to conventionally used drying processes, e.g., spray drying, was also carried out for the first time in literature. As a continuation, Chapter 8 uses the nanoextrusion process as a platform enabling the systematical assessment of extrudate

particle (matrix) size impact on the drug dissolution performance under both non-supersaturating and supersaturating conditions for nanocomposites as well as ASDs at two drug loading levels.

1.3 Objectives and Major Research Tasks

In view of the above mentioned issues, the goal of this dissertation is to enhance the dissolution performance of poorly water-soluble drugs using nanoparticle-based formulations and ASDs, compare their dissolution performance, and elucidate the mechanisms. To achieve this goal, three major objectives are targeted. The first major objective is to develop a processing–formulation understanding of wet stirred media milling process for fast–efficient production of drug nanoparticles in a stable nanosuspension form. To this end, combination of an adsorbing polymer–anionic surfactant was assessed for five poorly water-soluble drugs as a general stabilizing strategy; a microhydrodynamic model-based rationale was developed for optimal bead size selection that achieves the fastest production of drug nanoparticles; and a process intensification methodology for production of sub-100 nm stable drug nanoparticles with minimal product contamination was developed in view of the microhydrodynamic model. The second major objective is to elucidate the impact of various classes dispersants on drug release rate and mechanisms during the redispersion–dissolution of nanocomposites prepared via dying of the drug nanosuspensions. To this end, drug nanosuspensions were used as precursor materials for the production of nanocomposite microparticle powders (nanocomposites) via various drying techniques. Several classes of dispersants/stabilizers such as polymer,

surfactants, sugars, sugar-alcohols, and superdisintegrants (SDIs) were used at various concentration to modulate the drug nanoparticle release and dissolution rate. The role of drug nanoparticle stabilization and drug particle size in dissolution performance of the nanocomposites was also investigated as well as the roles/impact of dispersant type and concentration. Finally, the third major objective is to assess the dissolution enhancement imparted by drug nanocomposites vs. ASDs prepared via drying of drug nanosuspensions by a novel nanoextrusion process. To attain a scientific, head-to-head assessment of the two formulation platforms, nanocomposites and ASDs of the same drug were prepared using the nanoextrusion process, and the dissolution performance of drug nanocomposites vs. ASDs was evaluated at two drug loadings, three different matrix size, and two doses.

1.4 Dissertation Outline

This dissertation has been organized into various chapters as follows:

1) Chapter 2 assesses the combined use of non-ionic cellulosic polymers and anionic surfactants in stabilizing multiple drug nanosuspensions prepared via wet media milling. The aim is to provide a generally applicable stabilization strategy for multiple drug nanosuspensions.
2) With the established stabilization strategy for drug nanosuspensions in Chapter 2, Chapter 3 studies the impact of bead size on the drug breakage kinetics at different stirrer speeds and rationalizes the selection of bead size in view of a microhydrodynamic model for the optimal performance of wet stirred media milling.

3) Combining the knowledge generated in Chapter 2 on formulating stable drug nanosuspensions and Chapter 3 on bead size optimization, Chapter 4 presents an intensified wet media milling process with the objective of preparing sub-100 nm drug nanosuspensions with reduced energy consumption and low contamination under the guidance of a microhydrodynamic model.
4) Chapters 2–4 established fundamental understanding on the fast production of drug nanoparticles in the form of aqueous suspensions with desired drug particle size and minimal aggregation. In Chapter 5, the drug suspensions stabilized by polymer/surfactant are dried–coated on the Pharmatose® carriers in a fluidized bed processor, and the impact of the physical stability of drug nanosuspension and roles of polymer/surfactant in drug dissolution from the nanocomposites are elucidated.
5) Chapter 6 presents spray drying of the drug suspensions into nanocomposite microparticles to produce high drug-loaded, matrix-type nanocomposites. The impact of various classes of dispersants is investigated for the preparation of fast-dissolving, high drug-loaded, and surfactant-free nanocomposites. Further, the mechanisms for the enhanced dissolution of nanocomposites is elucidated.
6) With all the established knowledge on nanoparticle-based formulations in previous chapters, Chapter 7 aims to develop a nanoextrusion process, which allows for preparing nanocomposites vs. ASDs of the same drug and enables comparative assessment of their capability for drug dissolution enhancement. Depending on the selection of polymeric matrix, the same nanoextrusion process can produce extrudates with crystalline (nanocomposites) and amorphous (ASD)

forms of the same drug.

7) As a continuation of Chapter 7, Chapter 8 investigates the impact of polymeric matrix size on the dissolution performance of nanocomposites vs. ASDs at both low dose and high dose conditions.
8) Finally, Chapter 9 provides the conclusions and recommendations for future work that originate from interesting research questions/issues identified during the course of this investigation.

CHAPTER 2

A GENERAL STRATEGY FOR ENSURING PHYSICAL STABILITY OF BCS CLASS II DRUG NANOSUSPENSIONS

Ensuring the physical stability of drug nanosuspensions prepared via wet media milling has been a challenge for pharmaceutical scientists. The aim of this study is to assess the feasibility of combined use of nonionic cellulosic polymers and anionic surfactants in stabilizing multiple drug nanosuspensions as a general stabilization strategy. The particle size of five drugs, i.e., azodicarbonamide (AZD), fenofibrate (FNB), griseofulvin (GF), ibuprofen (IBU), and phenylbutazone (PB) was reduced separately in an aqueous solution of hydroxypropyl cellulose (HPC) with/without sodium dodecyl sulfate (SDS) via a stirred media mill. Laser diffraction, scanning electron microscopy, thermal analysis, rheometry, and electrophoresis were used to evaluate the breakage kinetics, storage stability, electrostatic repulsion, and stabilizer adsorption.

2.1 Materials and Methods

2.1.1 Materials

Azodicarbonamide (AZD; Pfaltz & Bauer, Waterbury, CT), fenofibrate (FNB; BP grade, Jai Radhe Sales, Ahmedabad, India), griseofulvin (GF; BP/EP grade, Letco Medical, Decatur, AL), ibuprofen (IBU; PH.EUR/USP/JP/IP grade, Alfa Chem, Kings Point, NY), and phenylbutazone (PB; USP grade, Medisca, Plattsburgh, NY) were used as-received in the wet media milling experiments. These drugs were selected as they belong to BCS Class II and have different physicochemical properties

(Table 2.1).

Table 2.1 Physicochemical Properties of the Drugs

Drug	Solubility in Water at 4°C (mg/l)	Molecular Weight (g/mol)	Melting Point (°C)	Log*P*
AZD	35	116.1	225	-1.7
FNB	0.7	360.8	80.5	5.3
GF	8.6	352.8	220	2.2
IBU	21	206.3	76	3.6
PB	32	308.4	105	3.2

Hydroxypropyl cellulose (HPC, SL grade) donated by Nisso America Inc. (New York, NY, USA) was used as model non-ionic cellulosic polymer and steric stabilizer. SDS purchased from Sigma-Aldrich (Milwaukee, WI, USA) was used as a model anionic surfactant that acts as a wetting agent and electrostatic stabilizer. Its critical micelle concentration (CMC) in water is 8.2 mM (0.24% w/w) at ambient temperature. Wear-resistant yttrium stabilized zirconia beads (Zirmil Y, Saint Gobain ZirPro, Mountainside, NJ), with a median size of 430 µm, were used as milling media.

2.1.2 Preparation of Suspensions via Wet Media Milling

Feed suspensions to be milled were prepared in a DLM 1638X1 shear mixer (Cat#. 14-503 Fisher Scientific Pittsburgh, PA, USA). The drug and HPC concentrations were kept at 10 and 2.5%, respectively, in all suspensions, with or without 0.5% SDS. Hence, HPC was present in all suspensions as the baseline stabilizer, whereas SDS

was used along with HPC in some additional suspensions prepared. All concentrations reported here are with respect to deionized water (250 g) unless otherwise specified. SDS, where applicable, was added to deionized water in a beaker gradually for 15 min while the mixer ran at a fixed speed of 300 rpm. Then, HPC was added to the SDS solution gradually for 30 min. The final HPC–SDS solution or HPC solution was further mixed for 15 min to ensure proper dissolution. The desired amount of drug powder was weighed and added to this solution gradually for 30 min while mixing continued.

The wet stirred media mill (Figure 2.1) used in this study was manufactured by Netzsch Fine Particle Technology, LLC. (Model: Microcer, Exton, PA). The milling chamber has a volume of 80 ml and is lined with zirconia. During milling, a peristaltic pump recirculated the suspension between the holding tank and the milling chamber, while a 200 µm screen kept the zirconia beads in the milling chamber, but allowing the passage of the drug suspension. The feed suspensions prepared using the shear mixer were poured into the holding tank and milled under the following conditions: bead loading of 50 ml (bulk), suspension flow rate of 126 ml/min and stirrer (rotor) speed of 3200 rpm corresponding to a tip speed of 11.7 m/s. Both the milling chamber and the holding tank were equipped with a cooling system (model number M1-.25A-11HFX, Advantage Engineering, Greenwood, IN) to keep the suspension below 35 °C. The procedure and the aforementioned processing parameters were selected based on Bhakay et al. (2013) and Bilgili and Afolabi (2012).

At pre-determined intervals, samples were taken at the outlet of the milling chamber for particle size analysis. The final suspensions (after 120 min milling) for all formulations were tested for apparent shear viscosity, zeta potential, and refrigerated at 8 °C for a period of 7 days. Particle size results obtained immediately after milling and after 7-day storage were compared for all suspensions to assess the short-term physical stability of the suspensions. In general, this study assumed the milled suspensions were intended to be dried shortly after milling, justifying the 7-day stability. On the other hand, particle sizes for GF suspension samples were also measured after 6-month storage at 8 °C to assess the long-term physical stability as GF suspensions exhibit severe aggregation in the absence of surfactants (Afolabi et al., 2014).

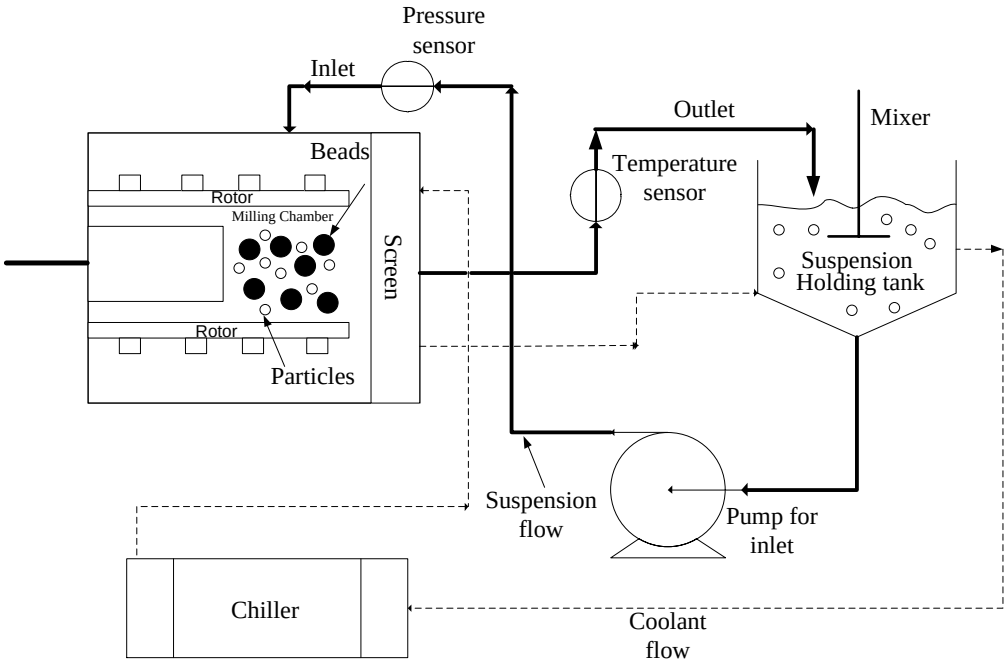

Figure 2.1 Schematic of a wet stirred media mill with recirculation mode of operation. Figure is not drawn to scale.

2.1.3 Particle Size Determination

Particle size distributions were measured using laser diffraction (LD) (LS 13 320, Coulter Beckman, Brea, CA, USA). A polarized intensity differential scattering (PIDS) obscuration water optical model was employed. The PIDS was maintained between 40% and 50% while the obscuration was maintained below 8% for all particle size measurements. Particle size distribution was computed by the equipment's software using the Mie scattering theory. Refractive index (RI) values are 1.68, 1.45, 1.65, 1.44, and 1.61, respectively, for AZD, FNB, GF, IBU, and PB particles, and 1.33 for the measurement medium (de-ionized water). Prior to the size measurement, ~2 ml samples of the milled suspensions were diluted with 8 ml solution of HPC or HPC–SDS depending on the stabilizer(s) used in the milling experiment. The refrigerated suspension samples after 7 days (all suspensions) and 6 months (GF only) of storage were mixed with the shear mixer running at 300 rpm for 5 min. Then, ~2 ml samples were taken and diluted for particle size measurement using the pertinent stabilizer solution.

2.1.4 Scanning Electron Microscopy

SEM imaging was used to examine the morphology of particles after milling and after 7-day storage and determine the primary particle sizes of various drugs. An aliquot of 1 ml drug suspension sample was diluted into 30 ml de-ionized water, vortex-mixed for 30 s and mounted on a silicon chip (Ted Pella, Inc., Redding, CA, USA), placed on top of carbon specimen holders, and dried in a desiccator. The

samples were then sputter coated with carbon and examined under a LEO 1530 SVMP (Carl Zeiss, Inc., Peabody, MA, USA).

2.1.5 Apparent Shear Viscosity of Stabilizer Solution and Milled Suspensions

The apparent shear viscosity of the milled suspensions and the stabilizer solutions was measured using an R/S Plus Rheometer (Brookfield Engineering, Middleboro, MA, USA) with a water jacket assembly Lauda Eco (Lauda-Brinkmann LP, Delran, NJ, USA). A coaxial cylinder (CC40) was used to provide a controlled shear rate on the samples from 0 to 1000 1/s for 60 s. The temperature of the jacket was kept constant at 25±0.5 °C. The raw data were analyzed using the Rheo 3000 software (Brookfield Engineering, Middleboro, MA, USA) of the equipment to obtain the apparent shear viscosity as a function of the shear rate.

2.1.6 Determination of the Polymer Adsorption on Milled Drug Particles

Polymer adsorption onto the drug particles was studied using a thermo-gravimetric technique. Fresh drug suspensions were prepared by wet stirred media milling under similar conditions to those described above, except for the milling time. The drugs were wet-milled for about 10 min, which yielded particles with Sauter mean diameter (D_{32}) values of 0.700±0.225 μm. Such colloidal sizes allowed for easier separation of the drug particles from the suspensions during the subsequent centrifugation step[22]. Each suspension was centrifuged (Sorvall RS-28S, DuPont Company, Wilmington, DE, USA) at 20,000 rpm for about 6 h. The polymer content in the supernatant solution was determined using a thermogravimetric analyzer (TGA): Mettler-Toledo

TGA/DSC1/SF, Stare system (Mettler Toledo, Inc., Columbus, OH, USA). A sample taken from the supernatant solution was heated to 200 °C under nitrogen at 10 °C/min to evaporate the water and determine the residual weight. The polymer concentration in the supernatant solution was determined using the initial weight and the residual weight. The amount of polymer adsorbed was back-calculated by subtracting the polymer concentration in the supernatant solution from the initial nominal polymer concentration in the suspension sample. Assuming sphericity of the drug particles, the external specific surface area (S) was calculated approximately from $S = 6/(\rho_p D_{32})$, where ρ_p is the true density of drug particles (i.e., AZD: 1.87 g/cm^3, FNB: 1.18 g/cm^3, GF: 1.45 g/cm^3, IBU: 1.12 g/cm^3, and PB: 1.54 g/cm^3), and D_{32} is the Sauter mean diameter of the milled particles, which was obtained from the LD measurement. The amount of polymer amount adsorbed divided by S was used to calculate the amount of polymer adsorbed per drug surface area.

2.1.7 Zeta Potential Measurement

The zeta potential of milled suspensions with and without SDS was measured using a zeta potential analyzer (Delsa Nano C, BeckmanCoulter, USA). The Delsa Nano C uses electrophoretic light scattering (ELS) for zeta potential determination; electrophoretic movement of charged particles was determined from the Doppler shift of scattered light under an applied electric field.

2.2 Results and Discussion

2.2.1 Apparent Breakage Kinetics

The time-wise variation of the 50% cumulative passing size or median size (d_{50}) and 90% cumulative passing size (d_{90}) is shown in Figure 2.2 for each of the five drugs wet-milled in the stirred media mill. While the apparent breakage kinetics of various drugs would be expected to be different due to their different mechanical and physico-chemical properties, Figure 2.2 illustrates some general trends that merit discussion first. Considering the relatively large micron-sized crystals initially present (at time t = 0 min), the data presented in Figure 2.2 suggest fast breakage of particles within the first 4 min for all drugs as the coarser particles were easier to break (Bilgili et al., 2004, 2006). In general, as milling continued, the apparent breakage rate decreased upon formation of smaller colloidal particles and nanoparticles, which can be explained by the difficulty to capture such small particles and their inherent high strength as compared to the coarser particles (Afolabi et al., 2014; Knieke et al., 2013). As a consequence, particle size approached or attained an equilibrium particle size. Another reason for the observed approach to such dynamic equilibrium is the competition between the particle breakage and aggregation (Bhakay et al., 2011; Bilgili et al., 2004; Sommer et al., 2006). The latter mechanism emerges to be significant as finer particles with large surface area and high surface energy were formed. Moreover, as the drug particle size decreased, particle number concentration in the suspension increased and the interparticle distance decreased, leading to more frequent collisions and potentially higher aggregation rate (Sommer et al., 2006). During prolonged milling of all drugs considered, the evolution of d_{50} and d_{90} in the

presence of SDS exhibited a monotonic decrease and approached a smaller plateau size compared to the absence of SDS. It must be noted that the presence of SDS shifts the dynamic equilibrium toward finer sizes through its positive impact on the prevention of aggregate formation. This effect was most pronounced for GF and FNB with relatively low solubility compared with the other drugs. Hence, the combined use of HPC and SDS appears to be beneficial in reducing the particle size during milling. However, the particle size of the suspensions may change during the storage, which will be explored below.

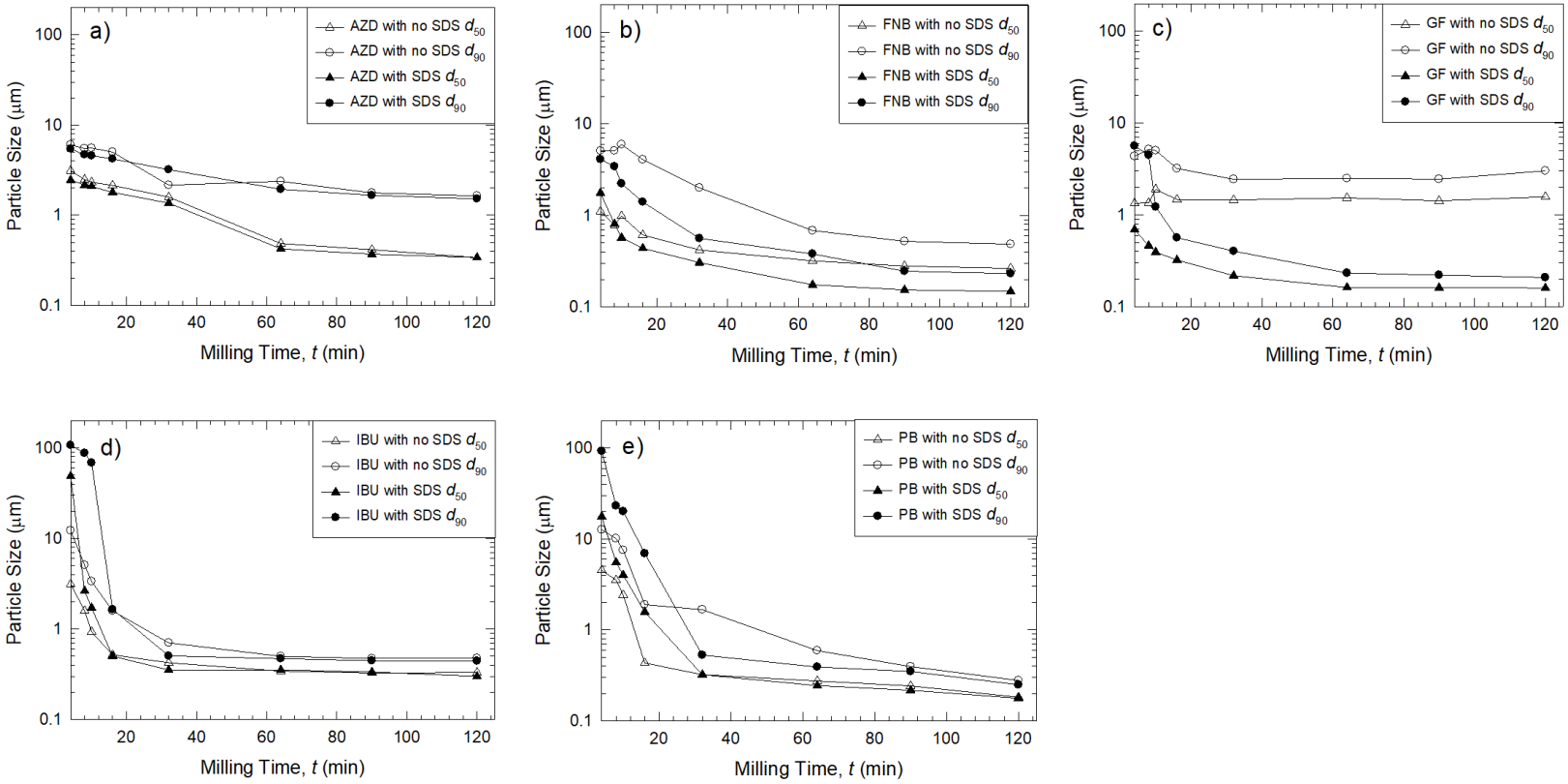

Figure 2.2 Temporal evolution of azodicarbonamide (AZD), fenofibrate (FNB), griseofulvin (GF), ibuprofen (IBU), and phenylbutazone (PB) particle sizes during wet media milling. All suspensions had 2.5% HPC with/without 0.5% SDS. The abscissa starts at t = 4 min for proper scaling of the curves. Initially, at t = 0 min, the AZD particles had d_{50} = 6.398 μm and d_{90} = 17.99 μm; the FNB particles had d_{50} = 17.32 μm and d_{90} = 40.88 μm; the GF particles had d_{50} = 27.74 μm and d_{90} = 58.00 μm; the IBU particles had d_{50} = 92.59 μm and d_{90} = 188.0 μm; and the PB particles had d_{50} = 71.82 μm and d_{90} = 445.5 μm.

2.2.2 Physical Stability of the Suspensions after Milling and Stabilization Mechanisms

The GF suspension with HPC as the sole stabilizer, reached an early median size plateau at 16 min (Figure 2.2 (c)). The final particle sizes (both d_{50} and d_{90}) for GF were greater than 1.3 µm (Table 2.2). Since the primary GF nanoparticles observed via SEM (Figure 2.3 (c)) had sizes in the range of 0.05–0.40 µm, the laser diffraction (LD) results suggest the significant extent of nanoparticle aggregation in the insufficiently stabilized GF suspension. Unlike the evolution of d_{50} and d_{90} in the absence of SDS, the evolution of both d_{50} and d_{90} exhibited a fast monotonic decrease in the presence of SDS and the particle size approached a plateau at about d_{50} = 0.160 µm and d_{90} = 0.208 µm. In view of the 0.05–0.25 µm primary particles produced (see Figure 2.3(d)) and the above information, the author can assert that the extent of aggregation in the 120 min milled suspension with SDS was low, and the breakage was the dominant mechanism, not the aggregation. This finding can be explained by the synergistic stabilizing action of HPC–SDS combination, as observed earlier by Bilgili and Afolabi (2012), where even 15% HPC alone was not able to stabilize a 10% GF suspension. In addition, Bhakay et al. (2011) reported that 0.1% SDS alone could not stabilize a 2% GF suspension either. However, a combination of HPC and SDS (2.5% HPC and 0.5% SDS) led to the narrowest particle size distribution and smallest d_{50} and d_{90} values of 10% GF suspension (Bilgili and Afolabi, 2012), which is due to synergistic effects of the HPC–SDS combination (Basa et al., 2008; Lee et al., 2008; Ryde and Ruddy, 2002). Similarly, HPC alone was not able to fully stabilize the FNB suspension. The apparent breakage rate of FNB was lower in the presence of HPC than in the presence of HPC–SDS (Figure 2.2(b) and Table 2.2)

because aggregation was still a significantly competing mechanism in the former case. For the FNB suspension milled with HPC–SDS, the sizes of the small primary nanoparticles shown in Figure 2.3(e) confirmed the LD size statistics in Table 2.2, which suggests that the HPC–SDS combination properly stabilized the milled FNB suspension.

Table 2.2 Effects of HPC and SDS on the Median Size (d_{50}) and 90% Passing Size (d_{90}) of Drug Suspensions after Milling and after 7-day Storage

Drug	With 2.5% HPC Only		With 2.5% HPC and 0.5% SDS	
	After Milling	After 7 Days	After Milling	After 7 Days
	d_{50}, d_{90} (μm)	d_{50}, d_{90} (μm)	d_{50}, d_{90} (μm)	d_{50}, d_{90} (μm)
AZD	0.339, 1.641	0.388, 1.909	0.340, 1.522	0.358, 1.682
FNB	0.264, 0.487	0.266, 0.472	0.148, 0.232	0.340, 1.190
GF	1.343, 2.183	1.546, 2.178	0.160, 0.208	0.164, 0.214
IBU	0.311, 0.477	0.346, 0.495	0.301, 0.445	0.386, 0.610
PB	0.182, 0.278	0.187, 0.305	0.177, 0.249	0.177, 0.253

AZD appears to have a relatively slow breakage after 4 min as shown in Figure 2.2(a). After 2 h milling, the d_{90} was still in the micron-range in the presence or absence of SDS. Unlike the case for GF and FNB with HPC, most of the coarse AZD particles were not aggregates of small primary nanoparticles; instead, they were large primary plate-like particles in the range of 0.80–2.40 μm as shown by the SEM images (Figure 2.3(a) and (b)). While the presence of SDS led to a smaller d_{90}, it did not eliminate the coarse micron-sized particles. These results imply that an AZD suspension with d_{90} less than 1 μm can only be produced if milling is carried out for more than 2 h and/or under more intense milling conditions.

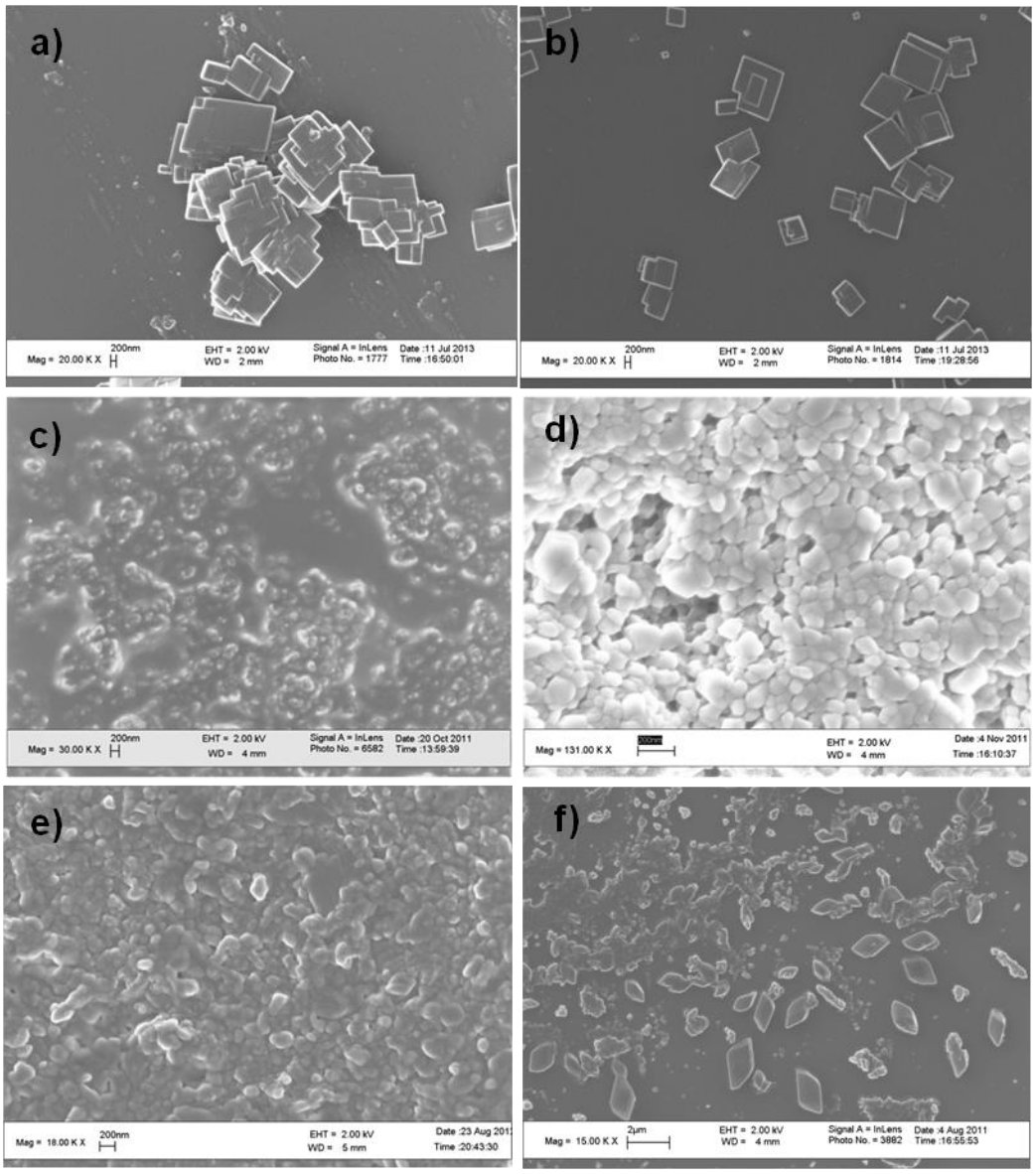

Figure 2.3 SEM images of drug particles: (a) the AZD particles milled for 120 min with HPC (marker size: 200 nm, 20k× magnification), (b) the AZD particles milled for 120 min with HPC–SDS (marker size: 200 nm, 20k× magnification), (c) the GF particles milled for 120 min with HPC (marker size: 200 nm, 30k× magnification), (d) the GF particles milled for 120 min with HPC–SDS (marker size: 200 nm, 131k× magnification), (e) the FNB particles milled for 120 min with HPC–SDS (marker size: 200 nm, 18k× magnification), (f) the milled FNB particles in the presence of HPC–SDS after 7-day storage at 8 °C (marker size: 2 μm, 15k× magnification).

Figure 2.2(d) and (e) show that the IBU and PB particles monotonically decreased in size and approached their equilibrium sizes, which were not significantly

affected by the presence of SDS, unlike the case for GF and FNB. Interestingly, the apparent breakage rate within the first 16 min of milling was lower in the presence of SDS, which is counterintuitive at first glance considering that SDS is an anionic surfactant which decreases surface tension, enhances wettability of hydrophobic drug particle surfaces, and minimizes aggregation through electrostatic forces (Kissa, 1999) (see Figure 1.1(b)). For IBU and PB, initially, micron-sized coarse particles present had a relatively low strength and a small surface area; hence, they were easier to break and stabilize; implying particle breakage mechanism to be the controlling mechanism during the first 16 min of milling. In view of this, the observed initial slower breakage of the drug particles in the presence of HPC–SDS vs. HPC alone can be explained by the higher viscosity of the HPC–SDS based drug suspension vs. HPC based drug suspension (see Figure 2.4). The higher the apparent shear viscosity of a suspension is, the higher the viscous dampening of the milling media or the beads, which leads to slower drug particle breakage (Bilgili and Afolabi, 2012). After the IBU and PB particles were broken into smaller particles following 16 min milling, the aggregation rate increased and the viscous dampening effect became weaker. In this regime, formulations with SDS exhibited higher apparent breakage rate. Interestingly, the higher viscosity and ensuing viscous dampening due to the use of SDS was not a significant factor for GF and FNB because particle aggregation was the controlling mechanism during milling, and the main effect of SDS was through stabilization. Despite the higher viscous dampening resulting from the use of HPC–SDS, the use of SDS in addition to HPC was generally beneficial due to the mitigation of the aggregation.

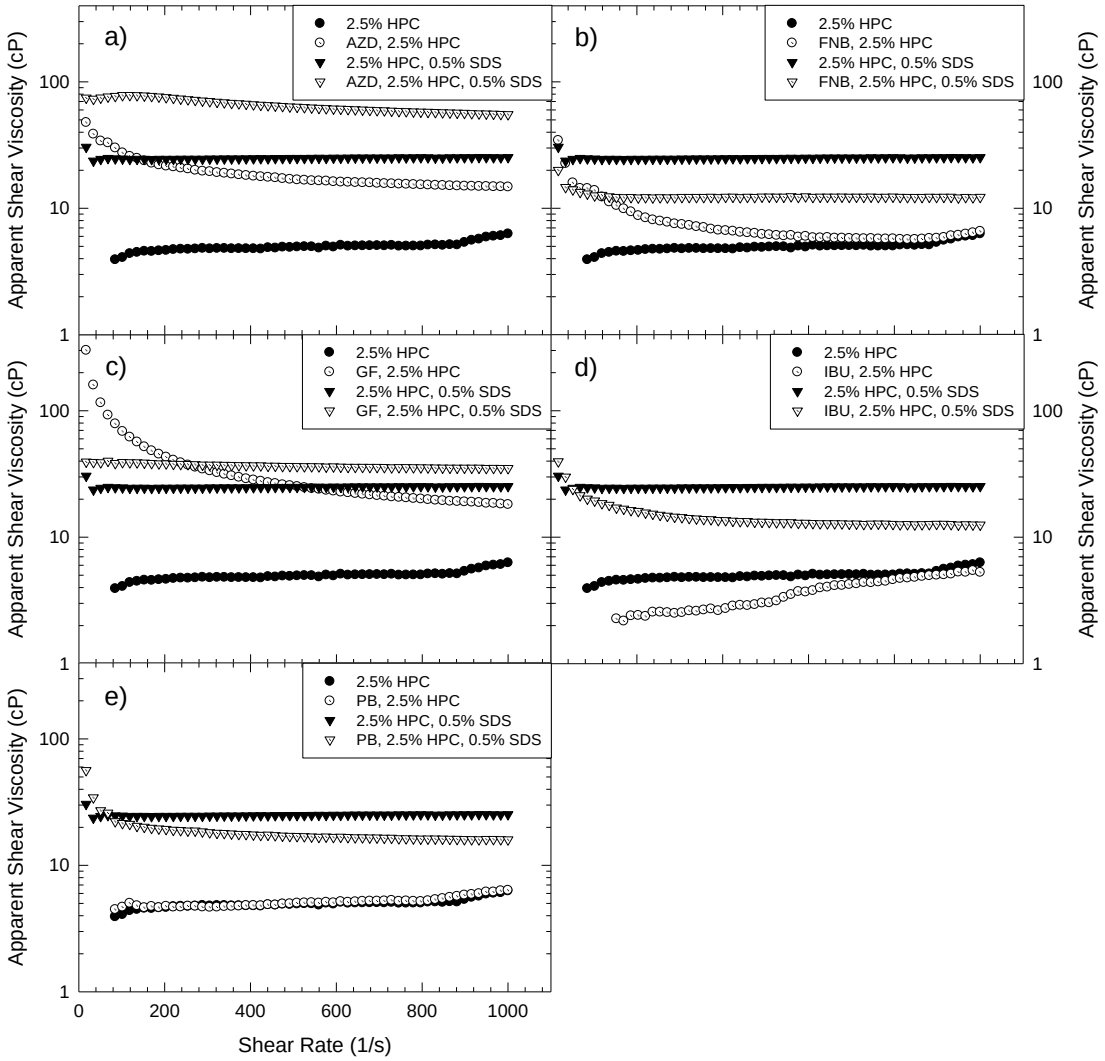

Figure 2.4 The apparent shear viscosity of 120 min milled drug suspensions in the presence of HPC alone and HPC–SDS: (a) AZD, (b) FNB, (c) GF, (d) IBU, and (e) PB.

2.2.3 Storage Stability of the Milled Suspensions

Milled drug suspensions were refrigerated at 8 °C for a period of 7 days to examine the aging effects. Note that all suspensions had 2.5% HPC as baseline stabilizer. All milled suspensions had smaller particles in the presence of SDS in addition to HPC (Table 2.2), which indicates that SDS helped to suppress the particle aggregation for

all drugs during the milling. After storage, the characteristic sizes of GF and PB suspensions with SDS remained unchanged within experimental accuracy, and AZD exhibited a slight increase in d_{90}. On the other hand, FNB and IBU suspensions with SDS exhibited significant size increase, whereas the suspensions of the same drugs without SDS (having HPC as the sole stabilizer) did not exhibit such a high size increase during the storage. While SDS helped to suppress aggregation of FNB and IBU particles during wet media milling, it unfortunately caused the growth of particles over 7 days, thus pointing to a need to optimize the SDS concentration.

The increase in particle size during storage can be attributed to two mechanisms: Brownian aggregation of the particles caused by insufficient stabilization and/or particle growth due to Ostwald ripening (Knieke et al., 2013; Verma et al., 2011). 2.5% HPC alone was not sufficient to stabilize FNB and GF suspensions via steric stabilization alone; hence, FNB and GF suspensions were already aggregated during the milling and interestingly GF showed no increase and FNB showed about 15% increase in the median size after 7-day storage (Table 2.2). The median size increase was less than 15% for all drugs in the absence of SDS. In the presence of 0.5% SDS, FNB and IBU showed a significant increase in both d_{50} and d_{90} after 7-day storage. The SEM image of FNB suspension after 7-day storage shows approximately 1×2 μm rhombohedral primary particles (Figure 2.3(f)) that did not exist in the milled suspension (Figure 2.3(e)). The presence of such rhombohedral crystals implies that the observed size increase was governed more by the Ostwald ripening than the aggregation. The water-solubility of FNB increases significantly with an increase in surfactant concentration especially above the critical micelle

concentration (CMC) of SDS, which in turn facilitates the ripening process (Ng et al., 1996). A similar effect with SDS was observed by Gosh et al. (2011) and Verma et al. (2011) for several drugs.

To mitigate Ostwald ripening and possible size increase during storage, while maintaining the positive effects imparted by combined HPC–SDS during the milling, the SDS concentration should be optimized. Knieke et al. (2013) constructed dynamic equilibrium curves to optimize surfactant concentration at constant HPMC loading with several SDS concentrations in a single milling experiment, and the particle sizes obtained after milling and after 7-day storage were compared to find the optimal SDS loading. In the current study, such a method was not used; but, an attempt was made to prove that optimization of the SDS concentration can mitigate the Ostwald ripening significantly. When 0.05% of SDS (below CMC), instead of 0.5% SDS (above CMC), was used in the presence of 2.5% HPC, FNB particles with d_{50} and d_{90} of 0.157 µm and 0.248 µm, respectively, were obtained after 120 min milling, and the d_{50} and d_{90} values were 0.171 µm and 0.342 µm, respectively, after 7-day storage. At 0.05% SDS, the positive impact of SDS on the suppression of particle aggregation was still maintained, while the negative impact via Ostwald ripening was significantly reduced, but not eliminated completely. Moreover, the FNB suspensions with HPC and 0.05% SDS had smaller sizes than those with HPC alone both after milling and after storage, again confirming the success of the HPC–SDS combination strategy. A similar reduction in SDS concentration could be applied to IBU case; however, this was not explored here because the beneficial effect of even 0.5% SDS was not pronounced for the milled IBU suspension as compared with the milled FNB

suspension, which can be inferred from the relatively small difference between particle sizes right after milling in the absence/presence of SDS (see Table 2.2). Additionally, the size increase during storage was much less pronounced for IBU than for FNB; hence, the benefit of using a smaller SDS concentration would be negligibly small. In a future study, the relative extent of Ostwald ripening could be investigated for different storage times and conditions, and SDS concentration could be optimized using the approach proposed by Knieke et al. (2013).

Since the milled suspensions are intended for immediate drying for eventual solid dosage manufacture, long-term stability of the suspensions was not a major focus of this work; it was studied only for one of the drugs, i.e., GF, which exhibited pronounced difference in the aggregation state depending on the presence/absence of SDS. When HPC was the sole stabilizer, not only did the GF particles aggregated extensively (refer to Table 2.2), but also they phase-segregated or settled after long-term storage due to the presence of coarse micron-sized aggregates (Figure 2.5(a) and (b)). The GF suspension with 2.5% HPC–0.5% SDS exhibited good long-term stability even without necessitating further formulation optimization. It did not show phase-segregation even after 6 months because all particles were colloidal and 90% of particles were smaller than ~300 nm (Figure 2.5(c) and (d)).

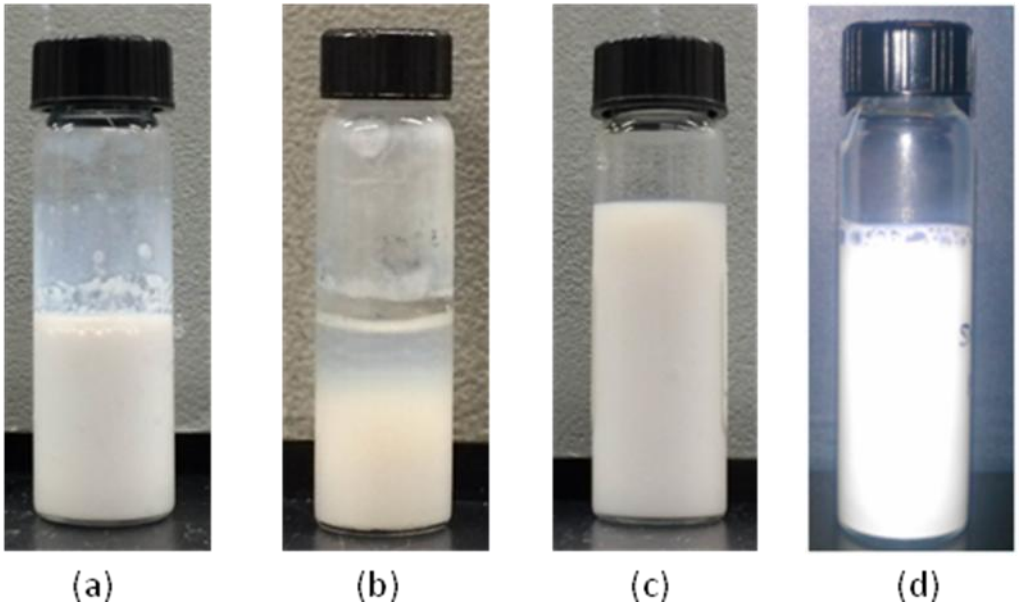

Figure 2.5 Images showing GF suspensions (a) after 120 milling in the presence of HPC alone (d_{50} = 1.343 µm and d_{90} = 2.183 µm), (b) after 6-month storage in the presence of HPC alone (d_{50} = 1.949 µm and d_{90} = 2.374 µm), (c) after 120 milling in the presence of HPC–SDS (d_{50} = 0.160 µm and d_{90} = 0.208 µm), (d) after 6-month storage in the presence of HPC–SDS (d_{50} = 0.186 µm and d_{90} = 0.301 µm).

2.2.4 HPC–SDS Synergistic Stabilization

The data presented in Table 2.2 have shown that the HPC–SDS combination gave finer milled particle sizes for five drugs as compared to the case with HPC alone as the sole stabilizer. Various researchers have pointed out the potential synergistic stabilization effects ensuing from the use of cellulosic polymers–anionic surfactant combinations (Basa et al., 2008; Bilgili and Afolabi, 2012; Knieke et al., 2013; Lee et al., 2008; Ryde and Ruddy, 2002). A manifestation of HPC–SDS interactions above the CMC of SDS is illustrated in Figure 2.4. The HPC–SDS solution had a much higher viscosity than the HPC solution, which can be attributed to the formation of HPC–SDS aggregates or micelle-like SDS clusters bound to the polymer (Berglund et al., 2003; Evertsson and Nilsson, 1997; Winnik and Winnik, 1990). It is expected that

such interactions could lead to enhanced electrosteric stabilization (see Figure 1.1(c)), i.e., the steric stabilization from the HPC and electrostatic repulsion from the negatively charged SDS.

To further elucidate the stabilization mechanisms, zeta potential and the extent of polymer adsorption on the drug nanoparticles were investigated. The value of the zeta potential indicates the strength of the electrostatic repulsive forces between particles at their surfaces, which is the basis for the physical stability imparted by the electrostatic mechanism besides the steric hindrance provided by the adsorbed polymer (Bilgili and Afolabi, 2012). For a physically stable nanosuspension stabilized by combined electrostatic and steric stabilization, a zeta potential value of ±20 mV may be sufficient (Müller et al., 2001). In general, the use of SDS led to higher (absolute) zeta potential in all drug nanosuspensions (Figure 2.6). The absolute values of the zeta potentials for FNB, GF, and PB in the presence of HPC–SDS were above 17 mV, which suggests a relatively stable suspension. However, the zeta potential of AZD suspension in the presence of HPC–SDS did not suggest a stable system even though the particle sizes from LD (Table 2.2) and SEM (Figure 2.3(b)) were very close. In addition, all suspensions had zeta potentials (absolute) less than 20 mV when HPC was used alone; yet, PB and IBU suspensions did not show significant aggregation. In fact, earlier work (Mishra et al., 2009) suggested that the adsorbed polymer layer can reduce the surface charge, and suspensions even with less than 20 mV (absolute) zeta potential could be stable via steric mechanism (Cerdeira et al., 2013a; Mishra et al., 2009). Thus, zeta potential alone may not adequately characterize the stability of all drug nanosuspensions stabilized with combined

stabilizers (Cerdeira et al., 2013a; Van Eerdenbrugh et al., 2009) and such results must be interpreted with caution (Cerdeira et al., 2013a).

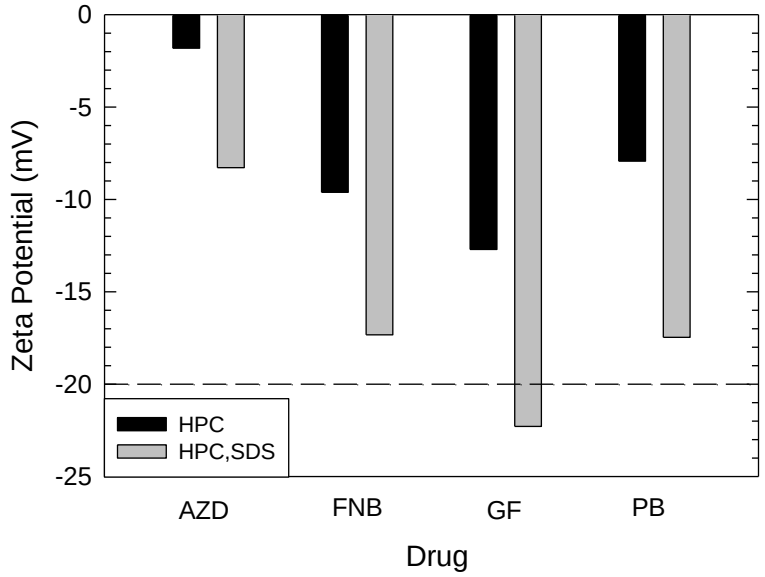

Figure 2.6 The zeta potential of drug suspensions after 120 min milling in the presence of HPC alone and HPC–SDS.

Polymer adsorption on drug particles in the absence–presence of SDS was explored following the same procedure of Bilgili and Afolabi (2012), where full adsorption isotherms for GF–HPC–SDS system suggested that the stabilizer adsorption was mainly due to HPC and, to a much smaller extent, by SDS at 0.5% concentration. In general, a thicker layer of the adsorbed polymer and strong adsorption are desirable for good steric stability (Bilgili and Afolabi, 2012; Knieke et al., 2013; Lee, 2003). Figure 2.7 shows that the amount of HPC adsorbed was much higher in the presence of SDS for all drugs potentially due to the co-adsorption of SDS with HPC and the facilitation of HPC adsorption by SDS (Bilgili and Afolabi, 2012; Cerdeira et al., 2010). The co-adsorbed layers can impart electrosteric stabilization to the GF particles (see Figure 1.1(c)); a sufficiently thick stabilizer layer

on drug particle surfaces provides a sufficiently high steric barrier to mitigate aggregation along with electrostatic charges (Knieke et al., 2013; Meng et al., 2012). Despite such possible advantages of higher amount of adsorption and associated lower d_{90} and improved stability for AZD, the AZD suspensions had d_{90} values greater than 1 µm because the coarse particles in the suspensions were mostly plate-like crystals (coarsely broken crystals), not solely aggregates of smaller primary particles. It should also be noted that while GF particles had higher amount of polymer adsorbed compared to other drugs (except AZD), its suspension was not stable in the absence of SDS whereas that of IBU with lower adsorption was relatively more stable. Hence, it appears that polymer adsorption alone does not predict the physical stability of all drugs with/without SDS. However, the presence of SDS led to both higher zeta potential and adsorption, which overall could explain the better physical stability of the milled suspensions with SDS. The storage stability, on the other hand, was affected by the Ostwald ripening, especially for FNB and IBU, thus necessitating the optimization of the SDS concentration.

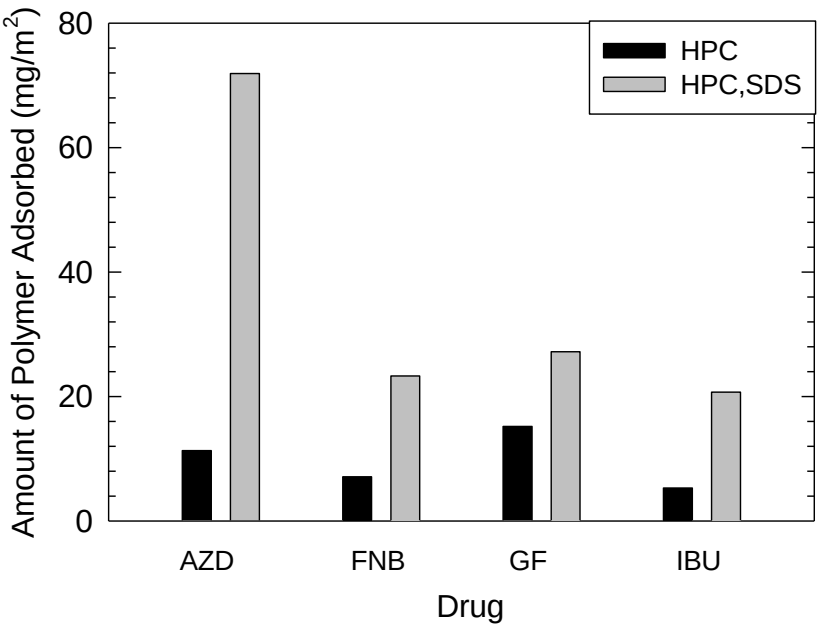

Figure 2.7 Amount of HPC adsorbed on milled drug particles in the absence and presence of SDS.

Finally, it is worth-mentioning a concern during milling, i.e., the formation of amorphous material from an initially crystalline drug. While such a concern needs further exploration and warrants in-depth study of crystallinity, the available literature suggests that wet milling does not significantly alter the crystallinity of most BCS Class II drugs including GF (Monteiro et al., 2013; Sievens-Figueroa et al., 2012), FNB (Sievens-Figueroa et al., 2012), IBU (Plakkot et al., 2011), naproxen (NPX) (Monteiro et al., 2013; Sievens-Figueroa et al., 2012), and indomethacin (IND) (Sharma et al., 2009). This is not surprising as water plays a major role in inhibiting the amorphization during wet milling of crystalline drugs (Sharma et al., 2009). Besides acting as a plasticizer, water present in the milling medium or suspension provides fast and effective cooling during particle breakage, which can minimize

formation of local hot spots on particle surfaces and thus reduce the extent of surface amorphization and oxidation (Monteiro et al., 2013).

2.2.5 On Correlations between Size Reduction/Physical Stability and Physico-Chemical Drug Properties

Mathematical correlations between measures of size reduction or drug suspension stability and physico-chemical drug properties, if exist, would benefit the formulators in developing drug nanoparticle formulations in a streamlined fashion. To quantitatively describe the extent of size reduction during milling, a size reduction ratio (*SRR*) (Bhakay et al., 2011; Verheezen et al., 2004) was defined for both d_{50} and d_{90}:

$$SRR_{50} = \frac{d_{50,\mathrm{ini}}}{d_{50,\mathrm{mil}}} \quad \text{and} \quad SRR_{90} = \frac{d_{90,\mathrm{ini}}}{d_{90,\mathrm{mil}}} \tag{2.1}$$

where the subscripts ini and mil refer to the initial (unmilled) drug particles and the final milled drug suspension, respectively. Similarly, a size growth ratio (*SGR*) was defined for both d_{50} and d_{90} in order to quantify the size increase during the 7-day storage:

$$SGR_{50} = \frac{d_{50,\mathrm{sto}}}{d_{50,\mathrm{mil}}} \quad \text{and} \quad SGR_{90} = \frac{d_{90,\mathrm{sto}}}{d_{90,\mathrm{mil}}} \tag{2.2}$$

In Eq. (2.2), the subscripts sto and mil refer to the 7-day stored suspension and the final milled drug suspension, respectively. Similar *SGR* definitions have been used to describe size enlargement during granulation (Sahoo, 2012). As opposed to more elaborate measures like agglomeration ratio (Knieke et al., 2015b), *SGR* defined in Eq. (2.2) was used due to its simplicity in describing size increase during the storage

of the milled suspensions. In general, a higher value of *SRR* suggests the greater extent of particle breakage, whereas the higher value of *SGR* suggests the greater extent of size increase during the storage and thus poorer physical stability. The *SRR* and *SGR* values for both d_{50} and d_{90} were calculated using the experimentally measured particle sizes of the drug suspensions with HPC as the sole stabilizer and the drug suspensions with HPC–SDS as the binary stabilizer system in two separate analyses. Then, an attempt was made to correlate the *SRR* and *SGR* with each one of the physico-chemical drug properties, i.e., molecular weight, melting point, log*P*, and solubility, via linear and nonlinear regression models in the comprehensive model library of SigmaPlot® (Version 11). In this study, a correlation is regarded as good if it has $R^2 > 0.95$ with statistical significance ($p < 0.05$ for both the model and each and every model parameter). In general, neither *SRR* nor *SGR* had good correlations with the physico-chemical drug properties when HPC was used as the sole stabilizer. There were only few good fits when HPC–SDS was used in the formulations (fits not shown). However, these few fits were so dependent upon one drug out of five (PB for *SRR* correlation with either molecular weight or log*P* and FNB for *SGR* correlation with either solubility or log*P*) that the removal of the respective drug from the fitting led to completely different and poor fits, signifying the low reliability of these correlations. Overall, our results from the statistical analysis appear to coincide with the findings from a more comprehensive study (Van Eerdenbrugh et al., 2009) using 13 stabilizers at 3 different concentrations to stabilize 9 drug compounds, which concluded that no correlation between physicochemical drug properties and stable nanosuspension formation exists.

The lack of any statistically significant and reliable correlation is mainly due to the complexity of the particle change mechanisms, i.e., particle breakage–aggregation–Ostwald ripening and the influence of multiple mechanical–physico-chemical properties of the drugs as well as the stabilizers during milling–storage. Empirically, one can use multiple non-linear regression, which requires a dense data set, to describe the effects of the multiple parameters. However, in this study, it was not even possible to fit a quadratic regression model with only two regressors due to the small number of drugs investigated. Another issue is that even if some statistically significant and reliable correlations were found, they would not imply causation. For example, the model fits of SRR to the physico-chemical drug properties alone cannot lead to correlations with causation because particle breakage is largely controlled by the mechanical properties including the strength parameters of the drug crystals, which are relatively hard to measure. Hence, elucidation of the impact of physico-chemical drug properties is elusive and warrants further investigation.

2.3 Conclusions

As a top-down approach, wet media milling has been investigated for the production of nanoparticles of five BCS Class II drugs to increase their total surface area, with the ultimate goal of increasing the dissolution rate and thus enhancing the bioavailability. The author assessed a recently suggested synergistic stabilization strategy with the use of a nonionic cellulosic polymer (HPC) and an anionic surfactant (SDS) to stabilize drug nanoparticles having different physico-chemical properties. Generally, using SDS, in addition to HPC, gave smaller particle sizes after

milling than in the absence of SDS, especially for GF and FNB. The combination of HPC and SDS led to the electrosteric stabilization of the drug nanosuspensions due to higher electrostatic repulsive forces (higher zeta potential) between the particles as well as enhanced steric hindrance from the adsorbed polymer, which was facilitated by the presence of SDS. However, after 7-day storage, FNB and IBU showed notable growth in the presence of SDS most likely due to Ostwald ripening. This negative effect was shown to be curtailed to a large extent by the use of smaller concentration of SDS for the FNB nanosuspension. In this study with five drugs, no correlation was found between the size reduction ratio for milling or the size growth ratio for storage stability and the physico-chemical drug properties.

Overall, this study suggests that the combination of nonionic cellulosic polymers and anionic surfactants generally provides physical stability for wet-milled drug suspensions provided that the surfactant concentration is optimized to mitigate the Ostwald ripening. Cellulosic polymers alone may still impart sufficient stability for some drug suspensions.

CHAPTER 3

A MICROHYDRODYNAMIC RATIONALE FOR SELECTION OF BEAD SIZE IN PREPARATION OF DRUG NANOSUSPENSIONS VIA WET STIRRED MEDIA MILLING

As has been indicated in Chapter 1, although wet stirred media milling has proven to be a robust process for producing nanoparticle suspensions of poorly water-soluble drugs and thereby enhancing their dissolution rate–bioavailability, selection of bead size, which is the most important design parameter in media milling, has been largely empirical, lacking any fundamental rationale. Chapter 3 aims to establish such rationale by investigating the impact of bead size at various stirrer speeds on the drug breakage kinetics via a microhydrodynamic model. A proper stabilizer formulation was selected based on Chapter 2 for the preparation of stable griseofulvin suspensions. The drug suspensions were milled at four different stirrer speeds (1000–4000 rpm) using various sizes (50–1500 μm) of the yttrium-stabilized zirconia beads. Laser diffraction, scanning electron microscopy (SEM), and X-ray powder diffraction (XRPD) were used for characterization. In order to elucidate the impact of bead size at different stirred speeds on characteristic process times, time-wise evolution of median particle size d_{50} and 90% passing cumulative particle size d_{90} in time was analyzed using piecewise cubic Hermite interpolation and an exponential model fit. The characteristic times reveal the existence of optimal bead sizes at different stirrer speeds. Then, the experimental observations were explained within the context of a microhydrodynamic model. Furthermore, the implications of our findings were indicated so as to develop a rationale for bead size selection in WSMM process and

offer an overarching explanation about the typical bead sizes used for all wet media milling processes with low–medium vs. high-energy levels.

3.1 Materials and Methods

3.1.1 Materials

EP/BP grade griseofulvin (GF) was purchased from Letco Medical (Decatur, AL, USA). GF is a BCS Class II drugs with an aqueous solubility of 8.9 μg/ml at 25 ˚C. Two stabilizers were used: a non-ionic cellulosic polymer, hydroxypropyl cellulose (HPC, SL grade, Nisso America Inc, New York, NY, USA) and an anionic surfactant, sodium dodecyl sulfate (SDS, 99% ACS reagent, Sigma Aldrich, Bellefonte, PA, USA). Zirmil Y grade yttrium-stabilized zirconia (YSZ) beads with *nominal* sizes of 50, 100, 200, 400, 800, and 1500 μm were purchased from Saint Gobain ZirPro (Mountainside, NJ, USA) as such media have been commonly used in many wet media milling studies (see Table 4.1) besides crosslinked polystyrene media. In this dissertation, the beads were labeled with their nominal sizes, while their actual median sizes are 54, 127, 215, 430, 798, and 1458 μm, respectively, as measured in dry dispersion mode via a laser diffraction particle size analyzer (Helos/Rodos, Sympatec, NJ, USA). The actual median sizes were used in the microhydrodynamic model. De-ionized water was used in all experiments.

Table 3.1 Recent Literature on Bead Sizes used in Pharmaceutical Wet Media Milling

References (Year)	Mill Type	Stirrer/ Circumference Speed (rpm)	Nominal Bead Size Investigated[a] (μm)	Optimal Bead Size[b] (μm)	Drug Particle Size Produced[d] (μm)
Konnerth *et al.* (2016)	Wet stirred media mill	2.9–6.4[c]	100–2,000	100	0.179[e]
Bitterlich *et al.* (2015)	Planetary ball mill	6.3[c]	100–500	500	~0.100[f]
Li *et al.* (2015)	Wet stirred media mill	11.7–14.7[c]	50–800	50	0.088[f]
Tuomela et al. (2015)	Planetary ball mill	600	5,000	5,000	0.550, 0.970[f]
Sarnes *et al.* (2014)	Planetary ball mill	1100	1,000	1,000	0.315[f]
Shah *et al.* (2014)	Wet media mill	400–1100	100 and 1,000	100	0.329[f]
Branham *et al.* (2012)	Planetary ball mill	200	15,000	15,000	0.355[g]
Ghosh *et al.* (2012)	Planetary ball mill	150	100–500	500	~0.600[f]
		400	100–500	100	~0.250[f]
Juhnke *et al.* (2012)	Wet stirred media mill	6–12[c]	100 and 200	100	~0.150[e]
Cerdeira *et al.* (2011)	Agitator media mill	2400–3600	400–800	400	~0.130[e]
Ghosh *et al.* (2011)	Wet stirred media mill	2500	100–500	200	0.230[f]
Niwa *et al.* (2011)	Oscillating beads-milling apparatus	2700	100–1,000	300	~0.250[e]
Singare *et al.* (2010)	Wet stirred media mill	2500–3400	200	200	0.211[i]
Ain-Ai and Gupta (2008)	Centrifugal ball mill	400	800	800	0.536[h]
Choi et al. (2008)	Ball mill	100	1,000	1,000	0.100[h]

[a]Bead made up of zirconium dioxide; [b]Bead size which led to the smallest final drug particle size or the only bead size chosen for the particular study; [c] m/s; [d]The smallest drug particle size produced using the optimal bead size; [e]d_{50}; [f] Z-average; [g]Sauter mean diameter; [h]Mean size; [i]d_{90}

3.1.2 Preparation of Suspensions via Wet Media Milling

The stabilizer types/concentrations and milling conditions were selected based on our recent investigations (Afolabi et al., 2014; Li et al., 2015b). First, about 225 g pre-suspensions were prepared by dispersing 10% drug particles in an aqueous solution of 2.5% HPC and 0.2% SDS under constant stirring at 300 rpm (Cat#. 14-503, Fisher Scientific, Pittsburgh, PA, USA) for a total of 90 min. Here, all percentages are w/w with respect to de-ionized water (200 g). The pre-suspensions were then milled for 256 min at the conditions presented in Table 3.2. A chiller (Model M1-.25A-11HFX, Advantage Engineering, Greenwood, IN, USA) provided cooling for both the milling chamber and the holding tank and kept the suspension temperature in the holding tank below 34 ^{o}C, as a maximum. The impact of bead size was studied at the stirrer speeds ω of 1000, 1600, 2800, and 4000 rpm. The highest speed was selected upon considering the maximum speed allowed by design, i.e., 4200 rpm. Speeds lower than 1000 rpm were not considered because they would cause extremely slow breakage and many practical processing issues (erratic flow, pressure build-up, etc.). Pre-suspensions were milled in a Microcer stirred media mill (Netzsch Fine Particle Size Technology, LLC, Exton, PA, USA) with a chamber volume V_m of 80 ml, lined with zirconia, and a zirconia shaft. The pre-suspension was added to the holding tank and recirculated between the holding tank and the milling chamber at a volumetric flow rate Q of 126 ml/min by a peristaltic pump (Cole-Parmer, Master Flex®, USA), based on previous work (Afolabi et al., 2014). Stainless steel screens with different opening sizes, which are approximately half of the nominal size of the beads, were used to keep the beads inside the milling chamber. The mass of beads was set constant in all

runs, i.e., 196 g, which corresponded to a fractional bead volume fraction *c* of 0.408 (40.8%) and was selected based on previous work (Afolabi et al., 2014). The Netzsch Microcer mill is limited to 50 µm beads in the recirculation mode by its design, which requires the use of a screen with an opening size of 25 µm. The bead sizes above 1500 µm are not desirable in this mill due to significant heat generation and inability to keep the temperature below 34 ^{o}C. In fact, even the use of 1500 µm beads at high speeds (2800 and 4000 rpm) caused excessive heat generation; hence, these runs were not considered in the analysis. Finally, 200 µm beads were used as the smallest beads at 1000 rpm and 100 µm beads at 1600 and 2800 rpm. Smaller beads than these resulted in clogging of the mill screen, erratic suspension flow, and sharp pressure rise at the indicated speeds, which all point to a practical processing limit; hence, these runs were not analyzed.

Suspension samples at several milling time points were collected from the outlet of milling chamber and used for particle size analysis. The sampling points were selected based on a geometric progression of 2 min (2^{s}, s = 0, 1, 2,...8). However, the author used additional time points (24 min, 48 min, and 96 min) so that there are sufficient data points available, without prolonging the total milling time, for reliable fitting and interpolation in the study of breakage kinetics. The final milled suspensions were stored in a refrigerator at 8 ^{o}C for 7 days and then their particle sizes were measured again to assess the physical stability.

The stirrer power per unit volume of the slurry (beads and drug suspension) in the milling chamber, shortly will be referred to as the stirrer power, i.e., $P_w = P/V_m$, was calculated as a time-averaged value. The stirrer power P was directly recorded

from the mill control panel. In the absence of the milling beads, the power input per unit volume of the suspension, i.e., ε_{ht}, was also measured at each stirrer speed. The specific energy consumption, i.e., $E^* = Pt_T/m_{sus}$, is the energy spent per unit mass of drug suspension, where t_T is the total milling time and m_{sus} is the total mass of the drug suspension. In all cases, the no-load power value obtained from a dry run of the mill rotor was subtracted from the power values used in the calculation of P_w, ε_{ht}, and E^*.

3.1.3 Particle Size Determination

Particle size distribution (PSD) of the GF suspensions at various milling times was determined by laser diffraction using LS 13-320 Beckman Coulter instrument (Brea, CA, USA). A refractive index of 1.65 and 1.33 was used for GF and water (measurement medium), respectively. In all measurements, the polarized intensity differential scattering (PIDS) was maintained between 40% and 50% while the obscuration was maintained below 8%. PSD was computed by the software using the Mie scattering theory. Prior to the size measurement, milled suspension samples (~ 2 ml) were diluted in a vial with 10 ml of HPC–SDS solution by using a vortex mixer (Fisher Scientific Digital vortex mixer, Model No: 945415, NH, USA), which rotates at 1500 rpm for 1 min. The particle size was measured four times (n = 4) and the average value was calculated together with the standard deviation (SD).

3.1.4 Scanning Electron Microscopy

Particle size and morphology of the as-received and milled drug particles were examined via SEM with a LEO 1530 SVMP (Carl Zeiss, Inc., Peabody, MA, USA). About 0.1 ml of the milled suspension was diluted with 30 ml de-ionized water, and a drop was placed on a silicon chip (Ted Pella, Inc., Redding, CA, USA), vacuum-dried, sputter coated, and observed in SEM.

3.1.5 X-ray Powder Diffraction

The crystallinity of the as-received drug, unmilled physical mixture of GF–HPC–SDS, and overnight dried, milled suspensions (Runs 4 and 14) was analyzed using XRPD (PANalytical, Westborough, MA, USA), provided with Cu K_α radiation (λ = 1.5406 Å). The samples were scanned for 2θ ranging from 5^o to 40^o at a scan rate of 0.165 s^{-1}.

3.1.6 Apparent Shear Viscosity of Milled Suspensions

The apparent shear viscosities μ_L of the milled suspensions were measured at 25 ± 0.5 ^{o}C using R/S plus Brookfield Rheometer (Brookfield Engineering, Middleboro, MA, USA) with a coaxial cylinder (CC40). The suspension was sheared from 0 to 1000 1/s in 60 s and the apparent shear viscosity at the maximum shear rate was taken (Bernhardt et al., 1999).

3.1.7 Density Measurement of Milled Suspensions

The density of the milled suspension was measured by weighing 25 ml of the milled

suspension. The weight of the suspension divided by its volume was used to calculate the suspension density.

Table 3.2 Operating Parameters Varied in the Wet Stirred Media Milling Experiments and Particle Size Statistics of the Suspensions after 256 min Milling and after 7-day Storage

Run No.[a]	Stirrer Speed, ω, Stirrer Tip Speed, u (rpm, m/s)	Bead Size, d_b (μm)	Particle Sizes After Milling (μm)			Particle Sizes After 7-Day Storage (μm)		
			d_{10} ± SD	d_{50} ± SD	d_{90} ± SD	d_{10} ± SD	d_{50} ± SD	d_{90} ± SD
1	1000, 3.67	200	0.122 ± 0.006	0.250 ± 0.005	0.456 ± 0.012	0.156 ± 0.008	0.276 ± 0.005	0.480 ± 0.004
2	1000, 3.67	400	0.100 ± 0.001	0.218 ± 0.003	0.405 ± 0.005	0.134 ± 0.008	0.232 ± 0.007	0.434 ± 0.006
3	1000, 3.67	800	0.161 ± 0.002	0.308 ± 0.006	0.607 ± 0.032	0.174 ± 0.005	0.325 ± 0.004	0.667 ± 0.033
4	1000, 3.67	1500	0.201 ± 0.007	0.422 ± 0.007	1.341 ± 0.016	0.210 ± 0.008	0.442 ± 0.009	1.373 ± 0.003
5	1600, 5.86	100	0.118 ± 0.000	0.160 ± 0.001	0.220 ± 0.001	0.117 ± 0.000	0.161 ± 0.000	0.227 ± 0.000
6	1600, 5.86	200	0.109 ± 0.000	0.160 ± 0.000	0.203 ± 0.001	0.124 ± 0.000	0.158 ± 0.001	0.208 ± 0.001
7	1600, 5.86	400	0.115 ± 0.001	0.161 ± 0.001	0.230 ± 0.001	0.112 ± 0.000	0.161 ± 0.000	0.234 ± 0.001
8	1600, 5.86	800	0.109 ± 0.000	0.171 ± 0.002	0.291 ± 0.010	0.093 ± 0.007	0.185 ± 0.001	0.332 ± 0.007
9	1600, 5.86	1500	0.144 ± 0.004	0.285 ± 0.002	0.537 ± 0.012	0.154 ± 0.007	0.293 ± 0.005	0.544 ± 0.004
10	2800, 10.3	100	0.093 ± 0.000	0.115 ± 0.000	0.143 ± 0.000	0.101 ± 0.000	0.125 ± 0.001	0.154 ± 0.001
11	2800, 10.3	200	0.119 ± 0.000	0.146 ± 0.001	0.178 ± 0.001	0.127 ± 0.002	0.157 ± 0.001	0.189 ± 0.001
12	2800, 10.3	400	0.129 ± 0.000	0.160 ± 0.001	0.199 ± 0.001	0.125 ± 0.001	0.159 ± 0.001	0.208 ± 0.001
13	2800, 10.3	800	0.110 ± 0.003	0.157 ± 0.001	0.232 ± 0.001	0.110 ± 0.000	0.160 ± 0.001	0.235 ± 0.000
14	4000, 14.7	50	0.095 ± 0.001	0.118 ± 0.001	0.145 ± 0.001	0.107 ± 0.001	0.129 ± 0.001	0.158 ± 0.001
15	4000, 14.7	100	0.097 ± 0.000	0.120 ± 0.001	0.146 ± 0.001	0.109 ± 0.001	0.135 ± 0.001	0.168 ± 0.001
16	4000, 14.7	200	0.107 ± 0.000	0.132 ± 0.001	0.162 ± 0.001	0.114 ± 0.000	0.141 ± 0.001	0.174 ± 0.001
17	4000, 14.7	400	0.124 ± 0.001	0.154 ± 0.001	0.195 ± 0.001	0.119 ± 0.002	0.153 ± 0.001	0.206 ± 0.002
18	4000, 14.7	800	0.109 ± 0.001	0.152 ± 0.001	0.223 ± 0.001	0.107 ± 0.000	0.151 ± 0.001	0.226 ± 0.000

[a]Drug (GF) loading of 10%, HPC/SDS concentration of 2.5%/0.2%, beads loading of c = 0.408, and suspension volumetric flow rate of Q = 126 ml/min were kept constant in all runs.

3.2 Theoretical

3.2.1 Analysis of Breakage Kinetics

Breakage kinetics during wet media milling can be studied by analyzing the time-wise evolution of the median particle size d_{50}, which usually decreases in time t and approaches a limiting value, provided that milling is continued for a prolonged time and particle aggregation is suppressed by a properly chosen stabilizer system (Bilgili et al., 2016a). The time-wise evolution of the median size can be described by a first-order exponential decay function as follows (Stražišar and Runovc, 1996; Varinot et al., 1999):

$$d_{50}(t) = d_{\lim} + \left[d_{50}(0) - d_{\lim}\right]\exp(-t/\tau_p) \tag{3.1}$$

where $d_{50}(0)$ and $d_{\lim}$ are the initial median size and the limiting median size, respectively, while τ_p is a characteristic time constant of the WSMM process. A lower τ_p value corresponds to faster breakage of the particles and a higher overall apparent breakage rate, which will be referred as the breakage rate in the rest of the dissertation for brevity. For the estimation of $d_{\lim}$ and τ_p, Eq. (3.1) was fitted to the measured d_{50} data via the Marquardt-Levenberg algorithm. Our preliminary analysis indicated that large particles with a d_{50} = 16.08 ± 0.05 μm broke faster initially (within the first minute) than the particles produced after one minute. Therefore, Eq. (3.1) with a single time constant τ_p was not able to fit the whole experimental data governed by two or potentially more characteristic time constants (Cho et al., 1996). Hence, the initial median particle size at 0 min was discarded, thus making the first-minute median size the initial size for better fitting capability. This approach was justifiably

adopted from earlier studies (Bilgili and Afolabi, 2012; Stražišar and Runovc, 1996; Varinot et al., 1999).

3.2.2 Microhydrodynamic Analysis

The dynamics of the inter-particle collisions in a dense slurry flow is referred to as microhydrodynamics. Eskin et al. (2005a, b) developed a model to calculate the mean velocity of bead oscillations in well-mixed slurries using the kinetic theory of granular flows and fundamental granular energy balance (Gidaspow, 1994). Salient features of this microhydrodynamic model with slight modification (Afolabi et al., 2014) in view of Eskin and Miller (2008) are presented here, and readers are referred to aforementioned literature for the assumptions and derivations. The power applied per unit volume of slurry P_{w} inside a stirred mill dissipates through several mechanisms, which are mathematically expressed as follows:

$$P_{\mathrm{w}} = \varepsilon_{\mathrm{visc}} + \varepsilon_{\mathrm{coll}} + \varepsilon_{\mathrm{ht}} \tag{3.2}$$

$$P_{\mathrm{w}} = \frac{54\mu_{\mathrm{L}} c\theta R_{\mathrm{diss}}}{{d_{\mathrm{b}}}^2} + \frac{12}{d_{\mathrm{b}}\sqrt{\pi}}\left(1-k^2\right)\left[\frac{1-0.5c}{(1-c)^3}\right]c^2\rho_{\mathrm{b}}\theta^{3/2} + \varepsilon_{\mathrm{ht}} \tag{3.3}$$

where $\varepsilon_{\mathrm{visc}}$ is the energy dissipation rate due to both the liquid–beads viscous friction and lubrication, $\varepsilon_{\mathrm{coll}}$ is the energy dissipation rate due to partially inelastic bead–bead collisions, and ε_{ht} is the power spent on shearing the equivalent liquid (milled drug suspension). In Eq. (3.3), μ_{L} is the apparent shear viscosity of the equivalent liquid, c is the bead volumetric concentration (volume fraction), θ is the granular temperature defined as the bead–equivalent liquid relative mean-square velocity, R_{diss} is the effective drag (dissipation) coefficient, d_{b} is the median size of the beads, k is the

restitution coefficient for the bead–bead collisions (0.76 from Tatsumi et al. (2009)), and ρ_b is the density of the zirconia beads (6000 kg/m^3).

The equivalent liquid properties μ_L and ρ_L as well as the power applied per unit volume in the presence of the beads P_w were measured. The energy dissipation rate for shearing the equivalent liquid ε_{ht} was found to be negligibly small (much smaller than P_w) due to the low viscosity of the suspensions. MATLAB's fsolve function was used to solve Eq. (3.3) for the granular temperature θ using P_w measured and R_{diss} values calculated (refer to Eqs. (A.1)–(A.5) in *Appendix A*). From the calculated θ, the frequency of single-bead oscillations ν and the average oscillation velocity of the beads u_b were determined as follows:

$$\nu = \frac{24c}{d_b}\left[\frac{1-0.5c}{(1-c)^3}\right]\sqrt{\frac{\theta}{\pi}} \tag{3.4}$$

$$u_b = \sqrt{\frac{8\theta}{\pi}} \tag{3.5}$$

Eskin et al. (2005a) advanced the microhydrodynamic model (Eskin et al., 2005b) by considering the elastic contact deformation of the beads along with the elastic–perfectly plastic deformation of the particles caught between the beads. While the beads frequently collide due to their fluctuating motions in a slurry, which are characterized by θ, u_b, and ν, the beads capture and compress the drug particles to be milled. The maximum contact pressure at the center of the contact circle σ_b^{max} of the two colliding beads is given by

$$\sigma_b^{max} = \frac{3}{2}\frac{F_b^n}{\pi\alpha_b^2} \tag{3.6}$$

where F_b^n and α_b are the average maximum normal force during the collision of two

elastic beads and the radius of the contact circle formed at the contact of two beads respectively (refer to Eqs. (A.6) and (A.7), respectively). The average frequency of drug particle compressions *a* equals the product of probability *p* of a single particle caught between beads (refer to Eq. (A.8)) and the frequency of single-bead oscillations ν as follows:

$$a = p\nu \tag{3.7}$$

It must be noted that only a small fraction of energy consumption is actually used for deforming the drug particles, which is explained by the energy dissipation rate resulting from the deformation of the particles per unit volume Π and expressed as (Eskin et al., 2005a):

$$\Pi = 2.23\frac{c^2(2-c)}{(1-c)^3}\frac{1}{\pi^{5/2}\varepsilon\sigma_y}\left(\frac{Y_b}{1-\eta_b^2}\right)^{18/15}\left(\frac{Y^*}{Y_p}\right)^{\gamma}\rho_b{}^{4/5}\frac{R_p}{R_b^2}\theta^{13/10} \tag{3.8}$$

where ε, Y^*, Y_p, η_b, σ_y, R_p, and R_b are the volume fraction of the drug particles in the suspension, reduced elastic modulus of the bead–drug particle contact, elastic modulus of the drug particles, Poisson's ratio of the beads, contact pressure in a drug particle captured when the fully plastic condition is reached, radius of the drug particle, and radius of the bead, respectively. To calculate Π, the mechanical properties of the drug particles (Y_p, η_p, σ_y) have to be known, and only scant information for drugs is available in the literature and they are also difficult to measure. Since the objective here is to rationalize the selection of bead size, the author decomposed Π multiplicatively into a material-dependent factor λ and a milling intensity factor *F*, similar to Afolabi et al. (2014), as follows:

$$\lambda = 2.23\frac{\rho_{\mathrm{b}}^{4/5} R_p}{\pi^{5/2}\sigma_{\mathrm{y}}}\left(\frac{Y_{\mathrm{b}}}{1-\eta_{\mathrm{b}}^2}\right)^{18/15}\left(\frac{Y^*}{Y_{\mathrm{p}}}\right)^{\gamma} \tag{3.9}$$

$$F = \frac{c^2(2-c)}{(1-c)^3}\frac{1}{\varepsilon R_{\mathrm{b}}^2}\theta^{13/10} \tag{3.10}$$

3.3 Results and Discussion

3.3.1 Effects of Wet Media Milling on the Drug Particle Size and Morphology

Two concerns during WSMM of BCS Class II drugs are physical instability of the milled drug suspensions and possible solid-state changes (Kesisoglou et al., 2007; Kumar and Burgess, 2014). To this end, Runs 4 and 14 suspensions were selected for SEM imaging and XRPD diffractograms because they led to the coarsest (slowest, least intense breakage) and finest (fastest, most intense breakage) drug particles after 256 min milling, respectively, among all different stirrer speed–bead size combinations (see Table 3.2). Figure 3.1 shows the SEM images of GF particles before and after 256 min milling. The SEM images show that as-received, coarse GF particles (Figure 3.1a) were broken into primary particles in the range of 0.20–2.00 μm for Run 4 (Figure 3.1b) and in the range of 0.05–0.20 μm for Run 14 (Figure 3.1c), which qualitatively agree with the particle sizes obtained from laser diffraction (Table 3.2). Results from laser diffraction and SEM images suggest that the drug suspension even with the smallest nanoparticles (Run 14) did not exhibit severe aggregation at the time scale of the milling process, and the electrosteric stabilization mechanism imparted by the HPC–SDS combination (Bilgili and Afolabi, 2012; Bilgili et al., 2016d) was effective. Hence, the presence of coarser primary particles in

Run 4 suspension can be attributed to the slower breakage in Run 4, which will be further elucidated.

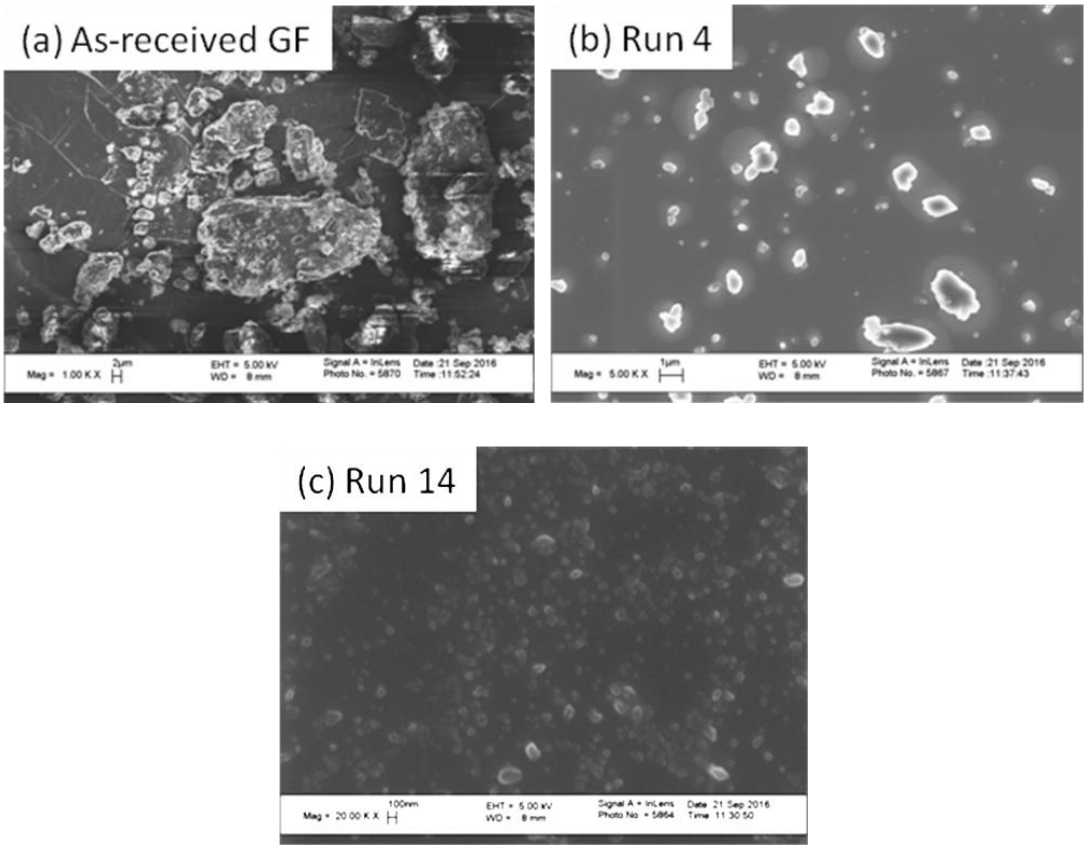

Figure 3.1. SEM images showing GF particle size and morphology: (a) before milling and after 256 min milling at (b) ω = 1000 rpm with d_b = 1500 μm beads (Run 4) and (c) 4000 rpm with d_b = 50 μm beads (Run 14). Before milling, the GF particles had d_{50} = 16.08 ± 0.05 μm and d_{90} = 35.47 ± 0.55 μm.

Short-term physical stability of the suspensions was studied for a storage period of 7 days at 8 °C (Table 3.2). The suspensions were physically stable and remained colloidal owing to the synergistic stabilizing action of the HPC–SDS combination. The slight size increase observed in most samples could have resulted from the temperature cycle during the sample preparation following the milling process, i.e., initial cooling to 8 °C and equilibration to room temperature after 7-day

storage, and associated particle aggregation. These observations are in line with our recent work (Bilgili et al., 2016d; Li et al., 2016b), where nanoparticles of GF and other poorly water-soluble drugs such as azodicarbonamide, phenylbutazone, and indomethacin were adequately stabilized by HPC–SDS. Long-term physical stability of the suspensions was not investigated in the present study. Reproducibility was established by repeating Run 4 (the slowest, least intense breakage among all runs) and Run 14 (fastest, most intense breakage among all runs), which essentially captures the full range of breakage dynamics observed in all milling experiments. For both runs, the time-wise evolution of PSD was almost identical in the repeated runs, with slight deviations within experimental accuracy of the size measurements (see Figure B2 in *Appendix B*). Hence, the milling process is considered reproducible, which is in line with some previous investigations on WSMM (see Li et al., (2016a), and the references cited therein).

Another potential concern with wet media milling is potential solid-state changes to the drugs. Figure 3.2 presents the XRPD diffractograms of as-received GF, unmilled physical mixture of GF–HPC–SDS, as well as 256 min milled GF suspensions (Runs 4 and 14) after overnight drying. The characteristic peaks of GF appeared in all diffractograms without a broad halo after milling, despite the contribution of amorphous HPC in the samples. As compared to the as-received GF pattern, a slight reduction in the GF peak intensities in the unmilled physical mixture is observed due to dilution and surface coverage of GF particles by HPC (Hecq et al., 2005). On comparing Runs 4 and 14 patterns with the unmilled physical mixture, it is noted that the peak positions remained the same despite a slight reduction in peak

heights after milling, which can be attributed to defect formation–accumulation during milling (Monteiro et al., 2013) besides more effective coverage of GF particles by HPC in dried Runs 4 and 14 samples than that in the physical mixture. While XRPD cannot detect minor amount of amorphous phase due to indirect inference and crystal orientation effects, the aforementioned XRPD results overall suffice to show that the crystalline state of GF was largely preserved after 256 min milling.

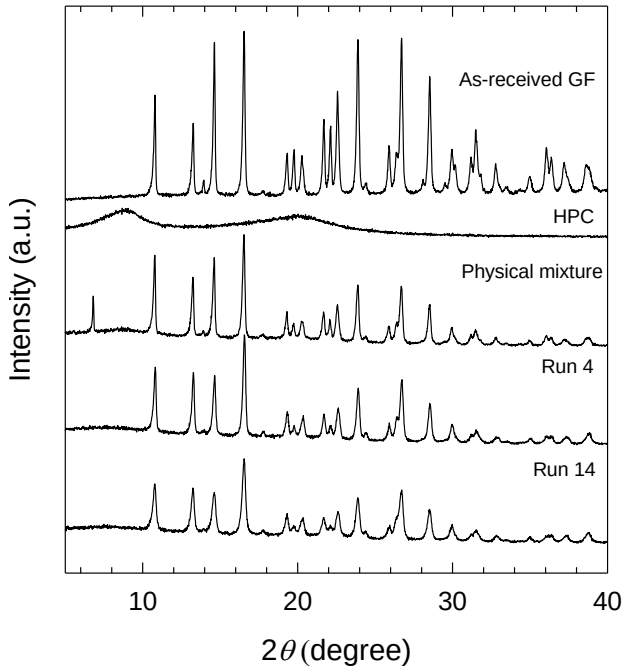

Figure 3.2 XRPD diffractograms of as-received GF, HPC, unmilled physical mixture of GF–HPC–SDS, and dried, milled suspensions of Runs 4 and 14. Run 4 refers to the drug suspension milled at ω = 1000 rpm with d_b = 1500 μm beads and Run 14 refers to the drug suspension milled at ω = 4000 rpm with d_b = 50 μm beads.

3.3.2 Effects of Bead Size at different Stirrer Speeds

A comprehensive investigation of the impact of bead size at various energetic conditions, i.e., different specific energy consumptions, was conducted by milling the

as-received GF particles using 50, 100, 200, 400, 800, and 1500 μm zirconia beads at a range of stirrer speeds from 1000 rpm to 4000 rpm. While Table 3.2 presents the particle size statistics of the suspensions after 256 min milling and 7-day storage only, Figure. B1 (*Appendix B*) illustrates the time-wise evolution of cumulative PSD during the wet stirred media milling in all 18 runs.

Temporal evolution of the median size d_{50} and 90% passing size d_{90} of the GF particles during the wet media milling was first analyzed to identify "general trends" (see Figure 3.3). In most runs, the characteristic particle sizes decreased monotonically in time and approached or tended to approach a limiting/plateau size, known as apparent grinding limit (Knieke et al., 2013; Knieke et al., 2009), except for 1000 rpm for which breakage was too slow, hence, it must be prolonged significantly to approach such plateau size. For a given bead size, an increase in stirrer speed led to faster breakage and smaller final milled particle sizes (see also Table 3.2); however, this effect got saturated at higher speeds and was less notable for 100 μm beads. The monotonic decrease of the drug particle size again suggests that particle breakage was the dominant mechanism. While Bhakay et al. (2011) noted severe aggregation and drastic increase in d_{50} of GF particles stabilized with HPMC (hydroxypropyl methylcellulose) alone, the author did not see such behavior here because aggregation of the particles was largely suppressed due to the synergistic action of HPC–SDS combination, as discussed in *Section 3.3.1*. Finally, a delay in the reduction of d_{90} along with some fluctuation/increase was noted for Runs 1 and 5 with the smallest beads used at 1000 rpm and 1600 rpm, respectively. For these runs only, coarse GF

particles were difficult to capture/break between the smallest beads used, leading to slower GF breakage initially and slightly irregular flow at the outlet of the mill.

In order to analyze the impact of bead size at different stirrer speeds on the apparent, overall breakage rate, shortly referred to as the breakage rate in the rest of this dissertation, various quantitative measures were used. A characteristic time constant τ_p, which considers all data points for each milling run, was obtained by fitting Eq. (3.1) to the evolution of the GF median size in Figure 3.3. The drug breakage rate can be calculated by $1/\tau_p$ (not reported). Most R^2 values from the fits were greater than 0.95 (all above 0.87), and the parameters were all statistically significant with p-value < 0.05 (details in Table B1 of Supplementary Material). Moreover, motivated by earlier work (Afolabi et al., 2014), two practical characteristic time constants were introduced: the milling time required to attain a median drug particle size d_{50} of 0.5 μm, t_{d50} and the milling time required to attain a 90% passing size d_{90} of 1 μm, t_{d90}. These measures mathematically represent the particle sizes of a nanosuspension with the majority of particles less than 1 μm, which is required for effective improvement of drug dissolution rate (Kumar et al., 2014; Muller and Keck, 2004). A piecewise cubic Hermite interpolating polynomials (MATLAB's pchip function) was used to calculate both t_{d50} and t_{d90}.

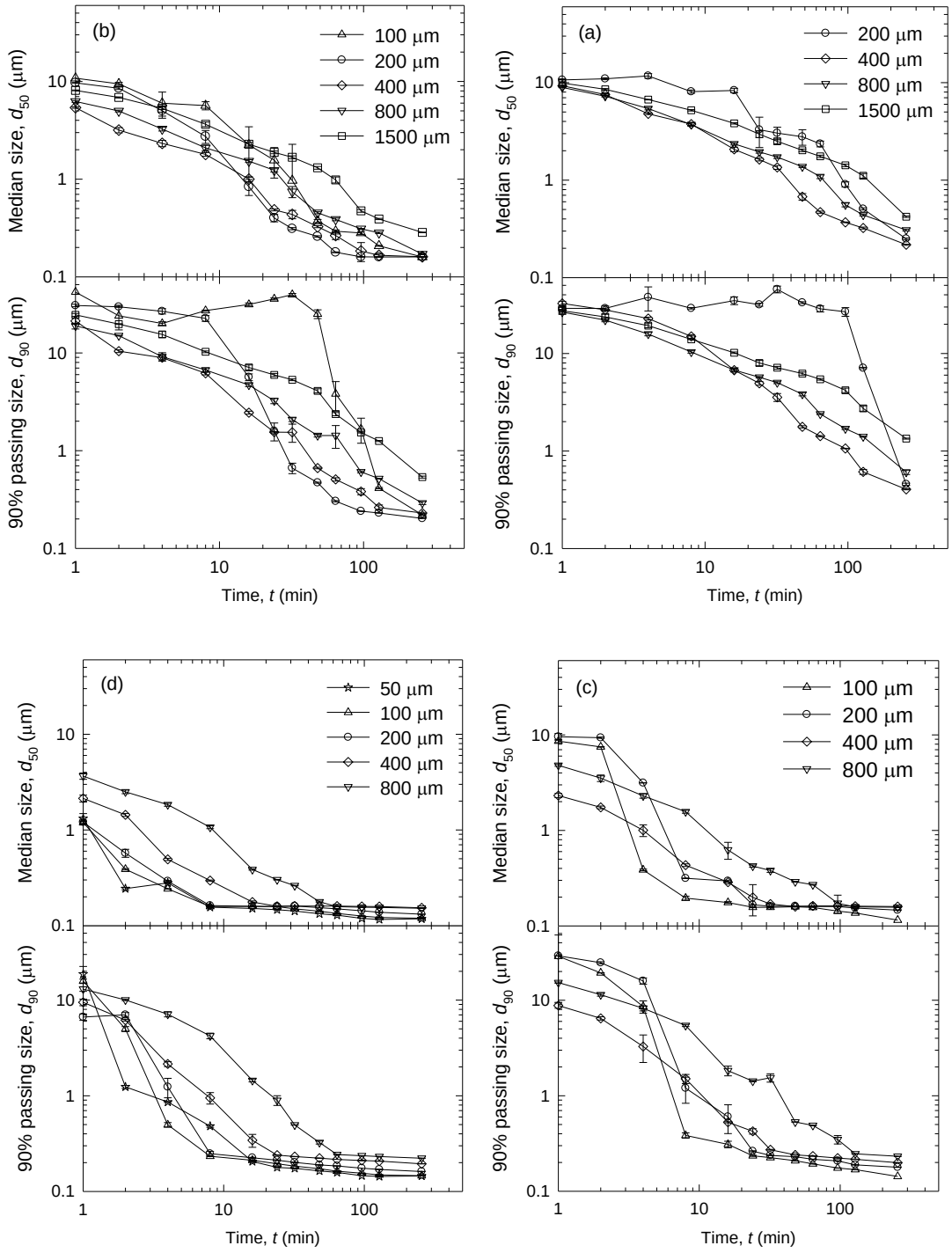

Figure 3.3 Effects of bead size d_b on the temporal evolution of GF particle sizes during wet stirred media milling at various stirrer speeds: (a) ω = 1000 rpm, (b) ω = 1600 rpm, (c) ω = 2800 rpm, and (d) ω = 4000 rpm. At t = 0 min, the GF particles had d_{50} = 16.08 ± 0.05 μm and d_{90} = 35.47 ± 0.55 μm.

Figure 3.4 presents all calculated characteristics time constants t_{d50}, t_{d90}, and τ_p for various bead sizes at different stirrer speeds. A quick comparison of all data presented in Figures 3.4a,b,c, and d reveals that they all decreased upon an increase in stirred speed, suggesting enhanced breakage kinetics at higher stirrer speeds observed by many researchers (e.g., (Afolabi et al., 2014; Hennart et al., 2010; Singh et al., 2011)), which gives credence to the use of these measures for the assessment of the impact of bead sizes as well. Moreover, all three characteristic time constants t_{d50}, t_{d90}, and τ_p exhibited clear minima (highest breakage rate) for the same bead size: 400 µm beads at 1000 rpm (Figure 3.4a). The use of either smaller or larger beads than 400 µm caused slower breakage (higher values of t_{d50}, t_{d90}, and τ_p). When 1500 µm beads were used at 1000 rpm, d_{90} = 1 µm was not even attained during 256 min milling (hence, t_{d90} not shown in Figure 3.4a). Similarly, Figure 3.4b indicates 200 µm beads being the optimal bead size at 1600 rpm. Hence, an interesting phenomenon emerges: an increase in stirrer speed shifted the optimal bead size to a smaller value. This trend continued when the stirrer speed was further increased to 2800 rpm and 4000 rpm for which 100 µm and 50 µm beads exhibited the lowest t_{d50}, t_{d90}, and τ_p (Figures 3.4c and d). However, at these higher speeds, t_{d50}, t_{d90}, and τ_p tended to decrease monotonically with a decrease in bead size; the minima occurred at the lower boundary of the experimentally feasible bead size domain unlike the clear minima that occurred within the bead size domain at 1000 rpm and 1600 rpm. It must also be noted that at 2800 and 4000 rpm, 100 µm and 50 µm were the smallest feasible sizes of the beads, respectively, due to the practical processing issues (*Section 3.2.1*) and the restriction imposed by the current mill design. Thus, they were regarded as the

practically attainable optimal size, leading to the fastest drug breakage at the corresponding speeds.

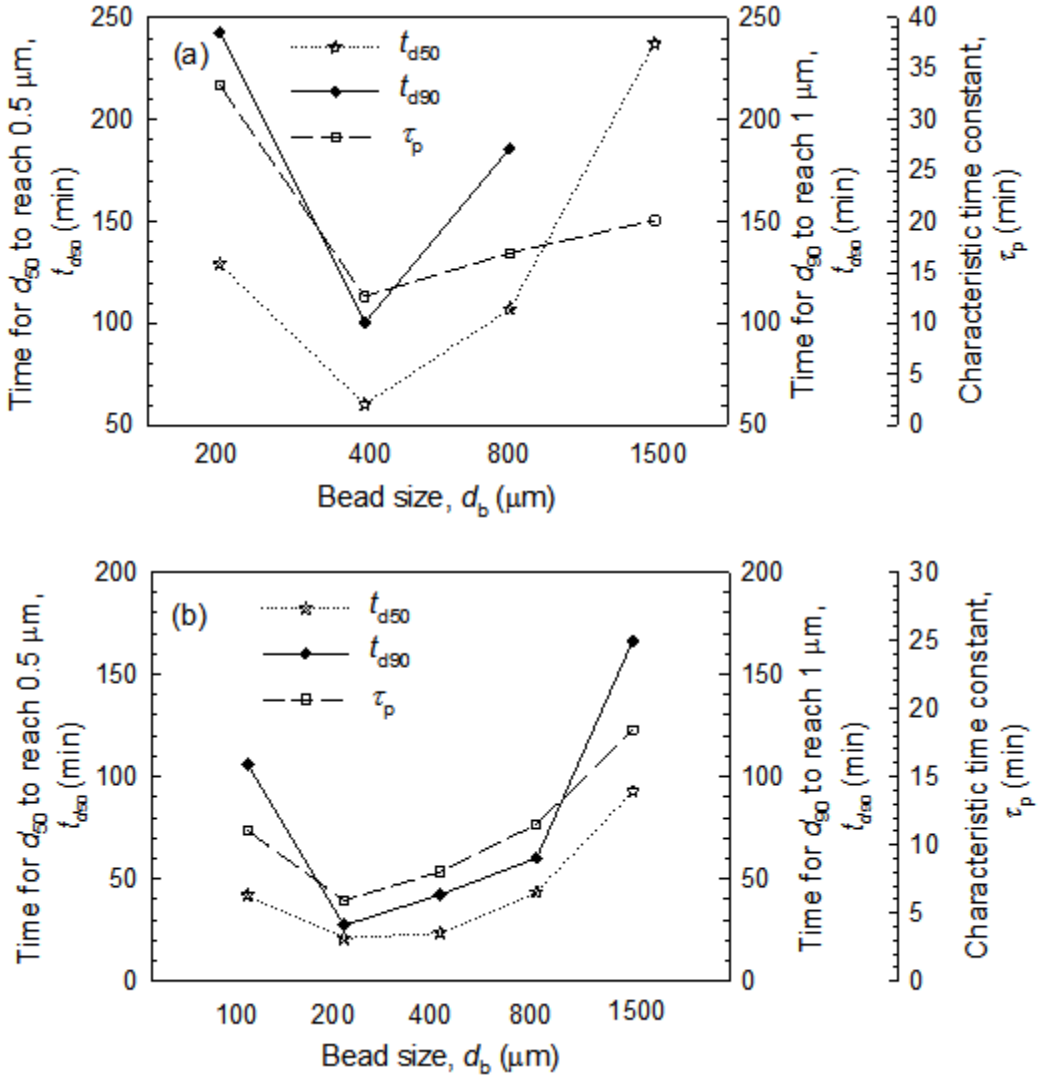

Figure 3.4 Effects of bead size d_b on the characteristic milling times t_{d50}, t_{d90}, and τ_p at various stirrer speeds: (a) ω = 1000 rpm, (b) ω = 1600 rpm, (c) ω = 2800 rpm, and (d) ω = 4000 rpm. Note that d_{90} = 1 µm was not reached during 256 min milling when 1500 µm beads were used at ω = 1000 rpm (Run 4). (Continued)

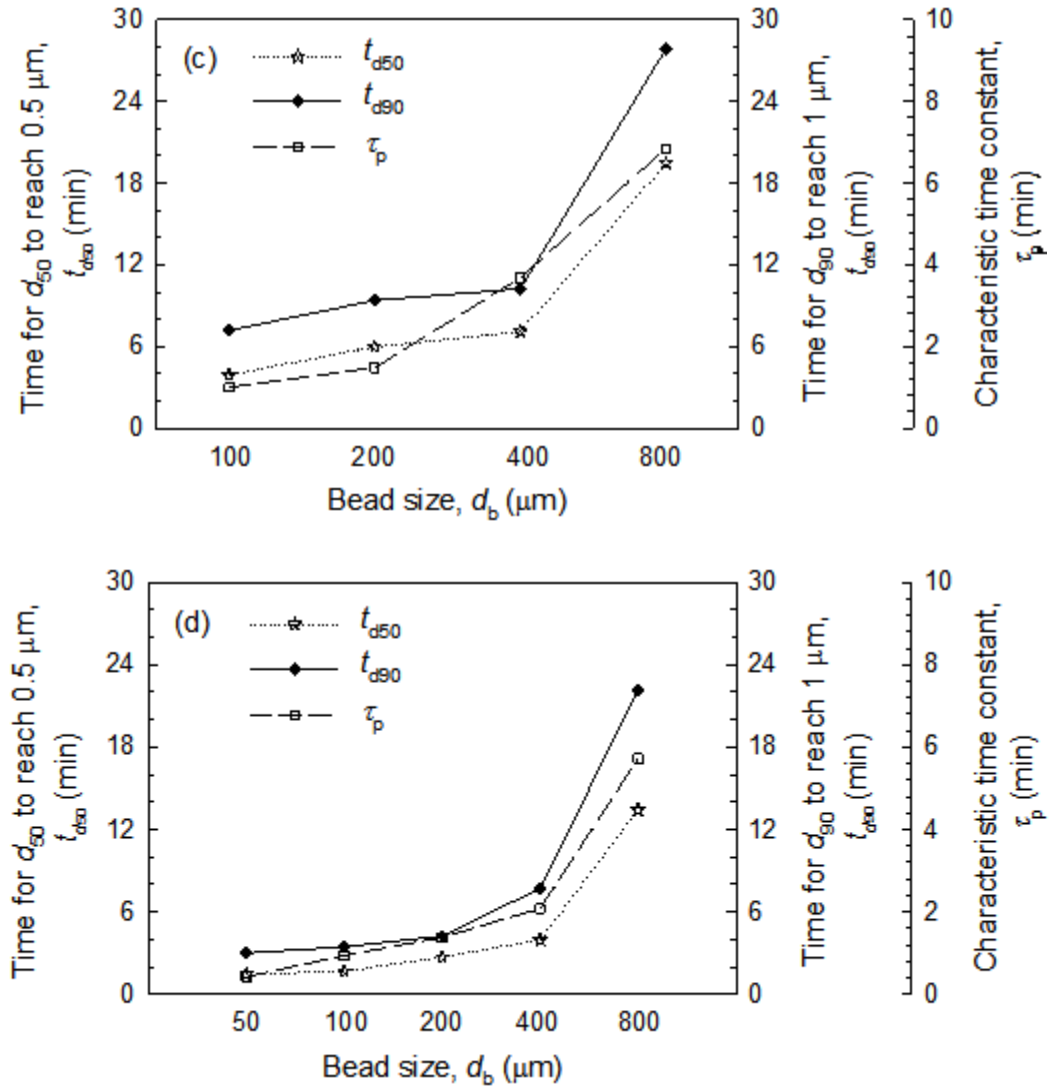

Figure 3.4 (Continued) Effects of bead size d_b on the characteristic milling times t_{d50}, t_{d90}, and τ_p at various stirrer speeds: (a) ω = 1000 rpm, (b) ω = 1600 rpm, (c) ω = 2800 rpm, and (d) ω = 4000 rpm. Note that d_{90} = 1 µm was not reached during 256 min milling when 1500 µm beads were used at ω = 1000 rpm (Run 4).

While the final milled particle sizes after 256 min milling (refer to Table 3.2) could be conveniently used to describe breakage kinetics, i.e., smaller d_{50} and d_{90} values corresponding to faster breakage, this approach may not be very reliable for several reasons. It only considers one time point (256 min) and that point corresponds to prolonged milling, at which differences that stem from different bead size–stirrer

speed might be reduced upon approach to the apparent grinding limit. Interestingly, the author notes from Table 3.2 that the smallest d_{50} and d_{90} values of the suspensions after 256 min milling, i.e., the fastest breakage, correspond to the *same* optimal bead sizes at the respective speeds as those revealed by t_{d50}, t_{d90}, and τ_p values, which were mentioned above. Hence, the calculated τ_p, t_{d50}, and t_{d90} as well as d_{50} and d_{90} for the 256 min milled suspensions all show (1) the significant impact of bead size on the drug breakage kinetics and milled particle sizes, (2) the existence of a different optimal bead size at each stirrer speed, and (3) the shift of the optimal bead size to smaller sizes at the higher stirrer speeds.

3.3.3 Microhydrodynamic Analysis of the Impact of Bead Size at Different Stirrer Speeds

Figure 3.5 shows the specific energy consumption E^* and the average power applied per unit volume of slurry P_w during 256 min milling of GF particles at different stirrer speeds when various bead sizes were used. At the same stirrer speed, higher mechanical energy was expended to stir a slurry with larger beads; hence, the higher E^* and P_w for larger beads. Similarly, higher mechanical energy was expended to stir a slurry with the same bead size at higher speeds; hence, higher E^* and P_w. The specific energy consumption E^* is known to correlate positively with the breakage rate and extent of size reduction (Kawatra, 2006). Hence, it is no surprise to see faster breakage at the higher stirrer speeds that also resulted in higher E^* and P_w. On the other hand, the optimal bead sizes were found to be 400 μm at 1000 rpm, 200 μm at 1600 rpm, 100 μm at 2800 rpm, and 50 μm at 4000 rpm (*Section 3.3.2*), which cannot be explained by E^* and/or P_w because E^* and P_w for the respective beads were either

too low or the lowest among all beads used at the respective speeds (refer to Figure 3.5 or Table B2 in *Appendix B*). This finding implies that the specific energy consumption E^* is not the sole factor that determines the breakage rate and that the impact of bead size *at a given stirrer speed* cannot be explained by E^* alone. Considering that only a small fraction of E^* or P_w is actually spent on deforming/breaking the (drug) particles to be ground (Eskin et al., 2005a), a microhydrodynamic analysis of the bead–bead collisions is required to explain the bead size impact on fundamental grounds.

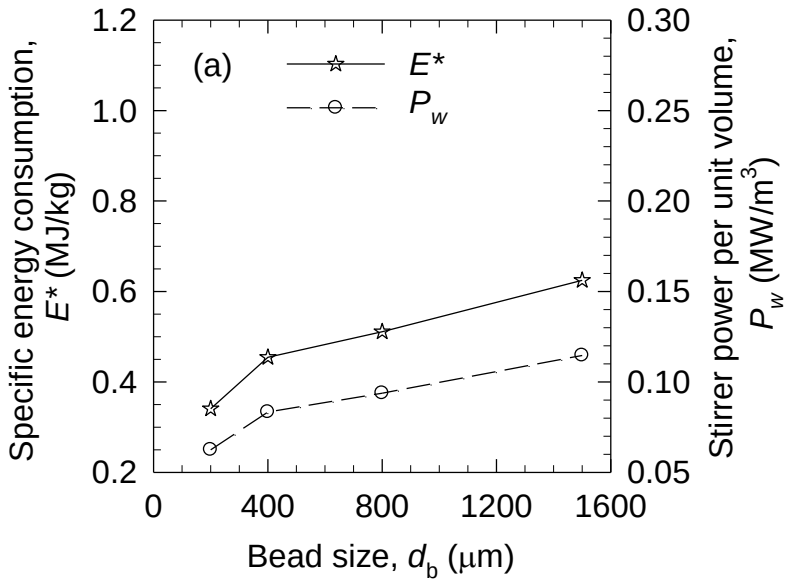

Figure 3.5 Effects of bead size d_b on the specific energy consumption E^* and the power applied by the stirrer per unit volume P_w for 256 min milling at various stirrer speeds: (a) ω = 1000 rpm, (b) ω = 1600 rpm, (c) ω = 2800 rpm, and (d) ω = 4000 rpm. (Continued)

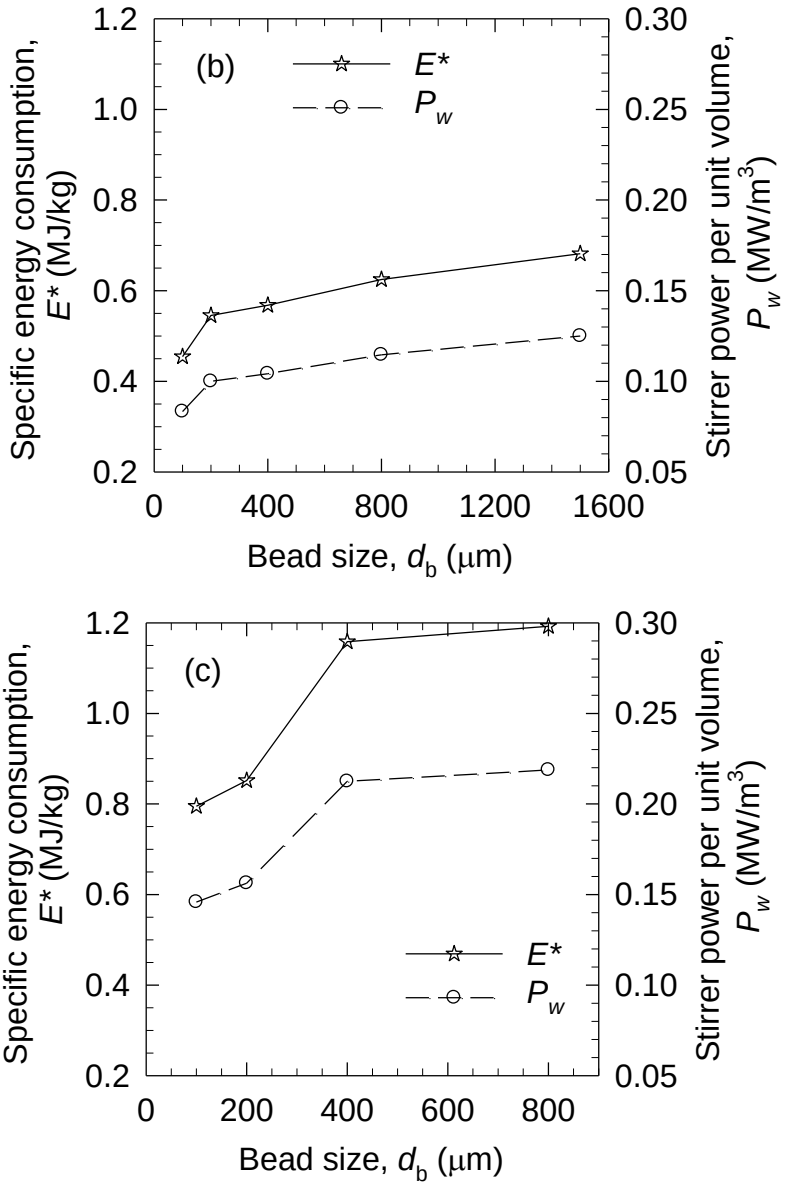

Figure 3.5 Effects of bead size d_b on the specific energy consumption E^* and the power applied by the stirrer per unit volume P_w for 256 min milling at various stirrer speeds: (a) ω = 1000 rpm, (b) ω = 1600 rpm, (c) ω = 2800 rpm, and (d) ω = 4000 rpm. (Continued)

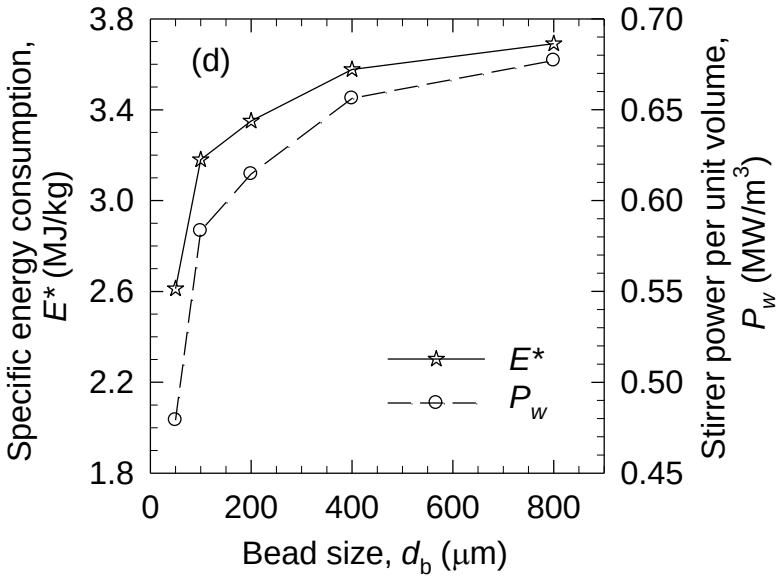

Figure 3.5 (Continued) Effects of bead size d_b on the specific energy consumption E^* and the power applied by the stirrer per unit volume P_w for 256 min milling at various stirrer speeds: (a) ω = 1000 rpm, (b) ω = 1600 rpm, (c) ω = 2800 rpm, and (d) ω = 4000 rpm.

To develop a fundamental understanding of the aforementioned dependency of optimal bead size on the stirrer speed, a microhydrodynamic analysis was performed and several microhydrodynamic parameters were calculated as a function of bead size at various stirrer speeds (see Figures 3.6 and 3.7). In general, at a given stirrer speed or tip speed u, bead loading c, and suspension flow rate Q, the microhydrodynamic parameters in Figures 3.6 and 3.7 show two major counteracting effects of the bead size. Smaller beads have a higher number concentration, which equals $6c/\pi d_b^3$, than larger beads for a given loading of the beads. On one hand, the fluctuating motion of the beads became less vigorous with a decrease in bead size as signified by the lower granular temperature θ (Figure 3.6). This decrease resulted from the decrease in the applied power P_w (Figure 3.5) and the increase in the bead number concentration. The slower fluctuating motion of the smaller beads was also

reflected in the lower average bead oscillation velocity u_b (Figure 3.6), which led to development of a lower maximum contact pressure σ_b^{max} (Figure 3.7), i.e., lower stress intensity. Up to this point, one may argue that the drug particle breakage would be slower with the use of smaller beads as the aforementioned changes in the microhydrodynamic parameters do not seem to favor particle breakage. On the other hand, the frequency of bead oscillations ν (Figure 3.6) and the average frequency of drug particle compression a (Figure 3.7) increased with a decrease in bead size due to the higher number concentration of the smaller beads. Figures 3.6 and 3.7 also show that ν and a approached a plateau or slightly decreased at the lowest bead size depending on the stirrer speed, which resulted from a secondary effect of reduced P_w. The overall increasing trend in ν and a with smaller beads correlates to higher number of stressing events and favors the drug particle breakage. In summary, upon a decrease in bead size, θ, u_b, and σ_b^{max} decreased, whereas ν and a increased up to a certain point, signifying more bead number of collisions yet with less energy/force. Hence, these two effects could counteract each other for a specific bead size, which can, in principle, explain the observed optimal bead size at a given stirrer speed.

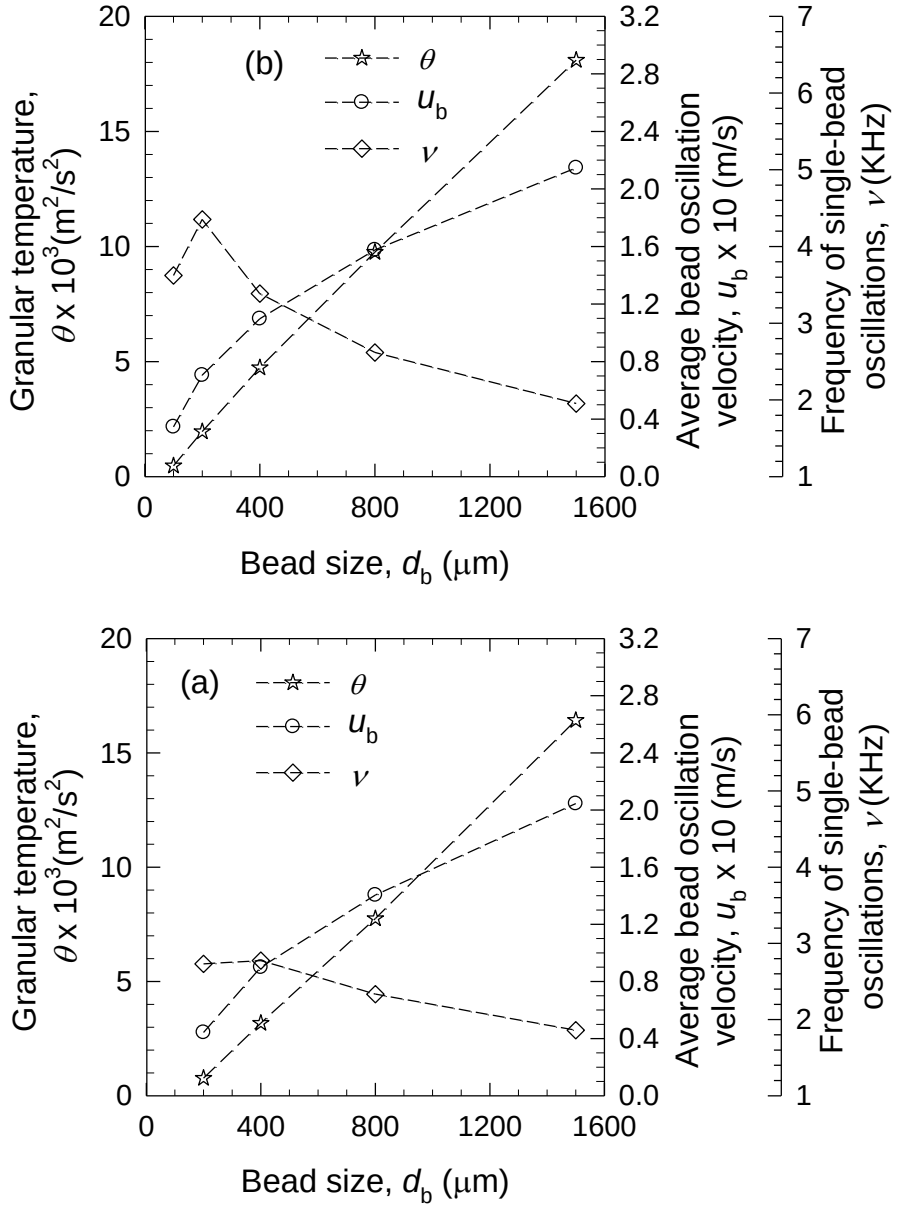

Figure 3.6 Effect of bead size d_b on the granular temperature θ, the average bead oscillation velocity u_b, and the frequency of single bead oscillations ν at various stirrer speeds: (a) ω = 1000 rpm, (b) ω = 1600 rpm, (c) ω = 2800 rpm, and (d) ω = 4000 rpm. (Continued)

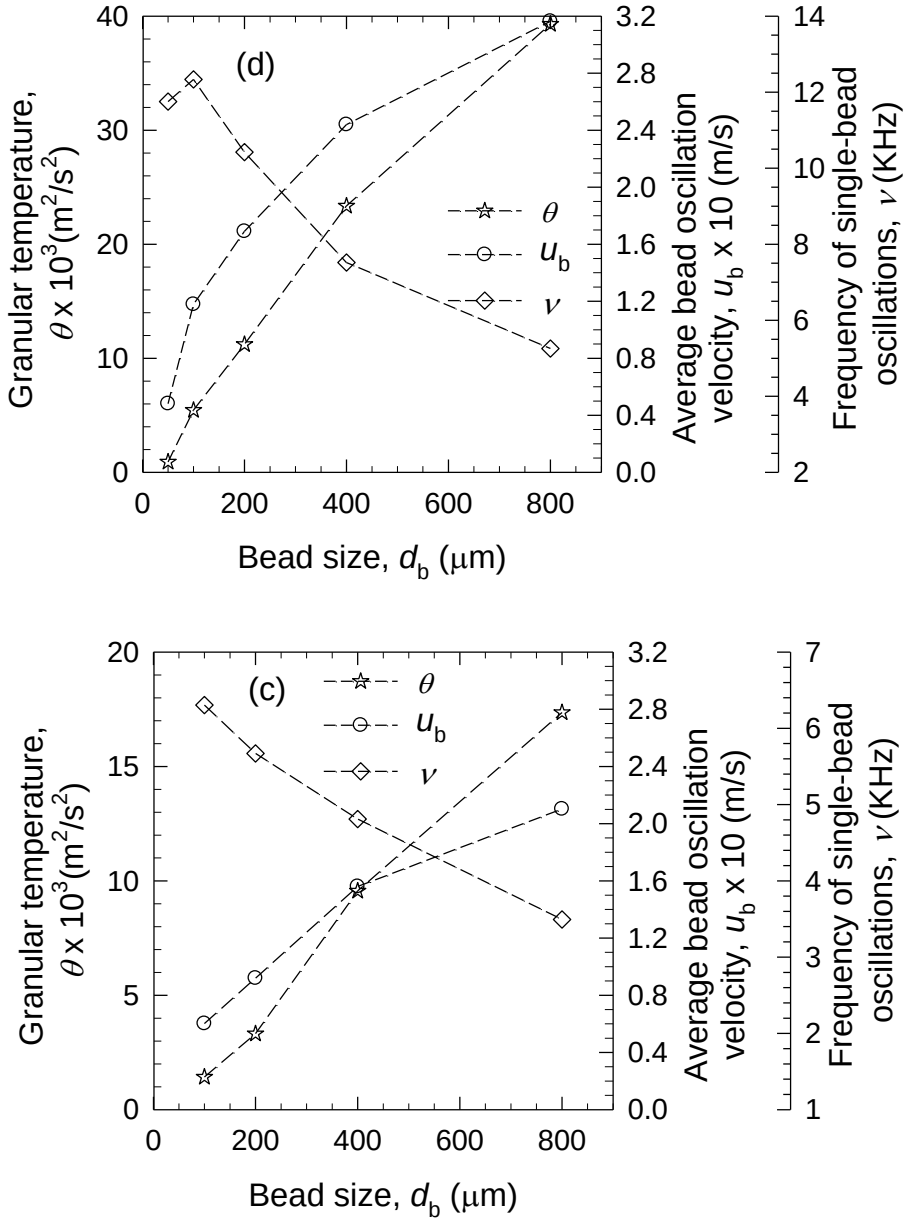

Figure 3.6 (Continued) Effect of bead size d_b on the granular temperature θ, the average bead oscillation velocity u_b, and the frequency of single bead oscillations ν at various stirrer speeds: (a) ω = 1000 rpm, (b) ω = 1600 rpm, (c) ω = 2800 rpm, and (d) ω = 4000 rpm.

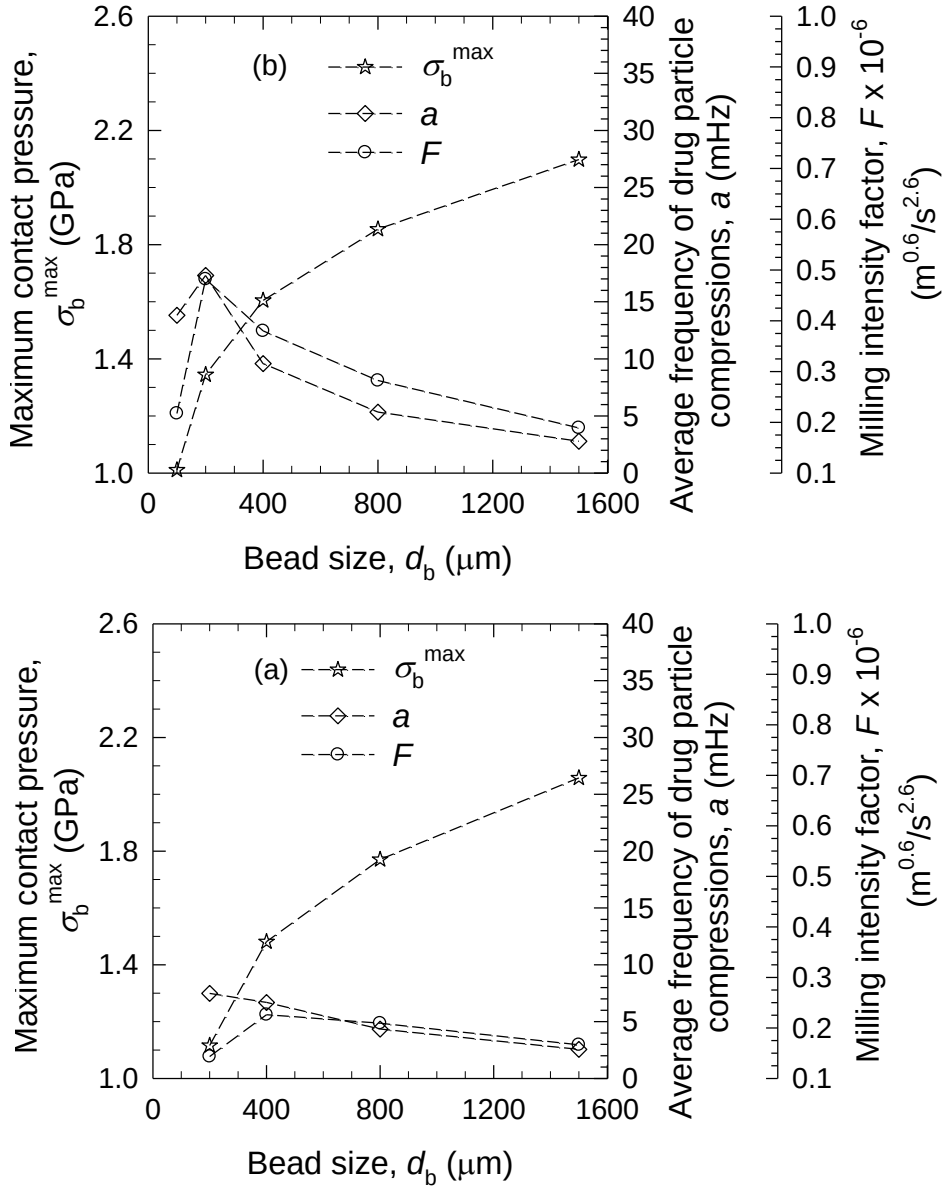

Figure 3.7 Effect of bead size d_b on the maximum contact pressure σ_b^{max}, the average frequency of drug particle compressions a, and the milling intensity factor F at various stirrer speeds: (a) ω = 1000 rpm, (b) ω = 1600 rpm, (c) ω = 2800 rpm, and (d) ω = 4000 rpm. (Continued)

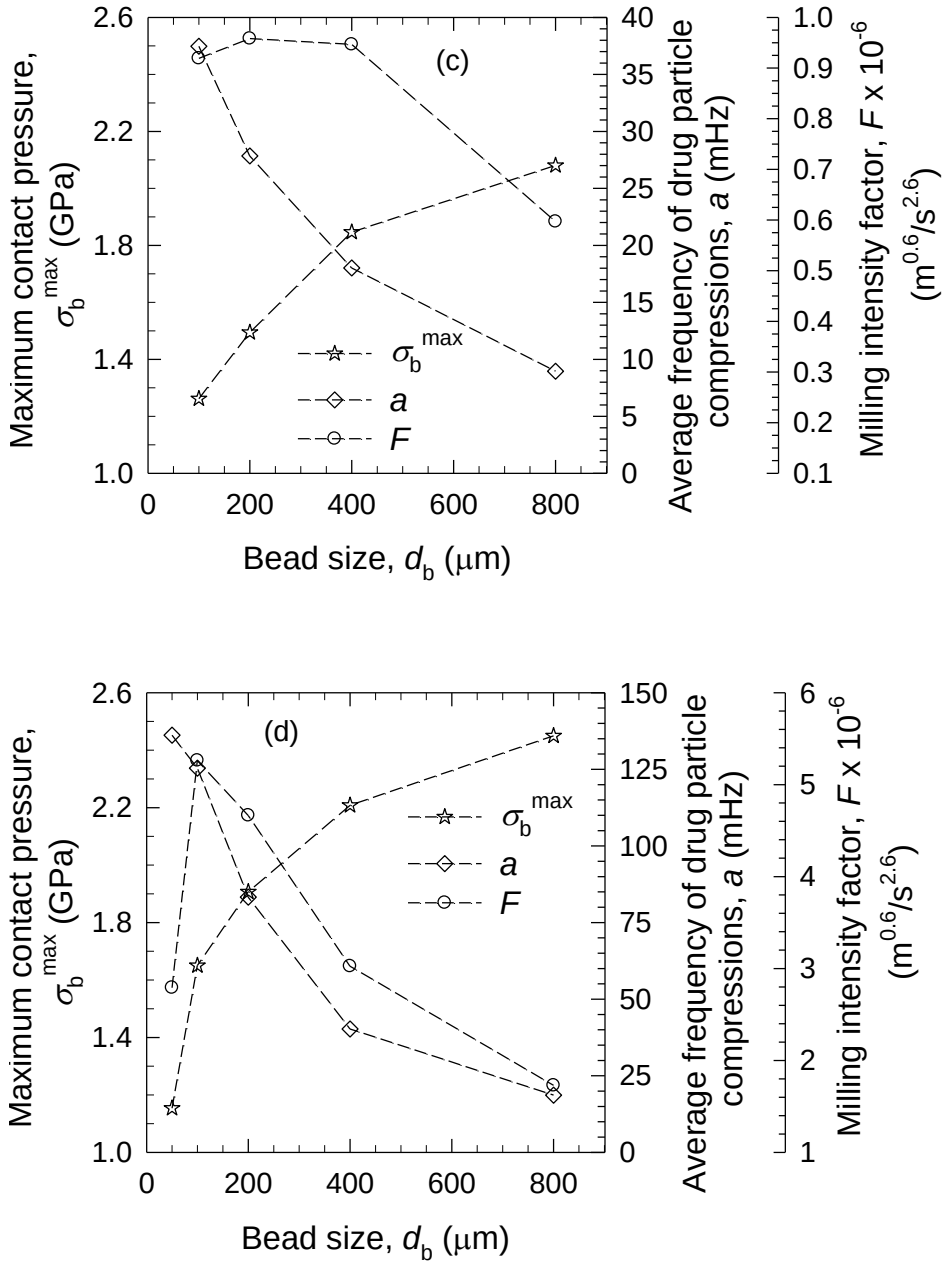

Figure 3.7 (Continued) Effect of bead size d_b on the maximum contact pressure σ_b^{max}, the average frequency of drug particle compressions a, and the milling intensity factor F at various stirrer speeds: (a) ω = 1000 rpm, (b) ω = 1600 rpm, (c) ω = 2800 rpm, and (d) ω = 4000 rpm.

While none of the microhydrodynamic parameters alone predicts the optimal bead sizes for different stirrer speeds perfectly (refer to Figure 3.4), it appears that the

experimentally observed optimal bead size corresponds to either the highest ν (except for 4000 rpm, Figure 3.6) or highest a (except for 1000 rpm, Figure 3.7) for each stirrer speed, i.e., highest frequency of bead oscillations or drug particle compressions. The parameters that relate to stress intensity and impact energies, i.e., θ, u_b, and σ_b^{max}, when considered alone, indicate the largest beads as optimal bead sizes, which contradicts the experimental findings. The above observations can be explained as follows: first, as mentioned earlier, the bead size has two major counteracting effects, which can only be characterized thoroughly by all microhydrodynamic parameters calculated. Second, a possible explanation for the dominant effect associated with ν and a on the breakage kinetics emerges from a damage mechanism called contact fatigue for the drug particles when they are captured multiple times by the colliding beads: multiple, frequent compressions of the particles with low stress intensity can cause nucleation of permanent structural defects that lead to crack initiation; the growth of cracks eventually results in particle fracture (Bilgili et al., 2006; Eskin et al., 2005a). Thus, it is likely that GF particles may break at lower stresses than their static fracture strength values, thus making their breakage rate more sensitive to the average frequency of drug particle compressions a than the maximum bead contact pressure σ_b^{max} under the specific milling conditions explored here. Further investigation is needed to elucidate these mechanisms, which is beyond the scope of this dissertation. Finally, the milling intensity factor F, which was originally developed by Afolabi et al. (2014) to explain the impact of milling process parameters using a single microhydrodynamic parameter, exhibited a maximum at the optimal bead sizes for the lower stirrer speeds

(1000 and 1600 rpm) (Figure 3.7). However, the maximum F occurred for larger beads at the higher speeds, i.e., 200 μm and 100 μm at 2800 and 4000 rpm, than for the experimentally found optimal beads, i.e., 100 μm and 50 μm, respectively. Since bead size is usually regarded as an equipment parameter in media milling (Kawatra, 2006), F alone cannot capture the bead size effects well; however, it explains the impact of stirrer speed (a process parameter) well, as will be mentioned below.

The impact of stirrer speed was analyzed here within the context of microhydrodynamics in order to elucidate why the optimal bead size shifted to lower values at higher speeds. Upon an increase of stirrer speed, both E^* and P_w increased (refer to Figure 3.5), all microhydrodynamic parameters increased monotonically for a given size of beads (refer to Figures 3.6 and 3.7 and Table B2 in *Appendix B*). Upon an increase in the stirrer speed, the fluctuating motion of the beads became more vigorous (higher θ). There were more frequent bead oscillations (higher v), which led to a more frequent compression of the drug particles (higher a). The beads had higher fluctuating velocity (higher u_b), which led to more impactful bead collisions and development of higher compressive stress (higher σ_b^{max}). An increase in stirrer speed significantly increased F, which indicates a more intensified milling process. These combined effects led to the aforementioned enhanced breakage kinetics with increasing stirrer speed for a given bead size. In view of the above, upon an increase in stirrer speed, even the smallest beads undergo more vigorous/energetic collisions. With the added advantage of having a higher number concentration leading to more frequent collisions, smaller beads become more advantageous at higher speeds. Hence, considering the counteracting effects of bead size, i.e., more bead–bead collisions yet

with less energy/force upon the use of smaller beads, small beads are favored more than larger beads at the higher stirrer speeds in terms of the balancing action of the two effects. This could explain the shift of the optimal bead size to smaller values at the higher stirrer speeds.

3.3.4 A Rationale for Bead Size Selection for WSMM with Implications for All Wet Media Mills

It is important to develop a rationale for the selection of optimal bead size as a function of stirrer speed on the basis of specific energy consumption E^* and the microhydrodynamic parameters. The optimal bead sizes at different stirrer tip speeds, determined in *Section 3.3.2* experimentally, exhibited a negative power-law correlation with E^* and the microhydrodynamic parameters (Figure 3.8). The R^2 values for the fittings of optimal bead size vs. stirrer speed and microhydrodynamic parameters were above 0.997, and the fitted parameters were all statistically significant with p-values < 0.0015. Some deviation occurred at higher energy consumption E^*, which resulted in an R^2 of 0.947 and p-value of 0.0266 for the optimal bead size–E^* correlation. Overall, these correlations suggest that smaller beads are more effective at higher stirrer tip speeds or when wet media milling was conducted under more energetic (higher E^*)/more intensified (higher F) conditions. These correlations between optimal bead sizes and the microhydrodynamic parameters describe the experimentally observed shift of the optimal bead size, i.e., smaller optimal bead sizes at higher stirrer speeds. This fundamental finding also rationalizes the global trend in the preparation of drug nanosuspensions: mills that typically impart lower power consumption/energy such as ball mills, planetary ball

mills, etc. usually use coarser beads than the highly energetic wet stirred media mills (refer to Table 3.1).

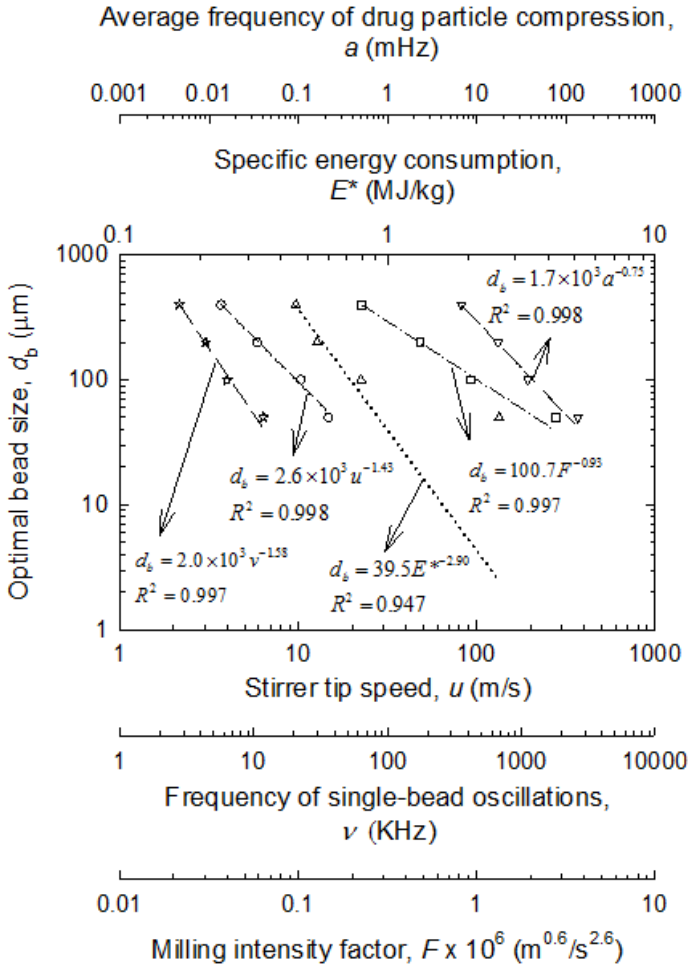

Figure 3.8 Scatter plots and power-law scaling for the dependence of optimal bead size on the stirrer tip speed *u*, the specific energy consumption *E**, the frequency of singe-bead oscillations *v*, the average frequency of drug particle compression *a*, and the milling intensity factor *F*.

3.4 Conclusions

This study has been driven by the importance of stable nanoparticle suspensions for bioavailability enhancement of poorly water-soluble drugs and the lack of

fundamental understanding of bead size effects and a scientific rationale for bead size selection in their preparation by wet media milling. To this end, the author has studied the milling of griseofulvin suspensions and elucidated the dependency of optimal bead size on the stirrer speed via combined breakage kinetic–microhydrodynamic models. Drug breakage kinetics, Hermite interpolation, and empirical model fitting indicated the existence of optimal bead size at each stirrer speed. More importantly, the optimal bead size decreased upon an increase in the stirrer speed. While all microhydrodynamic parameters provided significant physical insight, the existence of optimal bead size was overall explained by the two counteracting effects of bead size: more bead–bead collisions (more stressing events) with less energy/force (lower stress intensity) upon a decrease in bead size. The optimal bead size exhibited a negative power-law correlation with either the specific energy consumption or any of the microhydrodynamic parameters. Overall, this study has rationalized the use of smaller beads for more energetic wet media milling and provided an overarching explanation as to the use of smaller beads in wet stirred media mills than in low-energy mills such as ball mills and planetary ball mills. This study is expected to guide the design and optimization of wet media milling processes in terms of proper choice of bead size for optimal performance.

CHAPTER 4

SUB-100 NM DRUG PARTICLE SUSPENSIONS PREPARED VIA WET MILLING WITH LOW BEAD CONTAMINATION THROUGH NOVEL PROCESS INTENSIFICATION

As discussed in Chapter 1, there is sustained interest in sub-100 nm particles of poorly water-soluble drugs as such small particles offer improved permeation through various biological barriers and result in rapid onset of therapeutic action. Chapter 3 rationalized the selection of bead size at different stirrer speeds for the efficient production of drug nanosuspensions via the wet stirred media milling (WSMM) process. Not only the bead size, but also the other process parameters, such as stirrer speed, bead loading, and suspension flow rate, can affect the drug breakage. Chapter 4 aims to develop an intensified WSMM process to produce sub-100 nm BCS Class II drug particles. To this end, the impact of bead size on the drug particle size, breakage kinetics, energy consumption, and bead wear were investigated for griseofulvin, a poorly water-soluble drug, under highly energetic milling conditions in the turbulent flow regime. Laser diffraction, dynamic light scattering, scanning electron microscopy, and XRD were used to characterize the milled suspensions. Yttrium-stabilized zirconia beads with a nominal size ranging from 50 μm to 800 μm were used in the baseline process, which was subsequently intensified with the optimal bead size by increasing rotor tip speed, bead loading, and suspension flow rate stepwise, as guided by a microhydrodynamic model. After examining the breakage kinetics under the intensified conditions, shorter milling experiments, which targeted approximately 100 nm particle size, were performed to examine the energy consumption and bead wear along with the microhydrodynamics. The novel

intensification method, i.e., the use of optimal (50 μm) beads with the intensified process conditions as guided by the microhydrodynamic model, was also applied to wet-milling of indomethacin, another poorly water-soluble drug, confirming the generality of the novel model-guided process intensification method. In pursuit of the goal of preparing sub-100 nm drug particles fast, this study contributes to a fundamental understanding of the impact of bead size and process intensification while addressing all major issues associated with the WSMM process, i.e., excessively long processing time, high energy consumption, and potentially high media contamination in a holistic, model-guided approach.

4.1 Materials and Methods

4.1.1 Materials

EP/BP grade griseofulvin (GF) and USP grade indomethacin (IND) were purchased from Letco Medical (Decatur, AL, USA). GF and IND are two BCS Class II drugs with an aqueous solubility of 7.7 and 16 μg/ml, respectively (Merisko-Liversidge and Liversidge, 2011). Methocel E3 grade hydroxypropyl methyl cellulose (HPMC), which is commonly used as a neutral polymeric stabilizer, was a donation from Dow Chemical (Midland, MI, USA). Sodium dodecyl sulfate (SDS), which is an anionic surfactant, was purchased from Sigma Aldrich (Bellefonte, PA, USA), and nitric acid (65 wt%) was purchased from Fisher Scientific Inc. (Pittsburgh, PA, USA). Zirmil Y grade yttrium-stabilized zirconia (YSZ) beads with *nominal* sizes of 800, 400, 200, 100, and 50 μm were purchased from Saint Gobain ZirPro (Mountainside, NJ, USA) and used as the milling media. Throughout the dissertation, the beads were labeled

with their nominal sizes, while their actual median sizes, i.e., 802, 396, 214, 107, and 54 µm, respectively, measured in dry dispersion mode via a laser diffraction particle size analyzer (Helos/Rodos, Sympatec, NJ, USA) were used in the microhydrodynamic model. De-ionized water was used in all milling and particle sizing experiments. Fresh beads were rinsed with de-ionized water and sonicated for 40 min followed by a final rinse.

4.1.2 Preparation of Suspensions via Wet Media Milling

The stabilizer concentrations, milling procedure, and baseline process conditions were selected based on our recent investigations (Afolabi et al., 2014; Knieke et al., 2013). First, about 225 g pre-suspensions were prepared by dispersing 10% drug particles in an aqueous solution of 2.5% HPMC-E3 and 0.2% SDS under constant stirring at 300 rpm (Cat#. 14-503, Fisher Scientific, Pittsburgh, PA, USA) for a total of 90 min. Here, all percentages are w/w with respect to de-ionized water (200 g). The pre-suspensions were then milled at the conditions presented in Table 4.1. The impact of bead size d_b was studied through Runs 1–5, followed by process intensification experiments (Runs 6–8) guided by the microhydrodynamic model. Runs 9 and 10 were performed to establish the applicability of the intensification method to IND.

Wet milling was carried out in a Microcer stirred media mill (Netzsch Fine Particle Size Technology, LLC, Exton, PA, USA) with an 80 ml (V_m) milling chamber lined with zirconia and a zirconia shaft with a diameter D of 7 cm (Figure 2.1). The pre-suspension was added to the holding tank (500 ml) and recirculated

between the holding tank and the milling chamber at a controlled flow rate *Q* by a peristaltic pump (Cole-Parmer, Master Flex®, USA). Stainless steel screens with different opening sizes, which are approximately half of the nominal size of the beads, were used to keep the beads inside the milling chamber. The Netzsch Microcer mill is limited to ~50 µm beads in the recirculation mode by its design, which requires the use of a screen with an opening size of 25 µm. When 50 µm beads were used as the smallest beads, the presence of large GF particles and IND particles initially resulted in clogging of the screen and the pressure rose. This practical issue was resolved by using a higher rotor tip speed (14.7 m/s) and lower suspension flow rate (80 ml/min) shortly in Run 5, which were then restored back to the set values in Table 4.1. Similarly, in Runs 6–8 and 10, the milling with a lower flow rate (80 ml/min) was carried out; then the flow rate was restored back to the target value and milling continued up to the long duration presented in Table 4.1. A chiller (Model M1-.25A-11HFX, Advantage Engineering, Greenwood, IN, USA) provided cooling for both the milling chamber and the holding tank, which allowed for keeping the suspension temperature in the holding tank below 34 ^{o}C, as a maximum. Due to the low cooling capacity of this specific chiller, a cooling strategy similar to that in Afolabi et al. (2014) was adopted here: the mill was stopped for few minutes of additional, intermittent cooling after 3 h during Runs 1–5 and Run 9 and about every 8 min during Runs 6–8 and Run 10. The suspensions at several milling time points were collected from the outlet of milling chamber and used for particle size and morphology analysis. The final milled suspensions were also characterized and remaining suspensions were stored in a refrigerator at 8 ^{o}C for 7 days.

To study the impact of bead size on wear, additional 6 h milling experiments were performed under the same conditions of Runs 1–5 mentioned above using 800, 400, 200, 100, and 50 μm beads, respectively. These beads had already been used in the previous milling experiments as described above; hence, they are regarded as conditioned or pre-treated for the purpose of the wear study. Additional experiments were also performed with pre-treated 50 μm beads under Runs 6–10 conditions, including shorter milling times that allow for preparation of 100 nm drug particles. Bead wear was characterized on suspension samples following the procedure detailed in Section 4.1.3. The wet beads were oven-dried overnight at 40 °C following 40 min sonication–rinsing in de-ionized water before a new milling experiment.

The total energy consumption E was directly recorded from the mill control panel. Using this information, the average stirrer power applied per unit volume of the slurry (beads, drug, stabilizers, and water) P_w was calculated using

$$P_w = E/(V_m t_T) \tag{4.1}$$

where t_T is the total milling time. The specific energy consumption E^*, which is the energy spent per unit mass of drug suspension, was also calculated as follows:

$$E^* = E/m_{sus} \tag{4.2}$$

where m_{sus} is the total mass of the drug suspension.

Table 4.1 Parameters Varied in the Wet Milling Experiments. Fixed Parameters: Drug Loading of 10%, 200 g De-ionized Water, and HPMC/SDS Concentration of 2.5%/0.2% (Weight Percent with Respect to De-ionized Water)

Run No.	Drug	Nominal Bead Size d_b (µm)	Rotor Tip Speed u (rpm, m/s)	Bead Mass, Volume Fraction c (g), (–)	Suspension Flow Rate Q (ml/min)	Milling Time t (min)
1	GF	800	3200, 11.7	196, 0.408	126	360
2	GF	400	3200, 11.7	196, 0.408	126	360
3	GF	200	3200, 11.7	196, 0.408	126	360
4	GF	100	3200, 11.7	196, 0.408	126	360
5	GF	50	3200, 11.7	196, 0.408	126	360
6	GF	50	4000, 14.7	196, 0.408	126	120
7	GF	50	4000, 14.7	261, 0.543	126	120
8	GF	50	4000, 14.7	261, 0.543	343	120
9	IND	50	3200, 11.7	196, 0.408	126	360
10	IND	50	4000, 14.7	261, 0.543	343	120

4.1.3 Particle Size Determination

Particle size distribution (PSD) of the drug suspensions was determined using a combination of laser diffraction (LD) and dynamic light scattering (DLS) (see e.g., Schubert et al., 2006; Knieke et al., 2009 for a similar approach). LD was used to determine the PSD of all milled suspension samples. The measurements were performed in LS 13-320 Beckman Coulter instrument (Brea, CA, USA). A refractive index of 1.65, 1.50, and 1.33 were used for GF, IND, and water (measurement medium), respectively. For the particles with median particle size d_{50} above 200 nm, median particle sizes from LD were reported. The particle size was measured at least thrice and the average value was calculated together with standard deviation (SD). As DLS is more sensitive and accurate when the majority of particle sizes are less than 200 nm, the PSD of the milled suspension samples with d_{50} less than ~200 nm were determined by DLS using Delsa Nano C Particle analyzer (Beckman Coulter, Brea, CA, USA). About 0.5 ml of the milled suspension was diluted with 4 ml de-ionized water prior to measurement at 25 °C. The median size from LD and the Z-average (cumulant) size from DLS are referred to as the *particle size*.

4.1.4 Scanning Electron Microscopy

Particle size and morphology of the as-received and milled drug particles were examined via scanning electron microscopy (SEM) with a LEO 1530 SVMP (Carl Zeiss, Inc., Peabody, MA, USA). About 0.1 ml of the milled suspension was diluted with 30 ml de-ionized water, and a drop was placed on a silicon chip (Ted Pella, Inc., Redding, CA, USA), dried, sputter coated, and observed in SEM. Image J software

was used to analyze about 1500 particles and determine the average particle size based on equivalent projected-area diameters of the particles from the SEM images.

4.1.5 X-ray Powder Diffraction

The crystallinity of the as-received drug, unmilled physical mixture (overnight dried aqueous suspension with as-received drug, HPMC, and SDS), and overnight dried–milled suspensions was analyzed using X-ray Powder Diffraction (XRD, PANalytical, Westborough, MA), provided with Cu K_α radiation (λ = 1.5406 Å). The samples were scanned for 2θ ranging from 5^o to 40^o at a scan rate of 0.165 s^{-1}.

4.1.6 Apparent Shear Viscosity of Milled Suspensions

The apparent shear viscosities μ_L of the milled suspensions were measured at 25 ± 0.5 ^{o}C using R/S plus Brookfield Rheometer (Brookfield Engineering, Middleboro, MA, USA) with a coaxial cylinder (CC40). The suspension was sheared from 0 to 1000 1/s in 60 s and the apparent shear viscosity at the maximum shear rate was taken (Bernhardt et al., 1999).

4.1.7 Density Measurement of Milled Suspensions

The density of the milled suspension was measured by weighing 25 ml of the milled suspension. The weight of the suspension divided by its volume was used to calculate the suspension density.

4.1.8 Determination of Contamination in the Milled Suspensions

The elemental zirconium (Zr), the most abundant heavy metal in the beads and the main contaminant in the milled suspensions due mostly to bead wear, was measured by inductively coupled plasma mass spectrometry (ICP-MS) via an Agilent 7500i Bench-top ICP-MS System (Santa Clara, CA, USA) according to European Pharmacopeia 6.0 §2.2.58. The suspension samples were dried at 40 °C for 24 h in a convective drier (Gallenkamp, Netherlands), and the dried powder was finely ground by a mortar and pestle. Then, 1 g of ground powder was added to 40 ml of membrane-filtered de-ionized water, followed by addition of 40 ml of 65% nitric acid. The mixture was heated to 90 °C, and maintained at this temperature until a clear solution was observed. Finally, the resultant clear solution was cooled down to room temperature, diluted to 50 ml with the membrane-filtered deionized water, and subjected to ICP-MS analysis. The measurements were performed thrice, and an average value along with SD was reported.

4.2 Theoretical

The dynamics of the inter-particle collisions in a dense slurry flow is referred to as microhydrodynamics. Eskin et al. (2005a, b) developed a model to calculate the mean velocity of bead oscillations in well-mixed slurries using the kinetic theory of granular flows and fundamental granular energy balance (Gidaspow, 1994). Salient features of this microhydrodynamic model with slight modification (Afolabi et al., 2014) in view of Eskin and Miller (2008) are presented here, and readers are referred to aforementioned literature for the assumptions and derivations. The power applied

per unit volume of slurry P_w inside a stirred mill dissipates through several mechanisms, which are mathematically expressed as follows:

$$P_w = \varepsilon_{visc} + \varepsilon_{coll} + \varepsilon_{ht} \tag{4.3}$$

$$P_w = \frac{54\mu_L c\theta R_{diss}}{{d_b}^2} + \frac{12}{d_b\sqrt{\pi}}\left(1-k^2\right)\left[\frac{1-0.5c}{(1-c)^3}\right]c^2\rho_b\theta^{3/2} + \varepsilon_{ht} \tag{4.4}$$

where ε_{visc} is the energy dissipation rate due to both the liquid–beads viscous friction and lubrication, ε_{coll} is the energy dissipation rate due to partially inelastic bead–bead collisions, and ε_{ht} is the power spent on shearing the equivalent liquid (milled drug suspension). In Eq. (4.4), μ_L is the apparent shear viscosity of the equivalent liquid, c is the bead volumetric concentration (volume fraction), θ is the granular temperature defined as the bead–equivalent liquid relative mean-square velocity, R_{diss} is the effective drag (dissipation) coefficient, d_b is the median size of the beads, k is the restitution coefficient for the bead–bead collisions (0.76 from Tatsumi et al., 2009), and ρ_b is the density of the zirconia beads (6000 kg/m^3).

The equivalent liquid properties μ_L and ρ_L as well as the power applied per unit volume in the presence of the beads P_w were measured. The energy dissipation rate for shearing the equivalent liquid ε_{ht} was negligibly small (much smaller than P_w) due to the low viscosity of the suspensions. MATLAB's fsolve function was used to solve Eq. (4.4) for the granular temperature θ using P_w measured and R_{diss} values calculated (refer to Eqs. (A.1)–(A.5)). From the calculated θ, the frequency of single-bead oscillations ν and the average oscillation velocity of the beads u_b were determined as follows:

$$\nu = \frac{24c}{d_b}\left[\frac{1-0.5c}{(1-c)^3}\right]\sqrt{\frac{\theta}{\pi}} \tag{4.5}$$

$$u_b = \sqrt{\frac{8\theta}{\pi}} \tag{4.6}$$

Eskin et al. (2005b) advanced the earlier microhydrodynamic model (Eskin et al., 2005a) by considering the elastic contact deformation of the beads along with the elastic–perfectly plastic deformation of the particles caught between the beads. While the beads frequently collide due to their fluctuating motions in a slurry, which are characterized by θ, u_b, and ν, the beads capture and compress the drug particles to be milled. The maximum contact pressure at the center of the contact circle σ_b^{max} of the two colliding beads is given by

$$\sigma_b^{max} = \frac{3}{2}\frac{F_b^n}{\pi\alpha_b^2} \tag{4.7}$$

where F_b^n and α_b are the average maximum normal force during the collision of two elastic beads and the radius of the contact circle formed at the contact of two beads respectively (refer to Eqs. (A.6) and (A.7), respectively). The average frequency of drug particle compressions a equals the product of probability p of a single particle caught between beads (refer to Eq. (A.8)) and the frequency of single-bead oscillations ν as follows:

$$a = p\nu \tag{4.8}$$

It must be noted that only a small fraction of energy consumption is actually used for deforming the drug particles, which is explained by the energy dissipation rate resulting from the deformation of the particles per unit volume Π and expressed as (refer to Eskin et al., 2005b):

$$\Pi = 2.23\frac{c^2(2-c)}{(1-c)^3}\frac{1}{\pi^{5/2}\varepsilon\sigma_y}\left(\frac{Y_b}{1-\eta_b^2}\right)^{18/15}\left(\frac{Y^*}{Y_p}\right)^{\gamma}\rho_b{}^{4/5}\frac{R_p}{R_b^2}\theta^{13/10} \tag{4.9}$$

where ε, Y^*, Y_p, η_b, σ_y, R_p, and R_b are the volume fraction of the drug particles in the suspension, reduced elastic modulus of the bead–drug particle contact, elastic modulus of the drug particles, Poisson's ratio of the beads, contact pressure in a drug particle captured when the fully plastic condition is obtained, radius of the drug particle, and radius of the bead, respectively. To calculate Π, the mechanical properties of the drug particles (Y_p, η_p, σ_y) have to be known, and only scant information for drugs is available in the literature and they are also difficult to measure. Since the objective here is to gain insight and guide process intensification, similar to Afolabi et al. (2014), the author decomposed Π multiplicatively into a material-dependent factor λ and a milling intensity factor F as follows:

$$\lambda = 2.23\frac{\rho_b^{4/5}R_p}{\pi^{5/2}\sigma_y}\left(\frac{Y_b}{1-\eta_b^2}\right)^{18/15}\left(\frac{Y^*}{Y_p}\right)^{\gamma} \tag{4.10}$$

$$F = \frac{c^2(2-c)}{(1-c)^3}\frac{1}{\varepsilon R_b^2}\theta^{13/10} \tag{4.11}$$

4.3 Results and Discussion

4.3.1 Impact of Bead Size and Selection of Optimal Bead Size for Intensification

Proper selection of bead size can have a significant impact on the breakage kinetics, final milled particle size, energy consumption, and bead wear. A comprehensive analysis of the impact of bead size is presented in this section.

4.3.1.1 Effects of Bead Size on the Breakage Kinetics and Milled Particle Size.

GF particles were wet-milled using beads with different nominal sizes: 800, 400, 200, 100, and 50 μm at the baseline process conditions (Table 4.1, Runs 1–5). Figure 4.1 shows the temporal evolution of GF particle size during milling. For all bead sizes, the GF particle size decreased monotonically with a decreasing rate and slowly approached a limiting (plateau) size, also known as the grinding limit. Table 4.2 presents the particle sizes and their standard deviation (SD) as well as the polydispersity index (PDI) for 360 min milled suspensions. Sub-100 nm GF particles were only produced when 50 or 100 μm beads were used; these two bead sizes led to similar breakage profiles after 8 min (Figure 4.1). Reproducibility was established by repeat milling experiments on Runs 1 and 5. The particle sizes from the repeat experiments were 167 and 97 nm, respectively. The deviations of the repeat particle size values were less than or equal to 2%. In light of the low variability of the size measurements presented in Figure 4.1, the milling process is considered to be reproducible, which is consistent with our earlier investigations on the reproducibility of the wet milling process (e.g., Afolabi et al., 2014; Bilgili and Afolabi, 2012).

Table 4.2 Z-average Particle Size and its Standard Deviation (SD) as well as Polydispersity Index (PDI) Obtained from Dynamic Light Scattering (DLS) for Runs 1–10 Suspensions after Milling and 7 Days Storage.

Run No.	Milling Time (min)	After Milling		7 Days Storage	
		Particle Size (nm), SD	PDI	Particle Size (nm), SD	PDI
1	360	169, 1.1	0.158	174, 7.3	0.155
2	360	137, 4.8	0.144	148, 3.2	0.114
3	360	120, 4.4	0.246	124, 5.1	0.239
4	360	97, 1.0	0.272	115, 0.6	0.279
5	360	95, 2.0	0.241	108, 2.8	0.270
6	120	94, 3.9	0.228	104, 3.0	0.314
7	120	93, 3.3	0.250	104, 3.3	0.237
8	120	88, 2.7	0.269	97, 2.2	0.281
9	360	77, 2.7	0.272	85, 2.3	0.212
10	120	72, 2.1	0.338	87, 1.7	0.237

Reynolds number *Re*, which equals $ND^2\rho_L/\mu_L$, was calculated to be 47,300 ± 1,600 for all different sizes of the beads (Runs 1–5), which is greater than 35,000 (Kawatra, 2006), suggesting a *fully turbulent motion* in the mill. The use of low viscosity HPMC (E3 grade) and SDS as stabilizers in the suspensions helped to achieve these high *Re* values while mitigating viscous dampening. Having a fully turbulent motion, the baseline process is sufficiently aggressive for fast breakage, as seen from the attainment of a particle size less than 400 nm within 8 min (see Runs 3–5 in Figure 4.1). This proves that the baseline conditions were chosen rationally based on our earlier investigations (Afolabi et al., 2014; Knieke et al., 2013), setting the stage for the fast production of sub-100 nm particles via process intensification. Figure 4.1 and Table 4.2 overall suggest that the use of 100 and 50 μm beads can be advantageous for the fast production of finer GF particles.

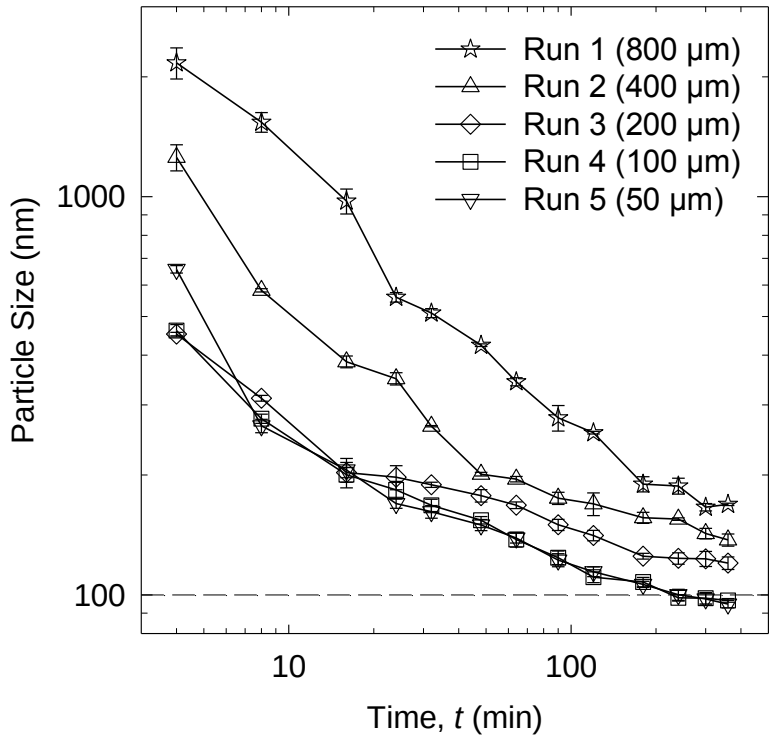

Figure 4.1 Temporal evolution of GF particle sizes during Runs 1–5. Runs 1, 2, 3, 4, and 5 refer to milling of GF with 800, 400, 200, 100, and 50 µm YSZ beads respectively at the baseline process conditions (u = 11.7 m/s, c = 0.408, and Q = 126 ml/min). At t = 0 min, the GF particles have d_{50} = 21.85 ± 1.25 µm and d_{90} = 57.77 ± 4.35 µm.

It is important to establish the aggregation state and physical stability of the milled suspensions. Figure 4.2 shows the SEM images of 4, 32, 120, 240, and 360 min milled GF particles with 50 µm beads (Run 5), capturing the evolution of the particle size and morphology. GF particles became smaller and more rounded as milling progressed. The average size of the 360 min milled particles (Figure 4.2(f)) calculated using the SEM images was 90 nm, which is slightly smaller than the Z-average particle size obtained from DLS (Table 4.2). These findings suggest that even the suspension with the smallest particles at the baseline conditions is not significantly aggregated at the time scale of the milling process, and the electro-steric

stabilization mechanism imparted by the HPMC–SDS combination was quite effective. Short-term physical stability of the suspensions was studied for a storage period of 7 days at 8 °C. Table 4.2 shows that the particle size did not change significantly after 7 days storage; hence, the suspensions were physically stable and remained colloidal mainly due to the synergistic stabilizing action of the HPMC–SDS combination. These observations are in line with our recent work (Bhakay et al., 2013; Knieke et al., 2013; Sievens-Figueroa et al., 2012), where nanoparticles of other poorly water-soluble drugs such as fenofibrate, naproxen, and phenylbutazone were properly stabilized in the presence of SDS with either HPC (hydroxypropyl cellulose) or HPMC. Long-term physical stability of the suspensions was not investigated in the present study as the milled suspensions are mainly intended for immediate drying with the ultimate goal of preparing solid dosage forms (similar to e.g., Bhakay et al., 2014; Kesisoglou et al., 2007).

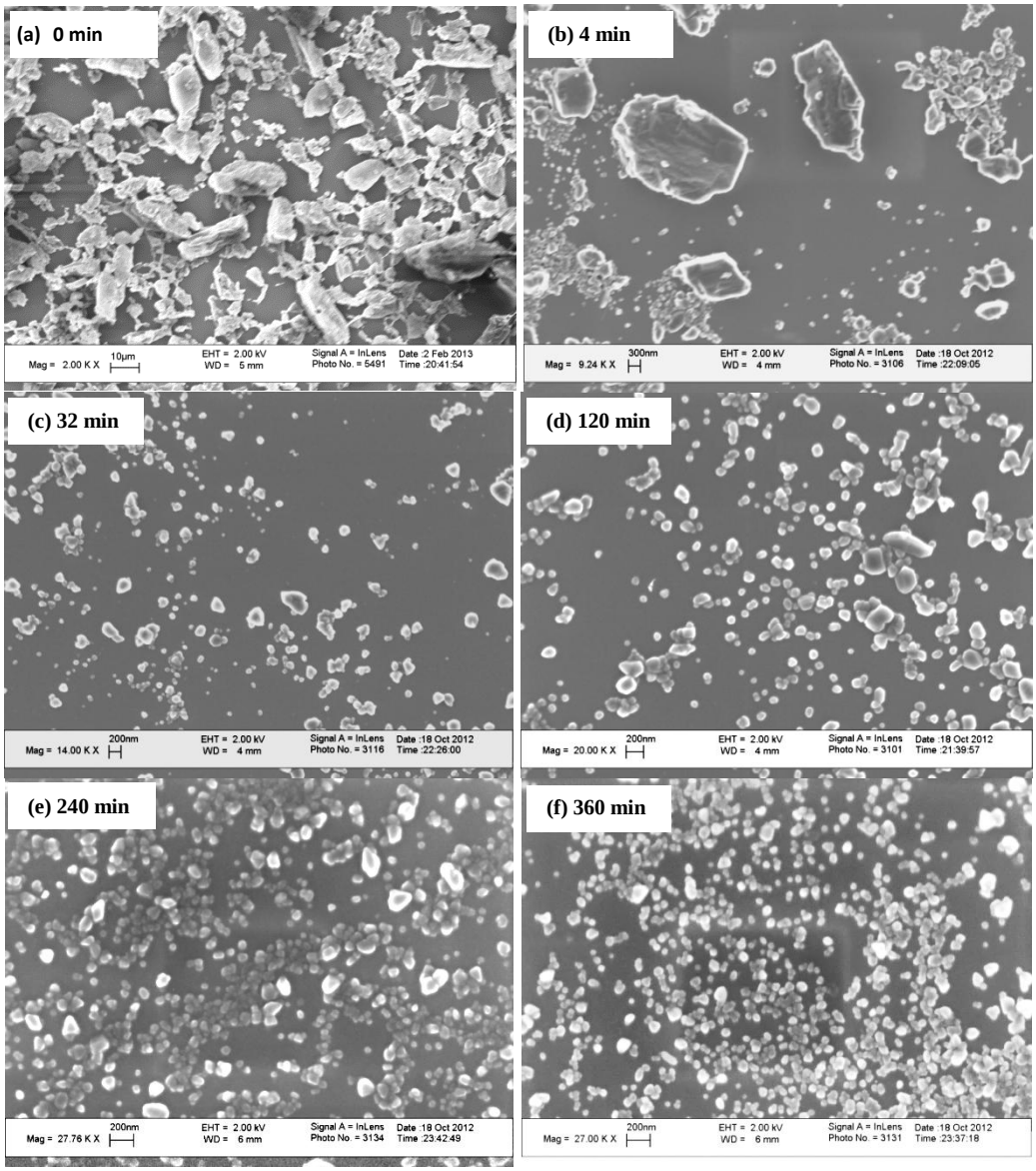

Figure 4.2 SEM images showing the evolution of GF particle size and morphology during Run 5: (a) particles before milling and after milling for (b) 4 min, (c) 32 min, (d) 120 min, (e) 240 min, and (f) 360 min. Run 5 refers to the use of 50 µm YSZ beads at the baseline process conditions (u = 11.7 m/s, c = 0.408, and Q = 126 ml/min). Initially, the GF particles have d_{50} = 21.85 ± 1.25 µm and d_{90} = 57.77 ± 4.35 µm.

Monotonic decrease of the particle size in Figure 4.1 as well as the similarity of the primary particle sizes from the SEM image and the particle size measured by

DLS suggest that particle breakage was the dominant mechanism and aggregation of the particles occurred at a smaller rate than the breakage in the presence of HPMC–SDS during most of the milling process. Hence, the commonly observed slow-down in Figure 4.1 is mainly attributed to the generation of smaller particles, which have a lower specific breakage rate (Bilgili et al., 2004, 2006), as milling continued. In addition, smaller particles especially nanoparticles are harder to capture by beads, and the intensity/number of stressing events due to compressions by the colliding beads may not be sufficiently high. Hence, the limiting size and the time to reach the limiting size are functions of both the material properties of the bead and the drug as well as the process parameters. Since 360 min was already too long, the author has not prolonged the milling to find the exact grinding limit in this study.

4.3.1.2 Effects of Bead Size on Wear and Product Contamination. Wear of the YSZ beads during milling can lead to undesirable contamination of the milled drug product with zirconium (Zr), the most abundant element in the beads. The toxicity of Zr is moderately low, as confirmed by both histological and cytological studies, and the average daily human uptake has been known to be as high as about 125 mg (Ghosh et al., 1992). However, its consumption has to be considerably reduced as Zr is prone to cross the blood brain-barrier and results in accumulation in the brain (Ghosh et al., 1992). GF suspensions milled for 360 min with the use of 800, 400, 200, 100, and 50 μm beads (Runs 1–5, respectively) were analyzed for elemental zirconium (Zr) level using ICP-MS. The elemental Zr levels, quantified as the mass ratio of Zr to milled drug in μg/g, were listed in Table 4.3. Juhnke et al. (2012) found

contamination with 100–500 µg/g Zr from three different grades of 100 µm YSZ beads when an undisclosed drug was wet-milled to 140 nm particles (unspecified time and batch size). In our study, Zr contamination was similar in order of magnitude, but reduced by a factor of 21.4 to 47 ± 1.2 µg/g when 50 µm beads were used as opposed to 800 µm beads, which accords well with the general trends in the previous bead wear studies in terms of the impact of bead size (Breitung-Faes and Kwade, 2008; Hennart et al., 2010).

Table 4.3 Power Applied per unit Volume of Slurry P_w, Specific Energy Consumption per unit Mass of Drug Suspension E^*, Zr Concentration in Milled Suspension per unit Mass of Drug for Runs 1–10

Run No.	Drug	Milling Time (min)	P_w (W/m^3)	E^* (MJ/kg)	Zr Level (µg Zr/g drug)	
					Average	SD
1	GF	360	3.13×10^5	2.40	1004	18.1
2	GF	360	2.92×10^5	2.24	832	5.9
3	GF	360	2.71×10^5	2.08	453	1.0
4	GF	360	2.29×10^5	1.76	307	5.8
5	GF	360	1.88×10^5	1.44	47	1.2
6	GF	120	2.32×10^5	0.59	36	0.4
7	GF	120	4.38×10^5	1.12	70	1.3
8	GF	120	5.00×10^5	1.28	83	3.8
9	IND	360	1.75×10^5	1.34	24	0.2
10	IND	120	5.00×10^5	1.28	56	2.6

4.3.1.3 Effects of Bead Size on Specific Energy Consumption and Applied Power. Figure 4.3 shows the specific energy consumption E^* and the average power applied per unit volume of slurry P_w for 360 min milling with various bead sizes. Both E^* and P_w were the lowest for 50 µm beads and they increased when larger beads were used. For a fixed rotor tip speed, more power is required to stir the

larger beads. It is well-known that at fixed milling conditions, the particle size decreases with an increase in the specific energy consumption or milling time (Kawatra, 2006). Interestingly, despite the resultant lower specific energy consumption at 360 min, 50 μm beads led to finer drug particles than the larger beads used (Figure 4.1). This finding implies that the specific energy consumption is not the sole or direct measure of particle fineness during wet media milling because only a small fraction of the specific energy is actually spent on deforming/breaking the drug particles, which is largely controlled by the microhydrodynamics of the bead–bead collisions, which is explored in *Section 4.3.1.4*.

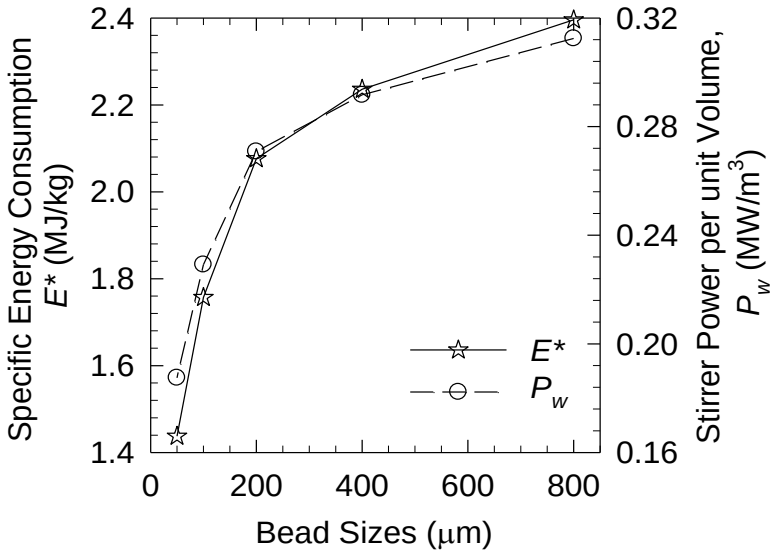

Figure 4.3 Specific energy consumption E^* and power applied by the mill stirrer per unit volume P_w for various bead sizes (Runs 1–5) during 360 min of milling at the baseline process conditions (u = 11.7 m/s, c = 0.408, and Q = 126 ml/min).

4.3.1.4 Microhydrodynamic Analysis of the Impact of Bead Size. To develop a fundamental understanding of the aforementioned bead size effects on the GF particle size, energy consumption, and bead wear, the microhydrodynamic parameters were

calculated and plotted as a function of bead size (Figure 4.4(a) and (b)). In general, smaller beads have a higher number concentration, which equals $6c/\pi d_b^3$, than larger beads for a given loading of the beads (constant c), and there are two major counteracting effects of the bead size. On one hand, the fluctuating motion of the smaller beads was less vigorous as indicated by the lower granular temperature θ. This effect can be explained by the decrease in the applied power P_w (see Table 4.4) and the increase in the bead number concentration. The slower fluctuating motion of the smaller beads was also reflected in the lower average bead oscillation velocity u_b, which led to development of a lower maximum contact pressure σ_b^{max}, i.e., lower stress intensity. Up to this point, one may argue that the drug particle breakage would be slower with the use of smaller beads as the aforementioned changes in the microhydrodynamic parameters do not favor particle breakage. On the other hand, the frequency of bead oscillations ν increased when smaller beads were used and tended to plateau below 200 μm bead size while the average frequency of drug particle compressions a increased dramatically and monotonically with a decrease in bead size due to the higher number concentration associated with the smaller beads. Obviously, this effect of the smaller beads, especially on a, favors faster breakage. The overall impact of the bead size is expected to be dependent upon which one of the two counteracting effects above is more pronounced and how they relate to the mechanical properties of the specific drug. This is why a universal explanation for the impact of bead size on all drugs appears to be elusive in terms of size on the breakage kinetics and final milled particle size. For example, due to the aforementioned

competing effects, an optimum bead size for maximum breakage rate can be found for a given set of milling conditions (e.g., Bilgili et al., 2004; Ghosh et al., 2011).

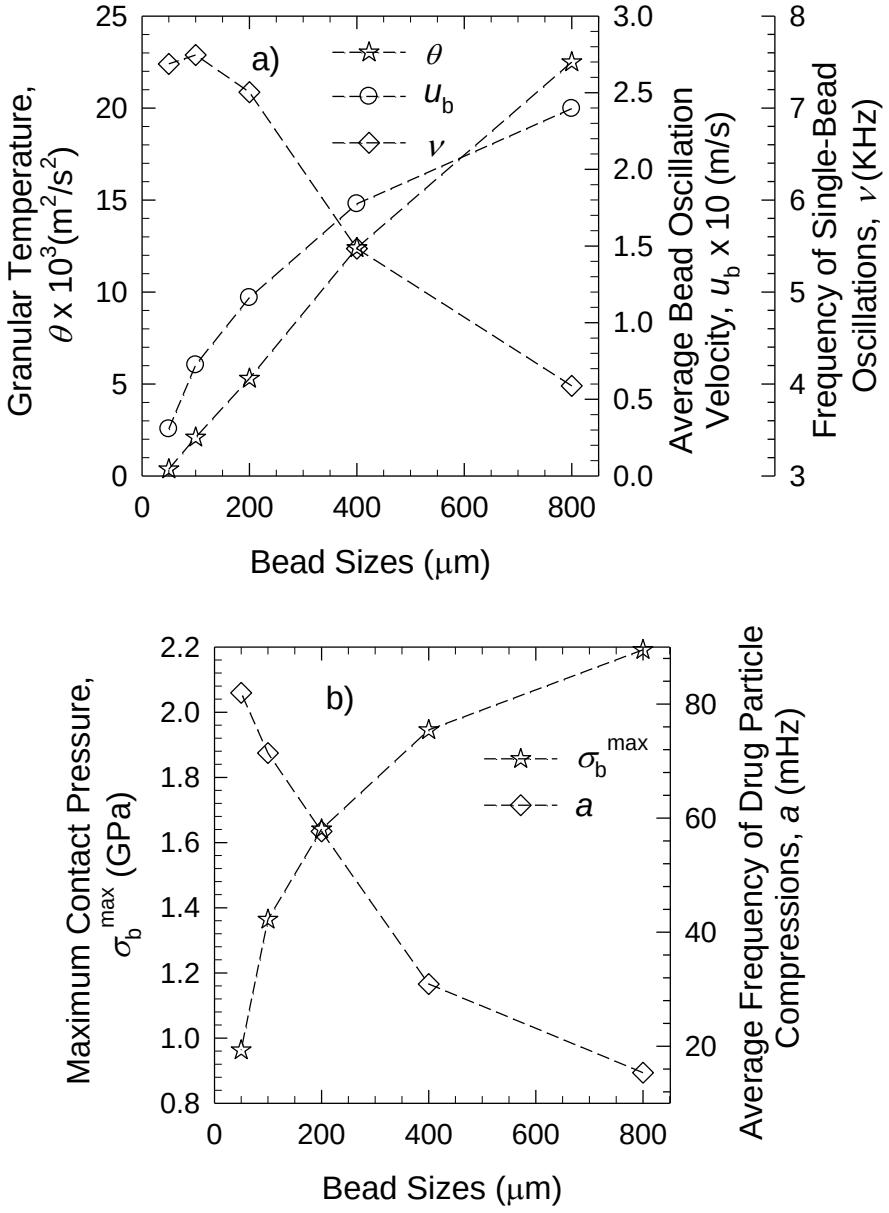

Figure 4.4 Effects of bead size on the microhydrodynamic parameters (Runs 1–5): (a) granular temperature θ, average bead oscillation velocity u_b, and frequency of single bead oscillations ν and (b) maximum contact pressure σ_b^{max} and average frequency of drug particle compressions a. Baseline process conditions: u = 11.7 m/s, c = 0.408, and Q = 126 ml/min.

In view of the above discussion, it may be difficult to predict the impact of bead size using a single microhydrodynamic parameter. Afolabi et al. (2014) successfully established a unified process correlation between the breakage kinetics and the milling intensity factor F for a *given drug–bead pair* in that an increase in F led to faster breakage of the drug particles; however, they did not investigate the impact of bead size. Table 4.4 shows that F exhibited a maximum with 200 μm beads while its value for 100 μm beads was slightly smaller. On the other hand, ν exhibited a maximum with 100 μm beads and a had the maximum with 50 μm beads. Considering that the size evolution for 50 and 100 μm beads were similar and faster than those of the coarser beads (refer to Figure 4.1), ν and a seems to explain the bead size impact better than F. This may also partly be due to the fact that while F can successfully explain the impact of process parameters (Afolabi et al., 2014), it may be inadequate to explain the impact of bead size, usually regarded as an equipment parameter in media milling. In summary, a holistic analysis of the results presented in Figures 4.1 and 4.4 and Table 4.4 suggests that an increased frequency of bead–bead collisions and drug particle compressions (the favorable effect of the smaller beads) dominates over the decreased stress intensity (the unfavorable effect of the smaller beads) in terms of their overall impact on the GF particle breakage rate. A possible explanation for the dominant effect associated with ν and a on the breakage kinetics emerges from a damage mechanism called contact fatigue for the drug particles when they are captured multiple times by the colliding beads: multiple, frequent compressions of the particles with low stress intensity can cause nucleation of permanent structural defects that lead to crack initiation; the growth of cracks

eventually results in particle fracture (Bilgili et al., 2006; Eskin et al., 2005b). Thus, it is likely that GF particles may break at lower stresses than their static fracture strength values, thus making their breakage rate more sensitive to the average frequency of drug particle compressions *a* than the maximum bead contact pressure σ_b^{max} under the specific milling conditions explored here. Further investigation is needed to elucidate these mechanisms, which is beyond the scope of this dissertation.

The observed reduction in Zr contamination with the use of smallest beads (50 µm) may be partly explained by the lower σ_b^{max} despite higher *a*. Smaller beads underwent less impactful collisions (lower σ_b^{max}) that resulted in less bead wear. On comparing σ_b^{max} for 800 µm (Run 1) and 50 µm (Run 5) beads (Table 5), σ_b^{max} was reduced by a factor of 2.3 upon the use of 50 µm beads, which could account for the reduced Zr contamination. Another possible explanation is that smaller beads may be more wear-resistant with a smaller number of inherently present surface/bulk defects.

Table 4.4 Power Applied per unit Volume of Slurry P_w, Measured Viscosity μ_L and Density ρ_L of the Milled Drug Suspensions, and the Microhydrodynamic Parameters (θ, u_b, ν, σ_b^{max}, a, and F) Calculated for Runs 1–10

Run No.	Milling Time (min)	P_w (W/m^3)	μ_L (mPa·s)	ρ_L (kg/m^3)	θ (m^2/s^2)	u_b (m/s)	ν (KHz)	σ_b^{max} (GPa)	a (Hz)	F (m$^{0.6}$/s$^{2.6}$)
1	360	3.13×10^{5}	5.97	1034	2.25×10^{-2}	2.40×10^{-1}	3.98	2.19	1.54×10^{-2}	8.37×10^{5}
2	360	2.92×10^{5}	5.73	1026	1.24×10^{-2}	1.78×10^{-1}	5.47	1.95	3.09×10^{-2}	1.33×10^{6}
3	360	2.71×10^{5}	5.51	1028	5.30×10^{-3}	1.16×10^{-1}	7.17	1.64	5.77×10^{-2}	1.76×10^{6}
4	360	2.29×10^{5}	5.63	1040	2.10×10^{-3}	7.24×10^{-2}	7.58	1.36	7.14×10^{-2}	1.52×10^{6}
5	360	1.88×10^{5}	5.64	1029	3.68×10^{-4}	3.06×10^{-2}	7.48	0.96	8.20×10^{-2}	8.62×10^{5}
6	120	2.32×10^{5}	5.84	1033	4.39×10^{-4}	3.34×10^{-2}	8.17	1.00	9.60×10^{-2}	1.08×10^{6}
7	120	4.38×10^{5}	5.64	1050	3.09×10^{-4}	2.81×10^{-2}	18.2	0.93	3.21×10^{-1}	2.43×10^{6}
8	120	5.00×10^{5}	5.56	1057	3.57×10^{-4}	3.01×10^{-2}	19.5	0.96	3.65×10^{-1}	2.92×10^{6}
9	360	1.75×10^{5}	5.64	1065	3.44×10^{-4}	2.96×10^{-2}	7.22	0.95	1.99×10^{-1}	7.44×10^{5}
10	120	5.00×10^{5}	5.74	1053	3.46×10^{-4}	2.97×10^{-2}	19.3	0.95	9.20×10^{-1}	2.66×10^{6}

4.3.2 Process Intensification

Developing an intensified milling process is important as it can increase the breakage rate, thereby achieving faster production of nanoparticles; however, such intensification can also cause a dramatic and unacceptable increase in bead wear and specific energy consumption, if not performed rationally. The results in *Section 4.3.1* suggest that the use of 50 μm beads led to the fastest GF breakage (similar to 100 μm beads) when an aggressive milling process with fully turbulent motion was carried out and that 50 μm beads were superior to 100 μm beads because the former led to lower bead contamination along with reduced specific energy consumption. The microhydrodynamic analysis and contamination results have elucidated the impact of the bead size and rationalized the use of 50 μm beads. Notwithstanding all the relatively favorable outcomes originated from the use of 50 μm beads, it took 240 min to obtain GF particles with a particle size of 100 nm at the baseline milling conditions (see Run 5 in Figure 4.1). Obviously, process intensification is required to reduce milling time to achieve sub-100 nm particle size. At this juncture, the question as to whether the intensification could cause a dramatic increase in bead wear and specific energy consumption must be answered.

4.3.2.1 Process Intensification Guided by the Microhydrodynamic Model.

Although milling intensity factor *F* may not be the best predictor of bead size impact (Section 4.3.1.4), it can successfully explain the impact of other milling parameters as established by Afolabi et al. (2014): an increase in *F* led to faster drug particle breakage for a given drug–bead pair (GF–YSZ beads), signifying a more intense

process. In view of this, the use of F in guiding the process intensification is deemed appropriate since the bead size was taken fixed (50 μm) based on the analysis in *Section 4.3.1*. As seen from Eq. (4.11), F strongly depends on bead volume fraction c, bead size d_b or radius R_b, and drug loading ε explicitly as well as all other process parameters including the rotor tip speed implicitly through the granular temperature θ, which is a monotone increasing function of the power consumption P_w (refer to Eq. (4.4)). A detailed analysis of Eqs. (4.4) and (4.11) suggests that a higher rotor tip speed leading to a higher P_w and/or higher bead loading may increase F, which accords well with the findings in Afolabi et al. (2014). In addition, it has been reported that an increase in suspension flow rate may lead to faster breakage (Monteiro et al., 2013; Stehr, 1984). Hence, the combination of higher rotor tip speed, higher bead loading, and higher suspension flow rate may allow for the development of the most intensified process.

In the preliminary intensifications experiments (Runs 6–8, Table 4.1), the baseline process (Run 5) was intensified by increasing the rotor tip speed, the bead loading, and the suspension flow rate sequentially one at a time while keeping all the other conditions the same. To avoid unnecessarily high damage to the beads, the study of breakage kinetics in Runs 6–8 was carried out with 120 min milling, as opposed to 360 min milling in the baseline process (Run 5). It should be noted that the maximum rotor tip speed allowed per our mill design is 4200 rpm (15.4 m/s); hence; a rotor tip speed of 14.7 m/s was used as the maximum to avoid stressing the mill close to the design limit. Similarly, a bead loading above 90% v/v of the milling

chamber (c = 0.543) results in pressure build-up and excessive heat generation; hence, 0.543 was taken as the maximum c value.

4.3.2.2 Impact of Process Intensification on the Breakage Kinetics. Figure 4.5(a) shows the temporal evolution of GF particles during 120 min milling in Runs 5–8. Compared to Run 5, the higher rotor tip speed in Run 6 led to faster particle breakage and consequently smaller particles, which is in line with previous studies (Afolabi et al., 2014; Ghosh et al., 2012). Unlike Run 5, sub-100 nm particle size (94 nm) was attained after 120 min in Run 6. Therefore, the high rotor tip speed of 14.7 m/s was used in the subsequent experiment (Run 7), where the bead volume fraction c was increased to 0.543. Due to the increase in bead loading, Run 7 exhibited faster breakage than Run 6, and 93 nm particle size was attained within 90 min of milling, which remained the same even after 120 min. Similar positive impact of the bead loading was reported previously (Afolabi et al., 2014; Sadler III et al., 1975). As compared with Run 7, the higher suspension flow rate (Run 8) resulted in faster breakage initially, but the difference diminished during prolonged milling, leading to particle sizes of 91 and 88 nm after 90 and 120 min (Figure 4.5(a)). Hence, the suspension flow rate had the smallest overall impact among all three parameters. As a most intensified process, Run 8 was close to the design limits of the milling equipment. Therefore, it is argued that a grind limit was attained for GF about ~90 nm particle size. Reproducibility was established by repeat milling experiments on Run 8. A particle size of 90 nm was attained after 120 min in the repeat experiment. Hence, the milling process was considered reproducible. SEM of the GF particles prepared in Run 8 (Figure 4.5(b)) shows the primary GF particles with an average

particle size of 74 nm. The small difference between the particles sizes measured via SEM and DLS could be due to the different basis for particle size distributions by the respective methods, i.e., number and intensity, different equivalent sphere size definitions, and the smaller sample size used in SEM.

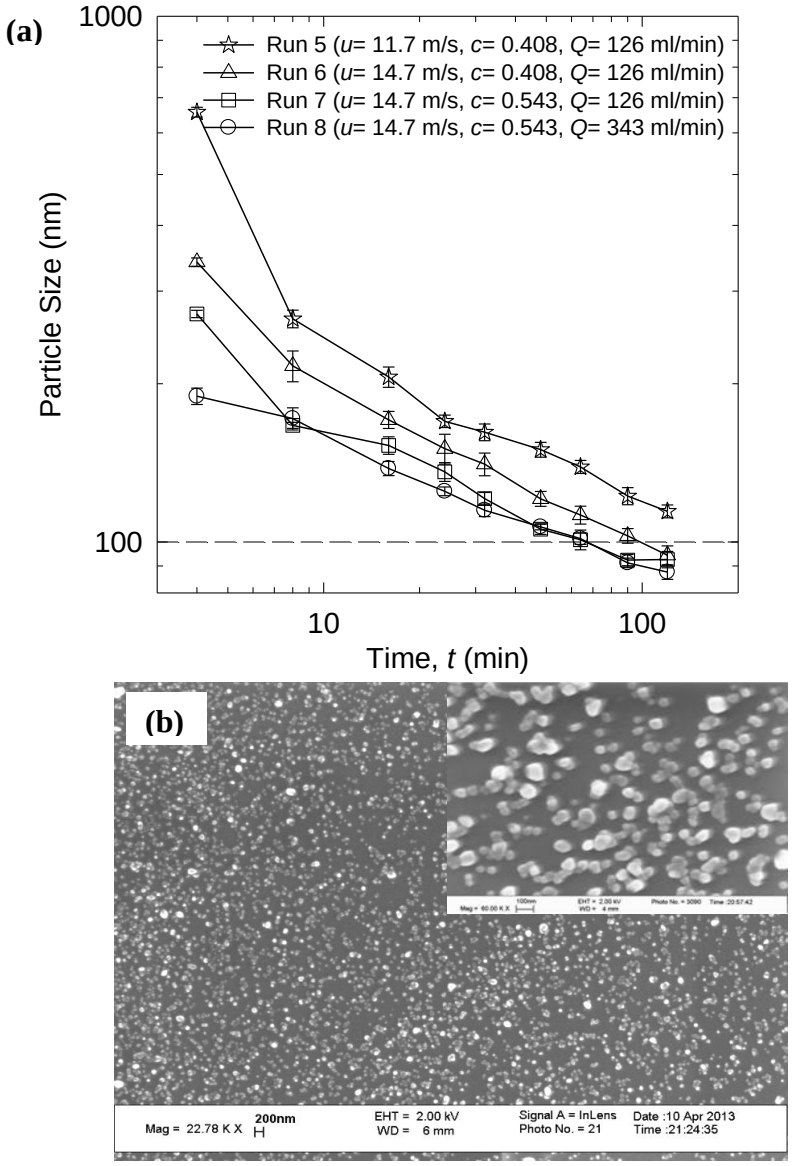

Figure 4.5 (a) Temporal evolution of GF particle sizes for Runs 5–8 with the use of 50 μm YSZ beads and (b) SEM images of the GF nanoparticles formed after 64 min milling at the intensified process conditions (Run 8: u = 14.7 m/s, c = 0.543, and Q = 343 ml/min). Inset SEM image shows magnified view of the GF nanoparticles. At t = 0 min, the GF particles have d_{50} = 21.85 ± 1.25 μm and d_{90} = 57.77 ± 4.35 μm.

4.3.2.3 Shorter Milling Experiments for the Preparation of ~100 nm Particles.

An overall analysis of the results for Runs 5–8 (Figure 4.5(a) and Table 4.3) suggests that a more intense milling process with 50 μm beads, signified by higher milling intensity factor F (Table 4.4), had also higher power consumption P_w and led to faster breakage. Although P_w was significantly higher in the intensified Runs 6–8 than in Run 5, the specific energy consumption E^*, which determines the electric utility cost, was lower because Runs 6–8 were carried out for a shorter time (120 min as opposed to 360 min). On the other hand, the intensification led to higher Zr contamination, which is still well below the 100–500 μg/g reported for YSZ beads in Juhnke et al. (2012). Hence, overall, the process intensification did not lead to a dramatic increase in the energy consumption and bead contamination although the GF breakage kinetics was enhanced and smaller GF particles were produced for a given milling time.

As compared with the aforementioned performance comparison, a more exacting comparison of the baseline and intensified processes would result if these processes were run so as to produce the same *desired product particle size* (e.g., 100 nm in the spirit of this dissertation). The milling time required to produce a GF particle size of 100 nm for Runs 5 and 8 was taken from the experimental data presented in Figures 4.1 and 4.5(a): 240 and 64 min, respectively. The milling time required to achieve ~100 nm was about 4 times lower when the intensified process (Run 8) was used as opposed to the baseline process (Run 5), which is attributed to the enhanced breakage kinetics upon intensification (see also Figure 4.5(a)). Hence, the intensified process (Run 8) can be run shorter to minimize specific energy consumption and media contamination for a desired product particle size. To prove

this point further, new milling experiments were performed under the same conditions of Runs 5 and 8, but at the *shorter milling times* that correspond to the attainment of a particle size of ~100 nm from Figure 4.5(a), i.e., 240 and 64 min, respectively. As would be expected from reproducible milling processes, these two additional experiments indeed led to final particle sizes of 101 nm (Run 5 at 240 min) and 100 nm (Run 8 at 64 min). The specific energy consumption E^* and the elemental Zr level were also determined for these shorter milling experiments. Although P_w was higher in Run 8 (5.00×10^5 W/m^3) than in Run 5 (1.88×10^5 W/m^3), E^* was lower in Run 8 (0.69 MJ/kg) than in Run 5 (0.96 MJ/kg) at the indicated times. The reduced energy consumption was explained by the shorter milling in Run 8. Second, the Zr levels for both Runs 5 and 8 at the indicated milling times were relatively low: 17 ± 0.3 µg/g, and 27 ± 1.2 µg/g, respectively. If the milling was carried out under Run 8 conditions for 120 min, then the Zr level would be higher, i.e., 83 ± 3.8 µg/g (Table 3.3). Hence, it is concluded that the enhanced breakage kinetics owing to process intensification allows for 4 times reduction in milling time and 28% reduction in the specific energy consumption when 100 nm particle size was desired with the relatively low media contamination (much lower than 100 µg/g).

Another potential concern with process intensification is that a more energetic milling process may lead to significant changes in the crystalline state of drugs. Figure 4.6 presents the XRD diffractograms of as-received GF, unmilled physical mixture (dried aqueous suspension with GF, HPMC, and SDS), as well as 240 min milled (baseline process, Run 5) and 64 min milled (intensified process, Run 8) GF suspensions after overnight drying. The characteristic peaks of GF appeared in all

diffractograms without a broad halo after milling, despite the contribution of amorphous HPMC in the samples. As compared to the as-received GF pattern, a slight reduction in the GF peak intensities in the unmilled physical mixture is seen, which is due to dilution and surface coverage of GF particles by HPMC (Hecq et al., 2005). On comparing Run 5 and Run 8 patterns with those of the physical mixture, the author notes that the peak positions remained the same despite a slight reduction in peak heights after milling, which can be attributed to defect formation and accumulation during milling (Monteiro et al., 2013). While XRD cannot detect minor amount of amorphous phase due to indirect inference, crystal orientation effects, and instrument-related intensity variations (Venkatesh et al., 2001), the aforementioned XRD results overall suffice to show that the crystalline state of GF was largely preserved after milling. Most importantly, the intensified process and the baseline process led to identical diffractograms, which demonstrates that the crystalline state of GF was not severely altered when the process intensification was carried for a shorter duration.

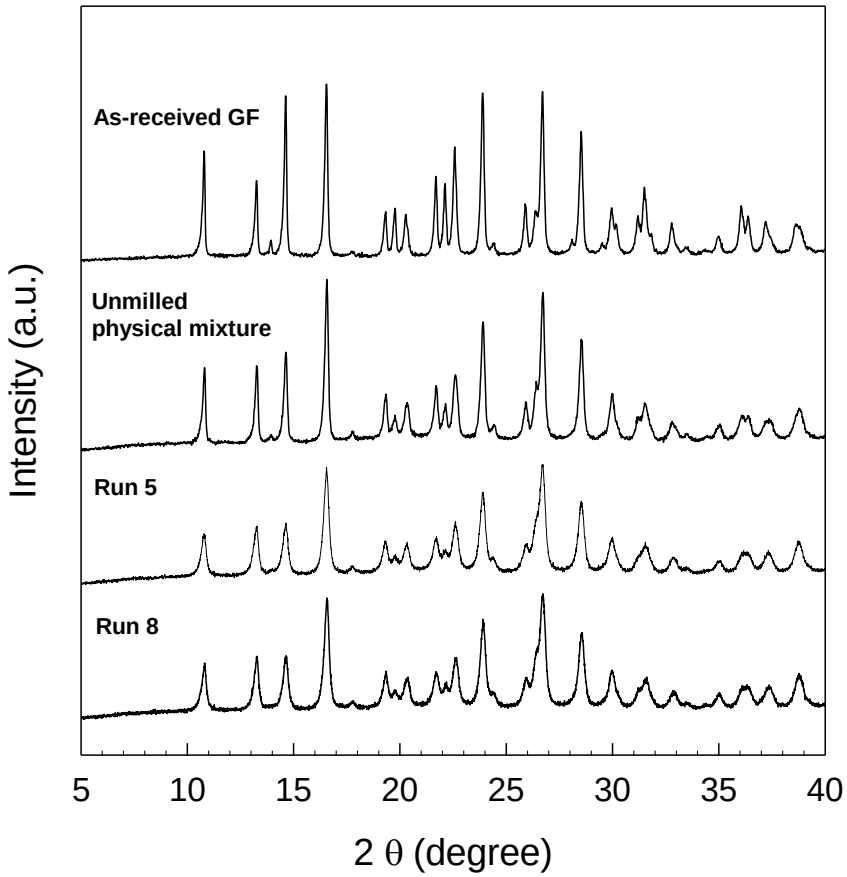

Figure 4.6 XRD diffractograms of as-received GF, unmilled physical mixture (dried aqueous suspension with GF, HPMC, and SDS), and dried, milled suspensions prepared with 50 μm YSZ beads. Run 5 refers to 240 min milling at the baseline process conditions (u = 11.7 m/s, c = 0.408, and Q = 126 ml/min), and Run 8 refers to 64 min milling at the intensified process conditions (u = 14.7 m/s, c = 0.543, and Q = 343 ml/min).

4.3.2.4 A Microhydrodynamic Analysis of the Intensified Process. Table 4.4 shows the calculated microhydrodynamic parameters for the baseline process (Run 5) and intensified process conditions (Runs 6–8). Here, the milling intensity factor F expressed in Eq. (4.11) was used to quantify the process intensification. At the higher rotor tip speed (Run 6), all microhydrodynamic parameters (θ, u_b, ν, σ_b^{max}, a, and F) increased as compared with those in Run 5, and F increased 1.3 times. These combined effects led to the aforementioned enhanced breakage kinetics, which allows

for shorter milling time required for a desired fineness of the drug particles. At the higher bead volume fraction c (Run 7), a counteracting effect was observed: θ, u_b, and σ_b^{max} were smaller, whereas ν, a, and F were greater as compared to Run 6 values (Table 4.4). In other words, the stress intensity decreased while the number of stressing events dramatically increased. The number concentration of the beads increased and the clearance between the beads decreased at higher c, both causing a dramatic increase in the bead–bead collisions and the average number of drug particle compressions per unit time (higher ν and a). On the other hand, despite the increase in the stirrer power P_w, higher number of inelastic bead–bead collisions and liquid-film squeezing events coupled with an increase in the effective drag coefficient R_{diss} led to greater energy dissipation, which explains smaller values of θ, u_b, and σ_b^{max}. Apparently, the extent of θ decrease was not sufficiently great to compensate for the significant positive impact of an increase in bead number concentration on ν and a, which was explained overall by higher F alone (see Afolabi et al., 2014), resulting in enhancement of the breakage kinetics presented in Figure 4.5(a). Finally, when a higher suspension flow rate was used in the most intensified process (Run 8), the *initial* breakage rate was further increased due to tighter residence time of the suspension in the mill chamber (Monteiro et al., 2013; Stehr, 1984) as well as the slight increase in P_w and all microhydrodynamic parameters. Overall, 3.4 times increase in F can be achieved with the most intensified conditions (Run 8) compared to the baseline conditions (Run 5), which in turn led to enhanced breakage kinetics, thus enabling shorter milling time (64 min) to attain ~100 nm particles with energy savings up to 28%, and low Zr contamination (27 µg/g).

4.3.3 Applicability of the Novel Process Intensification Method to Other Drugs

It is important to demonstrate the general applicability of the process intensification method on another drug. To this end, indomethacin (IND), another poorly water-soluble drug, was milled at the baseline process conditions (Run 9, 360 min) and the most intensified process conditions (Run 10, 120 min). The formulation was kept the same as that of GF. The breakage kinetics was first studied using the long milling times indicated above. Figure 4.7 shows the temporal evolution of IND particle sizes at both sets of conditions. Similar to the GF case, to produce 78 nm particles, the baseline process (Run 9) took almost 300 min, whereas the intensified process (Run 10) took only 48 min, which again proves that the process intensification can prepare sub-100 nm particle size much faster. The Zr contamination increased upon intensification, but still remained well below 100 μg/g (Table 3.3), and E^* slightly decreased despite a much higher P_w in the intensified process (Run 10). Table 4.4 shows the calculated microhydrodynamic parameters for Runs 9 and 10. The intensified process (Run 10) had a 3.6 times higher F than the baseline process condition (Run 9), and ν and a dramatically increased while other parameters did not change significantly upon intensification. Overall, the general trends and results were similar for both GF and IND, signifying the generality of the process intensification.

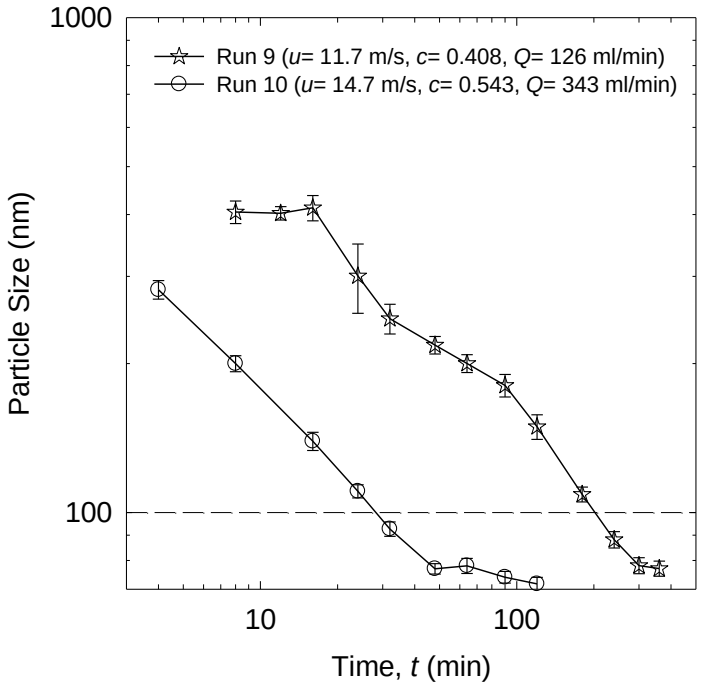

Figure 4.7 Temporal evolution of IND particle sizes milled with the use of 50 μm YSZ beads at the baseline process conditions (Run 9) and the intensified process conditions (Run 10). At t = 0 min, the IND particles have d_{50} = 56.56 ± 0.20 μm and d_{90} = 143.10 ± 1.28 μm.

To perform a more exacting comparison, additional milling experiments were also carried out to attain ~100 nm size under Runs 9 and 10 conditions. The milling time to achieve a 100 nm particle size was first estimated from the data in Figure 4.7 to be 201 min and 28 min for Runs 9 and 10, respectively, via piecewise cubic Hermite interpolating polynomials (MATLAB's pchip function). These values are only approximate as there are errors involved with any interpolation used, especially in the absence of a dense temporal data set. The particle sizes obtained from the additional milling experiments, after 201 min (Run 9) and 28 min (Run 10), were 106 and 105 nm, respectively, which confirms the success of the interpolation. XRD analysis of the dried suspensions also confirmed that crystalline state of milled IND

was not significantly altered (Figure 4.8). Zr level and specific energy consumption E^* were also determined after performing additional milling experiments with these shorter milling times. The E^* values were determined to be 0.75 MJ/kg and 0.30 MJ/kg, respectively, and the elemental Zr levels were 15 ± 1.1 µg/g and 18 ± 0.6 µg/g for Runs 9 and 10, respectively. Overall, a significant reduction in the milling time (7 times) was achieved upon intensifying the process, which allowed for about 60% energy savings while keeping the Zr contamination low. These trends appear to be similar to those for the milling of GF particles as discussed in *Section 4.3.2.3*, thus proving the general applicability of the process intensification method to multiple drugs.

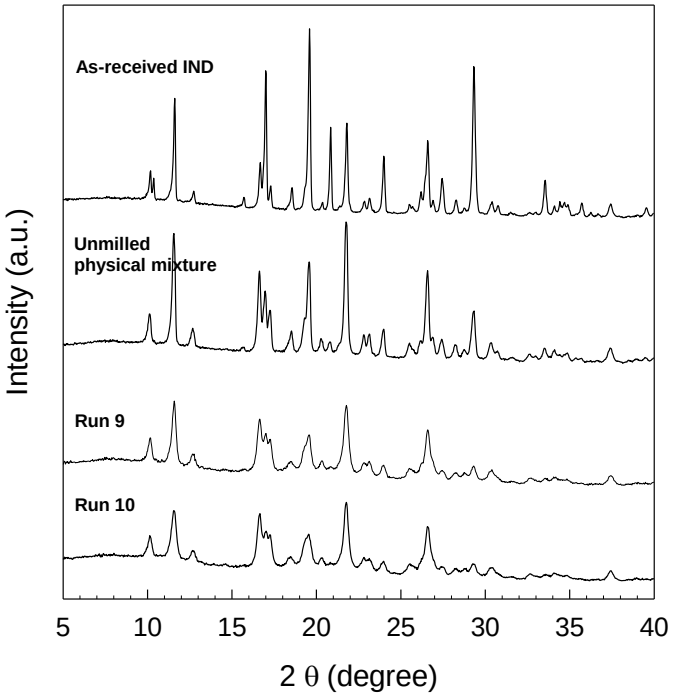

Figure 4.8 XRD diffractograms of as-received IND, unmilled physical mixture (dried aqueous suspension of IND, HPMC, and SDS), 201 min milled IND suspensions (Run 9) and 28 min milled IND suspension (Run 10) after drying. Run 9 refers to the use of 50 µm YSZ beads at the standard conditions: u = 11.7 m/s, c = 0.408, and Q = 126 ml/min. Run 10 refers to the use of 50 µm YSZ beads at intensified conditions: u = 14.7 m/s, c = 0.543, and Q = 343 ml/min.

4.4 Conclusions

This study has demonstrated, for the first time, the use of small beads in an intensified wet stirred media milling (WSMM) process for the faster production of sub-100 nm particles of two BCS Class II drugs while achieving reduced energy consumption and keeping Zr contamination low. A novel process intensification method based on microhydrodynamics has been used as opposed to ad-hoc trial-error. The grinding limit for two drugs has been proven to be in the sub-100 nm size domain. Provided that the WSMM process is sufficiently energetic with turbulent fluid motion in the mill, small (50 μm) beads can be very effective owing to their high number concentration for the same beads loading and small inter-bead distances despite generating relatively low bead contact pressures upon bead–bead collisions. This leads to a high number of drug particle compressions at lower specific energy consumption without causing significantly elevated wear, thus rendering process intensification feasible. The intensification can be realized by a simultaneous or sequential increase in rotor tip speed, bead loading, and suspension flow rate. Process intensification with small beads increases the breakage rate, thus allowing for reduction in milling time required for a desired product particle size. A shorter milling with the intensified process leads to reduced energy consumption and relatively low bead wear/contamination despite the higher mechanical power applied.

The model-guided intensification method empowers the WSMM for fast production of dense (>1% drug-loaded) suspensions of sub-100 nm drug particles, which can be incorporated into various solid and parenteral dosage forms upon drying and sterile filtration respectively with the ultimate goal of bioavailability

enhancement. Moreover, by following this general method, engineers can improve the existing WSMM processes in industry, which can lead to significant cycle time, energy, and cost savings, whether these processes are intended for sub-100 nm particles or not.

CHAPTER 5

A STUDY OF THE IMPACT OF POLYMER–SURFACTANT IN DRUG NANOPARTICLE COATED PHARMATOSE COMPOSITES ON DISSOLUTION PERFORMANCE

The preceding chapters have addressed the challenges associated with producing drug nanosuspensions with good physical stability (Chapter 2) and microhydrodynamic model-guided development of an intensified WSMM process with optimal bead size (Chapters 3 and 4). In order to preserve the nanosuspension stability over a long period of time and from a patient compliance perspective, these suspensions are usually dried into powders (nanocomposites), which are ultimately incorporated into final solid dosage forms such as tablets, capsules, sachets, etc. As discussed in Chapter 1, without a proper stabilizer formulation, drug nanoparticles can aggregate during the formation of nanosuspensions and their drying into nanocomposite powders, which in turn can cause inadequate bioavailability enhancement from nanoparticles and ensuing lack of therapeutic efficacy. No systematic and comprehensive study has been conducted to elucidate the impact of polymer concentration and molecular weight in the presence/absence of an ionic surfactant on the redispersion and drug dissolution from the nanoparticle-laden composites. The study presented in this chapter aims to fill this gap and develop an understanding of the relationships between the physical stability of drug nanosuspension, redispersion, and drug dissolution from the composites. Griseofulvin (GF) suspensions were wet-milled in a stirred media mill and then fluidized-bed dried–coated onto Pharmatose® carrier particles. Three grades of hydroxypropyl cellulose (HPC) having different molecular weights and sodium dodecyl sulfate (SDS) were used as non-ionic, adsorbing polymer and anionic surfactant,

respectively. HPC concentrations varied from 0.25% to 7.5% (w/w) for each polymer molecular weight/grade in the absence/presence of SDS. Laser diffraction, SEM, and UV spectroscopy were used to characterize the drug suspensions and the composites. Particle sizes of the redispersion samples were compared with those of the milled suspensions to assess drug nanoparticle recovery from the composites. Drug dissolution from the composites was measured using a USP II paddle apparatus. Besides elucidating the impact of HPC–SDS, this study also attempts to assess the validity of the commonly-held notion that the use of stable wet-milled drug nanosuspensions ensures fast redispersion and drug dissolution from the dried composites.

5.1 Materials and Methods

5.1.1 Materials

GF (BP/EP grade), a poorly water-soluble drug which belongs to Biopharmaceutics Classification System (BCS) Class II, was purchased from Letco Medical (Decatur, AL, USA) and used as-received in the wet media milling experiments. Three grades (SSL, SL, and L) of hydroxypropyl cellulose (HPC) with ~40, ~100, and ~140 kDa molecular weight, respectively, were donated by Nisso America Inc. (New York, NY, USA) and used as model non-ionic, cellulosic polymer which serves as a steric stabilizer during the milling and a film-former during the drying. SDS purchased from Sigma-Aldrich (Milwaukee, WI, USA) was used as a model anionic surfactant that acts as a wetting agent and electrostatic stabilizer. Its critical micelle concentration (CMC) in water is 8.2 mM (0.24% w/w) at ambient temperature (Kagotani et al., 2013). Pharmatose® DCL 11, a grade of lactose monohydrate

produced by DMV International (Netherlands), was used as the water-soluble carrier for fluidized bed drying–coating. Wear-resistant yttrium stabilized zirconia beads (Zirmil Y, Saint Gobain ZirPro, Mountainside, NJ, USA), with a median size of 430 μm, were used as the milling media.

5.1.2 Preparation of Suspensions via Wet Media Milling

The preparation of initial (feed) drug suspensions followed the same procedure used in Afolabi et al. (2014). The formulation of the suspensions is listed in Table 5.1. Drug concentration was kept at 10%. All concentrations reported here are with respect to deionized water (300 g). In the absence of SDS, only HPC SSL and L grades were investigated in the 0.25–7.5% (w/w) concentration range. At SDS loading of 0.05% (w/w), HPC concentrations varied from 0.25% to 7.5% (w/w) for all three grades. SDS concentration was purposefully selected well below the CMC so as to suppress the Ostwald ripening during the storage (Bilgili et al., 2016c; Knieke et al., 2013) because the aqueous solubility of GF is order of magnitude smaller below the CMC than that above the CMC (Rao et al., 1997).

A Microcer wet stirred media mill (Netzsch Fine Particle Technology, LLC, Exton, PA, USA) with 80 ml chamber was used to prepare the drug nanosuspensions. A peristaltic pump (Masterflex L/S Cole-Parmer Company, USA) recirculated the suspension between the holding tank and the milling chamber, while a screen with a 200 μm opening kept the zirconia beads in the milling chamber, but allowing the passage of the suspension. The feed suspensions prepared using a shear mixer (Fisher Scientific Laboratory Stirrer, Catalog no. 14-503, Pittsburgh, PA) were poured into

the holding tank and milled under the following conditions: bead loading of 50 ml (bulk), suspension flow rate of 126 ml/min, and rotor speed of 3200 rpm corresponding to a tip speed of 11.7 m/s. Both the milling chamber and the holding tank were equipped with a chiller (Advantage Engineering, Greenwood, IN, USA) to keep the suspension below 35 °C. The aforementioned processing parameters were selected based on Bilgili and Afolabi (2012). The particle sizes of the final suspensions (after 80 min milling) were determined, and the suspensions were refrigerated at 8 °C for one day before coating onto Pharmatose®.

5.1.3 Fluidized Bed Drying–Coating of Drug Suspensions onto Pharmatose®

The suspensions prepared by wet media milling, also referred to as precursor suspensions, were sprayed onto Pharmatose® carrier particles in a conventional bench-top fluidized bed processor (Mini-Glatt 5, Glatt Air, Ramsey, NJ, USA) with the top spray configuration. The operating conditions were selected based on Bhakay et al. (2013). 100 g Pharmatose® powder with d_{50} and d_{90} values of 123.6 μm and 195.2 μm was charged in the product bowl and fluidized at an inlet air pressure of 0.4–0.5 bar. After the powder was fluidized, the heater and suspension spray were turned on. About 200 g milled drug suspension was pumped through a peristaltic pump (Masterflex L/S Cole-Parmer Company, USA) at a constant rate of 0.6 ml/min. Sedimentation of the particles was prevented by constant stirring of the suspension during the spraying process. The suspensions were atomized through a bi-fluid nozzle with 0.5 mm tip diameter at an atomization air pressure of 1 bar. The fluidizing air temperature was set at 70 °C. The coated powder continued to fluidize and dried for

10 min after all suspension was sprayed. The coated powders (composites) were then tested for particle size and morphology, and used in redispersion–dissolution tests.

5.1.4 Particle Size Determination

Particle size distributions (PSDs) were measured using laser diffraction (LS 13 320, Coulter Beckman, Brea, CA, USA). A polarized intensity differential scattering obscuration water optical model was employed. It was maintained between 40% and 50% while the obscuration was maintained below 8% for all measurements. PSD was computed by the software using the Mie scattering theory. Refractive index values are 1.65 for GF and 1.33 for the measurement medium (deionized water). Prior to the size measurement, ~2 ml samples of the milled suspensions were taken from the outlet of mill chamber and diluted with 8 ml solution of water, HPC, SDS, or HPC–SDS depending on the stabilizer(s) used in the milling experiment. The particle size of the suspensions was also measured at the end of the drying process (about 30 h after milling) to assess aggregation in the suspensions during the storage–coating period, and this size was referred to as the size of the milled suspension before redispersion.

The particle size of the composite particles produced by the fluidized bed drying was measured by a Rodos/Helos laser diffraction system (Sympatec, NJ, USA) based on Fraunhofer theory. Approximately 1 g of the composites was placed on the sample chute of the Rodos dispersing system. As the sample chute was vibrated to feed the sample at a 50% setting, a dispersion pressure of 0.1 bar was imposed to suck in falling powder through the sample cell of the Rodos.

5.1.5 Determination of Drug Content in the Composite Powders

Maximum theoretical amount of GF in 100 mg composites is estimated to be 15.4 mg disregarding losses during the coating (Run 1). GF solubility in methanol is 3 mg/ml (Bhakay et al., 2013). 100 mg of the nanocomposite particles was dissolved in 20 ml of methanol and sonicated for 30 min to ensure that all GF had dissolved in methanol. The Pharmatose® particles do not dissolve in methanol and remain suspended. After sonication, they were allowed to sediment overnight, and an aliquot of 100 µl was taken from the supernatant. This aliquot was diluted to 10 ml methanol. The absorbance of all the samples was measured at the wavelength of 292 nm by Ultraviolet (UV) spectroscopy in a UV Spectrophotometer (Agilent, Santa Clara, CA, USA). Six replicates from each composite formulation were used to calculate the mean drug content along with the percent relative standard deviation (RSD).

5.1.6 Redispersion of the Drug Composites

The redispersion method was selected based on previous work (Bhakay et al., 2014a; Bhakay et al., 2013). 1 g of the composites was weighed and dispersed in 30 ml deionized water for 2 min. This early time point was purposefully selected because of its good discriminatory power for different formulations. The samples were paddle-stirred with a laboratory stirrer (CAT R18, Scientific Instrument Center Limited, Winchester, UK) at 200 rpm for 2 min to determine if the GF drug particles are redispersed from the composites fast. The maximum amount of drug that can dissolve in water during the redispersion test is very small (e.g., about 0.2% of GF particles for Run 1). Approximately, 0.5 ml aliquot of redispersed sample was taken while stirring

and its particle size was measured. HPC, SDS, and Pharmatose® are all water-soluble. Hence, unless otherwise indicated, the particle sizes obtained from the laser diffraction were mainly the sizes of GF particles and their clusters. The redispersion response in an aqueous solution of SDS at 0.05% was also studied for formulations with HPC alone. All redispersion tests were done thrice for each formulation and the average with standard deviation was reported.

5.1.7 Dissolution Test

Drug dissolution from the composites was determined via a Distek 2100C dissolution tester (North Brunswick, NJ, USA) according to the USP II paddle method. The dissolution medium was 1000 ml deionized water that was maintained at 37 °C, and a paddle speed of 50 rpm was used for all runs. Deionized water allowed for good discrimination of different formulations under non-sink conditions. The composites were weighed equivalent to a dose of 8.9 mg of GF. They were poured into the dissolution medium and 4 ml samples were taken out manually at 1, 2, 5, 10, 20, 30, and 60 min. These aliquots were filtered with a 0.1 μm PVDF membrane type syringe filter before UV spectroscopy measurements to minimize any confounding effect of the undissolved drug aggregates. The amount of GF dissolved was measured by UV spectroscopy at a wavelength of 296 nm. Deionized water was used as the blank.

5.1.8 Scanning Electron Microscopy (SEM)

SEM images of the milled drug particles, Pharmatose® particles, composite particles, and the dried sample after redispersion were taken with LEO 1530 SVMP (Carl

Zeiss, Inc., Peabody, MA, USA). For Pharmatose® particles and the composite particles, a carbon tape was placed on an SEM stub, the particles were then placed on the carbon tape. An aliquot of 1 ml drug suspension sample was diluted to 30 ml de-ionized water, vortex-mixed for 30 s, and mounted on a silicon chip (Ted Pella, Inc., Redding, CA, USA). For redispersed samples, after 2 min paddle stirring, a drop sample was mounted on a silicon chip. The stubs with liquid sample were put in a desiccator and allowed to dry overnight under vacuum. All samples were then sputter coated with carbon using BAL-TEC MED 020 (BAL-TEC AG, Balzers, Switzerland) prior to imaging.

5.2 Results and Discussion

5.2.1 Formation of Drug Nanoparticles via Wet Stirred Media Milling

Table 5.1 presents the formulations of the milled drug (GF) suspensions. The formation of GF nanoparticles was first explored in the absence of any stabilizers (Run 1) and in the presence of an anionic surfactant, SDS (Run 2). These two formulations were used as baseline to assess the impact of various stabilizers and physical stability of the resulting suspensions. The impact of HPC concentration was then studied in the absence (Runs 3–12) and presence of 0.05% SDS (Runs 13–27) using SSL, SL, and L grades of HPC with MW of ~40, ~100, and ~140 kDa, respectively.

Table 5.1 Formulations of the Milled Drug Suspensions and Drug Content of the Composites

Run No.	HPC Grade	Suspension		Composite
		HPC (% w/w)[a]	SDS (% w/w)[a]	Average, RSD (%w/w, %)[b]
1	-	-	-	15.2, 5.95
2	-	-	0.05	13.8, 7.28
3	SSL	0.25	0	15.0, 8.08
4	SSL	1	0	14.9, 3.36
5	SSL	2.5	0	12.5, 5.74
6	SSL	5	0	14.0, 4.61
7	SSL	7.5	0	12.5, 5.19
8	L	0.25	0	11.3, 1.72
9	L	1	0	12.3, 2.16
10	L	2.5	0	13.7, 1.12
11	L	5	0	11.7, 2.09
12	L	7.5	0	10.3, 4.67
13	SSL	0.25	0.05	12.1, 3.17
14	SSL	1	0.05	13.2, 0.16
15	SSL	2.5	0.05	13.5, 6.21
16	SSL	5	0.05	12.8, 1.31
17	SSL	7.5	0.05	11.6, 5.02
18	SL	0.25	0.05	13.5, 5.64
19	SL	1	0.05	11.5, 5.71
20	SL	2.5	0.05	11.3, 5.95
21	SL	5	0.05	10.6, 3.21
22	SL	7.5	0.05	11.2, 6.30
23	L	0.25	0.05	12.1, 4.08
24	L	1	0.05	14.3, 0.69
25	L	2.5	0.05	11.9, 2.88
26	L	5	0.05	12.0, 2.29
27	L	7.5	0.05	9.30, 6.43

[a] w/w with respect to deionized water in the suspension.
[b] w/w with respect to dried composite.

Figure 5.1 presents the PSD of the milled suspensions for Runs 1 and 3–12, where HPC was the sole stabilizer and its concentration varied from 0 to 7.5% for both SSL and L grades. When no stabilizer was used (Run 1), a coarse suspension with particles in the size range of 1–60 μm was formed (Figure 5.1), as measured by

laser diffraction. On the other hand, SEM images show that the as-received GF particles (Figure 5.2(a)) were broken into 50–400 nm primary nanoparticles (Figure 5.2(b)) upon milling in Run 1. Clearly, Figures 5.1 and 5.2 suggest that the nanoparticles formed upon breakage of the micron-sized GF particles severely aggregated due to high attractive inter-particle forces (van der Waals, hydrophobic forces, etc.). Similar observations were reported by Bilgili et al. (2016c) and Ain-Ai and Gupta (2008) for several wet-milled, poorly water-soluble drugs.

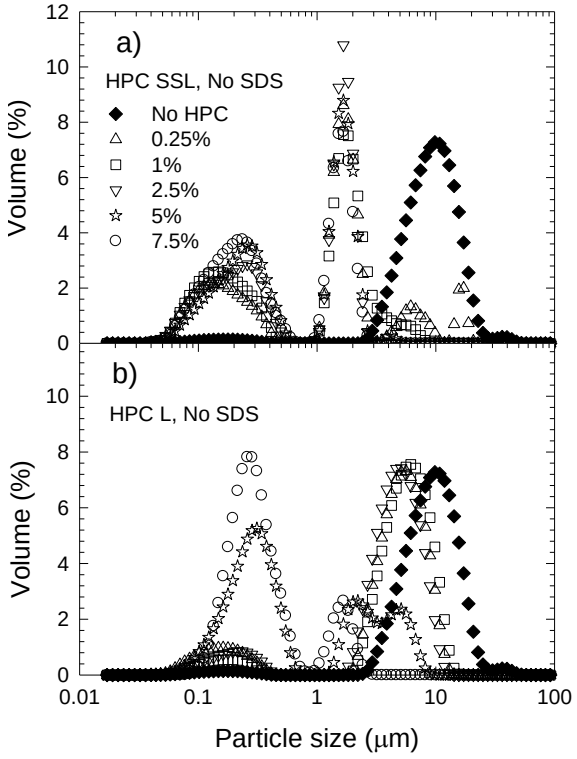

Figure 5.1 Volume frequency distributions of various milled drug suspensions containing HPC with different molecular weights: (a) 40 kDa (SSL grade, Runs 3–7) and (b) 140 kDa (L grade, Runs 8–12). Run 1 had no stabilizers.

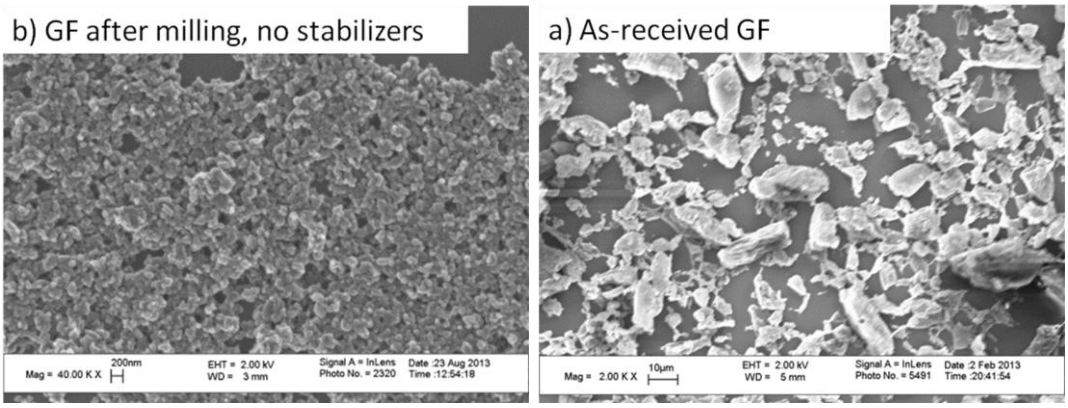

Figure 5.2 SEM images of drug (GF) particles: (a) before milling and (b) after milling (Run 1, without HPC/SDS).

When HPC (SSL and L grades) was used as the sole stabilizer especially at a higher concentration, the PSDs shifted to the finer particles, while showing bi-modality due to presence of aggregates (Figure 5.1). Although smaller aggregates were formed upon use of lower MW HPC (SSL grade) as compared with L grade, even 7.5% HPC SSL was insufficient to stabilize GF nanoparticles. Figure 5.3 shows PSDs for all formulations with 0.05% SDS (below the CMC of SDS). When SDS was used alone at this low concentration (0.05%, Run 2), a tri-modal PSD was observed. This indicates that 0.05% SDS alone was not able to stabilize the GF nanoparticles. A fine, uni-modal PSD was attained when HPC and SDS were used in combination. The use of HPC–SDS has synergistic stabilizing effects, as demonstrated on multiple drugs (Bilgili et al., 2016c). An increase in HPC concentration led to finer particles and narrower PSDs for the SL and L grades, whereas the PSD was less sensitive to the concentration for the SSL grade. SDS acts as a wetting agent, allowing for effective deaggregation of the milled particles and it may also impart some electrostatic stabilization, whereas non-ionic HPC adsorbs on GF particles and

sterically stabilize the nanoparticles (Bilgili and Afolabi, 2012). An increase in cellulosic polymer concentration is known to increase adsorption onto drug particles, thus offering enhanced steric stability via thicker adsorbed polymer layer (Knieke et al., 2013; Sepassi et al., 2007).

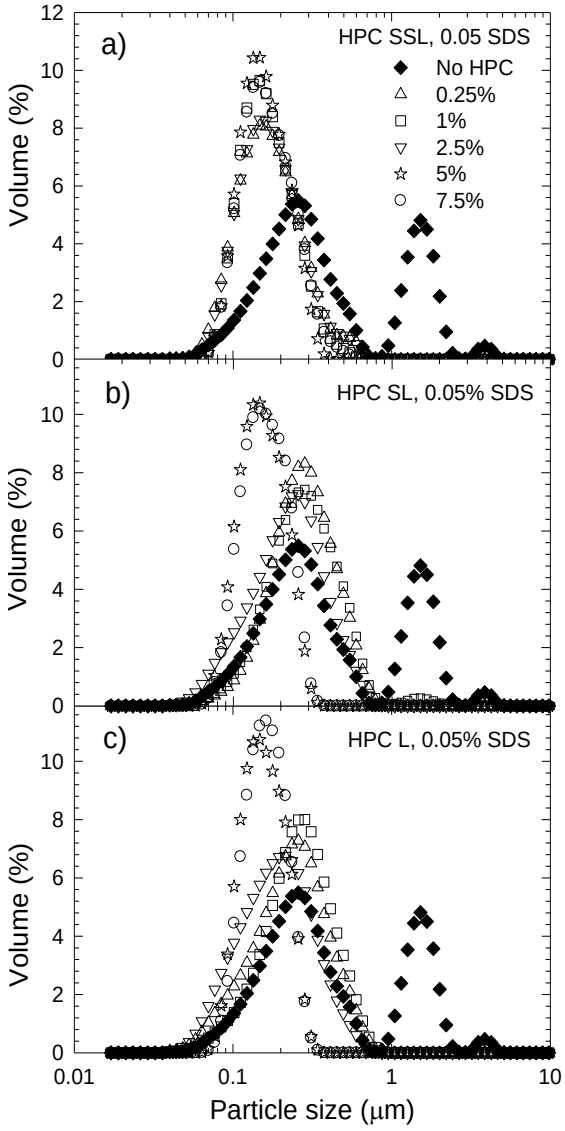

Figure 5.3 Volume frequency distributions of various milled drug suspensions containing 0.05% SDS and HPC with different molecular weights: (a) 40 kDa (SSL grade, Runs 13–17), (b) 100 kDa (SL grade, Runs 18–22), and (c) 140 kDa (L grade, Runs 23–27). Run 2 had only 0.05% SDS.

The reproducibility of wet stirred media milling of GF and other BCS Class II drugs has been established in several studies (Bilgili and Afolabi, 2012; Li et al., 2015b). In this study, the d_{50} and d_{90} values for the repeat of Run 20 were 0.236 ± 0.001 and 0.435 ± 0.002 μm, respectively. Compared to d_{50} = 0.230 ± 0.001 and d_{90} = 0.443 ± 0.001 μm in Run 20, the deviations in the repeated milling experiment were less than 3%. Also, as will be shown below, for most formulations, the suspensions did not exhibit a drastic shift in particle sizes after 30 h storage (before redispersion samples vs. after milling samples), and any variations could be partly attributed to the handling–sampling of the aggregated suspensions following refrigerated storage.

5.2.2 Formation of Drug Composites via Fluidized Bed Drying of the Precursor Drug Suspensions

The GF suspensions produced by milling were sprayed onto Pharmatose® carrier particles (see Figure 5.4(a)), which form the core of the composite particles, in a fluidized bed drier. Throughout the rest of the dissertation, all composites are labeled based on the formulation of the respective precursor drug suspension that was used as the feed during the drying. The mean drug content was in the range of 9.3–15.2% due to different stabilizer concentrations in the milled suspensions and variable drug/Pharmatose® losses to the filters and side walls of the drier (Table 5.1). Most importantly, the composite powders exhibited pharmaceutically acceptable content uniformity: RSD was less than 6% for most formulations. Upon atomization, droplets of the milled suspensions impinged on Pharmatose® carrier particles and dried, leading to the formation of a single coated composite particle (Figure 5.4(b)), which embeds GF nanoparticles on its shell (Figure 5.4(c)). Some SEM images (not shown

for brevity) indicated presence of granules, i.e., doublets, triplets, etc. at higher HPC L concentration, which is quantified by the presence of much coarser composite particles (see Table 5.2) than the uncoated Pharmatose® particles with d_{50}: 123.6±0.86 μm, d_{90}: 195.2±4.79 μm. The larger composite particles prepared at higher HPC concentration, especially with the use of L grade, can be explained by higher viscosity of the respective drug suspensions and coarser droplets formed upon atomization as well as higher coalescence probability of wetted Pharmatose® particles (Bhakay et al., 2013; Bilgili et al., 2011). SEM images of the composite particle surfaces with different suspension formulations were shown in Figure 5.4(c)–(g). Drug aggregates as well as primary nanoparticles encapsulated in the HPC film can be observed on the composite surface.

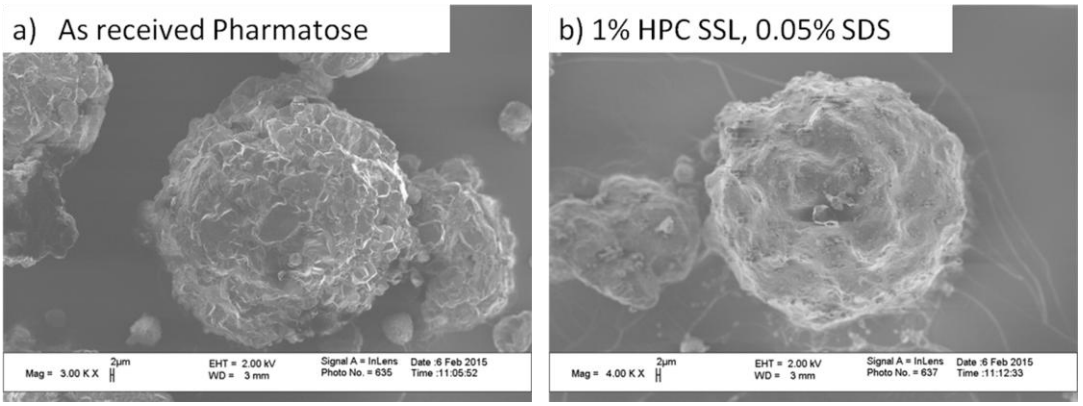

Figure 5.4 SEM images of the surfaces of (a) as-received Pharmatose® particles as well as the composites prepared using (b) 1% HPC SSL, 0.05% SDS (Run 14), (c) 1% HPC SSL, 0.05% SDS (Run 14, higher magnification), (d) 1% HPC SSL (Run 4), (e) 5% HPC SSL, 0.05% SDS (Run 16), (f) 1% HPC L, 0.05% SDS (Run 24), and (g) 5% HPC L, 0.05% SDS (Run 26). (Continued)

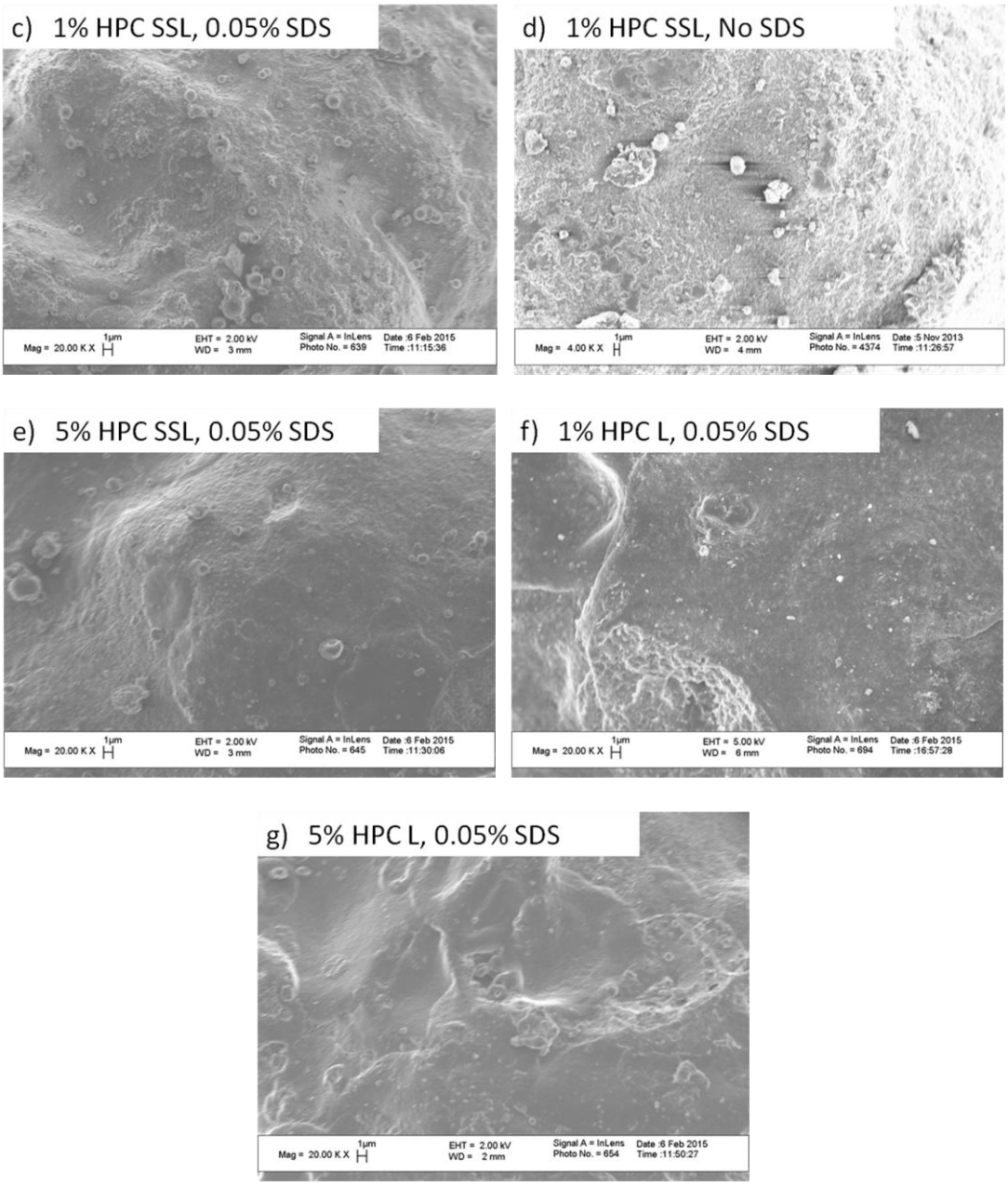

Figure 5.4 (Continued) SEM images of the surfaces of (a) as-received Pharmatose® particles as well as the composites prepared using (b) 1% HPC SSL, 0.05% SDS (Run 14), (c) 1% HPC SSL, 0.05% SDS (Run 14, higher magnification), (d) 1% HPC SSL (Run 4), (e) 5% HPC SSL, 0.05% SDS (Run 16), (f) 1% HPC L, 0.05% SDS (Run 24), and (g) 5% HPC L, 0.05% SDS (Run 26).

Table 5.2 Particle Sizes of the Composites Prepared using Various Precursor Suspensions

HPC Concentration (% w/w), Grade	Drug Composite Particle Size (μm)			
	Without SDS		With 0.05% SDS	
	d_{50}±SD	d_{90}±SD	d_{50}±SD	d_{90}±SD
0%, –	127.8±0.67	201.8±3.61	130.1±2.34	199.1±6.72
0.25%, SSL	123.2±0.75	187.7±2.58	123.4±2.17	199.0±8.25
1%, SSL	124.1±2.33	193.2±3.08	124.6±1.79	196.4±4.36
2.5%, SSL	124.6±3.94	199.4±7.63	127.4±3.24	201.0±5.85
5%, SSL	131.2±2.43	207.7±7.49	128.6±1.96	202.8±4.16
7.5%, SSL	152.9±5.53	320.5±25.2	145.3±0.52	229.1±6.09
0.25%, L	126.4±2.02	192.7±2.20	139.2±3.00	222.6±12.5
1%, L	137.7±0.96	212.5±1.93	154.3±3.45	236.4±7.93
2.5%, L	163.0±0.29	249.8±6.17	187.2±7.21	381.5±24.6
5%, L	238.4±2.71	436.0±26.5	251.1±6.55	428.8±18.4
7.5%, L	289.8±24.1	442.7±18.5	260.7±0.61	502.2±22.3

5.2.3. Recovery of the Drug Nanoparticles from the Composite Particles in Deionized Water

The composite particles produced via fluidized bed drying–coating of precursor GF suspensions onto Pharmatose® were redispersed in water to study the recovery of GF nanoparticles via gentle paddle stirring for 2 min. Figure 5.5 presents the particle size statistics of drug particles right after milling, before redispersion (30 h storage after milling), and after redispersion in deionized water for formulations without stabilizers and those with HPC alone having different MWs. Figure 5.5 shows that the particle sizes after the redispersion test were much greater than the drug particle sizes after milling and 30 h storage. Although there were some micron-sized particles in the milled suspensions (Figure 5.1), the clusters in the redispersed suspension samples had particle sizes above 10 μm (Figure 5.5), which are all larger than those in the milled suspensions, indicating poor redispersibility of the composites and potentially formation of large clusters during the drying. In fact, it is likely that the shell of some

composite particles did not break at all, keeping the core (Pharmatose®) intact for low HPC concentrations, and that coarse clusters might have appeared after redispersion. A higher polymer concentration (especially at and above 2.5%) led to smaller clusters after redispersion for both HPC grades.

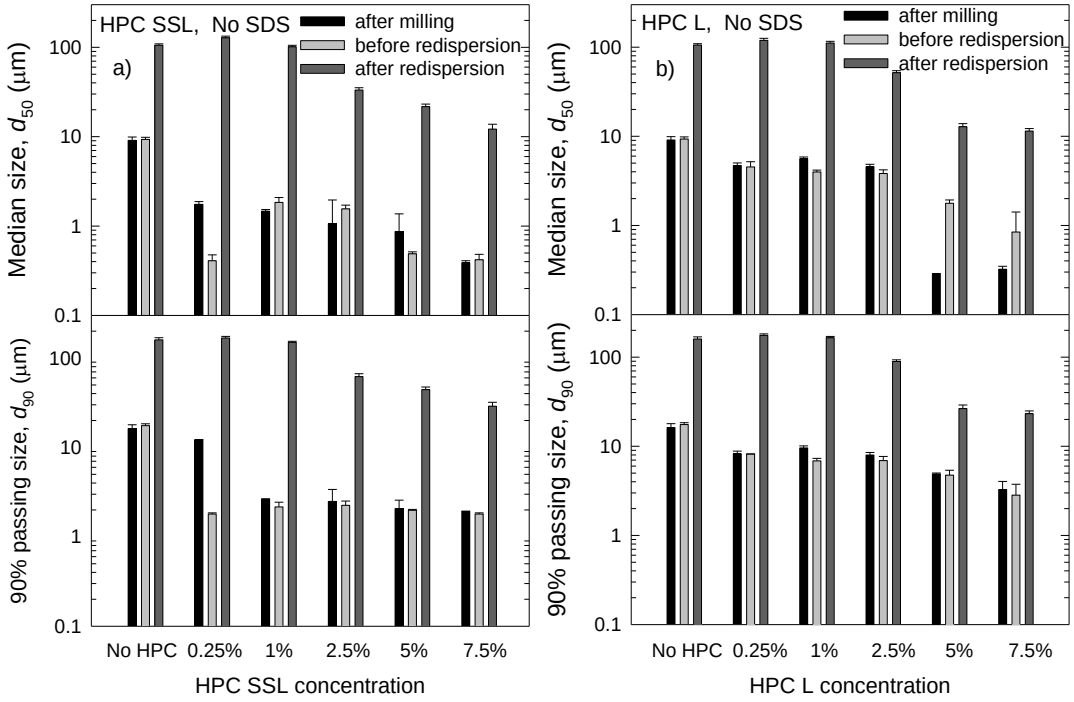

Figure 5.5 Particle sizes of the composites prepared using various precursor suspensions with (a) HPC SSL (40 kDa, Runs 3–7) and (b) HPC L (140 kDa, Runs 8–12) after 2 min redispersion in deionized water in comparison to the particle sizes of the suspensions after milling and after 30 h storage (before redispersion). Run 1 had no stabilizers.

A specific example of the poor redispersion is the composite particles with no stabilizer in the suspension (Run 1), which had the median size of 127.8 µm (Table 5.2). After redispersion in deionized water, the median size was 105.5 µm, whereas the milled suspension had GF median size of 9.1 µm (Figure 5.5). SEM images of the redispersed suspension samples following drying are shown in Figure 5.6. Figure

5.6(a) confirmed the aforementioned poor redispersion: the Run 1 composite particles slightly shrunk upon partial dissolution of Pharmatose® and the coated layer (shell structure) broke into large pieces. The poor redispersion is most likely due to hard aggregates formed upon removal of water during the drying; solid bridges could have formed upon re-crystallization of the small amount of dissolved GF. The hard aggregates might not have allowed for proper shell breakage and or full dispersion into primary GF nanoparticles. Moreover, without having any stabilizers, Run 1 composite particles are covered solely by hard aggregates of hydrophobic GF particles, which may have slowed down water penetration into the core. During the redispersion test, water penetrates through the pores in the shell of the composite particles and dissolves the Pharmatose® core, which is largely inhabited by the poor wettability of Run 1 composite, leading to the coarse clusters (Figure 5.6(a)).

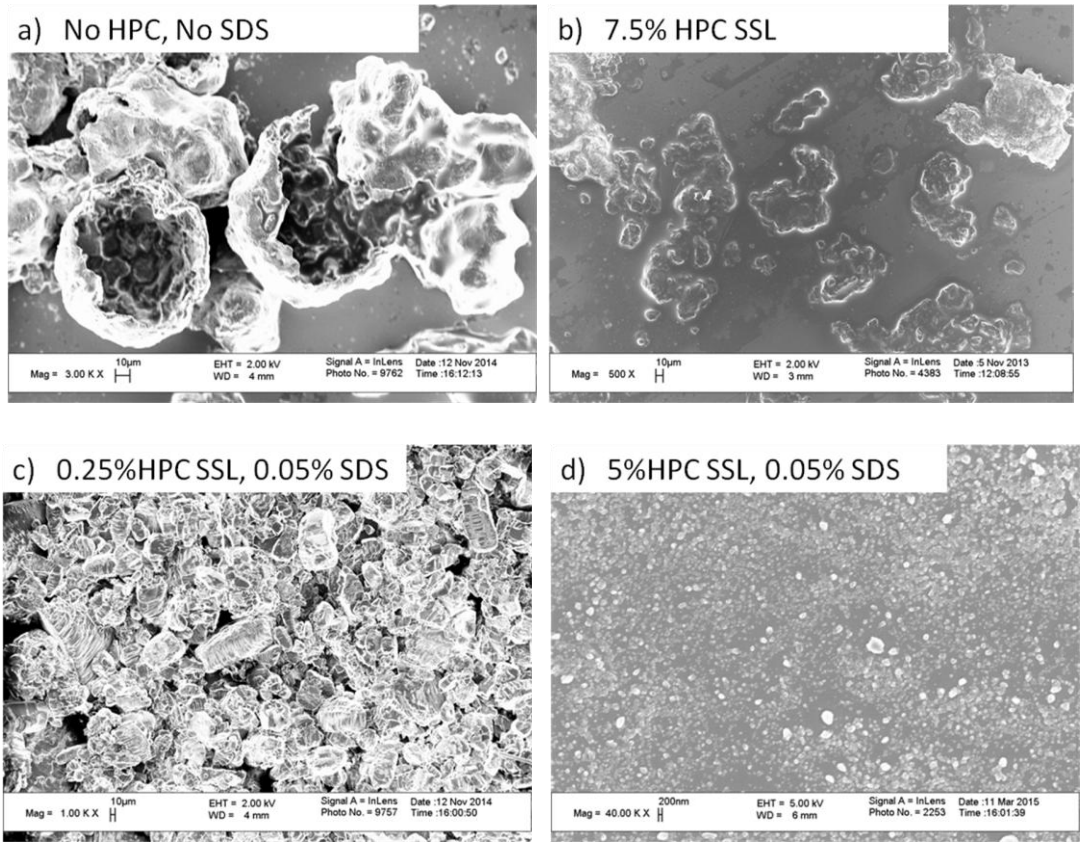

Figure 5.6 SEM images of the drug composites prepared using various precursor suspensions (a) without stabilizers (Run 1) as well as with (b) 7.5% HPC SSL (Run 7), (c) 0.25% HPC SSL, 0.05% SDS (Run 13), and (d) 5% HPC SSL, 0.05% SDS (Run 16) after 2 min redispersion in deionized water.

For composites with HPC as the sole stabilizer, HPC acts as a film former and partially covers hydrophobic GF nanoparticles (e.g., Figure 5.4(d)). Due to the dissolution of HPC and the mechanical action of paddle stirring, the shell of the composite particles broke down to smaller clusters in water, especially at higher HPC concentration as compared with Run 1 case (Figures 5.5 and 5.6(b)). On the other hand, even with 7.5% HPC, the primary drug nanoparticles cannot be recovered for both HPC grades. This is partly due to the slow dissolution of HPC and its relatively low wetting capability (Dalvi and Dave, 2010; Rasenack et al., 2003), which limited

the water penetration. Moreover, the hydrophobic nature of GF led to poor wetting of the clusters, thus slowing down the release of drug nanoparticles. Finally, the precursor suspensions with HPC as the sole stabilizer exhibited severe aggregation (see Figure 5.5). Hence, the redispersion of these composites at best might have resulted in aggregates whose sizes would be similar to those in the precursor suspensions; however, much larger clusters formed due to the poor wettability and the formation of hard aggregates especially below 2.5% HPC.

Figure 5.7 shows the particle size statistics for the composites with SDS and HPC of various MWs after redispersion and those of the corresponding precursor suspensions. As a baseline, Run 2 had only SDS in the precursor suspension. Drug nanoparticles in the milled suspension show significant particle size increase after 30 h storage (before redispersion) and drug nanoparticles were not recovered from its dried composite. SDS can impart excellent wettability and thus effective deaggregation of clusters that formed during or after the breakdown of the shell under the action of gentle paddle stirring (Bhakay et al., 2013). However, SDS alone was not able to provide sufficient coverage of the drug nanoparticles and prevent the formation of hard aggregates during drying. This, coupled with the presence of aggregates formed during the storage, could explain the poor redispersibility of Run 2 composite without any HPC. It appears that while wettability imparted by SDS and small aggregates formed during the milling upon use of SDS are both desirable, a minimum HPC concentration is still required.

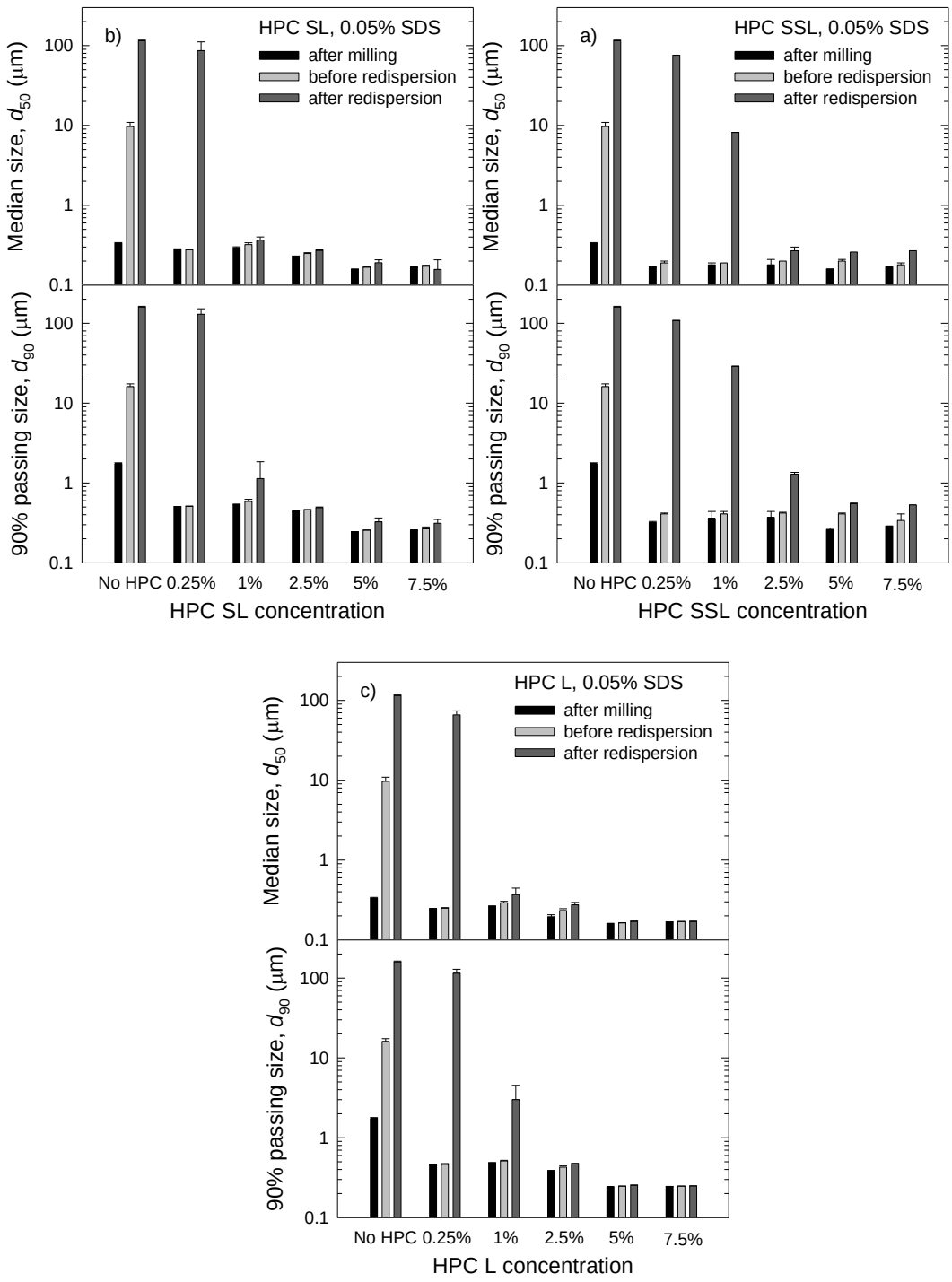

Figure 5.7 Particle sizes of the composites prepared using precursor suspensions with 0.05% SDS and (a) HPC SSL (40 kDa, Runs 13–17), (b) HPC SL (100 kDa, Runs 18–22), and (c) HPC L (140 kDa, Runs 23–27) after 2 min redispersion in deionized water in comparison to the particle sizes of the suspensions after milling and after 30 h storage (before redispersion).

The formulations with SDS (Figure 5.7) exhibited smaller drug particle sizes and lower extent of drug nanoparticle aggregation in the milled suspensions, enhanced wettability of the composites, and faster redispersion and recovery of the drug nanoparticles as compared with those without SDS (Figure 5.5), pointing out the criticality of SDS. Moreover, with 0.05% SDS, an increase in HPC concentration led to smaller milled particle sizes and faster/more complete recovery of the drug nanoparticles (Figure 5.7). Different from the formulations with HPC alone (Figure 5.5), the formulations with SDS led to effective recovery of the drug nanoparticles at 5% HPC SSL or 2.5% HPC SL or L. The SEM image (Figure 5.6(d)) qualitatively confirms the full recovery of nanoparticles from the composite with SDS. The excellent wettability and water penetration imparted by SDS led to the fast disintegration of the shell of the composites followed by fast dispersion of any clusters into drug nanoparticles. However, despite ensuring the formation of fine nanoparticles in the respective milled suspensions, the use of SDS did not allow for full nanoparticle recovery when HPC was below a threshold concentration (~1%) (see e.g., Figure 5.6(c)). This may be explained by the formation of hard aggregates during the drying process when HPC concentration was low. Considering that the respective milled suspensions with SDS had low extent of aggregation and were relatively stable, the existence of large clusters emanating from the redispersed composites (Figure 5.7) implies that a relatively stable nanosuspension did not guarantee full and fast recovery of nanoparticles from the composites. It is concluded that the presence of sufficient amount of HPC is critical for full recovery of drug nanoparticles, and a

lower HPC concentration may be needed for the higher molecular weight (SL or L grades).

5.2.4 Recovery of Drug Nanoparticles from the Drug Composite Particles in 0.05% SDS Solution

To further elucidate the role of SDS and investigate the impact of wettability of the composites, the composites with HPC alone (without SDS) were redispersed in 0.05% SDS solution (see Figure 5.8), in comparison to their redispersion in de-ionized water (Figure 5.5). This medium has the same SDS concentration as in the milled suspensions containing SDS (Figure 5.7). It should be noted that GF solubility is only slightly increased by SDS below the CMC (Rao et al., 1997). Interestingly, drug nanoparticles were effectively recovered only from the composites with high HPC concentration, at or above 5%, for both SSL and L grades (Figure 5.8) because 0.05% SDS in the redispersion medium enhanced the wetting and dispersed the drug aggregates, unlike the redispersion in de-ionized water (Figure 5.5). Drug nanoparticles could not be recovered from the composites with less than 5% HPC despite the presence of 0.05% SDS in the redispersion medium. Figures 5.5 and 5.8 both illustrate coarse clusters (>10 μm) at or below 1% HPC. These results can again be explained by the presence of significant fraction of aggregates in the composites without SDS (refer to Figure 5.1) and formation of hard aggregates during drying, which did not allow for fast shell breakage/disintegration even under paddle stirring with good wettability imparted by SDS. Similar results were obtained by de Villiers for aggregated drug powders (de Villiers, 1996).

A comparison of the redispersed particle sizes for the formulations with 0.05% SDS in the respective precursor suspensions, which led to an estimated 0.0026% SDS upon the redispersion of the respective composites in de-ionized water (see Figure 5.7(a), (c)), vs. those formulations with HPC/without SDS, redispersed in 0.05% SDS solution (see Figure 5.8a,b) sheds further insight. Despite the attainment of 0.0026% SDS concentration in the redispersion medium, 0.05% SDS in the milled suspension/composite led to smaller redispersed particles, i.e., more effective recovery of the GF nanoparticles, notably at the intermediate HPC concentrations, i.e., 1% and 2.5% HPC (Figure 5.7), as compared with 0.05% SDS added to the redispersion medium directly (Figure 5.8). A similar, albeit less pronounced difference occurred at 0 and 0.25% HPC because hard aggregate formation controlled the poor redispersibility observed at such low HPC concentration. These findings could be mainly explained by the presence of smaller aggregates in the precursor milled suspensions with SDS (refer to Figure 5.3) than without SDS (refer to Figure 5.1) besides facilitated disintegration of the composite shell with enhanced wettability during the redispersion test. At 5% and 7.5% HPC, a similar pattern was observed for the L grade, whereas an anomaly occurred for the SSL grade for which the smaller redispersed particles were obtained when 0.05% SDS was added to the redispersion medium directly. It seems the much higher SDS concentration, i.e., 0.05% vs. 0.0026%, in the redispersion medium affected the redispersion results differently at only for the high HPC SSL concentration.

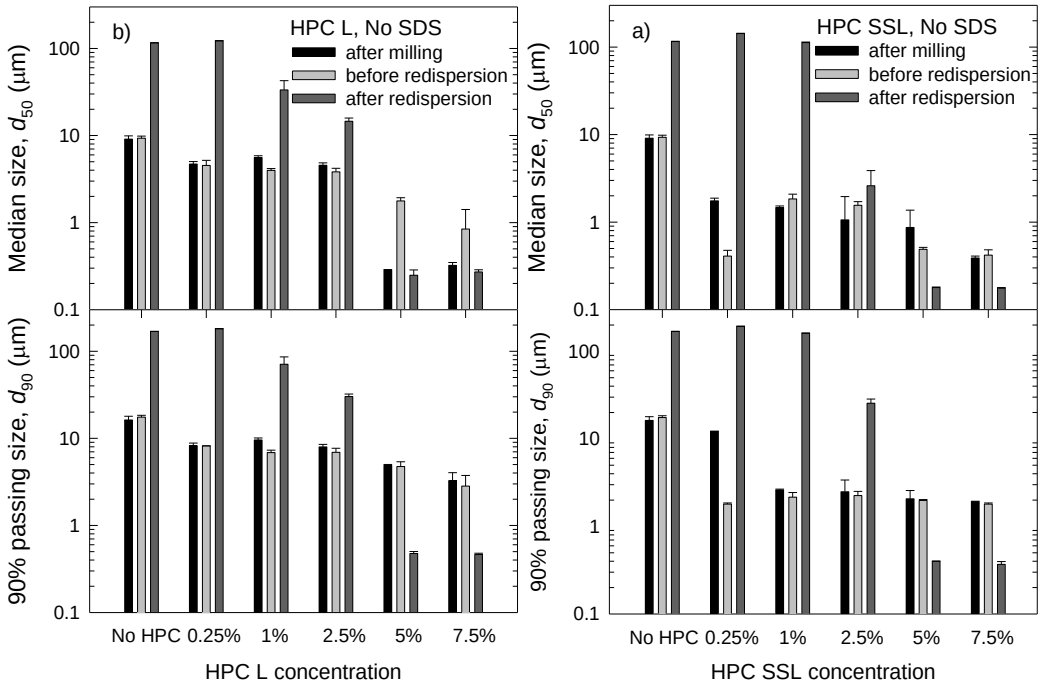

Figure 5.8 Particle sizes of the composites prepared using various precursor suspensions with (a) HPC SSL (Runs 3–7) and (b) HPC L (Runs 8–12) after 2 min redispersion in 0.05% SDS solution in comparison to the particle sizes of the suspensions after milling and after 30 h storage (before redispersion). Run 1 had no stabilizers.

Overall, the redispersion experiments with deionized water and 0.05% SDS solution as two separate media point out the need for preparing aggregate-free precursor (milled) drug suspensions upon use of HPC–SDS combination. Moreover, a minimum HPC concentration (within 0.25–1% in the precursor) is required to prevent hard-aggregate formation during drying and to give strength and proper film formation in the shell of the composite particles.

5.2.5 Drug Dissolution from the Composites

The composites produced via fluidized bed drying were dissolved in excess de-ionized water to allow for full dissolution of the poorly water-soluble drug.

Dissolution profiles of the composites without SDS in the precursor suspensions are shown in Figure 4.9. For both HPC SSL and L, dissolution rates increased with higher polymer concentration, but immediate drug release (80% dissolved within 20 min) was not realized for any formulation. These findings can overall be explained by the poor redispersibility of the composites without SDS and slow/incomplete nanoparticle recovery during the dissolution (see Figure 4.5). It is expected that GF nanoparticle recovery precedes GF dissolution from the composites considering the poorly water-soluble nature of this drug.

For HPC SSL at the highest concentration (7.5%), the dissolution of drug particles only reached 50.2% at 60 min. Applying f1 and f2 tests and t-test (Azad et al., 2015a; Moore and Flanner, 1996), the author found that the dissolution profiles of the composite formulations with 1–7.5% HPC SSL presented in Figure 4.9 were not statistically different. For 7.5% HPC L having the highest polymer molecular weight, the drug dissolution reached 68.8%, which is higher than that for HPC SSL at the same concentration. This may be due to the better coverage of the hydrophobic drug surfaces with higher MW HPC, despite its slower diffusion/dissolution in water. It should be noted that, in the absence of SDS, HPC as a film former in composites can only provide limited wettability for dissolution, which is the limiting mechanism for their dissolution performance.

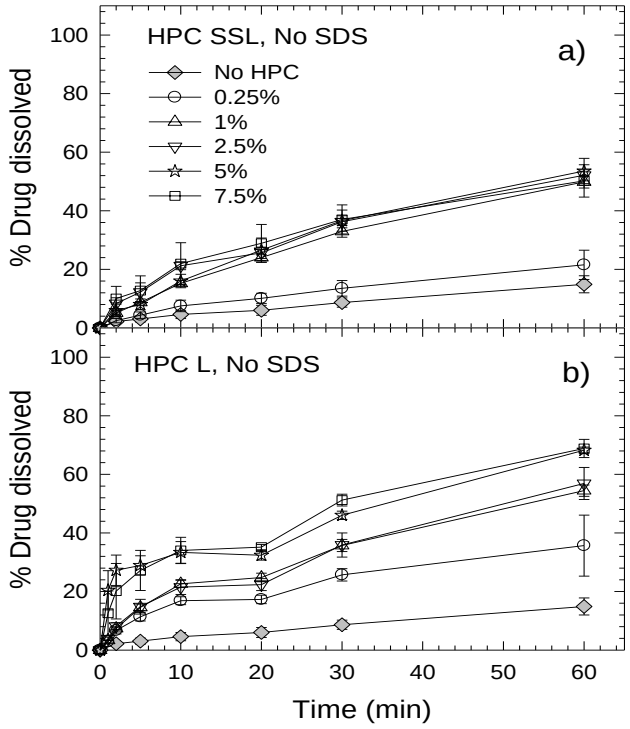

Figure 5.9 Drug dissolution profiles of the composites prepared using various precursor suspensions containing HPC with different molecular weights: (a) 40 kDa (SSL grade, Runs 3–7) and (b) 140 kDa (L grade, Runs 8–12). Run 1 had no stabilizers.

Dissolution profiles of the composites with 0.05% SDS in the precursor suspensions are shown in Figure 5.10. A comparative analysis of the results in Figures 5.9 and 5.10 suggests that most composites with SDS exhibited immediate drug release and faster drug dissolution than those without SDS, which can be overall explained by the enhanced redispersibility/faster nanoparticle recovery (refer to Figure 5.7) stemming from the excellent wettability and electrosteric stabilization imparted by the use of HPC–SDS. An increase in HPC concentration led to faster dissolution for all three HPC grades. This positive effect of HPC appears to saturate when the HPC concentration was above 2.5% for SSL and SL grades and 5% for L grade. These observations can again be explained by enhanced nanoparticle recovery

(smaller redispersed particle sizes) at higher HPC concentration and the tendency of the redispersed particle sizes to minimum values above 2.5% HPC (refer to Figure 5.7). At or below 5% HPC concentration, unlike the formulations without SDS, the formulations with HPC–SDS exhibited slower dissolution when a higher MW HPC was used. With SDS, the dissolution profiles are more sensitive to the dissolution–diffusion rate of HPC with various MW. The slower dissolution for the composites with higher MW HPC may be explained by the slower dissolution and diffusion of the higher MW HPC. In addition, the relatively large granules formed during the drying process for the higher MW HPC (L grade in Table 5.2) may also partly explain the slower dissolution profiles.

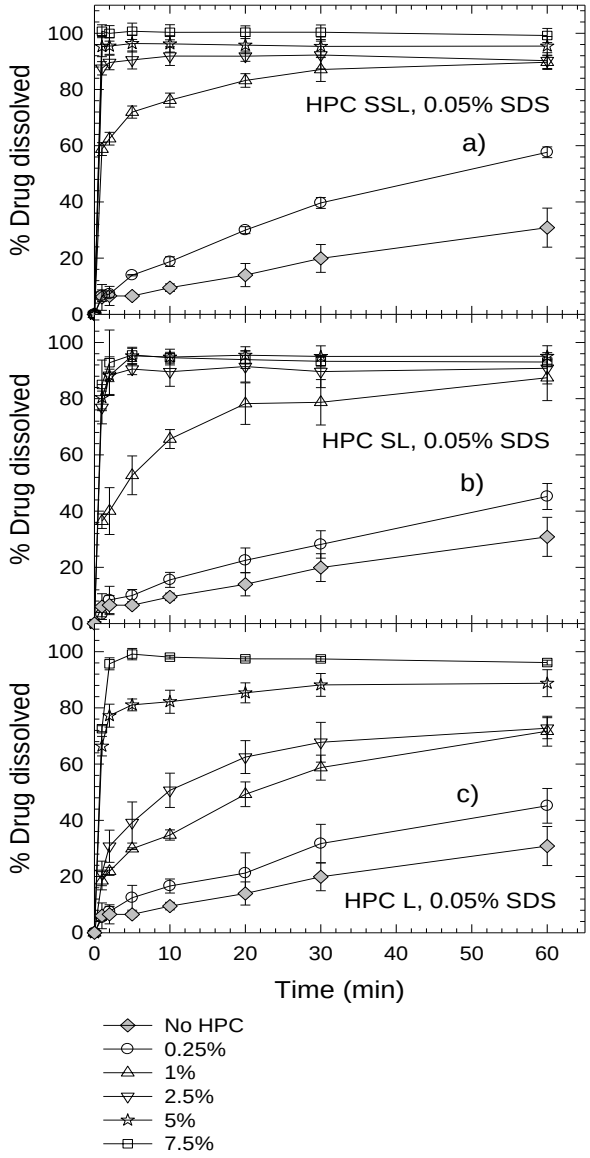

Figure 5.10 Drug dissolution profiles of the composites prepared using various precursor suspensions with 0.05% SDS and HPC with different molecular weights: (a) 40 kDa (SSL grade, Runs 13–17), (b) 100 kDa (SL grade, Runs 18–22), and (c) 140 kDa (L grade, Runs 23–27). Run 2 had only 0.05% SDS.

5.3 Conclusions

Nanocomposite microparticles were produced by fluidized bed drying–coating of wet stirred media-milled GF nanosuspension onto Pharmatose® carrier particles. The drug composites were redispersed in water and aqueous solution of SDS. Three

different HPC polymer molecular weights at varied concentrations in the absence/presence of SDS were investigated for their ability to enhance the redispersion and dissolution of the drug nanoparticles. The results overall suggest that well-stabilized drug nanosuspensions with minimal amount of aggregates is necessary to produce drug composites with good redispersion and fast dissolution. However, good physical stability and prevention of aggregation in the milled suspensions is not sufficient. The presence of a soluble, adsorbing polymer above a minimum concentration is also needed so as to suppress formation of hard aggregates during drying. Hence, our study concludes that proper stabilization of drug suspensions is a necessary condition for fast drug nanoparticles recovery and fast drug dissolution from the composites, but not sufficient. Sufficiency originates from the use of SDS in combination with HPC above the threshold concentration, which results in almost aggregate-free drug nanosuspensions and mitigates hard-aggregate formation. Immediate drug release is achieved when a lower molecular weight (SSL grade) HPC at or above 1% concentration was used along with 0.05% SDS. Despite the use of 0.05% SDS, the highest grade of HPC (L grade) entails relatively high concentrations to ensure immediate drug release from the composites.

CHAPTER 6

ENHANCED DISSOLUTION OF ITRACONAZOLE FROM HIGH DRUG-LOADED SURFACTANT-FREE NANOCOMPOSITE MICROPARTICLES

The previous chapter has developed an understanding of the relationships between the physical stability of drug nanosuspension, redispersion, and drug dissolution from the nanocomposites based on HPC–SDS formulations. The problem associated with the use of surfactant was discussed in detail in Chapter 1, which includes, for instance, Ostwald ripening of nanosuspensions during storage and irritation to the pulmonary epithelium. Thus, there is a need to find potential dispersants that can replace the surfactants to prepare surfactant-free formulations for certain pharmaceutical applications. The aim of Chapter 6 is to investigate the impact of various classes of dispersants, including the relatively novel class of swellable dispersants (e.g., superdisintegrants) on drug release from high drug-loaded, surfactant-free nanocomposites and elucidate the mechanisms for enhanced dissolution. To this end, precursor suspensions of itraconazole (ITZ) nanoparticles in the presence of various dispersants were prepared via wet stirred media milling and spray dried to form the nanocomposites. Hydroxypropyl cellulose (HPC, polymer) alone and sodium dodecyl sulfate (SDS, surfactant) alone as well as their combination were used as baseline stabilizers/soluble dispersants during milling and drying. Three commonly used superdisintegrants, which are insoluble swellable dispersants, i.e., sodium starch glycolate (SSG), crospovidone (CP), and croscarmellose sodium (CCS) were wet co-milled along with ITZ in the presence of HPC. In addition, two conventional soluble matrix formers, Sucrose and Mannitol, were dissolved in milled ITZ suspensions with

HPC. Laser diffraction, viscometry, scanning electron microscopy (SEM), X-ray powder diffraction (XRD), differential scanning calorimetry (DSC), and ultraviolet spectroscopy were used for characterization. In addition, drug wettability enhancement by soluble dispersants was investigated using the Washburn method so as to elucidate the mechanisms. Dissolution performance of the nanocomposites was determined, and dissolution profiles of selected formulations were compared by calculating the difference and similarity factors (Costa and Lobo, 2001). These methods and analysis allows for elucidating the impact of dispersants on both wet-milled particle size and drug dissolution.

6.1 Materials and Methods

6.1.1 Materials

Sodium starch glycolate (SSG, Primojel), croscarmellose sodium (CCS, Ac-Di-Sol, type-SD711), and crospovidone (CP, Polyplasdone XL-10) were donated by DMV Fonterra Excipients LLC (Princeton, NJ), FMC Biopolymer (Newark, DE), and ISP Chemicals (Wayne, NJ), respectively. Hydroxypropyl cellulose (HPC, SL grade) was donated by Nisso America, Inc. (New York, NY). Sodium dodecyl sulfate (SDS), Mannitol, and Sucrose were purchased from Fisher Scientific (Pittsburgh, PA), Pure Bulk Inc. (Roseburg, OR), and GFC Chemicals, Inc. (Columbus, OH), respectively. Itraconazole (ITZ) was purchased from Jai Radhe Sales (Ahmedabad, India). Mannitol is classified as a sugar alcohol with a solubility of 180 g/L in water, whereas sucrose is a common, naturally occurring sugar with a solubility of 2000 g/L. Superdisintegrants (SSG, CP, and CCS) are insoluble and highly swellable in water.

The swelling capacities of SSG, CP, and CCS in water are 23.6, 5.4, and 13.5cm3/g, respectively (Quadir and Kolter, 2006). As-received SSG and CCS were dry-sieved in a sieve shaker (Octagon 2000, Endecotts Ltd., London, England) for 1 h using the US Standard Testing Sieves (ASTM E-11 specification), and < 38 μm particles were collected. This step is intended to prevent potential clogging of the mill screen by water-swollen, coarse SSG/CCS particles during wet media milling (Azad et al., 2014b; Bhakay et al., 2014b). CP was used as is. The d50 and d90 values of the particles after sieving are 28.8 ± 0.1 μm and 41.0 ± 0.5 μm; 21.7 ± 0.3 μm and 49.0 ± 2.0 μm; and 34.5 ± 0.3 μm and 56.4 ± 0.1 μm for SSG, CP, and CCS respectively, as measured via the Rodos/Helos system (Sympatec, Pennington, NJ).

6.1.2 Preparation Methods

Drug precursor suspensions were prepared via wet media milling, followed by their spray drying into nanocomposite powders. The formulations of the drug precursor suspensions are presented in Table 6.1. Selection of the milling conditions and formulations were guided by our prior work on wet media milling (Azad et al., 2014b; Bilgili et al., 2016d). All percentages (%) refer to w/w with respect to total weight of deionized water (200 g). Unless otherwise indicated, suspensions and nanocomposites are labeled with the type–concentration of the dispersants in the precursor suspensions, which all contain 10% ITZ. The rationale behind the experimental design is as follows: since HPC is the only film-forming polymer in this study, which is essential to the formation of the nanocomposite structure, a minimum of 2.5% HPC was used in all formulations, except F2 (with 0.2% SDS alone).

Formulations F1–F3 allow one to examine the impact of HPC–SDS combination, which is known to be effective for stabilizing multiple drug nanosuspensions (see e.g., (Bilgili et al., 2016d)), on milled ITZ particle size with the respective controls (no SDS or no HPC). In F4–F6 and F7–F9 formulations, Mannitol and Sucrose were respectively used as soluble dispersants at 1%, 2%, and 4% levels and added right after milling to prepare precursor suspensions. Besides these soluble dispersants, SSG, CP, and CCS were used as insoluble, swellable dispersants at 1% and 2% levels and co-milled with ITZ (see below) to prepare F11–F16 precursor suspensions. F10 and F17 formulations had extra 4% and 2% HPC added before milling, without any additional dispersant, to enable comparative assessment of all dispersants at the same total dispersant concentrations of 6.5% and/or 4.5%.

Table 6.1 Formulations of the Precursor Suspensions used to Prepare Nanocomposites via Spray Drying and Drug Content of the Nanocomposites

Formula ID	HPC (% w/w)[a]	SDS (% w/w)[a]	Other Dispersants (% w/w)[a]	Theoretical Drug Content (%)	Drug Content (RSD) of the Nanocomposites (% w/w)[b]
F1	2.5	0	–	80.0	78.9 (5.19)
F2	0	0.2	–	98.0	N/M
F3	2.5	0.2	–	78.7	78.3 (4.66)
F4	2.5	0	1 (Mannitol)[c]	74.1	72.4 (5.59)
F5	2.5	0	2 (Mannitol)[c]	69.0	64.9 (4.68)
F6	2.5	0	4 (Mannitol)[c]	60.6	55.5 (5.76)
F7	2.5	0	1 (Sucrose)[c]	74.1	70.3 (4.20)
F8	2.5	0	2 (Sucrose)[c]	69.0	65.4 (5.94)
F9	2.5	0	4 (Sucrose)[c]	60.6	54.8 (5.03)
F10	6.5	0	–	60.6	55.2 (4.64)
F11	2.5	0	1 (SSG)[d]	74.1	74.0 (2.73)
F12	2.5	0	2 (SSG)[d]	69.0	66.8 (3.12)
F13	2.5	0	1 (CP)[d]	74.1	72.8 (4.30)
F14	2.5	0	2 (CP)[d]	69.0	64.4 (6.48)
F15	2.5	0	1 (CCS)[d]	74.1	74.0 (3.69)
F16	2.5	0	2 (CCS)[d]	69.0	66.6 (6.27)
F17	4.5	0	–	69.0	66.1 (3.81)

[a]Drug loading in all suspensions is 10%. % w/w is with respect to the weight of deionized water, 200 g.
[b]% w/w is the weight of ITZ with respect to the weight of NCMPs.
[c]Added to the suspension after milling.
[d]Co-milled along with ITZ for 15 min.

6.1.3 Preparation of Precursor Suspensions

For formulations, F1 and F3–F17, HPC at the indicated concentrations was dissolved in water using a shear mixer (Fisher Scientific Laboratory Stirrer, Catalog no. 14–503, Pittsburgh, PA). In Runs 2 and 3, 0.2% SDS was added in deionized water and 2.5% HPC solution, respectively. ITZ (10%) was then added to these stabilizer solutions and dispersed for 30 min with the shear mixer. Following the dispersion of the drug, each suspension was poured into the holding tank of a Netzsch mill (Microcer, Fine Particle Technology LLC, Exton, PA), pumped through the milling

chamber at a flow rate of 126 ml/min, and milled for 65 min (total milling time) at 4000 rpm stirrer speed (14.7 m/s tip speed). 196 g of yttria-stabilized zirconia beads with a nominal size of 400 μm were used as the milling media. A 200 μm screen was used to retain the beads in the milling chamber. The temperature inside the milling chamber was maintained below 34 ˚C with a chiller (Advantage Engineering, Inc., Greenwood, IN).

In preparation of F4–F9 precursor suspensions, Mannitol or Sucrose was dissolved in an already milled 10% ITZ–2.5% HPC suspension right after milling (65 min) while the suspension was still being stirred in the holding tank and re-circulated in the mill by the peristaltic pump. In Runs 11–16, superdisintegrants (SSG/CP/CCS) were added as additional dispersants after 50 min milling while the mill was operating and co-milled with ITZ for 15 min. This short milling time was selected based on the previous study (Azad et al., 2015b; Bhakay et al., 2014b), where short-milled CCS with multimodal size distribution enabled fastest recovery/dissolution of drug nanocomposites. To avoid clogging of the mill screen and associated pressure build-up (Azad et al., 2014b), superdisintegrant (SSG/CCS/CP) was added slowly. The particle size of the precursor suspensions was measured at the end of wet milling of ITZ or wet co-milling of ITZ–superdisintegrant or following the addition of Mannitol/Sucrose after wet milling. The milled suspensions were stored in a refrigerator at 8 ˚C. Particle size was also measured on samples stored in the refrigerator for 7 days to assess the impact of storage. Long-term stability was not studied as the precursor suspensions are intended to be dried following the wet media milling.

6.1.4 Spray Drying of the Precursor Suspensions

The precursor suspensions prepared via wet media milling were dried, within the same day of milling, using a spray dryer (4M8-Trix, Procept, Zelzate, Belgium) running in a co-current flow set-up. For each formulation, 150 g suspension was sprayed. The suspensions were atomized and spray-dried under identical conditions to those in Azad et al. (2015b). Drying air was fed co-currently at a temperature of 120 °C and a volumetric flow rate of 0.39–0.40 m3/min. The suspensions were pumped at a rate of 1.6 g/min using a peristaltic pump (Make-it-EZ, Creates, Zelzate, Belgium) and atomized through a bi-fluid nozzle with 0.6 mm tip diameter at an atomization air pressure of 2 bar. The dried nanocomposites were then tested for particle size and used in the dissolution test.

6.1.5 Particle Size Analysis

The particle size distributions (PSDs) of the precursor suspensions after milling and after 7-day refrigerated storage were measured by laser diffraction using Coulter LS 13 320 (Beckman Coulter, Miami, FL) based on Mie scattering theory following the procedure in Bilgili et al. (2016d). The refractive index of ITZ is 1.64. The area-based PSDs were also obtained upon transformation of the volume-based PSDs via the instrument's software. Unless otherwise indicated, all PSDs and their statistics reported throughout the dissertation are volume-based. The particle sizes of the spray-dried nanocomposites were measured by a Rodos/Helos laser diffraction system (Sympatec, NJ, USA) based on Fraunhofer theory following the procedure in Li et al. (2016b).

6.1.6 Scanning Electron Microscopy (SEM)

The morphology of as-received ITZ microparticles before milling, primary size of ITZ nanoparticles after milling (F1–F3, and F12) and nanocomposites (F1–F3, F5, F8, F12, F14, and F16) were examined via a scanning electron microscope (SEM) LEO 1530 SVMP (Carl Zeiss, Inc., Peabody, MA). Detailed sample preparation procedure can be found in Li et al. (2016b). The stub was coated with carbon using BAL-TEC MED 020 (BAL-TEC AG, Balzers, Switzerland) to reduce possible charging effects during the imaging.

6.1.7 Apparent Shear Viscosity of the Precursor Suspensions

The apparent shear viscosity of stabilizer solutions and the precursor suspensions was measured using an R/S Plus Rheometer (Brookfield Engineering, Middleboro, MA, USA) with a water jacket assembly Lauda Eco (Lauda-Brinkmann LP, Delran, NJ, USA). A coaxial cylinder (CC40) was used to provide a controlled shear rate on the samples from 0 to 1000 1/s for 60 s. The temperature of the jacket was kept constant at 25 ± 0.5 °C. The raw data were analyzed using the Rheo 3000 software (Brookfield Engineering, Middleboro, MA, USA) of the equipment to obtain the apparent shear viscosity as a function of the shear rate.

For selected stabilizer solutions (F1, F3, F6, F9, F10, F17) in the liquid penetration experiments, the viscosities at the lowest shear rate (i.e., 254 1/s) that are representative were reported. Due to the inaccuracy of the instrument at low viscosity region (< 5 cP), the viscosities of water and the F2 stabilizer solution were adopted

from Korson et al. (1969) and Kushner et al. (1952), respectively. For the stabilizer solutions of F9 and F10, 4% Mannitol/Sucrose was dissolved in 2.5% HPC solutions.

6.1.8 Determination of Drug (ITZ) Content of Nanocomposites

Nanocomposites (100 mg) were dispersed in 20 ml dichloromethane and then sonicated for 30 min to dissolve ITZ. The solubility of ITZ in dichloromethane is 239 mg/ml at 25 ˚C (Garg et al., 2013). After sonication, the solution was stored overnight during which insoluble superdisintegrants or Mannitol or Sucrose particles, if present, were allowed to settle. An aliquot (100 µl) was taken from the supernatant, diluted to 10 ml with dichloromethane, and the absorbance was measured at a wavelength of 260 nm by an Ultraviolet (UV) spectrophotometer (Agilent, Santa Clara, CA). The absorbance was then converted into the drug concentration via pre-established calibration curve of absorbance vs. concentration. Six replicates from each nanocomposite formulation were used to determine the mean drug content and the relative standard deviation (RSD), which are presented in Table 6.1.

6.1.9 X-ray Powder Diffraction (XRPD)

The crystallinity of the as-received ITZ, physical mixtures corresponding to F12 and F17 formulations, and overnight-dried ITZ precursor suspensions of F2, F12, and F17 was analyzed using XRPD (PANalytical, Westborough, MA, USA), provided with Cu Kα radiation (λ = 1.5406 Å). The samples were scanned for 2θ ranging from 5° to 30° at a scan rate of 0.165 s^{-1}. The precursor suspensions were centrifuged (Compact II centrifuge, Clay Adams® Brand, Sparks, MD, USA) at 3200 rpm for 90 min to

separate the solid and aqueous phase. The resulted solid phase was redispersed in deionized water followed by another centrifugation. The final solid phase was overnight-dried in a vacuum hood for XRD and differential scanning calorimetry (DSC) analysis.

6.1.10 Differential Scanning Calorimetry (DSC)

A Mettler–Toledo polymer analyzer DSC (PolyDSC, Columbus, OH, USA) was used to obtain the peak melting temperature and melting enthalpy of as-received ITZ, physical mixtures corresponding to F12 and F17 formulations, and overnight-dried ITZ precursor suspensions of F2, F12, and F17. The ITZ precursor suspensions were centrifuged–rinsed–centrifuged following the procedures in Section 6.1.9. ~6–7 mg powder sample was weighed before being placed in a sealed perforated aluminum pan and loaded into the DSC. All samples were heated from 25 to 220 ˚C at a rate of 10 ˚C/min. Nitrogen was used as the purge gas and protective gas at a flow rate of 50 ml/min and 150 ml/min, respectively. Data analysis was performed using STARe 10 software provided by Mettler–Toledo.

6.1.11 Thermogravimetric Analysis (TGA)

Thermogravimetric analysis (TGA) was performed using a TGA/DSC1/SF Stare system (Mettler Toledo, Inc., Columbus, OH) for the characterization of the residual water in the spray-dried nanocomposites. A 5 mg spray-dried nanocomposite powder (F1 and F12) was placed in a ceramic crucible and heated from 25 °C to 150 °C at a constant rate of 10 °C/min under nitrogen flow.

6.1.12 Liquid Penetration Study

Penetration of a liquid into a packed powder bed of a drug inside a cylindrical column allows for measurement of the drug powder wettability, based on the Washburn method (Hołownia et al., 2008; Washburn, 1921). Attension Sigma 700 (Biolin Scientific, Linthicum, MD, USA) set-up was used in this study. Experimental methods were presented in Li et al. (2017) and the details can be found in Supplementary Material. In this study, liquids and powder are deionized water/stabilizer solutions (HPC, SDS, HPC–SDS/Mannitol/Sucrose) and ITZ, respectively. For the stabilizer solutions with Mannitol/Sucrose, 4% Mannitol/Sucrose was dissolved in 2.5% HPC solutions. The apparent shear viscosity and surface tension of the liquids were respectively measured using R/S Plus Rheometer (Brookfield Engineering, Middleboro, MA, USA) and Attension Sigma 700 (Biolin Scientific, Linthicum, MD, USA), as described in *Section 6.1.7* and *Appendix C.1.1*, respectively. The ratio of the cosine of contact angles $\cos\theta_{ss}/\cos\theta_{w}$ was calculated using the Modified Washburn equation and used as a wetting effectiveness factor. Here, θ_{ss} is the contact angle between ITZ and the stabilizer solutions and θ_{w} is the contact angle between ITZ and deionized water. The ratio quantifies the drug wettability enhancement upon the use of different stabilizers (HPC, SDS, HPC–SDS/Mannitol/Sucrose) in water.

6.1.13 Dissolution

Dissolution experiments on nanocomposites were performed using a Distek Dissolution tester (North Brunswick, NJ) according to the USP II paddle method.

Nanocomposites containing an equivalent ITZ dose of 20 mg were weighed and added to 1000 ml dissolution medium (3 g/L SDS solution). The SDS solution was selected for quantification of the dissolution rate enhancement and also for providing the rank order/good discrimination between nanocomposite formulations, similar to Azad et al. (2016) and Cerdeira et al. (2013b). The dissolution medium was maintained at 37.0 ± 0.1 ˚C and a paddle speed of 50 rpm was used. After addition of the nanocomposites, 4 ml samples were taken manually at 1, 2, 5, 10, 20, 30, and 60 min and passed through a PVDF membrane type syringe filter with a nominal pore opening size of 0.1 µm. The amount of ITZ dissolved was measured by UV spectroscopy at a wavelength of 260 nm. SDS solution was used as the blank for UV measurements. Dissolution results are reported as ITZ release as a function of time for an average of six samples from each nanocomposite formulation.

To describe the drug release kinetics from different polymeric matrices and rank the dissolution rate from different nanocomposites, fitting of ITZ dissolution data to Korsmeyer–Peppas model (Ritger and Peppas, 1987a, b), as shown in Eq. (6.1), was performed using SigmaPlot's (Version 11) regression wizard.

$$\frac{M_t}{M_\infty} = kt^n \tag{6.1}$$

where *k* is a constant incorporating structural and geometric characteristics of the drug dosage form, *n* is the release exponent, indicative of the drug release mechanism, and $\frac{M_t}{M_\infty}$ is the fractional release of the drug. An apparent release mechanism was suggested in this dissertation based on the fitted *n* value and the specific geometry of the samples in view of various assumptions behind Eq. (6.1)

(refer to Ritger and Peppas (1987a)). Fitting of $\frac{M_t}{M_\infty}$ included data up to and including one point after attainment of $\frac{M_t}{M_\infty}$ value of 0.60. As the drug release rate (d($\frac{M_t}{M_\infty}$)/dt) is proportional to *kn* (Peppas, 1985), in this study, *kn* is used to compare dissolution rate of different formulations.

6.1.14 Statistical Analysis

All calculations were performed using Microsoft Excel® (Microsoft Office 2010, USA). Results for dissolution profiles are expressed as mean ± SD (standard deviation) while content uniformity results are expressed as mean with RSD% (relative standard deviation). Dissolution profiles of F2, F4–F17 were compared to F1 and F3, respectively, and those with 4.5% total dispersants (F5, F8, F12, F14, and F16) were compared to F17, using difference (f_1) and similarity (f_2) factors (Boateng et al., 2009; Costa and Lobo, 2001). Generally, f_1 values up to 15 (0–15) and f_2 values greater than 50 (50–100) ensure similarity/sameness/equivalence of the two profiles. When f_1 is greater than 15 or f_2 is smaller than 50, the dissolution profiles were regarded as statistically different.

6.2 Results and Discussion

6.2.1 Particle Sizes of the Precursor Suspensions

Particle size statistics of the milled drug (ITZ) suspensions are shown in Figure 6.1. Actual particle size data can be found in Supplementary Material. Unless otherwise indicated, all statistics refer to volume-based PSD. As-received ITZ particles has d_{10}:

4.8 ± 0.0 µm, d50: 15.5 ± 0.0 µm, and d_{90}: 45.8 ± 0.1 µm (see Figure 6.2a). When they were wet-milled in the presence of 2.5% HPC alone as a baseline steric stabilizer (F1), extensive breakage occurred and 200–600 nm primary ITZ particles with irregular shapes can be seen in the SEM image (Figure 6.2b). However, in the liquid medium, ITZ nanoparticles aggregated due to high attractive inter-particle forces (van der Waals, hydrophobic forces, etc) and d_{50} and d_{90} values of 289 nm and 1543 nm were measured by laser diffraction (Figure 6.1a). While HPC likely adsorbed on the ITZ particles, imparting some steric stability and enhancing the wettability (see Table 6.2 for the higher wetting effectiveness factor $\cos\theta_{ss}/\cos\theta_{w}$ of 2.5% HPC solution with respect to pure water), 2.5% HPC was not sufficient to prevent ITZ nanoparticle aggregation fully. Smaller aggregates were formed at the higher HPC concentrations of 4.5% (F17) and 6.5% (F10) because of enhanced wettability (higher $\cos\theta_{ss}/\cos\theta_{w}$, Table 6.2) and higher extent of ITZ adsorption as adsorption of cellulosic polymers like HPC and HPMC onto drug nanoparticles are known to follow Langmuir or Freundlich adsorption isotherms (Bilgili and Afolabi, 2012; Knieke et al., 2013). At higher HPC concentrations, a thicker layer of the adsorbed polymer and stronger adsorption could have occurred (Bilgili and Afolabi, 2012; Lee, 2003).

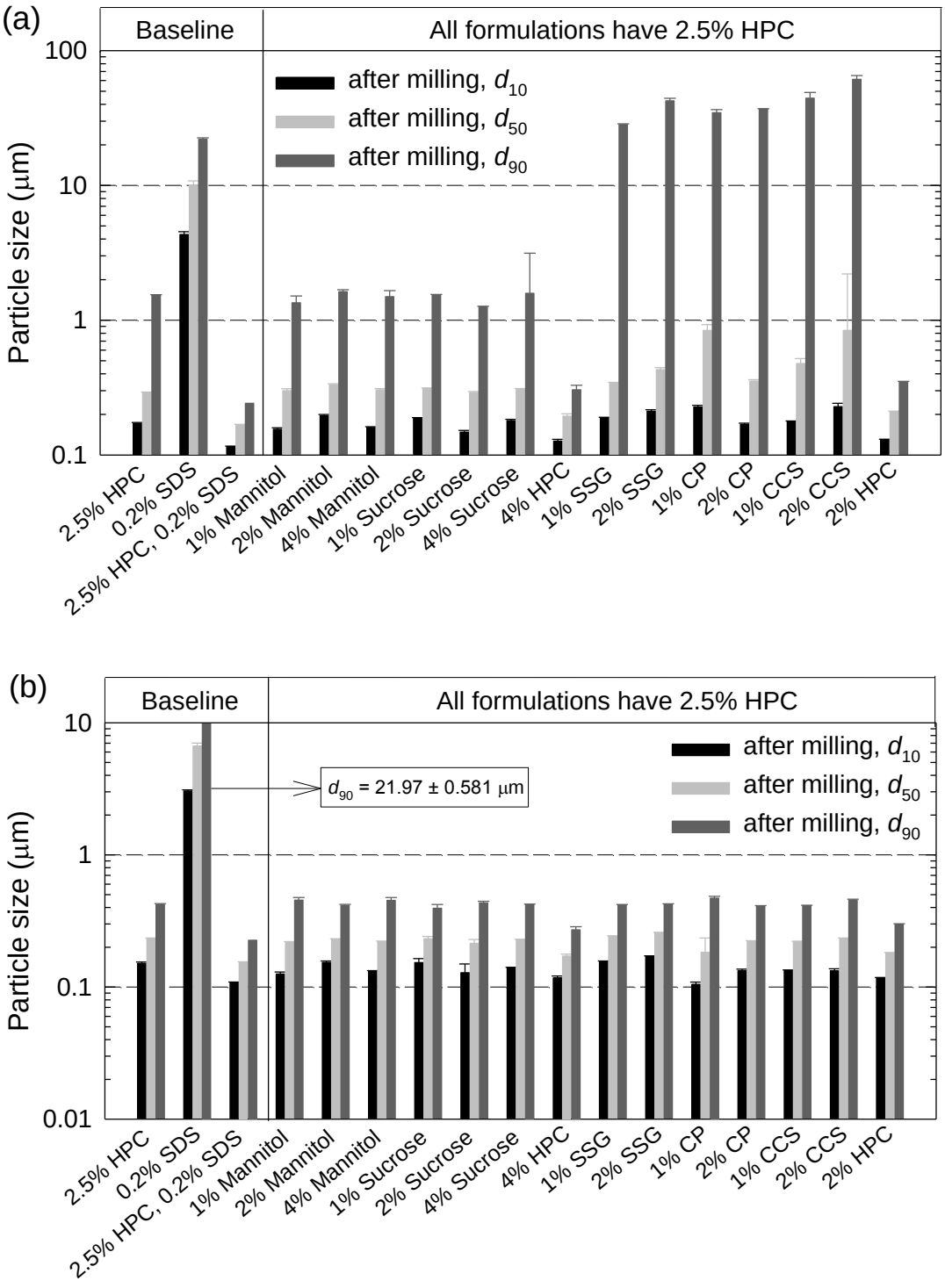

Figure 6.1 (a) Volume-based and (b) area-based particle size distributions of the ITZ precursor suspensions.

When 0.2% of the anionic surfactant (SDS) was used as the sole stabilizer in F2, a coarse suspension with d_{50} of 21.11 µm was formed (Figure 6.1a) and the large aggregate particle was observed in Figure 6.2c. It is likely that 0.2% SDS was not capable of imparting sufficient electrostatic stabilization and it imparted the lowest wettability enhancement among all dispersants studied (see Table 6.2). When 2.5% HPC–0.2% SDS combination was used, an ITZ nanosuspension with the smallest nanoparticles with d_{50} of 168 nm was obtained (Figure 6.1a). The sizes of the primary particles are in the range of 100–500 nm (Figure 6.2d). The synergistic stabilization effect can be seen from the markedly higher wettability enhancement by the combination of HPC–SDS vs. HPC or SDS alone. Such synergistic stabilization action has been previously reported for various BCS Class II drugs (Basa et al., 2008; Bilgili and Afolabi, 2012; Bilgili et al., 2016d).

In F4–F9, Mannitol or Sucrose was added to the milled ITZ suspension with 2.5% HPC as extra soluble dispersants with the ultimate objective of elucidating their impact on ITZ release from the nanocomposites. The addition of Mannitol or Sucrose in the presence of 2.5% HPC did not significantly affect ITZ particle sizes after milling (Figure 6.1a).

Table 6.2 Wetting Effectiveness Factor of Various Stabilizer Solutions Determined by the Modified Washburn Method

Formulation of the Stabilizer Solution[a]	$\eta/(C \rho^2 \gamma \cos\theta)$ (s/g^2)	R^2	η[b] (cP)	ρ (g/ml)	γ (mN/m)	$\cos\theta_{ss}/\cos\theta_w$
Water	93217	0.996	0.89c	1.000	70.8	1
2.5% HPC	2199	0.997	5.17	1.025	42.4	390
0.2% SDS	1802	1.000	0.94d	1.002	28.5	135
2.5% HPC, 0.2% SDS	1075	0.999	20.64	1.027	33.8	3974
4.5% HPC	466	0.992	16.44	1.045	42.3	5631
6.5% HPC	658	1.000	35.71	1.065	42.1	8393
2.5% HPC, 4% Mannitol	2098	0.998	5.673	1.065	42.2	433
2.5% HPC, 4% Sucrose	2119	0.994	5.685	1.065	42.3	429

[a]% w/w is with respect to the weight of deionized water.
[b]the viscosities at 254 1/s shear rate.
[c]adopted from Korson et al. (1968).
[d]adopted from Kushner et al. (1952).

In F11–F16, superdisintegrants were wet co-milled along with ITZ particles in the stirred media mill for 15 min. The short co-milling time allowed a wide PSD of superdisintegrants, which is known to be the most effective in the enhancement of nanocomposite dissolution rate (Azad et al., 2015b; Bhakay et al., 2014b). The shortly co-milled ITZ–superdisintegrants had a mixture of large swollen superdisintegrant particles and ITZ nanoparticles (Figure 6.2e), which was reflected by the high d_{90} values in Figure 6.1a. Note that the d_{50} and d_{90} of the SSG, CP, and CCS particles swollen in 2.5% HPC solution, without milling, are 113.7 ± 0.1 μm and 171.4 ± 0.2 μm; 29.9 ± 0.0 μm and 65.8 ± 0.3 μm; and 137.5 ± 0.3 μm and 213.8 ± 0.8 μm, respectively. Hence, albeit being short, the wet milling of the superdisintegrants seems to be effective for breakage of large swollen particles during the wet co-milling of ITZ–superdisintegrant.

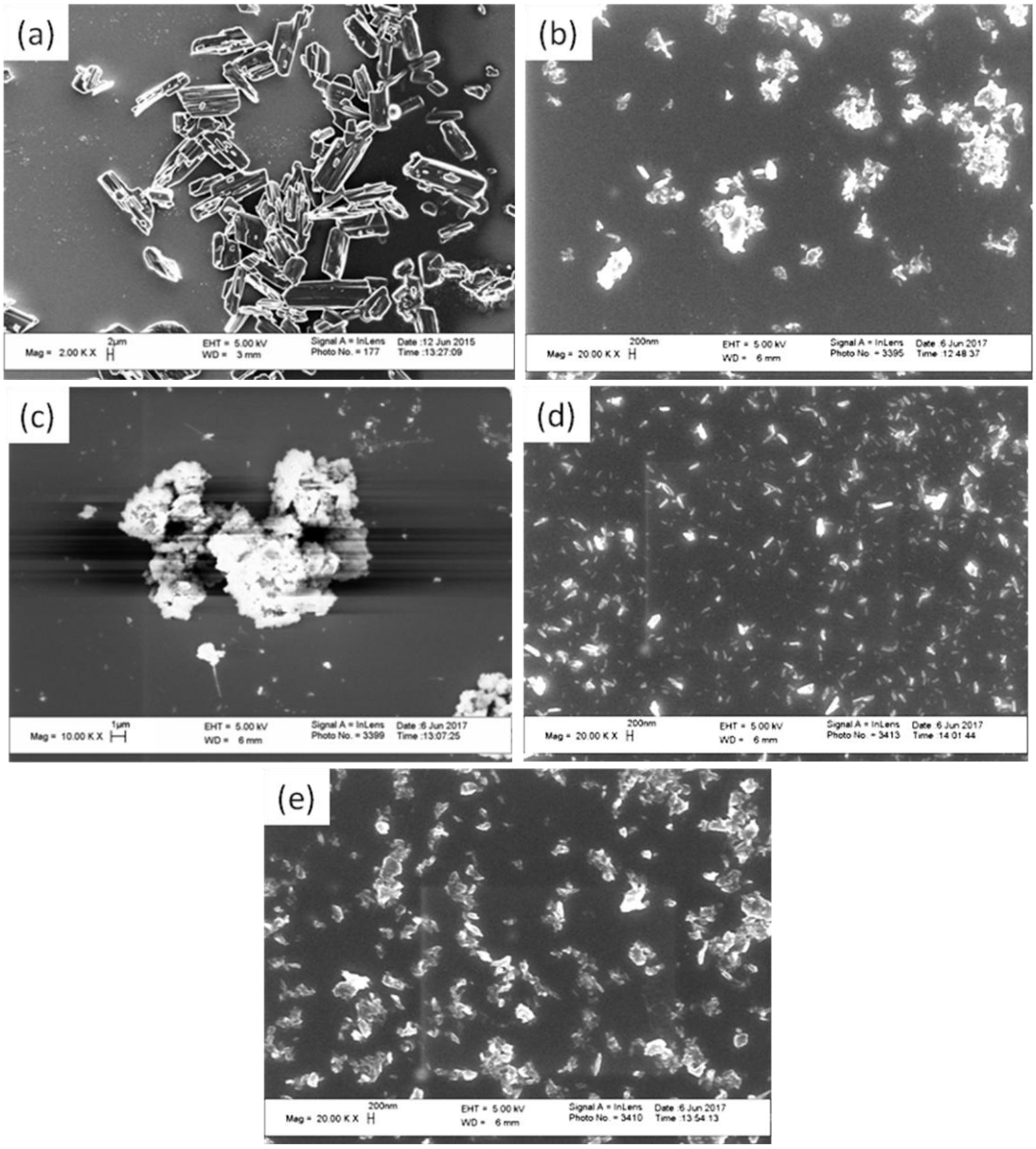

Figure 6.2 SEM images of the ITZ particles: (a) as-received ITZ before milling and the ITZ precursor suspensions with (b) 2.5% HPC (F1), (c) 0.2% SDS (F2), (d) 2.5% HPC–0.2% SDS (F3), (e) 2.5% HPC–2% co-milled SSG (F12).

As the volume-based PSD (Figure 6.1a) is much more heavily weighted by the large particles than smaller ones, the volume-based PSD of ITZ–superdisintegrants particles in F11–F16 suspensions is largely dominated by the large volume occupied by the swollen superdisintegrants. On the other hand, the area-

based distribution (Figure 6.1b) provides evidence of the presence of colloidal ITZ particles, while masking the effects of coarse swollen superdisintegrant particles (Azad et al., 2015b; Bhakay et al., 2014b), because, mathematically, coarse superdisintegrants weigh much less in the area-based PSD than in the volume-based PSD. In fact, when a suspension did not have a significant amount of aggregates and/or large superdisintegrant particles, the area-based particle size statistics were similar to the volume-based particle size statistics (e.g., for F3, F10, and F17).

Although the drug suspensions were spray dried into nanocomposite powders within the same day, a small portion of drug suspensions was kept at 8 ˚C for 7 days for the evaluation of short-term storage stability. For well-stabilized ITZ suspensions (F3, F10, and F17), little shift in particle sizes was observed (data can be found in *Appendix C* Table C1). However, for F1 suspension, wherein ITZ was stabilized by 2.5% HPC alone, ITZ particles were aggregated during/after milling and significant particle size increase was observed during the storage. Other suspensions with co-milled superdisintegrants, except 1% SSG (F11), also showed increased aggregation. While the presence of Mannitol or Sucrose did not change the ITZ size during milling, they seem to reduce the extent of aggregation during storage as compared to HPC alone (F1). These results support the need for a drying process like spray-drying to convert suspensions to nanocomposite powders for long-term storage.

6.2.2 A Rheological Characterization of the Precursor Suspensions

Laser diffraction involves a dilution step for particle sizing of the precursor suspensions, which affects the interpretation of the aggregation state of the drug.

Here, an orthogonal method, i.e., rheological characterization of the suspensions was carried out to further assess the aggregation state of the suspensions without dilution. The apparent shear viscosities of the stabilizer solutions (without the drug, corresponding to F1 and F3) and ITZ precursor suspensions of selected formulations (F1–3, F6, F9–17) were measured as a function of shear rate.

Figure 6.3a shows the viscosity of the stabilizer solutions. As the shear rate was increased, the viscosity of the stabilizer solution decreased slightly (shear-thinning behavior) and tend to an asymptotic value (Newtonian fluid behavior) above a shear rate of 200 1/s. Similar observation for stabilizer solutions was reported by Bilgili and Afolabi (2012). Besides, the addition of SDS in HPC solution significantly increased the viscosity due to the formation of HPC–SDS aggregates or micelle-like SDS clusters bound to the polymer (Berglund et al., 2003; Evertsson and Nilsson, 1997; Winnik and Winnik, 1990), which could be another manifestation of the synergistic action of HPC–SDS combination. Thus, for stabilizer solutions, HPC–SDS had the highest viscosity followed by HPC alone. The viscosity of SDS solution was not reported due to the inaccuracy of the instrument at low viscosity region (< 5 cP).

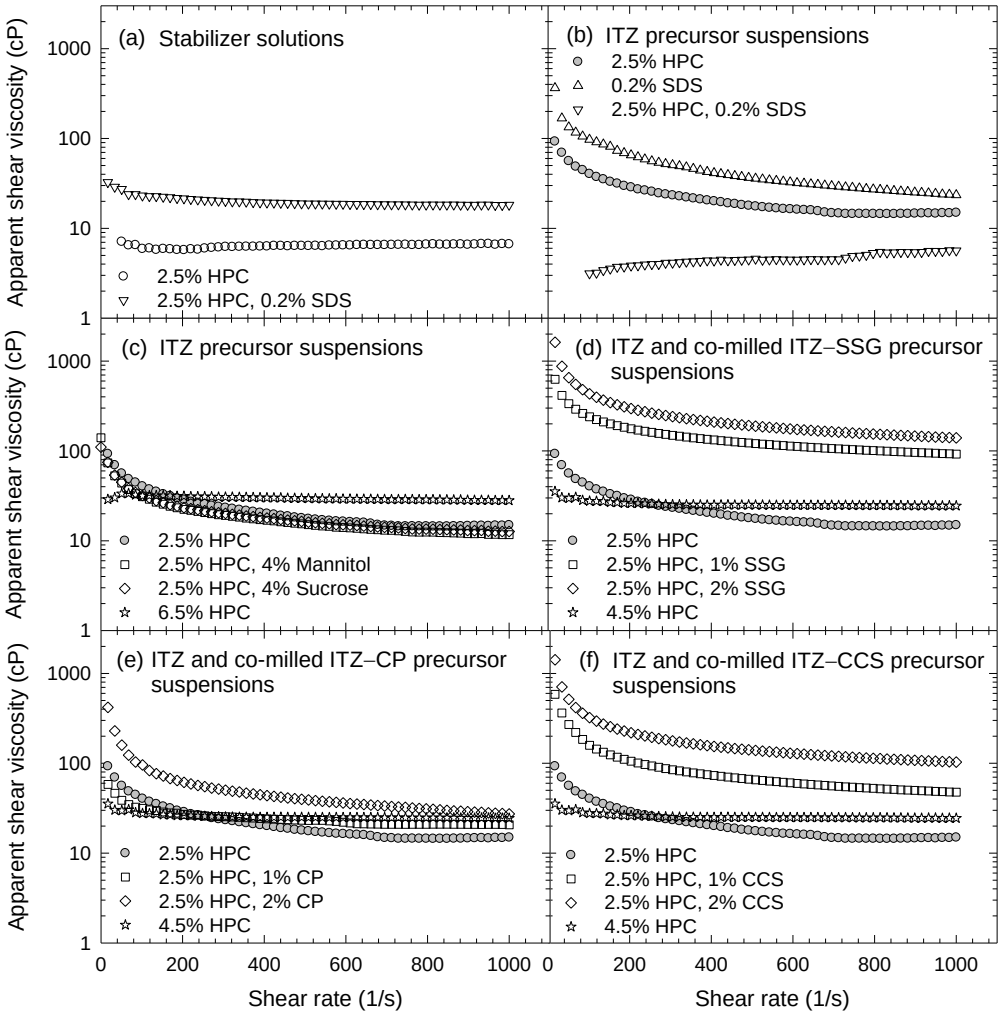

Figure 6.3 Apparent shear viscosity of (a) various stabilizer solutions (no drug) with HPC/SDS (F1 and F3), (b) ITZ precursor suspensions with HPC/SDS (F1–F3), (c) ITZ precursor suspensions with Mannitol (F6), Sucrose (F9), and wo/w extra HPC (F1/F10), (d) co-milled ITZ–SSG precursor suspensions (F11 and F12) and ITZ precursor suspensions wo/w extra HPC (F1/F17), (e) co-milled ITZ–CP precursor suspensions (F13 and F14) and ITZ precursor suspensions wo/w extra HPC (F1/F17), and (f) co-milled ITZ–CCS precursor suspensions (F15 and F16) and ITZ precursor suspensions wo/w extra HPC (F1/F17).

Drug precursor suspensions stabilized by 2.5% HPC (F1) or 0.2% SDS (F2) alone (Fig. 3b) show a high viscosity initially and exhibited strong shear-thinning behavior that was prevalent up to 700 1/s for F1 and 1000 1/s for F2. This finding accords well with other studies in literature and could be attributed to the higher

extent of aggregation breakage (deaggregation) at high shear rate (Barthelmes et al., 2003; Bernhardt et al., 1999). Presence of aggregates, which can occlude liquid in their void space, increases the effective volume fraction of the solid in a suspension with fixed solids loading. Hence, in general, an aggregated suspension had a higher shear viscosity than an otherwise fully dispersed suspension consisting of discrete primary particles. Since the ITZ aggregates broke more extensively at the higher shear rates, the apparent shear viscosity decreased with an increase in the shear rate. The drug precursor suspension stabilized by HPC–SDS (F3) had the lowest apparent shear viscosity with near Newtonian behavior (Figure 6.3b), which indicates the well-dispersed nature of the drug suspension and the least amount of aggregates. Overall, these findings corroborate the aggregation state assessment based on laser diffraction and SEM imaging in *Section 6.2.1*.

The apparent shear viscosity profiles of the precursor suspensions with 4% Mannitol or Sucrose or 4% extra HPC (6.5% HPC total) (F6, F9, and F10, respectively) are presented in Figure 6.3c. All formulations where additional dispersants were added have 2.5% HPC as a baseline in the precursor suspensions. The addition of even 4% Mannitol or Sucrose (the highest amount of extra dispersants added in this study) did not increase the shear viscosity of the precursor suspensions. Besides, they all show similar shear-thinning behavior, which indicates a significant amount of aggregates in the precursor suspensions. However, when extra 4% HPC was used (6.5% HPC in total), the suspension exhibited higher shear viscosity and near Newtonian behavior. The near Newtonian behavior indicates the

well-dispersed discrete primary particles (i.e., good physical stability) in F10 precursor suspension.

Unlike the addition of Mannitol or Sucrose, co-milling 1% SSG (Figure 6.3d) or 1% CCS along with ITZ (Figure 6.3f) significantly raised the viscosity of the drug precursor suspensions because of the removal of free water in the suspension via absorption by highly swellable superdisintegrants. On the other hand, co-milling 1% CP (Figure 6.3e) did not seem to raise the shear viscosity as significantly, which is due to the low swelling capacity of CP (i.e., 5.4 cm^3/g) as compared to 23.6 cm^3/g for SSG and 13.5 cm^3/g for CCS. The increase in superdisintegrant concentration led to the higher shear viscosity of the precursor suspensions. Moreover, all precursor suspensions with co-milled superdisintegrants exhibited shear-thinning behavior, which again indicates the existence of aggregates. When extra 2% HPC was added to the precursor suspension (4.5% HPC in total), the suspension shows very slight shear-thinning initially followed by Newtonian behavior, which indicates slightly aggregated suspension. In sum, the viscosity measurements (Figure 6.3) independently confirmed the aggregation state of the milled ITZ suspensions, agreeing well with the laser diffraction data (see Figure 6.1).

6.2.3 Crystallinity of the Drug Nanoparticles

The crystalline state of the ITZ particles in the precursor suspensions (after milling) was investigated via the XRPD and DSC on the pure ITZ, physical mixtures corresponding to F12 and F17 formulations, and overnight-dried ITZ precursor suspensions of F2, F12, and F17 after rinsing–centrifugation. ITZ showed distinct

crystalline peaks in the precursor suspensions as compared to as-received ITZ and its physical mixtures in XRPD diffractograms (Figure 6.4a). The peak positions for the precursor suspensions remained the same but with lower peak intensity, which could be attributed to defect formation and accumulation during milling (Azad et al., 2015b; Monteiro et al., 2013) and slight loss of crystallinity (Cerdeira et al., 2013b). Besides, the ITZ precursor suspensions also showed a more peak broadening compared to the physical mixture and the as-received ITZ, which might be due to the smaller drug particle sizes or stress and strain caused by the milling process (Bernard et al., 2008). Similar observation also reported by Van Eerdenbrugh et al. (2007) for loviride nanoparticles and by Cerdeira et al. (2013b) for ITZ nanoparticles.

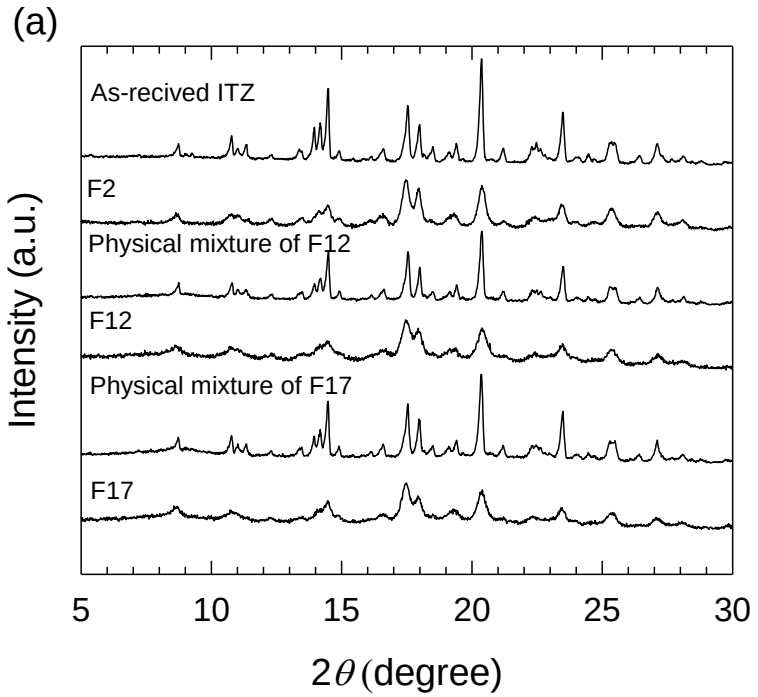

Figure 6.4 (a) XRPD diffractograms and (b) DSC thermograms of as-received ITZ, physical mixtures corresponding to F12 and F17 formulations, and overnight-dried ITZ precursor suspensions with 0.2% SDS (F2), 2.5% HPC–2% co-milled SSG (F12), and 4.5% HPC (F17). (Continued)

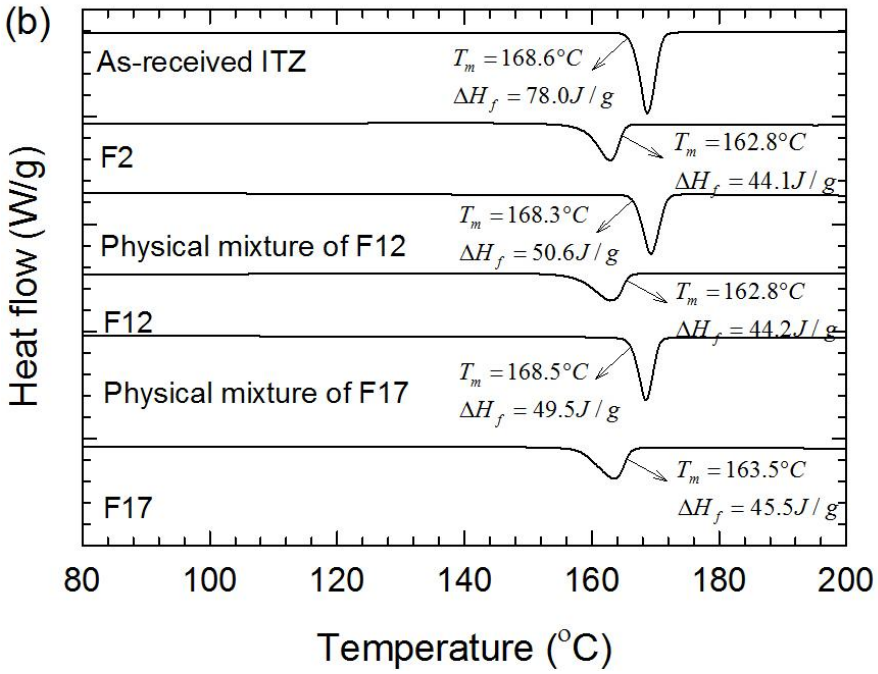

Figure 6.4 (Continued) (a) XRPD diffractograms and (b) DSC thermograms of as-received ITZ, physical mixtures corresponding to F12 and F17 formulations, and overnight-dried ITZ precursor suspensions with 0.2% SDS (F2), 2.5% HPC–2% co-milled SSG (F12), and 4.5% HPC (F17).

DSC thermograms of the physical mixtures and the precursor suspensions exhibited a notable endothermic event associated with the melting of crystalline ITZ (Figure 6.4b). The melting temperature of both as-received pure ITZ and its physical mixtures was detected at 168.4 ± 0.2 ˚C. A slight reduction of the peak melting temperature (T_m) in the precursor suspensions was observed (i.e., 5.5˚C and 5.0 ˚C for F12 and F17, respectively). Besides, there is a slight ΔH_m reduction with the precursor suspension comparing with its corresponding physical mixture (i.e., 12.6% and 8.1% for F12 and F17, respectively). The observed melting point reduction and peak reduction may due to the aforementioned defect formation–accumulation during milling–drying as well as the more efficient heat transfer during the DSC analysis for

the ITZ nanoparticles in comparison to that for the physical mixtures (Bonda et al., 2016; Liu et al., 2011; Shah et al., 2016). Besides, according to Gibbs–Thomson equation (Wu and Nancollas, 1998), the melting temperature of a material is proportional to its cohesive energy, which indicates that nanoparticles with reduced cohesive energy require less energy for melting, thus, resulting in a reduction of melting temperature and heat of fusion as compared to as-received drug microparticles. Based on the XRPD and DSC results, it can be concluded that wet media milling may have brought minor amorphous/defect formation in ITZ, but the crystallinity nature of ITZ was largely preserved.

6.2.4 Characterization of the Drug Nanocomposites

The precursor suspensions were spray dried into nanocomposite powders. Throughout the dissertation, all nanocomposites are labeled based on the formulation of the respective drug precursor suspension that was used as the feed during drying. The theoretical and actual drug contents of the nanocomposites are presented in Table 6.1. Table 6.1 presents that high drug-loaded nanocomposites (~55–80%) were prepared by spray drying process. Most nanocomposite powders had RSDs less than 6%, suggesting pharmaceutically acceptable content uniformity. The slight variations of actual drug content from the theoretical one may be attributable to preferential drug loss to the spray drying chamber, poor separation of finer particles in the cyclone of the spray drier, and the potential presence of residual moisture in the nanocomposite (Azad et al., 2015b). The mean moisture contents of selected nanocomposite powders, i.e., F1 and F12, were determined by weight loss via TGA. F1 and F12

nanocomposite powders had a residual moisture content of 2.6 ± 0.3% and 2.8 ± 0.4%, respectively, which demonstrates that most water in the drug precursor suspensions was removed during the spray drying process. Table 6.3 presents the particle sizes of the nanocomposites. For each dispersant class, an increase in the dispersant concentration led to slightly larger nanocomposites due to an increase in solids loading and viscosity. In general, spray drying produced small spherical and dimpled nanocomposite with drug nanoparticles embedded in the dispersant matrix (Figure 6.5). All formulations, except F2, contain HPC as a film–matrix former, which enables coverage and encapsulation of the drug nanoparticles. Note the irregular shapes of F2 nanocomposites (Figure 6.5b) and their smallest sizes among all nanocomposites indicate the criticality of HPC as a baseline dispersant.

It is likely that some large superdisintegrant particles may not be embedded into the nanocomposite particles. SSG, CP, and CCS were milled separately in the presence of 2.5% HPC for proper stabilization without drug (Azad et al., 2014b). After 15 min short milling (including 12 min addition of superdisintegrants to the mill), the produced d_{50} and d_{90} of SSG, CP, and CCS are 30.7 µm and 72.1 µm; 7.3 µm and 19.6 µm; and 39.3 µm and 91.2 µm, respectively, as measured by laser diffraction. Thus, the dried particle sizes of milled superdisintegrant particles were calculated based on their swelling ratio (refer to *Section 6.1.1*). The dried-milled d_{50} and d_{90} of SSG, CP, and CCS are estimated 7.7 µm and 17.2 µm; 5.3 µm and 14.6 µm; and 10.4 µm and 23.6 µm, respectively. Based on the study, there is also a possibility that drug nanoparticles were coated on the superdisintegrant particles and some superdisintegrant particles may be spray dried alone.

Table 6.3 Particle Size Distributions of the Nanocomposites Produced by Spray Drying

Formula ID	HPC (% w/w)[a]	SDS (% w/w)[a]	Other Dispersants (% w/w)[a]	Particle Sizes of the Nanocomposites					
				d_{10} (µm)	SD (µm)	d_{50} (µm)	SD (µm)	d_{90} (µm)	SD (µm)
F1	2.5	0	–	6.56	0.06	16.44	0.08	33.76	0.33
F2	0	0.2	–	1.97	0.15	8.43	1.18	18.74	1.80
F3	2.5	0.2	–	4.26	0.39	11.33	0.26	21.21	0.33
F4	2.5	0	1 (Mannitol)[b]	2.73	0.02	9.95	0.23	25.56	8.09
F5	2.5	0	2 (Mannitol)[b]	4.38	0.19	12.17	0.04	24.99	0.19
F6	2.5	0	4 (Mannitol)[b]	5.13	0.58	14.00	0.30	29.72	0.42
F7	2.5	0	1 (Sucrose)[b]	5.15	0.06	14.25	0.04	31.60	0.02
F8	2.5	0	2 (Sucrose)[b]	5.23	0.06	14.73	0.02	32.90	0.06
F9	2.5	0	4 (Sucrose)[b]	8.36	0.70	18.80	0.76	38.27	0.87
F10	6.5	0	–	7.56	0.24	20.53	0.38	48.45	1.27
F11	2.5	0	1 (SSG)[c]	7.97	0.08	16.30	0.13	31.75	0.62
F12	2.5	0	2 (SSG)[c]	9.90	0.13	19.67	0.13	36.63	0.10
F13	2.5	0	1 (CP)[c]	2.76	0.04	10.70	0.18	24.68	0.29
F14	2.5	0	2 (CP)[c]	5.80	0.17	15.51	0.17	33.66	0.41
F15	2.5	0	1 (CCS)[c]	6.67	0.03	13.73	0.18	25.93	1.21
F16	2.5	0	2 (CCS)[c]	9.43	0.35	20.36	0.23	40.03	0.33
F17	4.5	0	–	7.11	0.20	19.94	0.07	44.05	0.39

[a]Drug loading in all suspensions is 10%. % w/w is with respect to the weight of deionized water, 200 g.
[b]Added to the suspension after milling.
[c]Co-milled along with ITZ for 15 min.

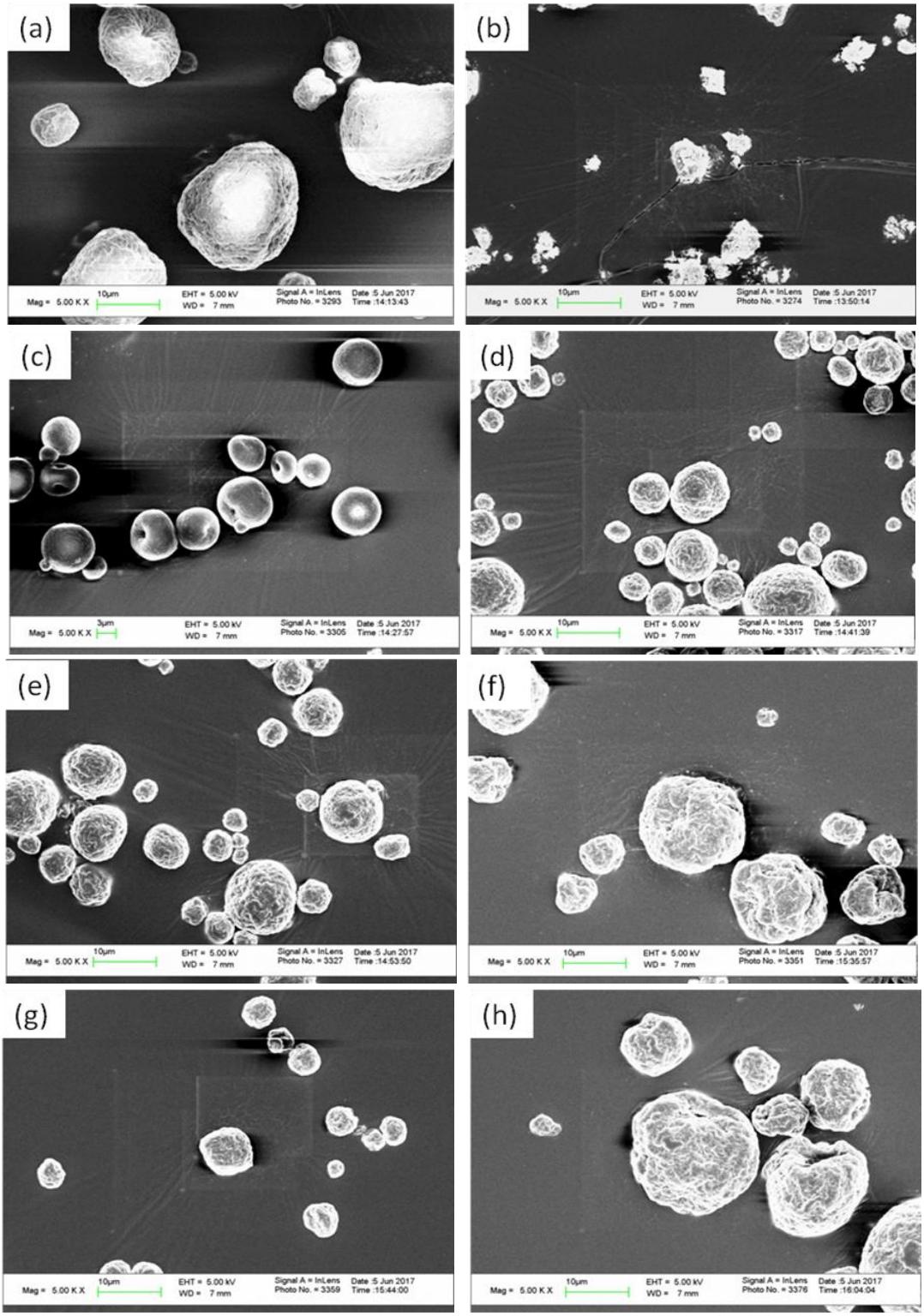

Figure 6.5 SEM images of the nanocomposites produced by spray drying of the ITZ precursor suspensions with: (a) 2.5% HPC (F1), (b) 0.2% SDS (F2), (c) 2.5% HPC–0.2% SDS (F3), (d) 2.5% HPC–2% Mannitol (F5), (e) 2.5% HPC–2% Sucrose (F8), (f) 2.5% HPC–2% co-milled SSG (F12), (g) 2.5% HPC–2% co-milled CP (F14), and (h) 2.5% HPC–2% co-milled CCS (F16).

6.2.5 Impact of Dispersants on the Drug Dissolution from Nanocomposites

The evolution of as-received (unmilled) ITZ and spray-dried nanocomposites was measured in 3 g/L SDS solution using a USP II apparatus. As discussed in Sections 6.2.1 and 6.2.2, both the laser diffraction and rheological characterization results presented in Figures 6.1 and 6.3 overall suggest that all drug precursor suspensions with 2.5% HPC, even with additional Mannitol/Sucrose/co-milled superdisintegrants, exhibited similar extent of aggregation during milling and larger particle sizes (d_{50}: ~210–260 nm and d_{90}: 400–470 nm, see Figure 6.1b) than the 2.5% HPC–0.2% SDS (F3), 6.5% HPC (F10), and 4.5% HPC (F17) suspensions, where aggregation was minimized. Hence, unless otherwise indicated below, for most dispersant formulations, the main impact of various dispersants on drug release during the dissolution is expected to be related to their capability to release drug nanoparticles from the nanocomposite particles, and much less related to the different drug particle sizes.

The as-received ITZ particles with d_{50}: 15.5 μm had extremely slow dissolution with only 7.3% of ITZ dissolved after 60 min, while the nanocomposites with wet-milled ITZ particles led to enhanced drug dissolution rate (Figure 6.6), regardless of the dispersants used. For nanocomposites with 2.5% HPC (F1) or 0.2% SDS (F2), the ITZ release was improved, i.e., 40.5% for F1 and 48.1% for F2 at 60 min. However, the dissolution rates from F1 and F2 are still low. Fast, immediate release was achieved when HPC and SDS (F3) were used in combination, i.e., 86.6% drug release within 5 min. All of these results can be explained by (i) the larger surface area of wet-milled ITZ as compared with as-received ITZ, (ii) enhanced

wettability of ITZ owing to the presence of dispersants (2.5% HPC–0.2% SDS >> 2.5% HPC > 0.2% SDS, refer to Table 6.2), which ensures the fast water penetration and dissolution-induced erosion/disintegration for F3, as well as (iii) the presence of smaller aggregates in precursor suspension of F3 as compared with those of F1 and F2 (Figure 6.2a).

In this study, the author aims to prepare high drug loaded, surfactant-free nanocomposites that can achieve fast immediate ITZ release similar to that of the F3 formulation by using additional soluble dispersants (Mannitol/Sucrose), swellable wet co-milled dispersants (SSG/CP/CCS) besides the baseline 2.5% HPC. Figure 6.6a and b also shows the impact of 1% dispersant. Upon addition of Mannitol (F4) or Sucrose (F7), the slight improvement on dissolutions was observed in Figure 6.6a, i.e., 48.9% for F4 and 50.8% for F7 at 60 min, but the dissolution profiles are still statistically similar to baseline nanocomposite (F1) according to similarity (f_2) and difference (f_1) factors (Table C3 in *Appendix C*). On the other hand, when 1% superdisintegrant, such as SSG (F11), CCS (F13), and CP (F15), were shortly co-milled with ITZ and thus incorporated into the nanocomposites, the dissolution performance of ITZ was significantly improved (Figure 6.6b). Quantitatively analysis of the dissolution data was carried out by using Korsmeyer–Peppas model (Korsmeyer et al., 1983). The drug release rates of nanocomposites with various dispersants are captured by *kn* in Table 6.4. All R^2 values are above 0.96, indicating a relatively good fitting by the Korsmeyer–Peppas model. According to Peppas (1985), a higher *kn* corresponds a faster drug release. Hence, superdisintegrants are better dispersants than sugar alcohol

or sugar at the same concentration (1%). More interestingly, their desirable impact positively correlated with their swelling capacity (SSG > CCS > CP).

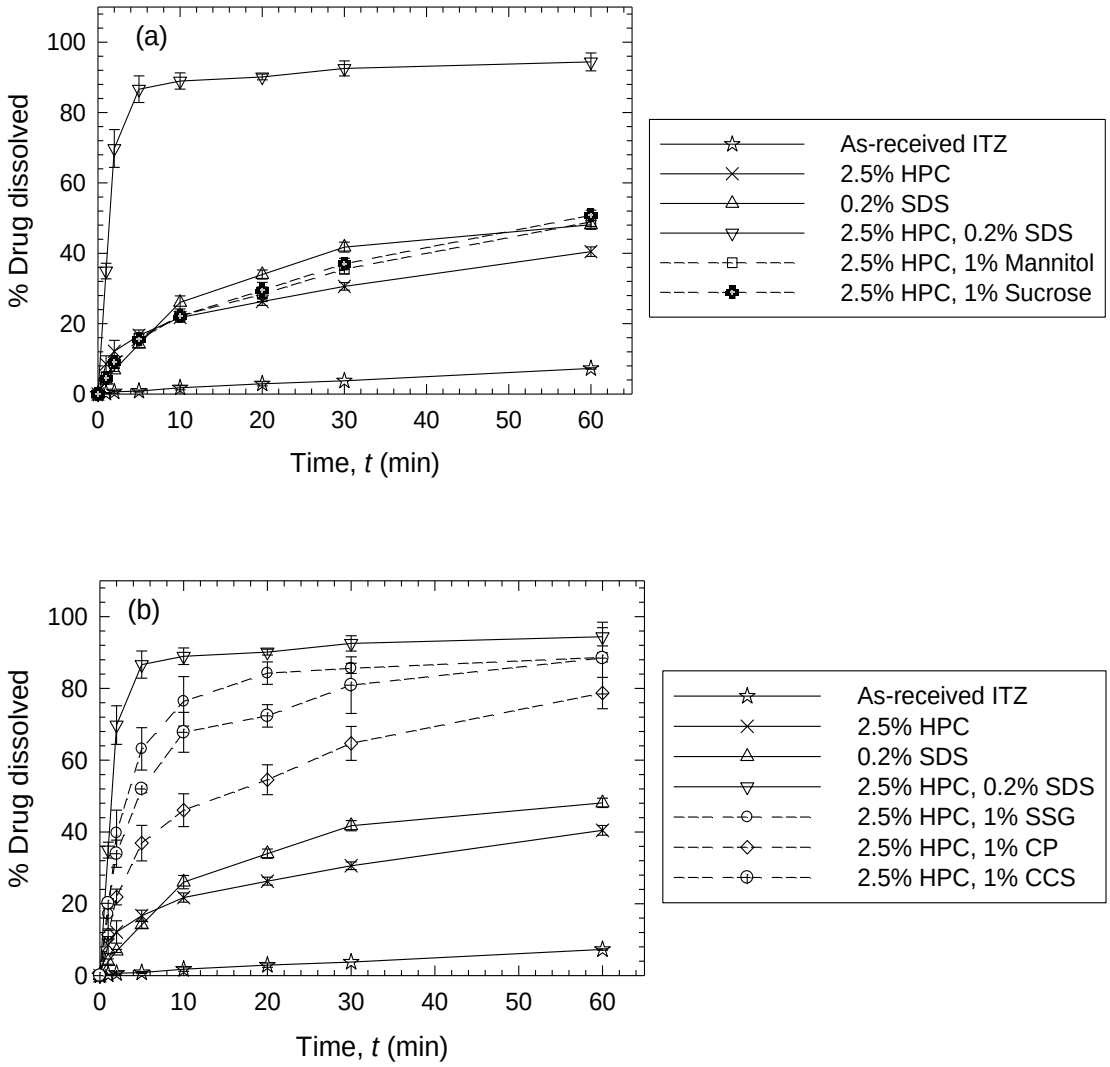

Figure 6.6 Evolution of ITZ dissolution from the nanocomposites prepared by spray drying of the ITZ precursor suspensions with 2.5% HPC–1% (a) Mannitol (F4), Sucrose (F7) and (b) co-milled SSG (F11), CP (F13), and CCS (F15). The figure includes dissolution performance of as-received ITZ and nanocomposite formulations with HPC/SDS (F1–F3) for comparison.

In general, the additional dispersants besides baseline 2.5% HPC led to a transition from diffusion controlled release to anomalous transport (Table 6.4). The

exceptions were F5 and F13. Conventional soluble dispersants such as HPC, Mannitol, and Sucrose, allows for drug release from the nanocomposite matrices via erosion/disintegration, which is initiated by their dissolution (Krull et al., 2016). On the other hand, the incorporation of shortly co-milled superdisintegrants along with soluble HPC facilitated erosion/disintegration of the nanocomposite matrix via both dissolution of HPC and swelling-induced degradation (Azad et al., 2015b; Bhakay et al., 2014b). The swellable superdisintegrant particles embedded in the nanocomposites tend to expand upon exposure to dissolution medium, but due to volumetric constraint within the matrix, mechanical stresses develop, facilitating the matrix erosion/disintegration. Apparently, simultaneous action of both mechanisms appears to be additive and more effective.

6.2.6 Impact of Higher Dispersant Concentration at 2% and 4% Levels

While dispersants at 1% level, besides 2.5% HPC, was shown to improve the ITZ release without SDS, even for the best performing superdisintegrant (1% SSG), the dissolution was still slower than/statistically different from 2.5% HPC–0.2% SDS nanocomposite, suggesting a need to increase the dispersant concentration. Hence, nanocomposites were also prepared by spray-drying 2.5% HPC and 2% dispersants. Generally, higher dispersant concentration improved the drug release rate for all dispersants as dissolution profiles were compared (Figure 6.7a vs. Figure 6.6), which also corresponded to a higher *kn* (Table 6.4). Again, the co-milled superdisintegrants are all superior to Mannitol/Sucrose with the same trend (release rates: SSG > CCS > CP). Furthermore, similarity and difference test (*f*1–*f*2 test) was conducted to

statistically compare the dissolution performance of ITZ–HPC–SDS (F3) and ITZ–HPC–SSG (F12). Their dissolution profiles are statistically similar to each other: $f1 = 7.2 < 15$ and $f2 = 62.3 > 50$ (Table C4 in *Appendix C*).

At 2% level, Mannitol/Sucrose in F5/F7 nanocomposites was not sufficient to improve the dissolution performance of ITZ to the extent that the F3 nanocomposite achieved. Thus, 4% Mannitol/Sucrose (F6/F9) was used as dispersants besides 2.5% HPC. These dispersants at 4% led to faster ITZ release from the nanocomposites (F6/F9) than at 2% level (F5/F7). Only when Mannitol/Sucrose (F5/F7) were used at 4% level, the dissolution profiles show a statistical difference from ITZ–HPC (F3) (Table C3 in *Appendix C*), but F5 and F7 still led to inferior performance as compared to F3 nanocomposites HPC–SDS (Figure 6.7b). While the use of higher than 4% Mannitol/Sucrose loading could further enhance the drug dissolution rate, this approach was not adopted here as it would cause a nanocomposite with much less than 50% drug loading.

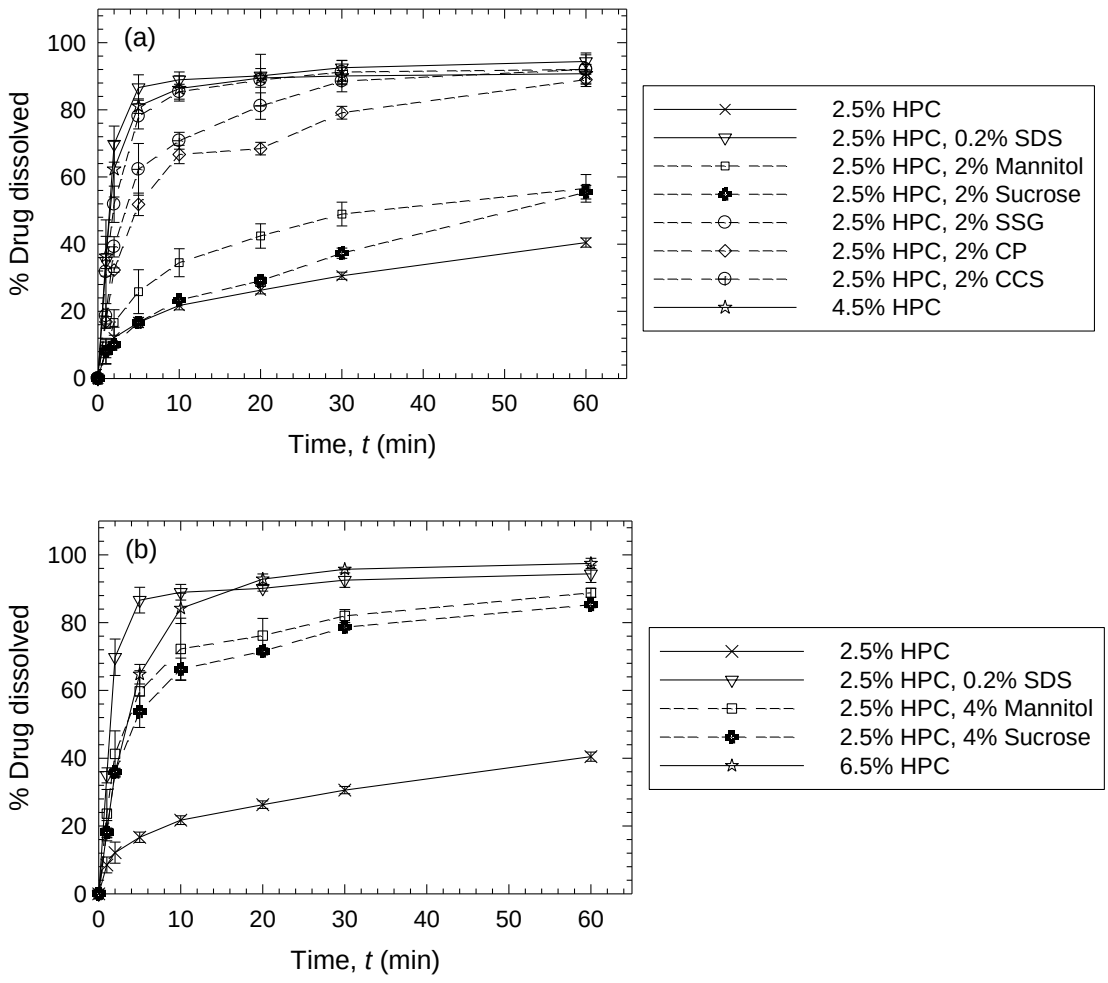

Figure 6.7 Evolution of ITZ dissolution from the nanocomposites prepared by spray drying of the ITZ precursor suspensions with (a) 2.5% HPC–2% Mannitol (F5), Sucrose (F8), co-milled SSG (F12), co-milled CP (F14), co-milled CCS (F16), and extra HPC (F17) and (b) 2.5% HPC–4% Mannitol (F6), Sucrose (F9), and extra HPC (F10). The figures also include dissolution performance of nanocomposite formulations with HPC/SDS (F1 and F3) for comparison.

Table 6.4 Statistical Analysis of the Fitting of the Drug Dissolution Profiles via Korsmeyer–Peppas Model

Formula ID	HPC (% w/w)[a]	SDS (% w/w)[a]	Other Additives (% w/w)[a]	Korsmeyer–Peppas Model[d]			*kn* (%min^{-n})
				n[d] (-)	*k* (%min^{-n})	R^2	
F1	2.5	0	–	0.360	9.155	0.998	3.30
F2	0	0.2	–	0.468	7.667	0.963	3.59
F3	2.5	0.2	–	0.998	34.95	1.000	34.86
F4	2.5	0	1 (Mannitol)[b]	0.484	6.795	0.995	3.29
F5	2.5	0	2 (Mannitol)[b]	0.414	12.33	0.985	5.10
F6	2.5	0	4 (Mannitol)[b]	0.516	26.45	0.989	13.64
F7	2.5	0	1 (Sucrose)[b]	0.498	6.682	0.997	3.33
F8	2.5	0	2 (Sucrose)[b]	0.498	7.070	0.995	3.52
F9	2.5	0	4 (Sucrose)[b]	0.462	23.69	0.978	10.95
F10	6.5	0	–	0.721	20.46	0.997	14.74
F11	2.5	0	1 (SSG)[c]	0.674	21.73	0.979	14.65
F12	2.5	0	2 (SSG)[c]	0.709	31.73	1.000	22.50
F13	2.5	0	1 (CP)[c]	0.296	17.17	0.979	5.08
F14	2.5	0	2 (CP)[c]	0.509	21.28	0.986	10.84
F15	2.5	0	1 (CCS)[c]	0.474	23.21	0.993	11.00
F16	2.5	0	2 (CCS)[c]	0.646	22.36	0.985	14.45
F17	4.5	0	–	0.776	36.40	1.000	28.26

[a]Drug loading in all suspensions is 10%. % w/w is with respect to the weight of deionized water, 200 g.
[b]Added to the suspension after milling.
[c]Co-milled along with ITZ for 15 min.
[d]$n \approx 0.43$ indicates diffusion-controlled release, $0.43 < n < 0.85$ indicates anomalous transport, while $n \approx 0.85$ indicates erosion-controlled release (Ritger and Peppas, 1987).

6.2.7 Additional Insight into the Dispersants

Finally, the author would like to examine the impact of higher HPC concentration, i.e., 6.5% (F10) and 4.5% (F17) as opposed to the use of additional dispersants such as Mannitol/Sucrose or superdisintegrants. Comparing the drug release rates of the nanocomposites at the same total dispersant level allows us to assess the relative impact of the dispersants. The dissolution performance of the nanocomposite with 4.5% HPC (F17) was compared to those with 2.5% HPC–2% additional dispersant (F5, F8, F12, F14, and F16) (see Figure 6.7a). Note that different from the addition of Mannitol/Sucrose to the milled ITZ suspension, additional 2% HPC (4.5% HPC total) was performed during the preparation of presuspension before milling. As mentioned in Section 6.2.1, higher HPC concentration (4.5% vs. 2.5%) led to smaller drug nanoparticle aggregates in the precursor suspension (F17 vs. F1, F5, F8, F12, F14, and F16). Hence, F17 nanocomposite embedded smaller drug nanoparticles than F1, F5, F8, F12, F14, F16 nanocomposites (see Figure 6.2a and Tables C1 and C2 in *Appendix C*). F17 nanocomposite (4.5% HPC) released ITZ similar to F12 nanocomposite (2.5% HPC–2% SSG combination), according to f_1–f_2 statistics (Table C5 in *Appendix C*), and both released ITZ faster than the nanocomposites with 2.5% HPC–2% Mannitol/Sucrose combination, with a 4.5% total dispersant concentration. Since the presence of extra HPC reduced ITZ drug nanoparticle aggregation in the precursor suspension (Figure 6.1), upon the erosion of F17 nanocomposite matrix, more discrete drug nanoparticles were released and dissolved in dissolution media as compared with the nanocomposites with HPC–Mannitol/Sucrose.

Since Mannitol/Sucrose has been used at a higher concentration for the effective dissolution improvement, 6.5% HPC (F10) was compared to 2.5% HPC–4% Mannitol/Sucrose (F6 and F9). Having more HPC than F17 precursor suspension (4.5%), F10 precursor suspension (6.5% HPC) exhibited the least aggregation and smallest particle sizes in the absence of SDS. The resultant F10 nanocomposite released ITZ faster than F6/F9 nanocomposite with HPC–Mannitol/Sucrose at the same total dispersant concentration. Hence, better dissolution improvement imparted by HPC vs. Mannitol/Sucrose can be ascribed to (i) the smaller ITZ aggregates and the release of discrete fast-dissolving drug nanoparticles when 6.5% HPC alone was used and (ii) the significantly enhanced wettability of ITZ (6.5% HPC >> 2.5% HPC–4% Mannitol > 2.5% HPC–4% Sucrose, refer to Table 6.2), which ensures the fast water penetration and dissolution-induced erosion/disintegration for F10. Interestingly, a comparison of ITZ release profiles for the nanocomposites with higher HPC concentration, i.e., 2.5% (F1), 4.5% (F17), and 6.5% (F10) HPC in the respective precursor suspensions in Figure 6.7a and b, one notes an optimum HPC concentration leading to the fastest drug release, which is 4.5% HPC. Despite the enhanced wetting efficiency with higher HPC concentration (Table 6.2) and smaller ITZ nanoparticle aggregates in the respective precursor suspension, 6.5% HPC led to slower ITZ 4.5% HPC. This seemingly anomalous behavior could be due to gelling-induced slow erosion/dissolution of the polymeric matrix, which has been commonly observed in the literature (Knieke et al., 2015a; Möckel and Lippold, 1993; Shah and Sheth, 1976). Overall, the use of higher HPC concentration can be another strategy

for producing fast-dissolving, surfactant-free, high drug-loaded nanocomposite, but its concentration should not be increased beyond an optimal level.

6.3 Conclusions

Nanocomposites of itraconazole (a BCS Class II drug) was prepared by spray-drying precursor wet media milled drug suspensions with various classes of dispersants with the goal of elucidating their roles in drug nanoparticle stabilization and drug release from the nanocomposites during dissolution. The highest dissolution enhancement was obtained via 2.5% HPC (soluble polymer)–0.2% SDS (anionic surfactant) combination due to enhanced ITZ wettability and presence of smallest drug nanoparticles in the precursor suspension. To achieve similar fast, immediate release without the surfactant, either wet co-milled superdisintegrants (SSG, CCS, CP) at 2% level must be used along with 2.5% HPC or 4.5% HPC must be used. Wet co-milled superdisintegrants are much more effective dispersants than conventional, water-soluble, low molecular weight dispersants like Mannitol/Sucrose. More importantly, the impact of superdisintegrants positively correlated with their swelling capacity (SSG>CCS>CP), signifying a swelling-induced erosion/disintegration mechanism for fast drug dissolution. The release and dissolution of drug nanoparticles from nanocomposites is governed by both the aggregates sizes of the drug and erosion/disintegration of the nanocomposite matrix. Dispersants affect and modulate the drug release through their impact on both. Erosion/disintegration of the nanocomposite is caused by the dissolution of the soluble polymer or sugar/sugar alcohol and/or the swelling-induced degradation induced by the wet co-milled

superdisintegrants. Overall, this study demonstrates that fast-dissolving, high drug-loaded, surfactant-free nanocomposites could be prepared with either HPC–co-milled superdisintegrant or optimal HPC concentration via spray drying.

CHAPTER 7

A COMPARATIVE ASSESSMENT OF NANOCOMPOSITES VS. AMORPHOUS SOLID DISPERSIONS PREPARED VIA NANOEXTRUSION FOR DRUG DISSOLUTION ENHANCEMENT

Previous chapters have demonstrated the impact of producing nanocrystals with large surface area on the dissolution enhancement of poorly water-soluble drugs. However, compared to amorphous form of the drug, the achieved increase in dissolution rate via nanoparticle-based formulations is limited and insufficient to provide significant enhancement of bioavailability for drugs with very low aqueous solubility. Interestingly, there is no head-to-head comparison established in literature to assess the dissolution enhancement of these drugs in both nanoparticles-based formulations as well as amorphous solid dispersions. In Chapter 7, the author proposes to use the nanoextrusion process as a platform enabling comparative assessment of nanocomposites vs. ASDs for drug dissolution enhancement. By using different polymers, the same nanoextrusion process can produce extrudates with crystalline and amorphous forms of the same drug, i.e., micro/nanocrystalline drug dispersed in the polymeric matrix (micro/nanocomposites) and amorphous drug molecularly dispersed within the polymer (ASD), respectively. To this end, hydroxypropyl cellulose (HPC) and Soluplus® were used to stabilize wet-milled griseofulvin (GF) suspensions and form the matrix of the extrudates during nanoextrusion. To assess the impact of drug particle size, GF suspensions with different GF particle sizes were prepared by wet stirred media milling using HPC and Soluplus® in the presence/absence of sodium dodecyl sulfate (SDS), an anionic surfactant. These

suspensions along with additional polymer (HPC/Soluplus®) were fed to a co-rotating twin-screw extruder, which dried the suspensions and formed various extrudates. The extrudates were milled into powders via mortar–pestle and sieved for further analysis. As a comparison to nanoextrusion, nanocomposite particles were also prepared via spray drying of the GF nanosuspension. The suspensions were characterized via laser diffraction, while the extrudates and their milled powders were characterized by laser diffraction, BET nitrogen adsorption, SEM, and XRD. Digital microscopy was used to visualize the changes of different polymeric matrices when exposed to water. Drug wettability enhancement by HPC and Soluplus® solutions with SDS was studied using the modified Washburn method. In general, a relatively low drug dose, i.e., 8.9 mg, was used to investigate the dissolution response under non-supersaturating conditions. To gain additional insight, few experiments used extrudate powder samples with excess drug (100 mg dose) to allow for supersaturation in the bulk dissolution medium. It is hypothesized that drug nanocrystals in the nanocomposites can dissolve faster than the amorphous drug in ASDs when the drug dose is so low not to cause supersaturation in the bulk dissolution medium (low drug dose), depending on the polymeric matrix. The effects of drug particle size in the feed suspensions and polymeric matrix type–size of the milled extrudates were also examined.

7.1 Materials and Methods

7.1.1 Materials

BP/EP grade griseofulvin (GF) was purchased from Letco Medical (Decatur, AL, USA). GF is a Biopharmaceutical Classification System (BCS) Class II drug with an aqueous solubility of 8.9 mg/L at 25 °C and 14.5 mg/L at 37 °C, melting point of 220 °C, and a glass transition temperature of 79 °C. Hydroxypropyl cellulose (HPC, SL grade, Nisso America Inc., New York, NY) and Soluplus® (BASF, Tarrytown, NY) were used as a polymeric stabilizer during wet media milling and polymeric matrix former during nanoextrusion and spray-drying processes. HPC is an amorphous polymer with two softening points at 68 and 178 °C, and has been commonly used to produce nanoparticle-laden nanocomposites of several BCS Class II drugs (Azad et al., 2015b; Bhakay et al., 2014a). Soluplus® is an amphiphilic polyvinyl caprolactam–polyvinyl acetate–polyethylene glycol graft copolymer. It is amorphous with a single glass transition temperature of 73 ± 2 °C and is widely used to prepare ASDs of various poorly water-soluble drugs via traditional HME process (Hardung et al., 2010; Kyerematen et al., 2014; Li et al., 2015a). Sodium dodecyl sulfate (SDS, GFS Chemicals, Inc., Columbus, OH) was used as an anionic surfactant to enhance the drug wettability and stabilize drug particles during milling. Its critical micelle concentration (CMC) in water is 0.23 wt.% at ambient temperature. Methanol (ACS reagent, ≥ 99.8%), purchased from Fisher Scientific (Suwanee, GA), was used as a solvent. Yttrium stabilized zirconia beads (Zirmil Y, Saint Gobain ZirPro, Mountainside, NJ, USA) with a median size of 430 µm were used as the milling media.

7.1.2 Preparation of Suspensions via Wet Media Milling

Table 7.1 presents the formulations of the GF (drug) suspensions. Drug concentration was kept at 22.4 wt.% in all suspensions. The concentrations reported for suspensions are with respect to the total suspension mass. Based on a previous milling study on GF (Bilgili and Afolabi, 2012), various GF suspensions were prepared to elucidate the potential impact of drug particle size on the dissolution. The F1 suspension had as-received, unmilled GF particles in HPC–SDS solution, whereas GF was milled for the preparation of F2, F4, and F5 suspensions in the presence of HPC or Soluplus® and SDS. SDS was avoided purposefully in F3 suspension in order to prepare a GF suspension with aggregated drug nanoparticles. A Microcer wet stirred media mill (Netzsch Fine Particle Technology, LLC, Exton, PA, USA) with 80 ml chamber was used to mill the drug suspensions. Feed suspensions were milled for 120 min under identical conditions to those reported in Bilgili and Afolabi (2012). The particle sizes of the suspensions after milling were determined using laser diffraction, and the suspensions were refrigerated at 8 °C for one day before nanoextrusion or spray drying.

Table 7.1 Formulations of the Drug (GF) Suspensions Fed in Nanoextrusion and Spray-Drying Processes and Drug Content in the Produced Composites and Amorphous Solid Dispersion (ASD)

Formula ID	Drug Suspension				Composites/ASD Powder[a]		
	Polymer (% w/w)[b]	SDS (% w/w)[b]	Drug Particle Size (µm)		Drug Content (RSD) (% w/w)[c]	Particle (Matrix) Size (µm)	
			D_{50}, SD	D_{90}, SD		D_{50}, SD	D_{90}, SD
F1	HPC, 1.9	0.2	15.28, 0.123	37.48, 0.973	22.7 (5.79)	127.9, 6.3	199.1, 13.6
F2	HPC, 1.9	0.2	0.155, 0.001	0.225, 0.001	23.0 (0.33)	121.8, 2.4	214.3, 11.9
F3	HPC, 1.9	0	3.763, 0.349	7.488, 1.114	23.7 (4.64)	113.0, 0.5	236.4, 1.2
F4	Soluplus®, 1.9	0.2	0.154, 0.000	0.205, 0.000	23.4 (5.81)	121.9, 9.0	202.7, 13.1
F5[d]	HPC, 1.9	0.2	0.154, 0.000	0.220, 0.000	24.1 (5.59)	17.9, 2.6	39.0, 3.5

[a]Additional polymer was added to the drug suspension at 1:1.5 mass ratio during nanoextrusion and prior to spray drying.
[b]w/w with respect to total suspension mass. GF concentration in the suspension was 22.4% w/w for all formulations.
[c]w/w with respect to total composite/ASD mass.
[d]Suspension was spray-dried following the addition of extra HPC to form the nanocomposites.

7.1.3 Nanoextrusion Process

Nanoextrusion was performed with a Nano-16 co-rotating twin-screw extruder (Leistritz Extrusionstechnik GmbH, Nürnberg, Germany) with a die having a 0.8 mm hole. The extruder barrel has three temperature-controlled zones, which are individually heated with electric heaters and cooled with water. The temperatures of the individual heating zones and the die are shown in Figure 6.1. The screw-speed was kept at 50 rpm. Additional HPC and Soluplus®, which were used as polymeric matrix formers during nanoextrusion besides acting as stabilizers in wet media milling, were fed in feeding section before Zone 1 via an Accurate 102M volumetric feeder (Schenck Process, Whitewater, WI) at the rate of 0.8 g/min. Zone 1 with all conveying elements served to soften the polymer. Zone 2 had kneading elements with 60° offset angle and served as a mixing zone. Each drug suspension was fed to Zone 2, ahead of the kneading elements, by using a peristaltic pump (Masterflex L/S Cole-Parmer Company, USA) at the constant rate of 1.2 g/min. Kneading elements provided intense mixing, which ensured homogeneous dispersion and distribution of the suspension within the molten polymeric matrix. After intense mixing via forward kneading elements in Zone 2, most of the water in the feed suspension evaporated in Zone 3, with conveying elements in place and 150 ºC barrel temperature. The extrudates that exit the die at 160 ºC were cooled to room temperature and milled into powders with D_{50} ranging 113–128 μm (Table 7.1) with a mortar–pestle to eliminate/minimize the potential confounding effect of matrix size on the dissolution rate among different formulations. Besides, a portion of F4 extrudate powder was passed through 90 μm sieve with the objective of studying the matrix size effect.

These powders will be generally referred to as extrudate powders throughout the dissertation, unless otherwise specified as micro/nanocomposites or ASDs, where more appropriate.

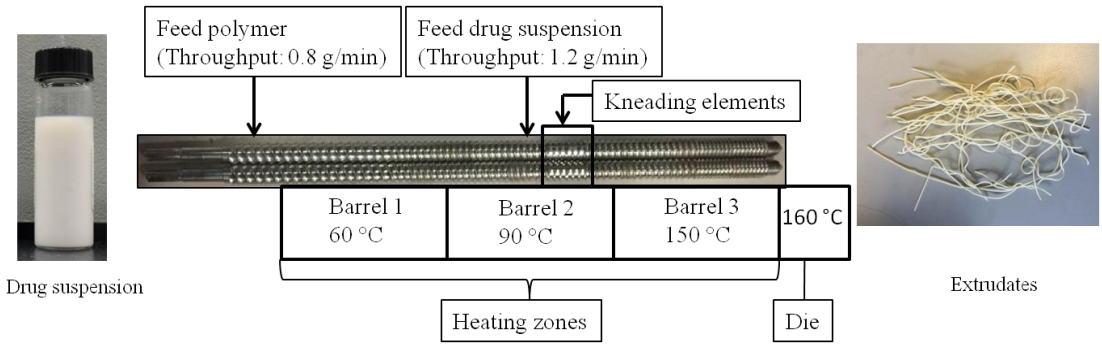

Figure 7.1 Schematic illustration of the extruder setup, including the process temperature of the barrel zones, the screw configuration, and the throughput of the feeder before barrel 1 and the liquid side-feeding device in barrel 2.

7.1.4 Spray Drying Process

One nanosuspension (F5) prepared via wet media milling was also dried using a spray dryer (4M8-Trix, Procept, Zelzate, Belgium), which is a more common method to dry a wet-milled suspension. The spray dryer was run in a co-current flow setup. Additional HPC was added to the milled suspension (F5) to ensure that the dried nanocomposite powder would have the same drug–polymer concentration as the extrudates. The suspensions were atomized and spray-dried under identical conditions to those in Azad et al. (2015b).

7.1.5 Measurement of Particle Size, External Surface Area, and Specific Total Surface Area

Drug particle sizes in suspensions were measured using laser diffraction (LS 13 320, Coulter Beckman, Brea, CA, USA) based on Mie scattering theory following the procedure in Bilgili et al. (2016d). The particle sizes of the extrudate powders and the spray-dried nanocomposites were measured by a Rodos/Helos laser diffraction system (Sympatec, NJ, USA) based on Fraunhofer theory following the procedure in Li et al. (2016b). Assuming that the GF particles in the GF suspensions are approximately spherical with smooth surfaces, the geometric (external) surface area (S_{ext}) of the drug particles was calculated from the particle size distribution data using the relationship $S_{ext} = 6/D_{32}$ (Allen, 2003; Jelinek and sz. Kovats, 1994; Monteiro et al., 2013), where D_{32} is the surface-weighted diameter (Allen, 2003), also known as the Sauter mean diameter.

F1–F4 extrudate powders, spray-dried nanocomposites (F5), sieved F4 extrudate powder, and cylindrical threads of F2 and F4 extrudates were subjected to BET nitrogen adsorption with the objective of determining the specific surface area (S_v). The samples were degassed under vacuum at 45 ^oC for 4 h to remove atmospheric moisture bound to the particle surface prior to nitrogen adsorption. The specific surface area was determined from 11-point nitrogen adsorption isotherm using a Nova 3200 BET analyzer (Quantachrome Instruments, Boynton Beach, FL, USA).

7.1.6 Microscopy

The presence of the drug particles in extrudate threads was explored via imaging of their cross-sections by a LEO 1530 SVMP (Carl Zeiss, Inc., Peabody, MA, USA) scanning electron microscope (SEM). The extrudates (F1–F4) in thread form were quenched in liquid nitrogen and manually broken to generate a relatively smooth cross-section. The cross-sections cut were placed on an aluminum stub using carbon tape. All samples were then sputter coated with carbon using BAL-TEC MED 020 (BAL-TEC AG, Balzers, Switzerland) prior to imaging. Multiple images were taken to ensure consistent visualization from each sample.

A VH-Z100 digital microscope (KEYENCE Corp., Osaka, Japan) was used to observe the morphological changes of a mortar–pestle milled extrudate particle with different polymeric matrices, when exposed to deionized water. A milled particle with selected formulation (F2 and F4) was placed on a glass slide kept under VH-Z100. A 3 μl drop of deionized water was placed on the particle and images were captured at different times. Since the extrudate particle could not be fixed on the glass slide, more water droplets were not added, which would have allowed for full dissolution of the particles.

7.1.7 X-ray Powder Diffraction (XRD)

Drug dissolution from the nanocomposites/ASD was determined via a Distek 2100C dissolution tester (North Brunswick, NJ, USA) according to the USP II paddle method. The dissolution medium was 1000 ml deionized water that was maintained at 37 °C, and a paddle speed of 50 rpm was used for all runs. Deionized water allowed

for good discrimination of different formulations under non-sink conditions. The nanocomposites/ASD were weighed equivalent to a dose of 8.9 mg of GF. Relatively low dose was selected purposefully in this study. The dose number calculated based on 8.9 mg GF was 0.36, which is much smaller than the most BCS Class drugs (Kasim et al., 2004). The nanocomposites/ASD were poured into the dissolution medium and 4 ml samples were taken out manually at 1, 2, 5, 10, 20, 30, and 60 min. These aliquots were filtered with a 0.1 µm PVDF membrane type syringe filter before UV spectroscopy measurements to minimize any confounding effect of the undissolved drug aggregates. The amount of GF dissolved was measured by UV spectroscopy at a wavelength of 296 nm. Deionized water was used as the blank.

7.1.8 Thermogravimetric Analysis (TGA)

Thermogravimetric analysis (TGA) was performed using a TGA/DSC1/SF Stare system (Mettler Toledo, Inc., Columbus, OH) for the characterization of residual water. A 5 mg extruded composite powder (F1 and F2) or as-received HPC was placed in a ceramic crucible and heated from 25 °C to 150 °C at a constant rate of 10 °C/min under nitrogen flow.

7.1.9 Drug Wettability by HPC and Soluplus® Solutions with SDS

Wettability was studied via liquid penetration into a (drug) powder bed, also known as the modified Washburn method (Hołownia et al., 2008; Washburn, 1921), using Attension Sigma 700 (Biolin Scientific, Linthicum, MD, USA), which measures the mass of liquid penetrated into the drug powder bed as a function of time.

Experimental details can be found in *Appendix D*. In this study, liquids and powder are deionized water/stabilizer solution (HPC/Soluplus® with SDS) and GF, respectively. The apparent shear viscosity and surface tension of the liquids were respectively measured using R/S Plus Rheometer (Brookfield Engineering, Middleboro, MA, USA) and Attension Sigma 700 (Biolin Scientific, Linthicum, MD, USA). The ratio of the cosine of contact angles $\cos\theta_{ss}/\cos\theta_{w}$ was calculated using the Modified Washburn equation and used as a wetting effectiveness factor. Here, θ_{ss} is the contact angle between GF and the stabilizer solutions and θ_{w} is the contact angle between GF and deionized water. The ratio quantifies the drug wettability enhancement upon use of different stabilizers (polymers–surfactant) in water.

7.1.10 Determination of Drug Content and Drug Release

Maximum theoretical amount of GF in 100 mg extrudates was estimated to be 24.6 mg (F3). GF solubility in methanol is 3 mg/ml (Bhakay et al., 2014b). Hence, 100 mg of the extrudate powders was dissolved in 20 ml of methanol and sonicated for 30 min, followed by storage overnight to ensure that all GF had dissolved. An aliquot of 100 µl was taken from the GF solution and diluted into 10 ml methanol. The absorbance of all samples was measured at the wavelength of 292 nm by Ultraviolet (UV) spectroscopy in a UV Spectrophotometer (Agilent, Santa Clara, CA, USA), and drug concentration was determined based on a pre-established calibration curve. Six replicates from each formulation were used to calculate the mean drug content along with the percent relative standard deviation (RSD).

Unless otherwise stated, all dissolution testing in this study was conducted with low drug dose (8.9 mg GF), which did not lead to supersaturation in the bulk dissolution medium. Drug release from the composites and ASD samples was determined via a Distek 2100C dissolution tester (North Brunswick, NJ, USA) according to the USP II paddle method. The dissolution medium was 1000 ml deionized water at 37 °C, and a paddle speed of 50 rpm was used. Deionized water allows for good discrimination of different GF formulations under non-sink conditions (Bhakay et al., 2014a; Li et al., 2016b). The composites and ASD were weighed equivalent to a dose of 8.9 mg of GF. This relatively low drug dose, which could emulate highly-potent drugs, was purposely selected in this study to ensure non-supersaturating conditions in the dissolution medium as the GF solubility in water at 37 ^{o}C is 14.5 mg/L. The composites/ASD powders were poured into the dissolution medium and 4 ml samples were taken out manually at 1, 2, 5, 10, 20, 30, and 60 min. These aliquots were filtered with a 0.1 µm PVDF membrane-type syringe filter before UV spectroscopy measurements to minimize any confounding effect of the undissolved coarse drug aggregates. The amount of GF dissolved was measured by UV spectroscopy at a wavelength of 296 nm and determined based on a pre-established calibration curve. Deionized water was used as the blank.

To describe the drug release kinetics from different polymeric matrices, fitting of GF dissolution data to Korsmeyer–Peppas model (Ritger and Peppas, 1987a, b), as shown in Eq. (7.1), was performed using SigmaPlot's (Version 11) regression wizard.

$$\frac{M_t}{M_\infty} = kt^n \qquad (7.1)$$

where k is a constant incorporating structural and geometric characteristics of the drug dosage form, n is the release exponent, indicative of the drug release mechanism, and $\frac{M_t}{M_\infty}$ is fractional release of drug. An apparent release mechanism was suggested in this dissertation based on the fitted n value and the specific geometry of the samples in view of various assumptions behind Eq. (7.1) (refer to Ritger and Peppas (1987b)). Fitting of $\frac{M_t}{M_\infty}$ included data up to and including one point after attainment of $\frac{M_t}{M_\infty}$ value of 0.85.

To gain further insight into the dissolution mechanisms, additional dissolution experiments were conducted with excess drug (100 mg dose), which allowed for supersaturation in the bulk dissolution medium. In these experiments, as-received GF powder, F2 extrudate (nanocomposite powder), and F4 extrudate (ASD powder) were used in excess, with an equivalent dose of 100 mg GF under the same dissolution conditions, as described above. Dissolution testing was conducted for duration of 120 min with additional sampling at 90 and 120 min. The filtered samples were diluted with 37 ^{o}C deionized water at a ratio of 1 to 7 before UV spectroscopy measurement.

7.2 Results and Discussion

7.2.1 Wet Stirred Media Milling of Drug Suspensions

Table 6.1 presents the formulations of drug (GF) suspensions and their particle sizes as measured by laser diffraction. Several suspensions with different GF sizes were prepared to affect the drug dissolution rate from dried extrudates. F1–F3 and F5 suspensions have the same polymer (HPC) and surfactant (SDS) with identical

concentrations. F1 has as-received unmilled GF microparticles (D_{50} = 15.3 μm) in the suspension, whereas F2 and F5 have stabilized GF nanoparticles (D_{50} = 155 nm) obtained by wet media milling. HPC–SDS combination is known to stabilize GF nanosuspensions due to synergistic stabilizing action (Bilgili and Afolabi, 2012), which has been shown to work for multiple BCS Class II drugs (Bilgili et al., 2016d). HPC was also used as the sole stabilizer (F3), which lead to aggregated GF nanoparticles in the milled suspension (D_{50} = 3.76 μm). Although primary GF nanoparticles can be produced upon wet media milling, as shown by previous work (Bilgili and Afolabi, 2012; Bilgili et al., 2016d), without sufficient amount of polymeric stabilizers or addition of SDS, the GF nanoparticles aggregated significantly due to high attractive inter-particle forces (van der Waals, hydrophobic forces, etc.). Essentially, for F3 suspension, laser diffraction measured the size distribution of soft aggregates, i.e., loose clusters of nanoparticles held together by the attractive forces. Soluplus®–SDS combination was used as stabilizers in F4, where a different polymeric stabilizer/matrix was investigated as a comparison to F2. The sizes of the milled drug particles produced by F4 were very close to those produced by F2 and F5 with HPC–SDS as stabilizers. Similarity of the particle sizes in F2 and F5 suspensions with identical formulations and processing variables signifies reproducibility of the wet media milling process as the deviations were less than 2%. All suspensions were stored in a refrigerator at 8 ºC for one day before drying.

7.2.2 Preparation and Characterization of Composites and Amorphous Solid Dispersion

The nanoextrusion process used drug suspensions mentioned above and additional extrusion polymer as two separate feeds and continuously produced extrudates that contain the drug. The mean moisture content of as-received HPC and selected extrudates, i.e., F1 and F2 formulations, was determined by weight loss via TGA. As-received HPC had moisture content of 2.35% and final extruded composites had a residual moisture content of 2.48 ± 0.18%, which demonstrates that most water in the drug suspensions was removed during the nanoextrusion process.

It is hypothesized that depending on the polymer chosen and polymer–drug miscibility (Qian et al., 2010; Thakral and Thakral, 2013), extrudates could be either in the form of ASD with amorphous form of the drug molecularly dispersed in the polymeric matrix or drug micro/nanocomposites embedding crystalline drug particles in the polymeric matrix, respectively. SEM images of the cross-section of various extrudates are presented in Figure 7.2 GF microparticles in the range of 2–16 μm were embedded in the HPC matrix of F1 extrudate (Figure 7.2a and b). GF nanoparticles in the size range of 50–400 nm were well-dispersed in the HPC matrix of F2 extrudate (Figure 7.2c and d). These observations accord well with the sizes of the drug particles in the feed suspensions, as measured by laser diffraction (refer to Table 7.1). Some aggregates of the drug nanoparticles were observed in the cross-section of F3 extrudate (Figure 7.2e). SEM images overall show that F1, F2, and F3 extrudates had drug particles dispersed throughout the HPC matrix; hence, these extrudates can be referred to as microcomposites (extrudate with drug microparticles embedded) (Figure 7.2a and b), nanocomposites (extrudate with drug nanoparticles

embedded) (Figure 7.2c and d), and nanocomposite with aggregated GF (extrudate with aggregated drug nanoparticles embedded) (Figure 7.2e), respectively. To confirm the crystalline state of the drug in the composites, F2 was selected for XRD analysis together with as-received GF microparticles, F1-physical mixture, and HPC (Figure 7.3). Theoretically, F1 and F2 had identical formulations with different drug particle sizes in the feed suspensions. As-received GF microparticles exhibited intense characteristic crystalline peaks (Figure 7.3), whereas the physical mixture of the as-received GF particles (F1 physical mixture) exhibited similar characteristic peaks with significantly reduced intensity, which is clearly attributable to dilution and surface coverage of the GF particles by HPC. Considering that F2 extrudate shows almost identical XRD diffractogram to that of the physical mixture, the author concludes that the GF nanoparticles in the HPC matrix (F2 extrudate) were largely crystalline. Besides the dilution effect of the polymer, reduction of drug particle size during milling could have resulted in some XRD peak broadening (Deng et al., 2008).

Besides HPC, Soluplus® was used to produce extrudates (F4), for which Soluplus® was already used as steric stabilizer in combination with SDS producing well-stabilized feed nanosuspension (Table 7.1). No particle was observed in the cross-section in SEM images of F4 extrudate (Figure 7.2f). On comparing F4 diffractogram with those of as-received GF microparticles and Soluplus®, no GF characteristic peak appeared for F4 (Figure 7.3). GF was molecularly dispersed within the Soluplus® matrix, forming a single-phase amorphous mixture also known as ASD. Similar observation was reported by Hardung et al. (2010) for GF–Soluplus® obtained via traditional HME. Good miscibility between the drug and

the polymeric matrix is the fundamental requirement for the formation of ASD (Craig, 2002; Marsac et al., 2009). The difference between the drug–polymer solubility parameters is widely used to estimate their miscibility. Namely, if the difference is < 7.0 $MPa^{1/2}$, they are likely to be miscible and form an ASD; if > 10 $MPa^{1/2}$, they are likely to be immiscible and formation of an ASD is unlikely (Forster et al., 2001; Greenhalgh et al., 1999). The solubility parameters of GF, HPC, and Soluplus® are 12.2 (Thakral and Thakral, 2013), 24.0 (Choi et al., 1994), and 19.4 (Kolter et al., 2012) $MPa^{1/2}$, respectively. The solubility parameter differences between GF–HPC and GF–Soluplus® are calculated to be 11.8 and 7.2, respectively. Hence, the lower solubility parameter difference close to 7 could explain the formation of ASD when Soluplus® was used as the extrusion polymer as opposed to HPC.

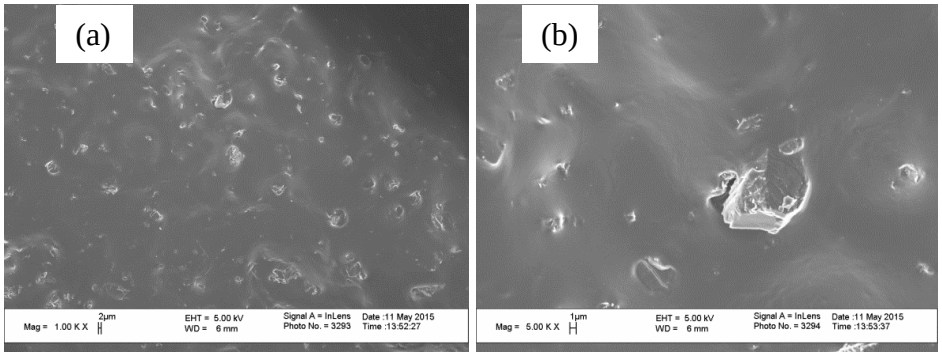

Figure 7.2 SEM images of the cross-sections of various extrudate threads: (a) and (b) F1 (microcomposite), (c) and (d) F2 (nanocomposite), (e) F3 (nanocomposite with aggregated GF), and (f) F4 (ASD). (Continued)

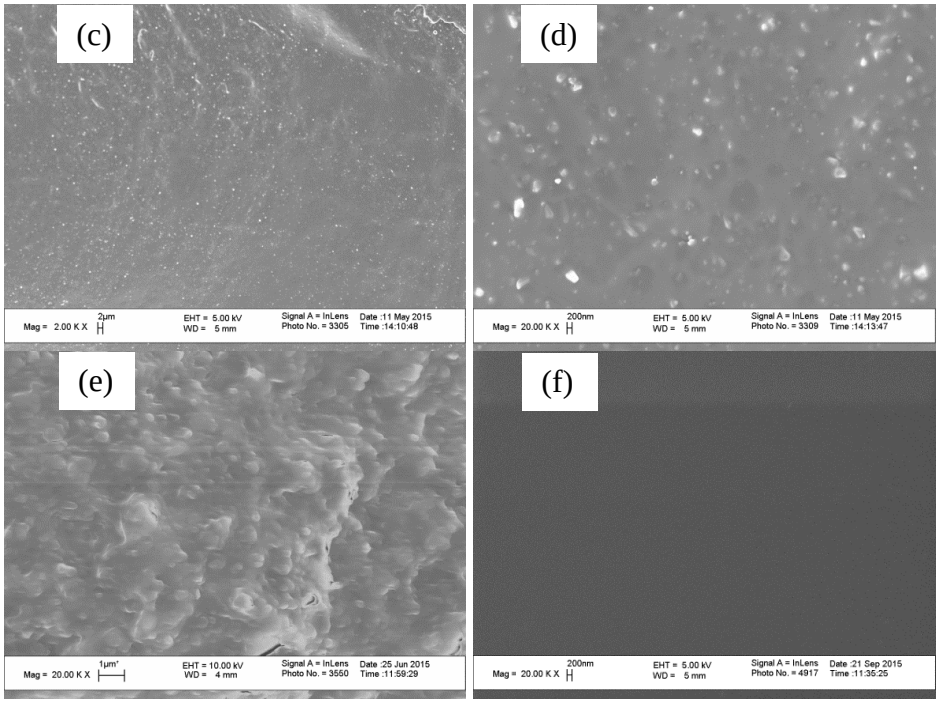

Figure 7.2 (Continued) SEM images of the cross-sections of various extrudate threads: (a) and (b) F1 (microcomposite), (c) and (d) F2 (nanocomposite), (e) F3 (nanocomposite with aggregated GF), and (f) F4 (ASD).

One milled suspension (F5) was also spray-dried to produce drug nanocomposites, in comparison to nanoextrusion (F2). F5 had the same formulation as F2, where HPC and SDS were used as the stabilizers in the milled suspension. Extra HPC, as a matrix former, was added to the milled GF suspension prior to spray drying. Spray-drying produced smaller nanocomposite particles than the nanoextrusion process (see F5 vs. mortar–pestle processed F1–F4 extrudate powders in Table 7.1). XRD results confirm that F5 powder had crystalline GF dispersed in the HPC matrix (Figure 7.3). Since GF was largely present as nanoparticles in the HPC–SDS solution (F5)/melt (F2) and GF–HPC miscibility is poor, drug nanocomposites (F5 and F2), with nanocrystals dispersed in the HPC matrix, were formed regardless of the drying method used.

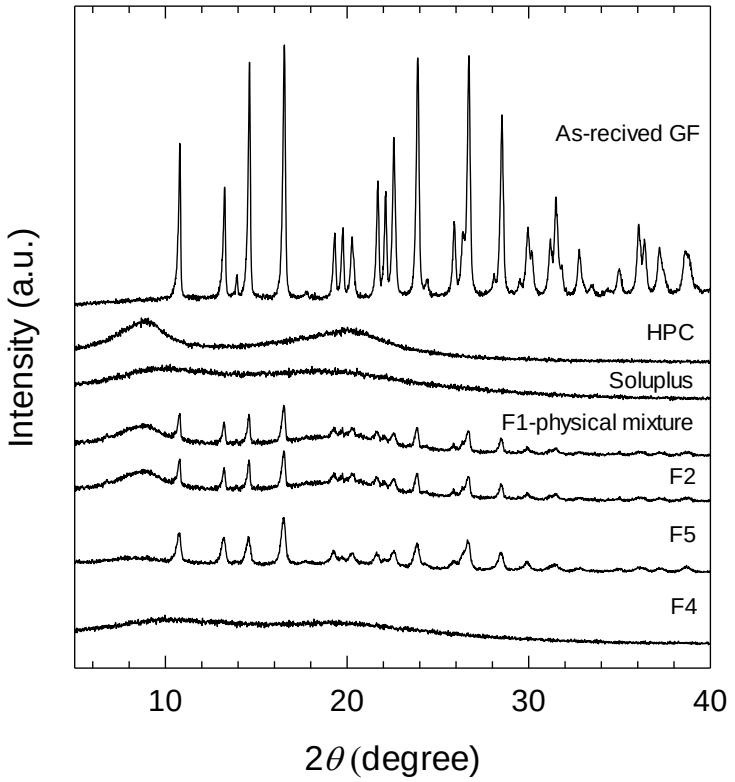

Figure 7.3 XRD diffractograms of as-received GF microparticles, HPC, Soluplus®, F1-physical mixture, F2 extrudate (nanocomposite powder), F4 extrudate (ASD powder), and F5 spray-dried nanocomposite powder.

The mean drug content was in the range of 22.7–24.1% (Table 7.1) with F2 showing the lowest RSD. Having the same formulation during milling and drying process, the F2 extruded nanocomposite had extremely low RSD, i.e., 0.33%, compared to the spray-dried nanocomposites (F5), which signifies the advantage of nanoextrusion process in preparing uniformly distributed and reproducible solid dosage forms. This finding is in line with a recent study which investigated the content uniformity of a low-dose drug using the nanoextrusion process (Park et al., 2013). Note that the nanoparticles in the feed suspension (F2) were well-stabilized and the extent of aggregates was extremely low. The F1 extrudate (microcomposite) and the F3 extrudate (nanocomposite with aggregated GF) had higher RSD than the

F2 extrudate (nanocomposite), which may be explained by the presence of larger drug particles, i.e., unmilled drug microparticles in F1 and nanoparticle aggregates of several microns in F3. Slightly higher RSD in drug content was also observed for F4 (ASD) and F5 (spray-dried nanocomposites).

7.2.3 Dissolution Performance of Composites and Amorphous Solid Dispersion

The evolution of GF dissolution was measured in de-ionized water using a USP II apparatus and presented in Figure 6.4. Milling of the extrudates via mortar–pestle allowed for preparing F1–F4 extrudate powder samples with similar sizes: D_{50} ranged 113–128 μm (Table 7.1). The specific surface areas for F1–F4 extrudate powders were found to be identical (0.31 m^2/g), as measured by BET nitrogen adsorption. The drug nanoparticles and microparticles (F1–F3) were covered and encapsulated by the polymer (HPC) well and their surface areas did not contribute to the specific surface area of the extrudate powders, resulting in F1–F3 surface areas identical to that of the F4 extrudate powder without drug particles (ASD). This finding suggests that the impact of polymeric matrix type and drug form/size on the dissolution can be investigated, with little to no confounding due to the matrix size (particle size of the extrudate) and extrudate surface area.

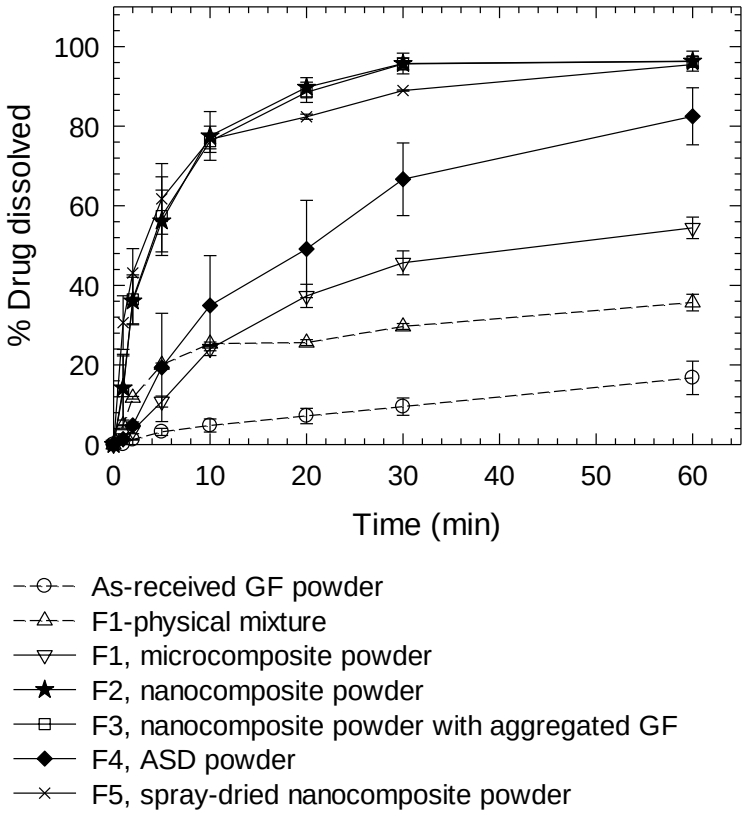

Figure 7.4 Evolution of GF dissolution from as-received GF microparticle powder, F1-physical mixture, F1 extrudate (microcomposite powder), F2 extrudate (nanocomposite powder), F3 extrudate (nanocomposite powder with aggregated GF), F4 extrudate (ASD powder), and F5 spray-dried nanocomposite powder in a USP II apparatus. Sample size equivalent to 8.9 mg GF dose.

Let us first examine the impact of *drug particle size* by comparing the dissolution performance of as-received GF microparticle powder, F1-physical mixture, F1 extrudate (microcomposite powder), F2 extrudate (nanocomposite powder), and F3 extrudate (nanocomposite with aggregated GF). The geometric (external) surface area (S_{ext}) of the drug particles is inversely proportional to the drug particle size, which was obtained from laser diffraction measurement. The respective XRD diffractograms in Figure 7.3 proved that GF particles were largely crystalline in these samples. A comparison of dissolution profiles of as-received GF and F1-

physical mixture (Figure 7.4) shows that the GF dissolution was faster in the presence of HPC–SDS even without wet media milling–nanoextrusion. This could be explained by the wetting enhancement of the hydrophobic drug (GF) particles in the presence of HPC–SDS dissolved in water. The wetting effectiveness factor for HPC–SDS solution was 127 (see *Appendix D* for details), which suggests a significant enhancement in wettability due to presence of HPC–SDS in water as compared with deionized water.

The dispersion of as-received GF microparticles in the HPC matrix (F1) via nanoextrusion process resulted in further improvement of the dissolution (Figure 7.4). This suggests that embedment of as-received drug microparticles into HPC matrix, even without milling, enhanced the drug dissolution as nanoextrusion achieves intimate and uniform mixing/dispersing of GF with HPC, as compared with simple blending (physical mixture). However, the dissolution rate was still low, i.e., 37.4% at 20 min. When drug nanoparticles obtained from wet milling, as opposed to as-received drug microparticles, were incorporated into HPC matrix during the nanoextrusion process (F2 vs. F1), a significant increase in dissolution rate was observed and 89.8% GF was released at 20 min. This finding is expected as GF nanoparticles with D_{50} = 155 nm (S_{ext} = 38.46 m^2/cm^3) dissolved faster than GF microparticles with D_{50} = 15.28 μm (S_{ext} = 0.63 m^2/cm^3) owing to larger surface area of the former. No significant difference in the dissolution profile was observed between F2 and F3, which indicates that aggregates of drug nanoparticles in F3 suspension with reduced surface area (S_{ext} = 5.31 m^2/cm^3) did not seem to affect the drug dissolution performance. One possible explanation is that the extra HPC added

to the milled nanosuspension during the nanoextrusion could have redispersed some of the aggregates in the HPC matrix, thus reducing the sensitivity of the dissolution to the presence of drug aggregates. These results overall suggest that presence of drug nanoparticles in the composites enhanced the dissolution significantly and that the nanoextrusion is capable of continuously producing GF nanocomposites that provide immediate release of GF. Moreover, the nanoextrusion allows for proper dispersion of GF aggregates, mitigating any potential negative effect on the dissolution.

A direct comparison of the dissolution performances of the nanocomposites (F2) and the ASD (F4) allows us to analyze the impact of the physical state of GF and the polymeric matrix. GF was nanocrystalline in F2 extrudate and amorphous in F4 extrudate although both F2 and F4 extrudates were produced by the same nanoextrusion process, but in different polymeric matrices, i.e., HPC and Soluplus®, respectively. Note that both extrudates had similar milled particle (matrix) sizes and identical surface areas (S_v = 0.31 m^2/g), which allows a head-to-head comparison. It is surprising that amorphous GF in ASD (F4) dissolved much slower than the crystalline GF nanoparticles in F2 composite (Figure 7.4). Previous *in vivo* animal studies and *in vitro* dissolution studies demonstrated that the amorphous form of a drug exhibited higher extent of drug dissolution and higher bioavailability than the nanocrystalline form of the drug (e.g., as in refs. (Fakes et al., 2009; Zhang et al., 2013; Zheng et al., 2012)) when a high drug dose was used. In previous investigations on ASDs, a relatively high drug dose was used to achieve supersaturation in the dissolution medium (Knopp et al., 2016b; Konno et al., 2008; Langham et al., 2012). However, here most dissolution experiments purposefully used a low drug dose (8.9 mg GF),

considering that the solubility of GF is 14.5 mg/L at 37 ^{o}C. Hence, the supersaturation in the bulk dissolution medium was not possible in these dissolution experiments. Under these non-supersaturating conditions in the bulk dissolution medium, nanocomposites allowed for faster GF dissolution than ASD. At this point, the author hypothesizes that the slower GF dissolution from ASD resulted from the slower drug release from the Soluplus® matrix than the HPC matrix under the non-supersaturating dissolution conditions investigated here. While drug nanocrystals could provide some supersaturation locally (microenvironment around nanocrystals) and contribute to enhanced dissolution due to their high curvature, such supersaturation would be expected to be very pronounced for drug nanoparticles with sizes below 100 nm (Shegokar and Müller, 2010). The relative supersaturation capability of the amorphous drug (ASD) vs. nanocrystalline drug present in the nanocomposites will be elucidated in *Section 7.2.4* via additional dissolution experiments by using excess extrudate powder samples with higher drug dose (equivalent of 100 mg GF).

The author also compares the drug dissolution performance from F2 nanocomposite powder prepared via nanoextrusion followed by mortar–pestle milling to that from F5 nanocomposite powder prepared via spray-drying, which is a commonly used drying process to prepare nanocomposites. F2 and F5 have the same formulation in their suspensions and dried nanocomposites. Although the spray-dried nanocomposites have smaller particles with larger specific surface area (D_{50} = 17.9 μm, S_v = 0.85 m^2/g) than the F2 extruded nanocomposites (D_{50} = 121.8 μm, S_v = 0.31 m^2/g), both nanocomposites exhibited fast, immediate release similarly. This finding

suggests that (1) GF nanoparticles well-distributed in a hydrophilic polymeric (HPC) matrix were released in water fast regardless of the drying method and size of the polymeric matrix, and (2) nanoextrusion can be used for producing fast-dissolving drug nanocomposites continuously, similar to spray drying.

7.2.4 On Dissolution Mechanisms with Different Polymeric Matrices

The interaction of a milled nanocomposite particle (F2) and ASD particle (F4) with a water droplet was visualized using a digital microscope (Figure 7.5). The HPC matrix of F2 disappeared upon wetting and subsequent fast dissolution, thus releasing drug nanoparticles immediately when exposed to water (Figure 7.5a). Unlike HPC matrix, Soluplus® matrix of F4 particle swelled and its larger dimension increased by about 60% in water while preserving the shape without significant erosion or disintegration (Figure 7.5b). Although this visualization is qualitative in nature and a water droplet was stationary during this experiment unlike voluminous water under stirring during the dissolution test, it is clear that HPC and Soluplus® matrices containing GF behaved differently in water, which could provide some evidence for the observed slower GF dissolution from Soluplus® matrix. To further elucidate the behavior of HPC and Soluplus® matrices in water, drug (GF) powder wetting by the respective polymer–SDS solutions was investigated. The calculated wetting effectiveness factor (i.e., $\cos\theta_{ss}/\cos\theta_{w}$) for HPC–SDS and Soluplus®–SDS were 127 and 20, respectively. This finding suggests that while both polymer–SDS combinations enhanced the wettability of the hydrophobic drug significantly, a higher hydrophilicity and wettability enhancement to GF was provided by HPC–SDS in water than by

Soluplus®–SDS in water. The greater wettability enhancement of GF by HPC–SDS could be one reason for the fast redispersion and release of drug nanoparticles observed in Figure 7.5a and associated immediate drug release in the dissolution testing (F2). Similar slower release from Soluplus®-based extrudates, albeit prepared by traditional HME process, was observed by Pudlas et al. (2015), where it was shown that copovidone-based extrudates released ibuprofen faster than Soluplus®-based extrudates. This was explained by the higher hydrophilicity and faster dissolution of copivodone in water as compared with Soluplus®; the latter aspect was clearly observed in their FTIR imaging. In other HME studies (Liu et al., 2012; Maniruzzaman et al., 2013; Song et al., 2015), Soluplus®-based extrudates exhibited a higher extent of drug release than extrudates with other polymers. These different observations in the above studies suggest that the aforementioned polymeric matrix effect was drug-specific, which could originate from specific drug–polymer interactions and differing wettability improvement of the hydrophobic drugs by various polymers (Knopp et al., 2016a; Konno et al., 2008).

(a)

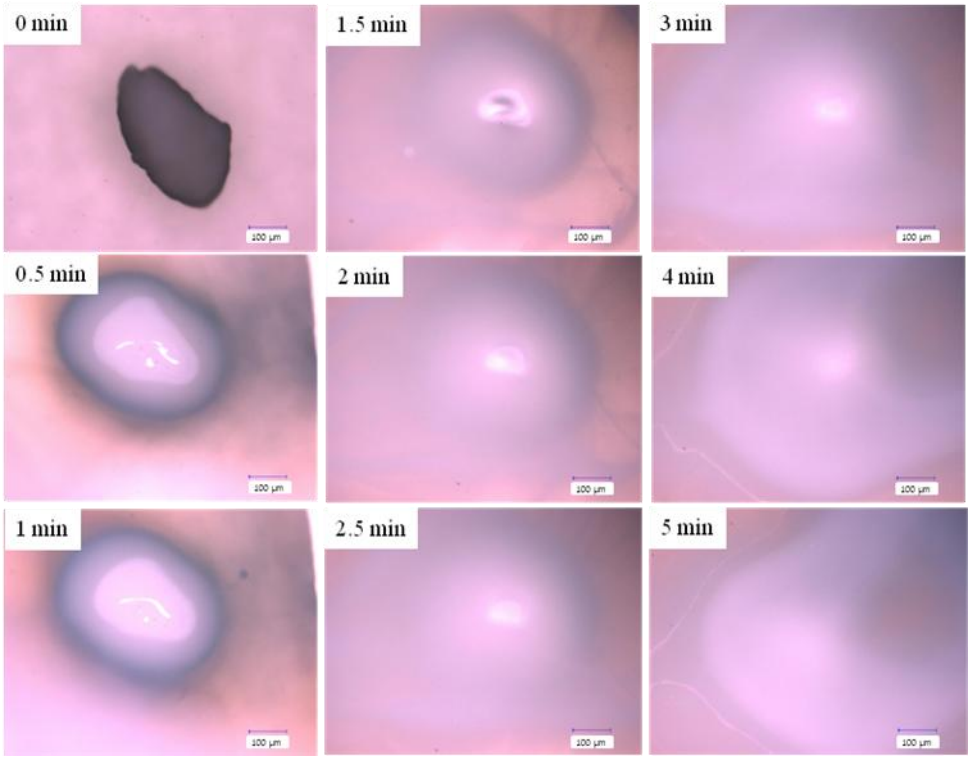

(b)

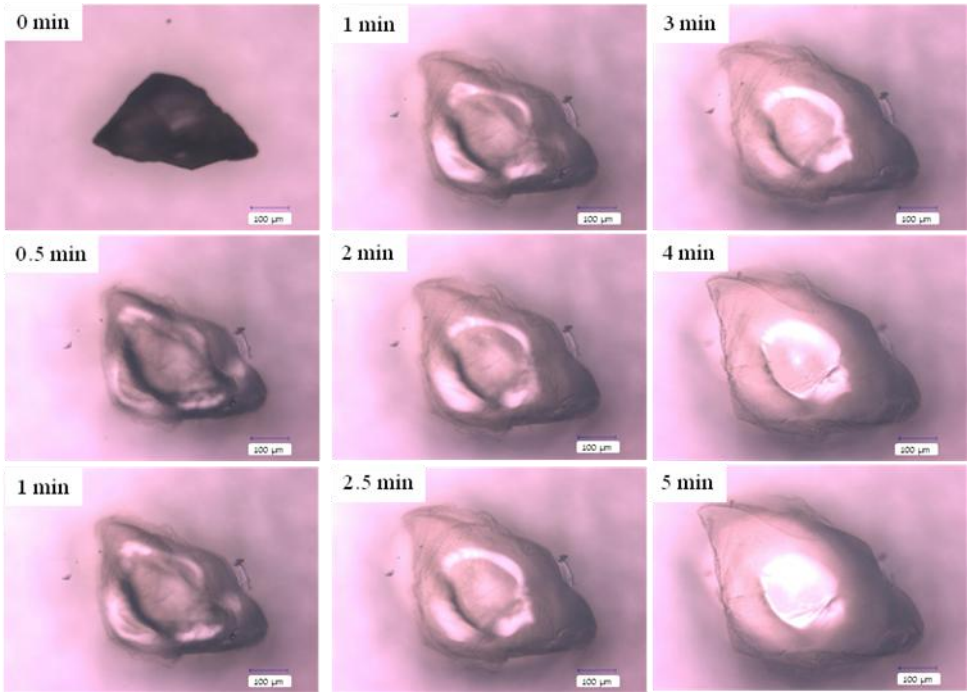

Figure 7.5 Digital microscope images showing the evolution of polymeric matrix erosion of (a) F2 nanocomposite (ground particle) (b) F4 amorphous solid dispersion (ASD, ground particle) in 3 µl deionized water.

Quantitative analysis of the dissolution data was carried out by using the Korsmeyer–Peppas model (Korsmeyer et al., 1983). As can be seen form Eq. (6.1), it relates the drug release to the elapsed time, and release exponent *n* could be used to characterize various release mechanisms (Peppas, 1985). This model is generally used to analyze the release of pharmaceutical polymeric dosage forms, when the release mechanism is not well-known or when more than one type of release phenomena could be involved (Costa and Sousa Lobo, 2001). The *n* values together with R^2 values obtained for F2 and F4 are listed in Table 6.2. Both R^2 values are above 0.96, indicating a relatively good fitting by the Korsmeyer–Peppas model (Korsmeyer et al., 1983). The *n* values for F2 and F4 milled *extrudate powders* appear to suggest that drug nanocomposite with HPC as the matrix (F2) exhibits diffusion-controlled release ($n \approx 0.43$) (Ritger and Peppas, 1987a), whereas Soluplus® matrix (F4) exhibits anomalous transport ($0.43 < n < 0.85$) (Ritger and Peppas, 1987a), for which swelling was observed under microscope in Figure 7.5b, and erosion might also have played a role.

Table 7.2 Statistical Analysis of the Fitting of the Drug Dissolution Profiles via Korsmeyer–Peppas Model

Formulation, Matrix	State of Extrudates	Crystallinity of GF	*n*	R^2
F2, HPC	Milled powders	Crystalline	0.42	0.963
F4, Soluplus®		Amorphous	0.58	0.969
F2, HPC	Cylindrical thread	Crystalline	0.72	0.981
F4, Soluplus®		Amorphous	0.84	0.999

Another possible reason for the slower drug release from ASD (F4) may be due to the recrystallization of amorphous GF. It is known that amorphous drugs can

crystallize during dissolution, as they become hydrated and when they generate supersaturated solution (Alonzo et al., 2010; Hancock and Parks, 2000). Since a low dose of GF was selected below its crystalline solubility, recrystallization in the bulk dissolution medium is not very likely to happen. Moreover, GF was classified as an intermediate crystallizer, whose recrystallization tendency from amorphous solids could be observed only between 0.25–1 h upon hydration (Van Eerdenbrugh et al., 2014) without any polymeric matrix. Due to the presence of up to ~76% Soluplus® in the F4 matrix, the recrystallization tendency of GF is expected to be slow or retarded (Alonzo et al., 2010; Konno and Taylor, 2006). To support these theoretical considerations and to gain additional insight into the supersaturation capability of the ASD vs. drug nanocomposites, additional dissolution testing was conducted with excess extrudate powder (equivalent of 100 mg GF). Figure 7.6 presents the dissolution performance under such supersaturating conditions. When a powder sample with 100 mg GF was used in the dissolution medium, F2 nanocomposite containing GF nanocrystals supersaturated (22.1 ± 0.9 mg/L at 120 min) and dissolved faster than the as-received GF microparticles, which did not exhibit supersaturation (14.3 ± 0.3 mg/L at 120 min). Although F2 nanocomposite supersaturated and dissolved faster than the F4 ASD, the extent of supersaturation and drug dissolution achieved by the ASD was much greater than that of F2 nanocomposite, i.e., 61.6 ± 4.5 mg/L vs. 22.1 ± 0.9 mg/L at 120 min. Within 2 h dissolution, no significant recrystallization of GF was seen for the ASD, providing evidence for the crystallization inhibiting action of Soluplus®. Hence, as expected from basic thermodynamic considerations and in line with previous literature (Zhang

et al., 2013), for high drug dose, the amorphous form of the drug attained higher supersaturation and exhibited higher extent/amount of drug dissolution than the nanocrystalline form of the drug in the nanocomposites. Overall, Figure 7.6 shows that the ASDs could indeed outperform drug nanocomposites in terms of higher extent of drug dissolution when a high drug dose is used to allow for supersaturation in the bulk dissolution medium. As shown in Figure 7.4, the reverse is true when the drug dose is low: the high supersaturating capability of the ASDs appears to have a smaller effect on dissolution, and dissolution enhancement is affected more by the relative wettability/ hydrophilicity, swelling–erosion, and size of the respective polymeric matrix (HPC vs. Soluplus®).

In summary, the faster GF dissolution from F2 composite with HPC matrix than that from F4 ASD with Soluplus® matrix appears to mainly stem from the faster erosion/dissolution of the hydrophilic HPC matrix with its higher wettability enhancement to GF as compared with the amphiphilic Soluplus® matrix, under the *non-supersaturating dissolution conditions* (low drug dose). When a high drug dose was used in the dissolution medium, the extent of drug dissolution enhancement provided by the drug nanoparticles was lower than that provided by the amorphous form of the drug in the ASD because the latter provided a much higher supersaturation. Interestingly, even for the high drug dose case, as can be seen from Figure 7.6, the HPC-based nanocomposite released the drug faster than the Soluplus®-based ASD up to the occurrence of the plateau, which was set by the apparent solubility of the drug.

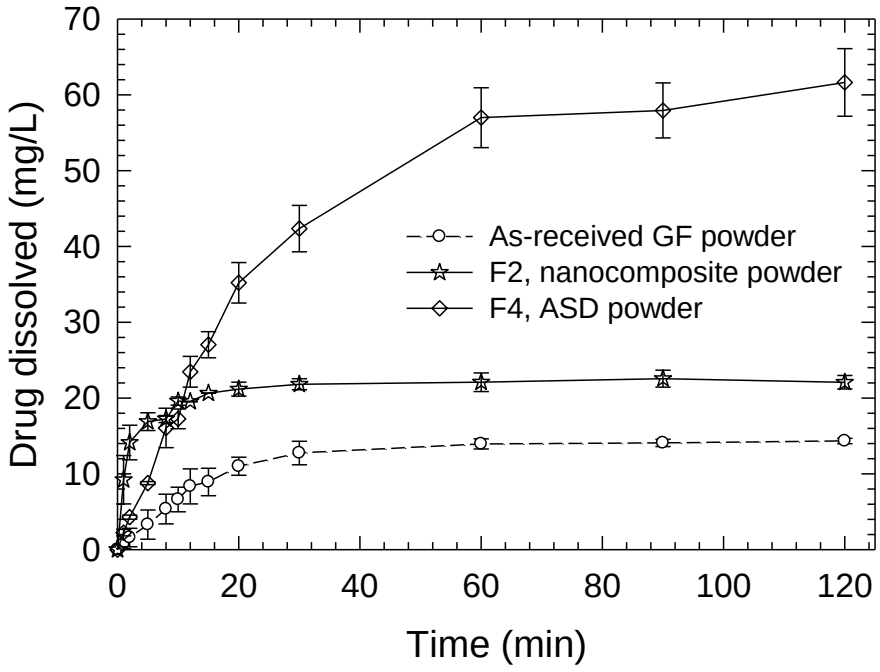

Figure 7.6 Evolution of GF dissolution from as-received GF microparticle powder, F2 extrudate (nanocomposite powder), and F4 extrudate (ASD powder) under supersaturating condition in a USP II apparatus. Sample size equivalent to 100 mg GF dose.

7.2.5 Elucidating the Matrix Size Effect

To elucidate the impact of matrix size on the drug dissolution rate, dissolution performances of a milled extrudate powder and a cylindrical thread were compared for F2 and F4 formulations. The milled matrix (particle) sizes of the extrudates are reported in Table 7.1. Single cylindrical threads of F2 and F4 extrudates (diameter × length of 1 mm × 31 mm) with the drug dose of 8.9 mg were used for the dissolution tests**.**

Cylindrical threads of the extrudates exhibited slower drug dissolution than the milled extrudate powders (Figure 7.7a and 7.7b), especially for F4 (ASD), due to their larger matrix sizes and negligibly small surface areas, which were measured to

be zero by BET method, as compared with 0.31 m^2/g for the F1–F4 extrudate powders. The release exponent values for the cylindrical threads in Table 7.2 could suggest anomalous transport ($0.45 < n < 0.89$) (Ritger and Peppas, 1987a), where matrix swelling/erosion plays a role, which is expected for these relatively coarse threads. For F2 extrudates, wherein drug nanoparticles were dispersed, the dissolution rate from the thread was slower than the milled extrudate powder initially but caught up quickly in 30 min (Figure 7.7a). 80% of the drug release was achieved within 20 min in both nanocomposite powder and cylindrical nanocomposite thread for F2. In general, HPC matrix allowed for fast GF release with slight dependence on matrix size. This finding is in line with the earlier finding that F2 and F5 composites prepared via nanoextrusion/spray drying exhibited similar drug dissolution performance despite their differences in matrix size and specific surface areas (0.31 m^2/g vs. 0.85 m^2/g, respectively). All these findings accord well with the fast release of drug nanoparticles from the hydrophilic HPC matrix, as shown in the microscopic visualization study (Figure 7.5a). In contrast, for F4 (ASD), the drug dissolution rate from the cylindrical ASD thread was remarkably slower than the ASD powder (Figure 7.7b). The dissolution of amorphous drug from the cylindrical threads in Soluplus® matrix was even slower than the as-received GF microparticles, suggesting Soluplus® matrix almost acted as a barrier to drug release. It is clear that the slower erosion/dissolution of the Soluplus® matrix appears to have a slowing-down effect on drug dissolution, especially from larger matrices.

In an attempt to achieve fast drug release from F4 extrudate (ASD), the milled extrudate powder was passed through a 90 μm sieve. The sieved F4 powder had D_{50}

and D_{90} of 51.4 ± 4.3 µm and 107.7 ± 9.9 µm, respectively, and S_v = 0.45 m^2/g. Upon further reduction in matrix/particle size of F4 (ASD) following sieving and resulting increase in the specific surface area from 0.31 m^2/g (milled extrudate) to 0.45 m^2/g (milled–sieved extrudate), 76.8 ± 8.3% drug release was achieved in 20 min. Besides the increase in specific surface area, the significantly improved dissolution rate from F4 extrudate (ASD) following milling and sieving also resulted from the reduced diffusion length of the drug from the swollen Soluplus® matrix as the matrix size was smaller. A quick comparison of Figure 7.7a and Figure 7.7b suggests that although the amorphous drug in ASD dissolved slower than the drug nanocrystals in the nanocomposites with similar extrudate particle (matrix) sizes, faster drug dissolution from ASDs can be achieved by size reduction of the extrudate particles.

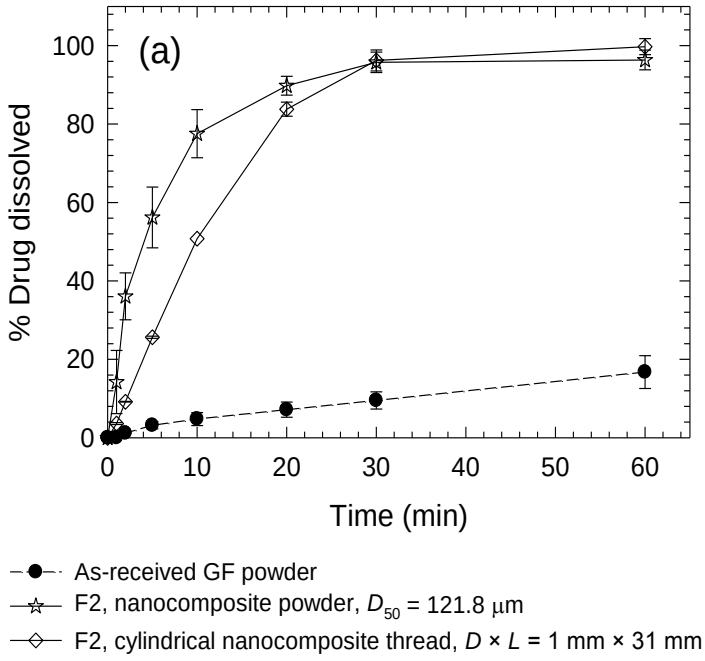

Figure 7.7 Evolution of GF dissolution from different polymeric matrices and matrix sizes: (a) F2 (nanocomposite) particles and (b) F4 (ASD) particles in a USP II apparatus. Sample size equivalent to 8.9 mg GF dose. (Continued)

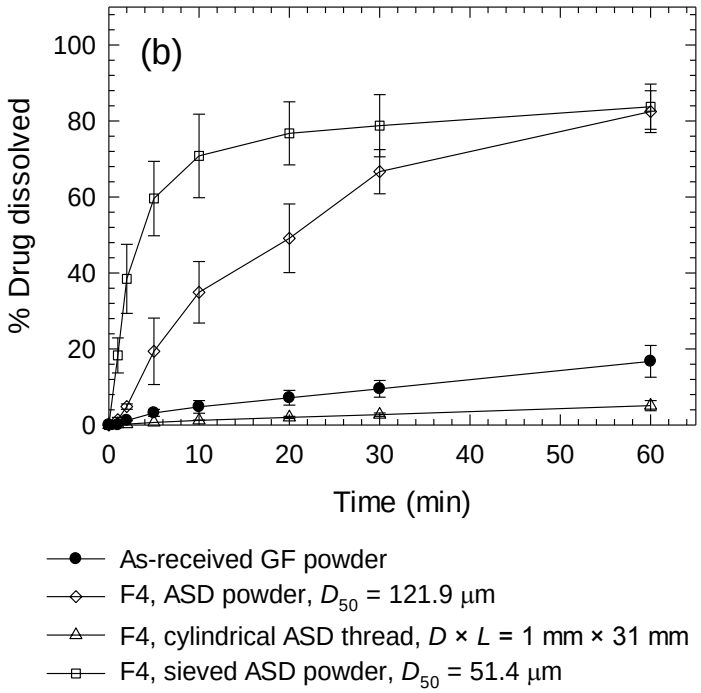

Figure 7.7 (Continued) Evolution of GF dissolution from different polymeric matrices and matrix sizes: (a) F2 (nanocomposite) particles and (b) F4 (ASD) particles in a USP II apparatus. Sample size equivalent to 8.9 mg GF dose.

7.3 Conclusions

Extrudates with different forms of griseofulvin (GF) were prepared via nanoextrusion by making use of two extrusion polymers (HPC and Soluplus®) with different drug–polymer miscibility: crystalline GF micro/nanoparticles dispersed in the HPC matrix (micro/ nanocomposites) and amorphous GF molecularly dispersed within Soluplus® (ASD). In the composites, GF particle size as modulated by wet media milling/formulation was the dominant factor that affected the GF dissolution performance, whereas the extrudate particle (polymeric matrix) size or even the drying method (nanoextrusion vs. spray drying) did not seem to have a significant impact. On the contrary, the matrix size appears to play a major role in GF dissolution

from ASD. A head-to-head comparison of the dissolution performance of the nanocomposites vs. ASD with the same drug loading and similar polymeric matrix sizes was made possible by using the same nanoextrusion process as a platform technology followed by dry milling. Under non-supersaturating conditions in the dissolution medium (low dose), drug nanocrystals in the nanocomposites with HPC matrix can dissolve faster than amorphous drug molecularly dispersed in Soluplus® matrix of the ASD. Fast release/dissolution of GF nanocrystals from fast eroding/dissolving, hydrophilic matrix of HPC as compared with the slower drug release from the slowly eroding/dissolving Soluplus® matrix was found to explain this observation. Microscopic examination and drug powder wettability testing provided significant insight into the fast nanoparticle redispersion from HPC matrix vs. swollen Soluplus® matrix and higher wettability enhancement to GF by HPC–SDS than Soluplus®–SDS. When a high drug dose was used in the dissolution medium, the ASD formulation provided higher drug supersaturation than the nanocomposite. Overall, the findings in this study imply that drug nanocomposites with fast eroding/dissolving, hydrophilic polymers like HPC could be competitive to drug ASDs with Soluplus® in enhancing the dissolution rate of low dose (e.g., highly potent) BCS Class II drugs.

CHAPTER 8

IMPACT OF PARTICLE (MATRIX) SIZE ON DISSOLUTION ENHANCEMENT FROM GRISEOFULVIN-LADEN EXTRUDATES PREPARED VIA NANOEXTRUSION

In Chapter 7, a head-to-head comparison of the dissolution performance of the nanocomposites vs. ASD with the same drug loading and similar polymeric matrix sizes was made possible by using the same nanoextrusion process as a platform technology followed by dry milling. As a continuation, Chapter 8 systematically investigates the effects of particle (matrix) size and the form of the drug (crystalline vs. amorphous) on the drug release from extrudates at both non-supersaturating and supersaturating dissolution conditions. Soluplus® (Sol), Kolliphor® P407 (Kol), and Hydroxypropyl cellulose (HPC) were used to stabilize wet-milled drug suspensions and form matrices of the extrudates. The wet-milled suspensions along with additional polymer (Sol/Kol/HPC) were fed to a co-rotating twin-screw extruder, which dried the suspensions and formed various extrudates. The extrudates were dry-milled and sieved into samples with various extrudate particle (matrix) sizes. Two forms of the drug were prepared: extrudates with nanocrystalline drug particles dispersed in the Kol or HPC matrices as a secondary phase (nanocomposites) and extrudates with amorphous drug molecularly dispersed within the Sol matrix (ASD) with two drug loadings in each polymeric matrix type. The produced extrudates with different polymeric matrix sizes, forms of drugs (crystalline vs. amorphous), and two different drug loadings were subjected to further characterization.

8.1 Materials and Methods

8.1.1 Materials

BP/EP grade griseofulvin (GF) was purchased from Letco Medical (Decatur, AL, USA). GF is a Biopharmaceutical Classification System (BCS) Class II drug with an aqueous solubility of 8.9 mg/L at 25 °C and 14.5 mg/L at 37 °C, melting point of 220 °C, and a glass transition temperature of 79 °C. Soluplus® (Sol, BASF, Tarrytown, NY), Kolliphor® P407 (Kol, BASF, Tarrytown, NY), and Hydroxypropyl cellulose (HPC, SL grade, Nisso America Inc., New York, NY) and were used as the polymeric stabilizer during wet media milling and polymeric matrix former during nanoextrusion. HPC is an amorphous polymer with two softening points at 68 and 178 °C. Kolliphor® P407 is a crystalline nonionic triblock copolymers composed of a central hydrophobic chain of polyoxypropylene (poly(propylene oxide)) flanked by two hydrophilic chains of polyoxyethylene (poly(ethylene oxide)) with a melting temperature at 57 °C. Soluplus® is an amphiphilic polyvinyl caprolactam–polyvinyl acetate–polyethylene glycol graft copolymer. It is amorphous with a single glass transition temperature of 73 ± 2 °C. Sodium dodecyl sulfate (SDS, GFS Chemicals, Inc., Columbus, OH) was used as an anionic surfactant to enhance the drug wettability and stabilize drug particles during milling. Its critical micelle concentration (CMC) in water is 0.23 wt.% at ambient temperature. Methanol (ACS reagent, ≥ 99.8%), purchased from Fisher Scientific (Suwanee, GA), was used as a solvent. Yttrium stabilized zirconia beads (Zirmil Y, Saint Gobain ZirPro, Mountainside, NJ, USA) with a median size of 430 µm were used as the milling media.

8.1.2 Wet Stirred Media Milling Process

Table 8.1 presents the formulations of the GF (drug) suspensions. The suspensions consisted of 22.4% GF dispersed in a stabilizer solution of 1.9% polymer (i.e., Sol/Kol/HPC) and 0.15% SDS. All percentages (%) refer to w/w with respect to total suspension mass. Selection of the milling conditions and formulations were guided by our prior work on wet media milling (Azad et al., 2014b; Bilgili et al., 2016d). A Microcer wet stirred media mill (Netzsch Fine Particle Technology, LLC, Exton, PA, USA) with 80 ml chamber was used to mill the drug suspensions. Feed suspensions were milled for 120 min under identical conditions to those reported in Bilgili and Afolabi (2012). The particle sizes of the suspensions after milling were determined using laser diffraction, and the suspensions were refrigerated at 8 °C for one day before nanoextrusion. A single suspension was used for formulations with the same polymer as stabilizer/matrix former.

Table 8.1 Formulations of the Drug (GF) Suspensions Fed in Nanoextrusion

Formulation ID[a]	Polymer[b]	Drug Particle Size after Milling (μm)		
		D_{10}, SD	D_{50}, SD	D_{90}, SD
10% GF-Sol	Soluplus®	0.113, 0.000	0.156, 0.001	0.228, 0.001
2% GF-Sol	Soluplus®	0.113, 0.000	0.156, 0.001	0.228, 0.001
10% GF-Kol	Kolliphor® P407	0.100, 0.008	0.185, 0.004	0.358, 0.049
2% GF-Kol	Kolliphor® P407	0.100, 0.008	0.185, 0.004	0.358, 0.049
10% GF-HPC	HPC	0.121, 0.001	0.159, 0.000	0.215, 0.001
2% GF-HPC	HPC	0.121, 0.001	0.159, 0.000	0.215, 0.001

[a] all suspension formulations have 22.6% GF, 1.9% polymer, 0.15% SDS. w/w with respect to total suspension mass.
[b] extrudates with the same polymer matrix used the same drug nanosuspension in the nanoextrusion process; hence, they had identical drug particle sizes.

8.1.3 Nanoextrusion Process

Nanoextrusion was performed with a Process 11 co-rotating twin-screw extruder (Thermo Fisher Scientific, Waltham, MA) with a die having a 2.0 mm hole. Six temperature-controlled zones were used, which are individually heated with electric heaters and cooled with water. Polymer (i.e., Sol/Kol/HPC) and drug nanosuspensions were fed in Zone 1 and Zone 3, respectively, as two separate feedings (Figure 8.1), similar to Li et al. (2017). The temperatures of the individual heating zones and the die and the polymer and suspension feeding rates are shown in Table 8.2. Polymers were used polymeric matrix formers during nanoextrusion besides acting as stabilizers in wet media milling and were fed via a volumetric feeder (Thermo Fisher Scientific, Waltham, MA). The drug suspensions were fed ahead of the kneading elements, by using a peristaltic pump (Thermo Fisher Scientific, Waltham, MA). The ratio of polymer and suspension feeding rates determined the final drug loading of various extrudates. Two drug loadings were produced in each polymeric matrix. The produced extrudates were labeled with the expected drug content, the drug, and the polymeric matrix. For example, 10% GF-Sol has 10% GF in the polymeric matrix of Sol. The screw-speed was kept at 100 rpm. Zones 4 and 5 had kneading elements with 60° offset angle and served as a mixing zone. Kneading elements provided intense mixing, which ensured homogeneous dispersion and distribution of the suspension within the molten polymeric matrix. Most of the water in the feed suspension evaporated in Zones 4–5, with conveying elements in place and elevated barrel temperature. The extrudates that exit the die were cooled to room temperature and stored in a desiccator for further

characterization. Due to the comparably low processing temperature and the resulting insufficient water evaporation, the Kol formulations were subjected to additional drying, i.e., 24 h storage in a desiccator. A higher processing time is not desirable for the production of Kol threads.

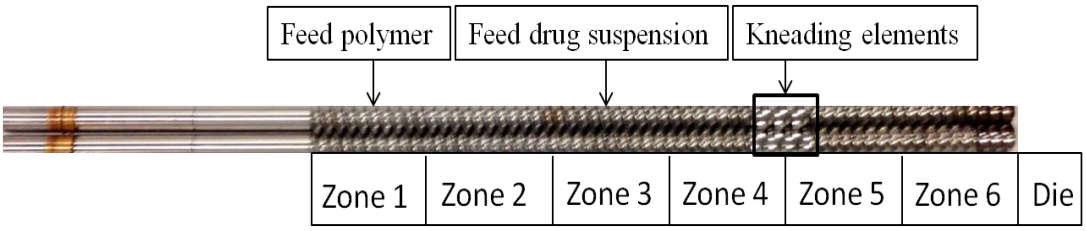

Figure 8.1 Schematic illustration of the extruder setup, the screw configuration, and the locations of the volumetric feeder feeding polymer powders (zone 1) and the peristaltic pump at zone 3 feeding drug nanosuspensions.

8.1.4 Microscopy

The presence of the drug particles in extrudate threads was explored via imaging of their cross-sections by an LEO 1530 SVMP (Carl Zeiss, Inc., Peabody, MA, USA) scanning electron microscope (SEM). The extrudates in thread form were quenched in liquid nitrogen and manually broken to generate a relatively smooth cross-section. The cross-sections were placed on an aluminum stub using carbon tape. All samples were then sputter coated with carbon using BAL-TEC MED 020 (BAL-TEC AG, Balzers, Switzerland) prior to imaging. Multiple images were taken to ensure consistent visualization from each sample.

An Axio Scope.A1 microscope (Carl Zeiss Microscopy, LLC, Thornwood, NY) was used to observe the morphological changes of a milled extrudate particle when exposed to deionized water. A milled particle with selected formulation (10 GF-Sol, 10 GF-Kol, and 10 GF-HPC) in the size range of 125–250 µm was placed on

a glass slide kept under the microscope. A 3 μl drop of deionized water was placed on the particle and images were captured at different times. Since the extrudate particle could not be fixed on the glass slide, more water droplets were not added, which would have allowed for full dissolution of the particles.

Table 8.2 Processing Temperature, Feeding Rate, and Residence Time for Each Formulation. The Extrusion is Run at 100 rpm

Formulation ID	Polymer	Feeding Rate (g/min)		Processing Temperature (°C)							Residence Time (s)
		Polymer[a]	Suspension[b]	Zone 1	Zone 2	Zone 3	Zone 4	Zone 5	Zone 6	Die	
10% GF-Sol	Soluplus®	2.9	1.4	70	70	100	100	165	165	165	120
2% GF-Sol	Soluplus®	2.7	0.25	70	70	90	100	165	165	165	115
10% GF-Kol	Kolliphor® P407	2.9	1.4	10	25	100	100	110	110	90	120
2% GF-Kol	Kolliphor® P407	2.8	0.28	10	25	95	100	110	110	85	110
10% GF-HPC	HPC	2.8	1.4	70	120	120	140	140	140	140	116
2% GF-HPC	HPC	2.8	0.27	70	120	120	140	140	140	140	120

[a] Refers to the additional polymer mixed with the drug nanosuspension during the nanoextrusion process.
[b] The drug nanosuspension has 22.6% w/w GF, 1.9% polymer, and 0.15% SDS for all formulations. w/w with respect to total suspension mass.

8.1.5 X-ray Powder Diffraction (XRD)

The crystallinity of the as-received GF, as-received polymers, physical mixtures, and extrudate powders with various polymeric matrices were analyzed using XRD (PANalytical, Westborough, MA), provided with Cu Kα radiation (λ=1.5406 Å). The samples were scanned for 2θ ranging from 5° to 40° at a scan rate of 0.165 s^{-1}.

8.1.6 Thermogravimetric Analysis (TGA)

Thermogravimetric analysis (TGA) was performed using a TGA/DSC1/SF Stare system (Mettler Toledo, Inc., Columbus, OH) for the characterization of residual water. A ~8 mg as-received GF/Sol/Kol/HPC or extrudate powder was placed in a ceramic crucible and heated from 25 °C to 150 °C at a constant rate of 10 °C/min under nitrogen flow.

8.1.7 Drug Wettability by Soluplus®, Kolliphor® P407, and HPC Solutions

Wettability was studied via liquid penetration into a (drug) powder bed, also known as the modified Washburn method (Hołownia et al., 2008; Washburn, 1921), using Attension Sigma 700 (Biolin Scientific, Linthicum, MD, USA), which measures the mass of liquid penetrated into the drug powder bed as a function of time. Experimental methods were presented in Li et al. (2017) and the details can be found in *Appendix E*. In this study, liquids and powder are deionized water/stabilizer solution (Sol/Kol/HPC) and GF, respectively. The apparent shear viscosity and surface tension of the liquids were respectively measured using R/S Plus Rheometer (Brookfield Engineering, Middleboro, MA, USA) and Attension Sigma 700 (Biolin

Scientific, Linthicum, MD, USA). The ratio of the cosine of contact angles $\cos\theta_{ss}/\cos\theta_{w}$ was calculated using the Modified Washburn equation and used as a wetting effectiveness factor. Here, θ_{ss} is the contact angle between GF and the stabilizer solutions and θ_{w} is the contact angle between GF and deionized water. The ratio quantifies the drug wettability enhancement upon the use of different stabilizers (polymers) in water.

8.1.8 Determination of Drug Content and Drug Release

Maximum theoretical amount of GF in 100 mg extrudates was estimated to be 10 mg (10% GF-polymer). GF solubility in methanol is 3 mg/ml (Bhakay et al., 2014b). Hence, 100 mg of the extrudate powders was dissolved in 20 ml of methanol and sonicated for 30 min, followed by storage overnight to ensure that all GF had dissolved. An aliquot of 100 µl was taken from the GF solution and diluted into 10 ml methanol. The absorbance of all samples was measured at the wavelength of 292 nm by Ultraviolet (UV) spectroscopy in a UV Spectrophotometer (Agilent, Santa Clara, CA, USA), and drug concentration was determined based on a pre-established calibration curve. Six replicates from each formulation were used to calculate the mean drug content along with the percent relative standard deviation (RSD).

Drug release from the extrudate samples was determined via a Distek 2100C dissolution tester (North Brunswick, NJ, USA) according to the USP II paddle method. The dissolution medium was 1000 ml deionized water at 37 °C, and a paddle speed of 50 rpm was used. Deionized water allows for good discrimination of different GF formulations under non-sink conditions (Bhakay et al., 2014a; Li et al.,

2016b). Two doses (i.e., 8.9 mg and 100 mg) of GF were tested for the dissolution performance of the produced extrudate threads and milled powders. The relatively low drug dose (i.e., 8.9 mg), which could emulate highly-potent drugs, was selected to ensure non-supersaturating conditions in the dissolution medium as the GF solubility in water at 37 ^{o}C is 14.5 mg/L. The nanocomposites/ASD powders were poured into the dissolution medium and 4 ml samples were taken out manually at 1, 2, 5, 10, 20, 30, and 60 min. These aliquots were filtered with a 0.1 µm PVDF membrane-type syringe filter before UV spectroscopy measurements to minimize any confounding effect of the undissolved coarse drug aggregates. Excess drug (i.e., 100 mg) was selected to allow for supersaturation in the bulk dissolution medium. Dissolution was conducted for 210 min with additional sampling at 90, 120, 150, 180, and 210 min. The filtered samples were diluted with 37 ^{o}C deionized water at a ratio of 1 to 7 before UV spectroscopy measurement. The amount of GF dissolved was measured by UV spectroscopy at a wavelength of 296 nm and determined based on a pre-established calibration curve. Deionized water was used as the blank.

To rank the drug dissolution rate from different polymeric matrices and matrix sizes, fitting of GF dissolution data to Korsmeyer–Peppas model (Ritger and Peppas, 1987a, b), as shown in Eq. (8.1), was performed using SigmaPlot's (Version 11) regression wizard.

$$\frac{M_t}{M_\infty} = kt^n \tag{8.1}$$

where *k* is a constant incorporating structural and geometric characteristics of the drug dosage form, *n* is the release exponent, indicative of the drug release mechanism, and $\frac{M_t}{M_\infty}$ is the fractional release of the drug. An apparent release

mechanism was suggested in this dissertation based on the fitted *n* value and the specific geometry of the samples in view of various assumptions behind Eq. (8.1) (refer to Ritger and Peppas (1987a)). Fitting of $\frac{M_t}{M_\infty}$ included data up to and including one point after attainment of $\frac{M_t}{M_\infty}$ value of 0.60. As the drug release rate (d($\frac{M_t}{M_\infty}$)/d*t*) is proportional to *kn* (Peppas, 1985), in this study, *kn* is used to compare dissolution rate of different formulations.

8.2 Results and Discussion

8.2.1 Wet Stirred Media Milling of Drug Suspensions

Table 8.1 presents the formulations of drug (GF) nanosuspensions and their particle sizes and standard deviation (SD) as measured by laser diffraction. All drug nanosuspensions have 1.9% polymer (Sol/Kol/HPC) and 0.15% surfactant (SDS) as steric and electrostatic stabilizers, respectively. Polymer–SDS combination is known to stabilize GF nanosuspensions due to synergistic stabilizing action (Bilgili and Afolabi, 2012), which minimizes the extent of drug nanoparticle aggregation during milling and storage. As-received unmilled GF microparticles have D_{10} = 4.67 ± 0.06 μm, D_{50} = 14.27 ± 0.25 μm, and D_{90} = 37.46 ± 0.38 μm. After milling, all the suspensions have D_{50} in the range of 0.156–0.185 μm, indicating a similar drug particle size after milling despite the use of different polymeric stabilizers. The slightly higher particle size in the formulation of Kol–SDS indicates presence of aggregates. All suspensions were stored in a refrigerator at 8 ºC for one day before nanoextrusion process.

8.2.2 Preparation and Characterization of Amorphous Solid Dispersion and Nanocomposites

The nanoextrusion process used milled drug suspensions and additional extrusion polymer as two separate feeds and continuously produced extrudates by removing water via evaporation. Depending on the feeding rate ratio of polymer and nanosuspension, two drug loadings were produced in each polymeric matrix. The produced extrudates were labeled with the expected drug content, the drug, and the polymeric matrix, as introduced in *Section 8.1.3*. The produced extrudates were kept in a desiccator. The mean moisture content of the Sol and HPC formulations was measured immediately after the nanoextrusion process, while due to the comparably low processing temperature and the resulting insufficient water evaporation, the moisture content of the Kol formulations was measured after additional drying, i.e., 24 h storage in a desiccator. The mean moisture content was reported in Table 8.3. Considering the moisture of the raw materials, it can be concluded that most water in the drug suspensions was removed. The extrudate threads were then subjected to other characterizations. The mean drug content was also reported in Table 8.3. All the produced extrudates had very low RSD, i.e., 0.95–2.22%, which signifies the advantage of nanoextrusion process in preparing uniformly distributed and reproducible solid dosage forms even with low drug loading (~ 2%) formulations. This finding is in line with the previous research (Li et al., 2017) and a recent study which investigated the content uniformity of a low-dose drug using the nanoextrusion process (Park et al., 2013).

Table 8.3 Drug Content and Moisture Content in the Produced Extrudates and Matrix Sizes of the Extrudate Powders after Grinding and Sieving

Formulation ID	Drug Content (RSD) (% w/w)[a]	Moisture Content ± SD[b] (% w/w)[a]	<63 µm			125–250 µm			425–710 µm		
			D_{10}, SD	D_{50}, SD	D_{90}, SD	D_{10}, SD	D_{50}, SD	D_{90}, SD	D_{10}, SD	D_{50}, SD	D_{90}, SD
10% GF-Sol	9.8 (1.52)	3.6 ± 0.02	12.9, 0.1	51.7, 0.1	103.7, 0.2	103.5, 1.6	145.7, 0.8	194.7, 3.7	469.2, 16.5	716.1, 28.9	844.8, 3.5
2% GF-Sol	1.9 (1.91)	3.2 ± 0.46	13.7, 0.3	42.8, 0.6	90.7, 0.5	103.6, 1.5	157.5, 3.5	230.1, 3.6	480.1, 19.5	726.4, 31.7	846.7, 4.3
10% GF-Kol	9.7 (2.22)	0.8 ± 0.22	12.7, 3.4	40.0, 2.3	81.0, 9.9	123.0, 24.5	194.7, 9.9	277.8, 6.8	370.8, 7.7	497.0, 28.6	580.9, 14.0
2% GF-Kol	2.1 (1.86)	0.7 ± 0.14	17.1, 0.9	39.6, 1.2	67.5, 6.7	137.8, 2.3	210.2, 8.7	279.5, 3.4	380.2, 4.7	492.3, 22.1	603.5, 13.9
10% GF-HPC	10.3 (0.95)	2.9 ± 0.24	16.9, 1.7	43.9, 12.9	114.6, 7.6	126.0, 3.3	194.9, 5.1	293.5, 16.1	464.3, 29.0	633.5, 24.0	811.7, 11.5
2% GF-HPC	2.1 (1.36)	2.8 ± 0.18	21.3, 1.4	57.1, 0.6	122.5, 18.6	126.6, 2.4	185.1, 8.8	266.2, 22.6	446.2, 50.8	615.9, 46.1	798.5, 9.0

[a]w/w with respect to total nanocomposite/ASD mass.
[b]Moisture content of raw materials: GF 0.2%, Soluplus® 2.4%, Kolliphor® 0.3%, HPC 2.6%.

Depending on polymer–drug miscibility, extrudates could be either in the form of ASD with amorphous form of the drug molecularly dispersed in the polymeric matrix or drug nanocomposites embedding crystalline drug particles in the polymeric matrix, respectively (Li et al., 2017; Qian et al., 2010; Thakral and Thakral, 2013). SEM images of the cross-section of various extrudates are presented in Figure 8.2. GF nanoparticles in the range of 50–300 nm are embedded in the Kol and HPC matrices, for which Kol/HPC was already used as a steric stabilizer in combination with SDS producing well-stabilized feed nanosuspensions (refer to Table 8.1). The drug particle sizes observed in the SEM images in Figure 8.2 accord well with the sizes of the drug particles in the feed suspensions, as measured by laser diffraction (Table 8.1). SEM images overall show that drug nanoparticles were dispersed throughout the Kol and HPC matrices; hence, these extrudates can be referred to as nanocomposites (extrudate with drug nanoparticles embedded). To confirm the crystalline state of the drug in the nanocomposites, XRD analysis was conducted for each extrudate together with as-received GF microparticles, polymer, and physical mixture (Figure 8.3). As-received GF microparticles exhibited intense characteristic crystalline peaks (Figure 8.3), whereas the physical mixture of the as-received GF particles exhibited similar characteristic peaks with significantly reduced intensity, which is clearly attributable to dilution and surface coverage of the GF particles by the polymer. Considering that GF-Kol/HPC extrudate shows almost identical XRD diffractogram to that of their physical mixture, the author concludes that the GF nanoparticles in the HPC/Kol matrix were largely crystalline. Besides the dilution effect of the polymer, reduction of drug particle size during milling could

have resulted in some XRD peak broadening (Deng et al., 2008). It is noted that 2% drug crystal concentration for 2% GF-Kol/HPC is close to the detection limit of XRD; while the SEM images clearly showed drug nanocrystals forming a secondary phase.

Besides Kol/HPC, Sol was used to produce extrudates, for which Sol was also used as a steric stabilizer in combination with SDS producing well-stabilized feed nanosuspension (Table 8.1). No particle was observed in the cross-section in SEM images of Sol extrudate (Figure 8.2a and b). On comparing GF-Sol extrudate diffractogram with those of as-received GF microparticles and Sol, no GF characteristic peak appeared (Figure 8.3a). GF was molecularly dispersed within the Sol matrix, forming a single-phase amorphous mixture also known as ASD. A similar observation was reported by Hardung et al. (2010) for GF–Soluplus® obtained via traditional HME and Li et al. (2017) via nanoextrusion process.

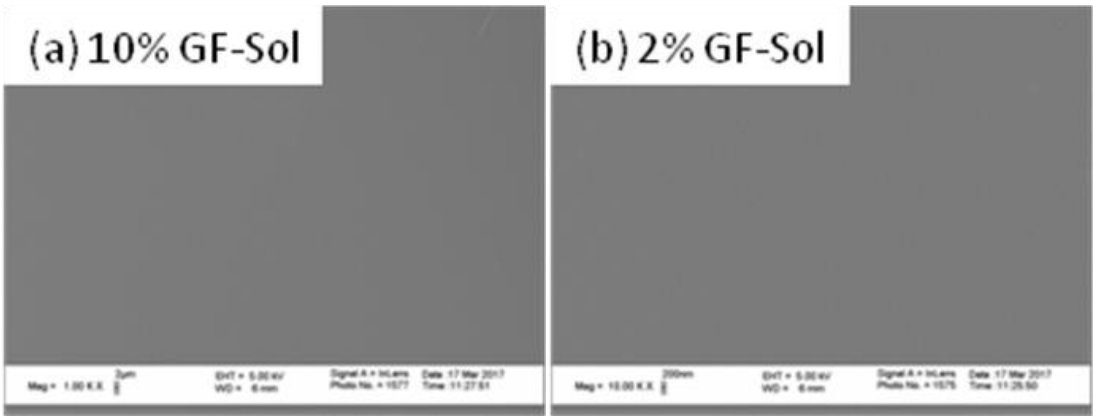

Figure 8.2 SEM images of the cross-sections of various extrudate threads: (a) 10% GF-Sol (ASD), (b) 2% GF-Sol (ASD), (c) 10% GF-Kol (nanocomposite), (d) 2% GF-Kol (nanocomposite), (e) and (f) 10% GF-HPC (nanocomposite), and (g) and (h) 2% GF-HPC (nanocomposite). (Continued)

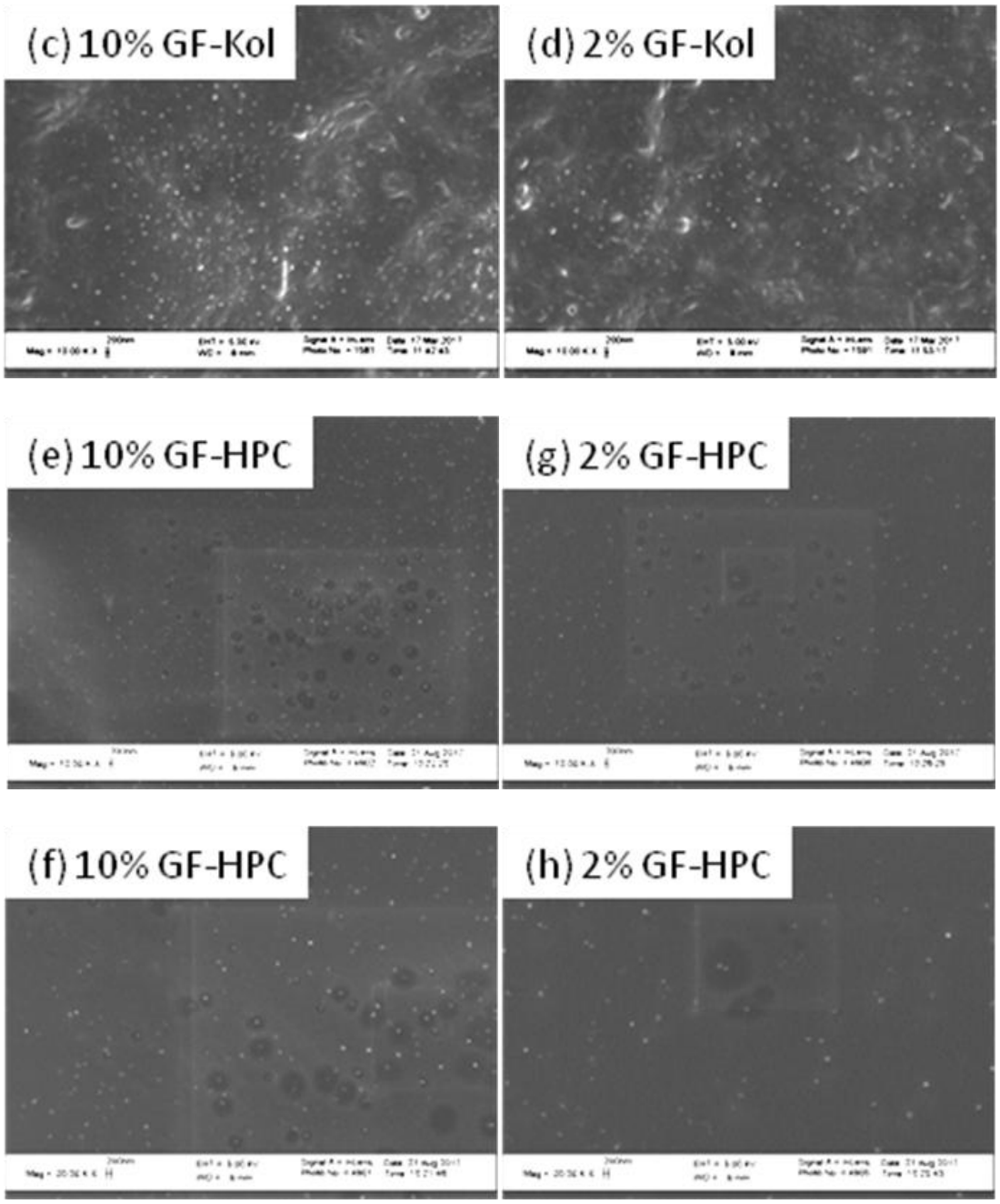

Figure 8.2 (Continued) SEM images of the cross-sections of various extrudate threads: (a) 10% GF-Sol (ASD), (b) 2% GF-Sol (ASD), (c) 10% GF-Kol (nanocomposite), (d) 2% GF-Kol (nanocomposite), (e) and (f) 10% GF-HPC (nanocomposite), and (g) and (h) 2% GF-HPC (nanocomposite).

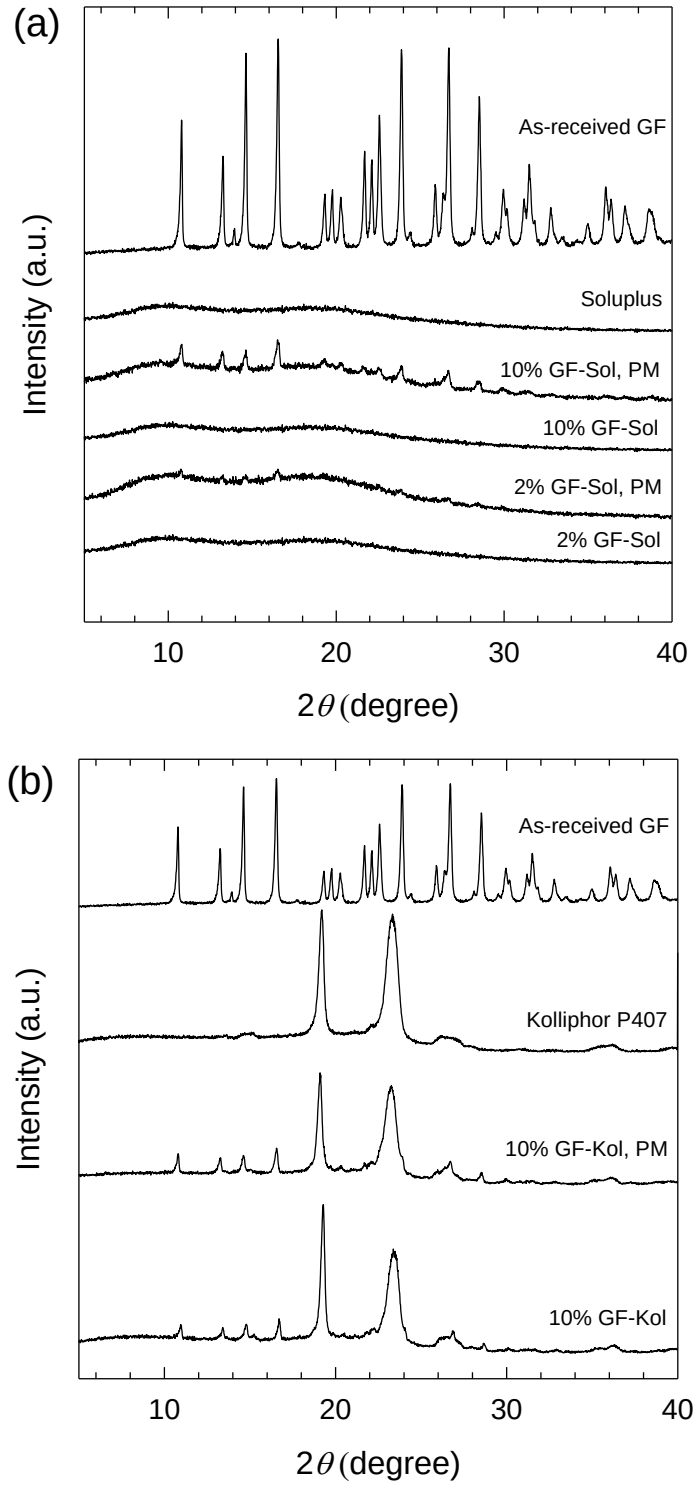

Figure 8.3 XRD diffractograms of as-received GF microparticles, Soluplus®, Kolliphor® P407, HPC, physical mixtures and extrudate powders of (a) 10% GF-Sol and 2% GF-Sol, (b) 10% GF-Kol, (c) 2% GF-Kol, (d) 10% GF-HPC and 2% GF-HPC. (Continued)

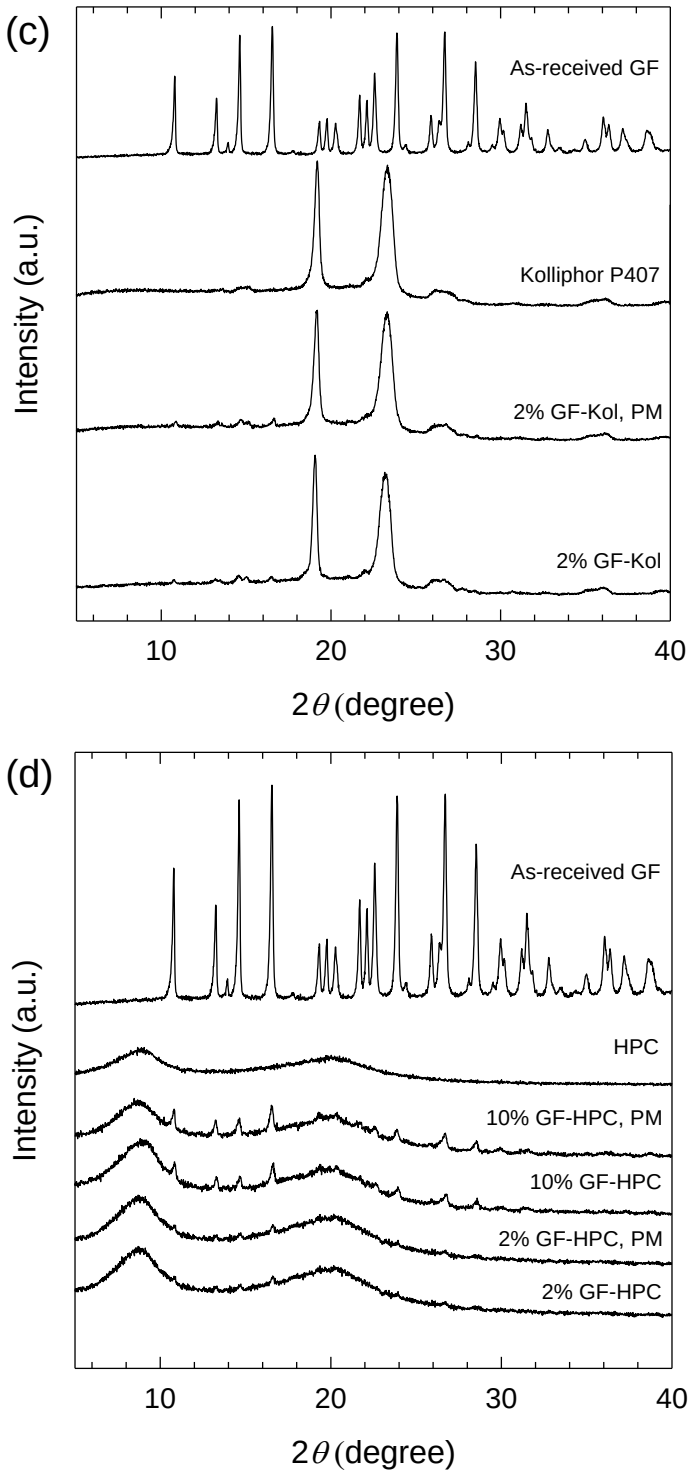

Figure 8.3 (Continued) XRD diffractograms of as-received GF microparticles, Soluplus®, Kolliphor® P407, HPC, physical mixtures and extrudate powders of (a) 10% GF-Sol and 2% GF-Sol, (b) 10% GF-Kol, (c) 2% GF-Kol, (d) 10% GF-HPC and 2% GF-HPC.

8.2.3 Effect of Polymeric Matrix Size at Non-supersaturating Condition

The XRD diffractograms in Figure 8.3 proved that GF was amorphous in the Sol matrix and largely crystalline in the Kol and HPC matrices. The extrudates were milled into powders using a coffee grinder and sieved into three different sizes: < 63 μm, 125–250 μm, and 425–710 μm. Their average sizes are reported in Table 8.3 together with the standard deviation (SD). The evolution of GF dissolution was measured in de-ionized water using a USP II apparatus and presented in Figure 8.4. Under the non-supersaturating condition, drug dose of 8.9 mg was used for the dissolution tests, while the solubility of GF is 14.5 mg.

A comparison of dissolution profiles of as-received GF and the physical mixtures with the corresponding extrudate formulations (Figure 8.4) shows that the GF dissolution was faster in the presence of polymer–SDS even without wet media milling–nanoextrusion. This could be explained by the wetting enhancement of the hydrophobic drug (GF) particles in the presence of polymer dissolved in water, as shown by the wetting effectiveness factors (Table E1, *Appendix E*). However, by producing GF ASD in Sol matrix as a cylindrical thread, i.e., 10%/2% GF-Sol, the expected dissolution enhancement was not achieved under non-supersaturating condition (e.g., only 6.8 ± 0.31% drug dissolved in 60 min for 10% GF-Sol ASD thread, even lower for 2% GF-Sol). Surprisingly, the amorphous drug in the cylindrical thread of 10% GF-Sol dissolved slower than the as-received GF microparticle powder (Figure 8.4(a)), suggesting Sol matrix almost acted as a barrier for drug release. Although the amorphous drug in ASD dissolved very slow in the cylindrical threads, faster drug dissolution from ASDs was achieved by size reduction

of the GF-Sol extrudate matrices, indicating a negative correlation between matrix size and the dissolution rate. Immediate release (i.e., 80% drug release in less than 20 min) was achieved when the matrix size of 10% GF-Sol was < 250 μm.

The dissolution rate of the extrudate with various matrix sizes as well as as-received GF microparticle powder and physical mixtures was quantitatively described by using Korsmeyer–Peppas model (Korsmeyer et al., 1983). The drug release rates are captured by *kn* in Table 8.4. According to Peppas (1985), a higher *kn* corresponds a faster drug release. The fitted *kn* values in Table 8.4 suggest the following general trends: (i) smaller extrudate particles or smaller polymeric matrices led to faster drug release for all formulations; (ii) higher drug loading (10% vs. 2%) accompanied with a reduction of polymer loading led to faster release; and (iii) drug release from the ASDs with the Sol matrix exhibited markedly stronger dependence on matrix size than the nanocomposites (10%/2% GF-Kol and 10%/2% GF-HPC). Similarly, no significant matrix size was observed when the matrix size is < 250 μm for both Kol and HPC matrices at two drug loadings.

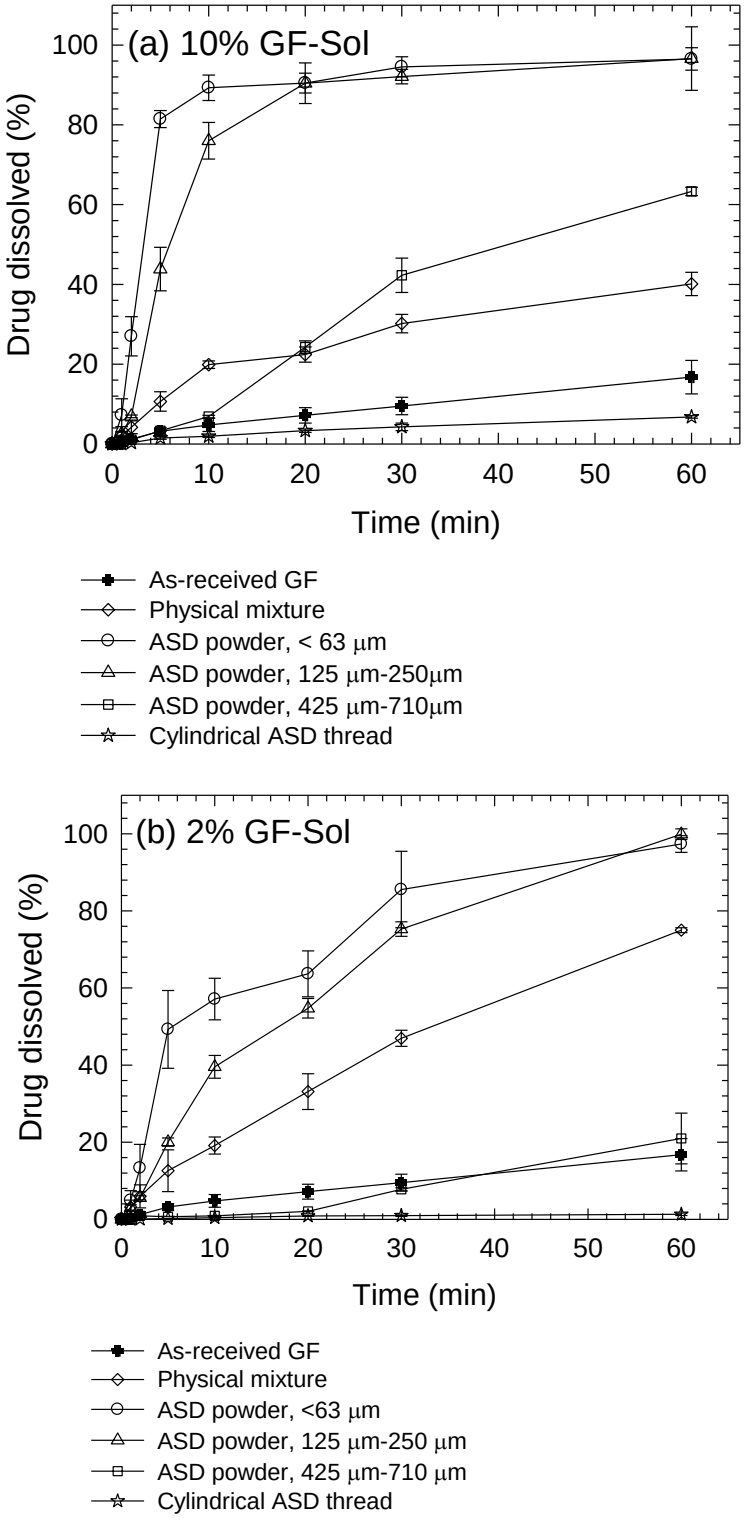

Figure 8.4 Evolution of GF dissolution from as-received GF microparticle powder, physical mixtures, and extrudates with various sizes of (a) 10% GF-Sol, (b) 2% GF-Sol, (c) 10% GF-Kol, (d) 2% GF-Kol, (e) 10% GF-HPC, and (f) 2% GF-HPC in a USP II apparatus. Sample size equivalent to 8.9 mg GF dose. (Continued)

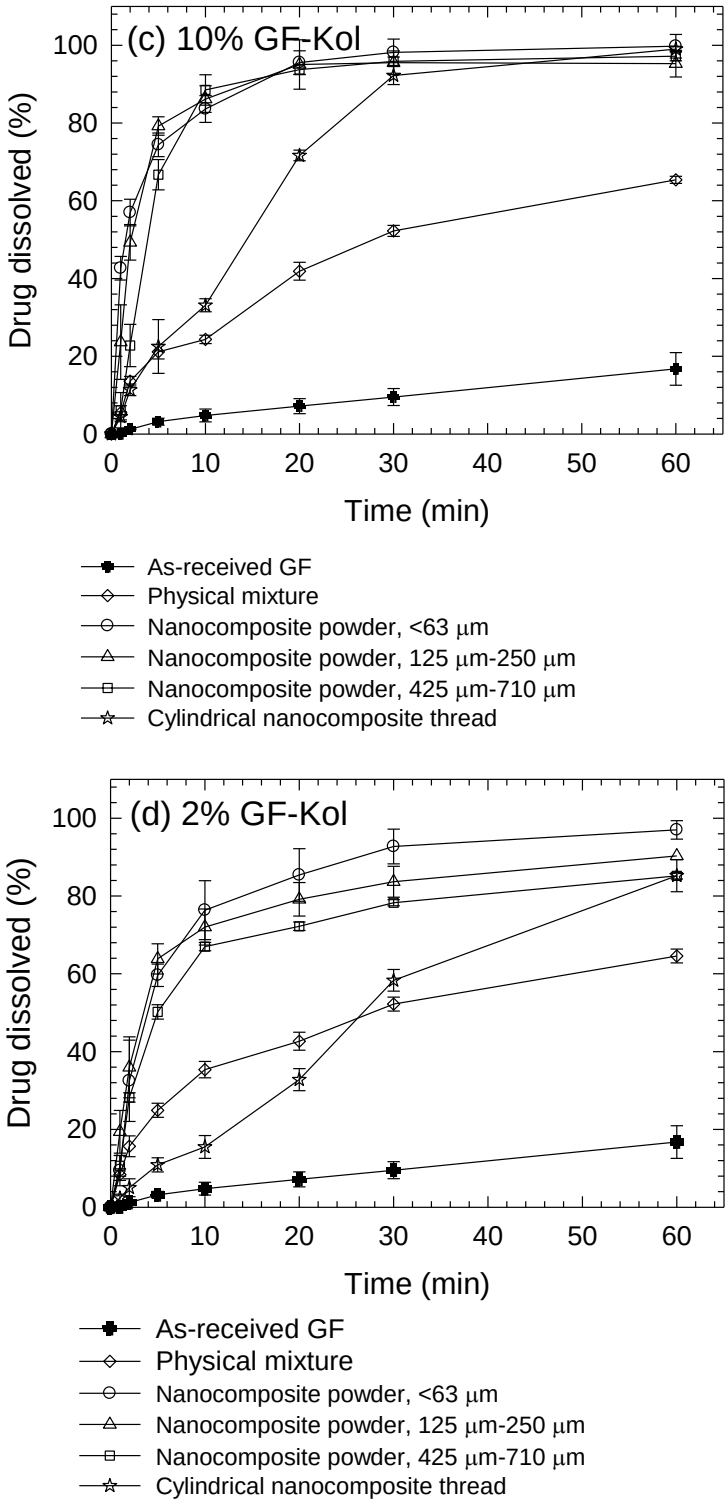

Figure 8.4 Evolution of GF dissolution from as-received GF microparticle powder, physical mixtures, and extrudates with various sizes of (a) 10% GF-Sol, (b) 2% GF-Sol, (c) 10% GF-Kol, (d) 2% GF-Kol, (e) 10% GF-HPC, and (f) 2% GF-HPC in a USP II apparatus. Sample size equivalent to 8.9 mg GF dose. (Continued)

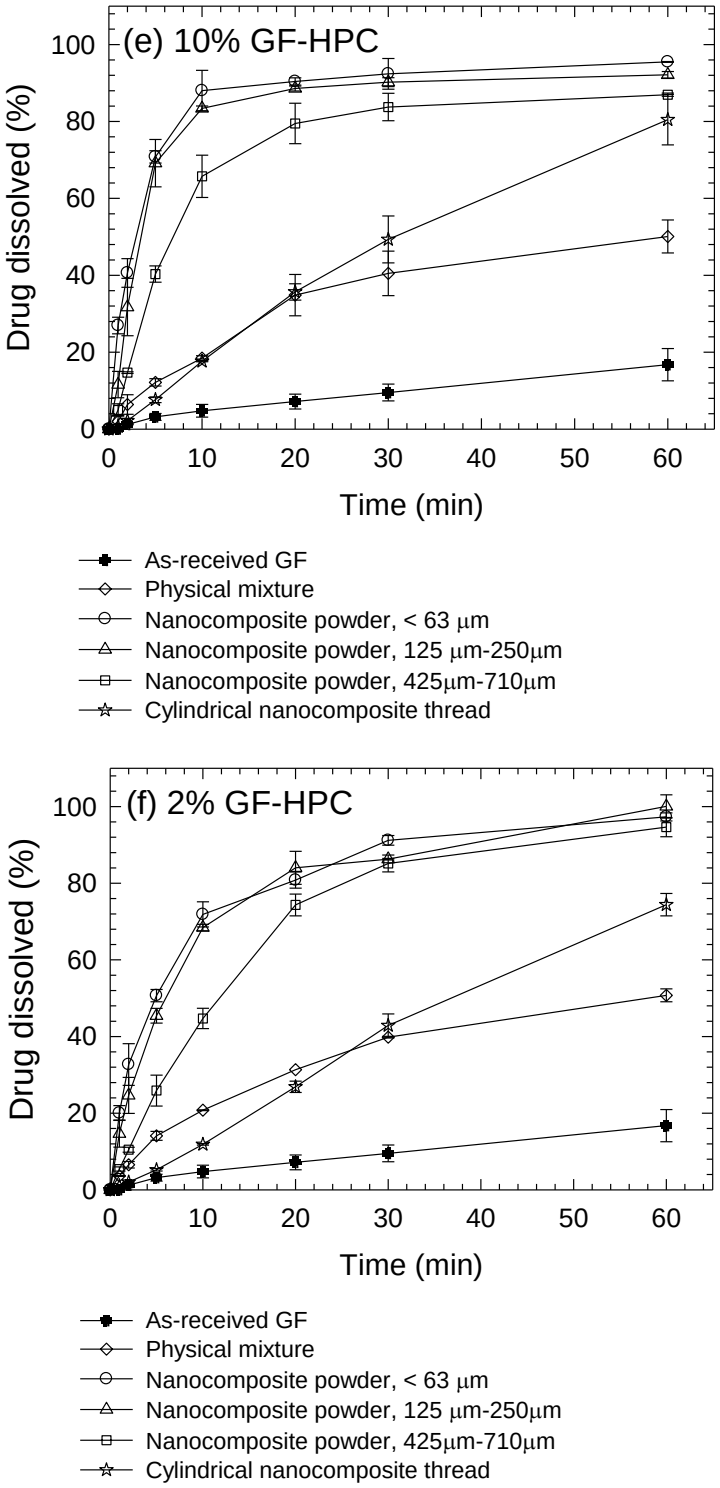

Figure 8.4 (Continued) Evolution of GF dissolution from as-received GF microparticle powder, physical mixtures, and extrudates with various sizes of (a) 10% GF-Sol, (b) 2% GF-Sol, (c) 10% GF-Kol, (d) 2% GF-Kol, (e) 10% GF-HPC, and (f) 2% GF-HPC in a USP II apparatus. Sample size equivalent to 8.9 mg GF dose.

Table 8.4 Statistical Analysis of the Fitting of the Drug Dissolution Profiles via Korsmeyer–Peppas Model

Formulation ID	Matrix Size (μm)	Korsmeyer–Peppas Model[a]			*kn* ($\%min^{-n}$)
		n (-)	*k* ($\%min^{-n}$)	R^2	
As-received GF	–	0.746	0.785	0.992	0.58
10% GF-Sol	PM	0.530	4.720	0.965	2.50
	<63	1.297	10.14	0.991	13.15
	125–250	1.101	6.187	0.953	6.81
	425–710	0.932	1.46	0.963	1.36
	Thread	0.697	0.40	0.988	0.28
2% GF-Sol	PM	0.737	3.693	0.999	2.72
	<63	0.506	15.54	0.769	7.86
	125–250	0.745	6.041	0.979	4.50
	425–710	1.430	0.06	0.989	0.09
	Thread	0.628	0.11	0.948	0.07
10% GF-Kol	PM	0.492	9.060	0.976	4.46
	<63	0.389	43.07	0.981	16.76
	125–250	0.527	30.952	0.939	16.32
	425–710	1.271	8.66	0.990	11.01
	Thread	0.903	4.70	0.984	4.24
2% GF-Kol	PM	0.406	12.659	0.981	5.14
	<63	0.616	19.59	0.900	12.06
	125–250	0.477	25.546	0.886	12.17
	425–710	0.434	21.53	0.860	9.34
	Thread	0.824	3.01	0.981	2.48
10% GF-HPC	PM	0.546	5.756	0.953	3.14
	<63	0.603	26.83	1.000	16.17
	125–250	0.963	14.790	0.978	14.24
	425–710	0.894	8.59	0.977	7.67
	Thread	0.826	2.80	0.991	2.31
2% GF-HPC	PM	0.528	6.105	0.981	3.23
	<63	0.521	21.77	0.995	11.34
	125–250	0.641	15.759	0.997	10.10
	425–710	0.795	6.95	0.997	5.52
	Thread	0.945	1.58	0.994	1.49

[a] $n \approx 0.43$ indicates diffusion-controlled release, $0.43 < n < 0.85$ indicates anomalous transport, while $n \approx 0.85$ indicates erosion-controlled release (Ritger and Peppas, 1987).

8.2.4 Effect of Polymer Type at Non-supersaturating Condition

A direct comparison of the dissolution performances of the ASD and nanocomposites allows us to analyze the impact of the GF physical state and the polymeric matrix type (refer to Figure 8.4). GF is amorphous in Sol extrudate and nanocrystalline in Kol and HPC extrudates although all the extrudates were produced by the same nanoextrusion process. All extrudates were milled–sieved into same size ranges, which allows a head-to-head comparison on the physical state of GF and the polymeric matrix. Since ASDs allow for higher drug solubility than nanocomposites containing crystalline drug nanoparticles, one would expect that ASDs should outperform the nanocomposites. It is surprising that amorphous GF in ASD dissolved much slower than the crystalline GF nanoparticles at the non-supersaturating condition, except when the matrix size is < 63 μm for 10% GF-Sol/Kol/HPC (Figure 8.4a, c, and e). Apparently, under these non-supersaturating conditions in the bulk dissolution medium, nanocomposites allowed for faster GF dissolution than ASD. The *kn* values also confirmed the rank order of the dissolution rate from different polymeric matrices, which is Kol > HPC > Sol at all matrix sizes and both drug loadings, except for 10% GF-Sol/Kol/HPC with the smallest matrix size, i.e., < 63 μm.

The observed polymeric matrix effect can be further elucidated by its interaction with water. A water droplet was added to a milled ASD particle (10% GF-Sol) or a milled nanocomposite particle (10% GF-Kol and 10% GF-HPC), and the changes to the extrudate particles were visualized using a digital microscope (Figure 8.5). The Kol and HPC matrices disappeared upon wetting and subsequent fast

dissolution, thus releasing drug nanoparticles immediately when exposed to water (Figure 8.5). Unlike Kol and HPC matrices, Sol matrix preserved the shape without significant erosion or disintegration. Although this visualization is qualitative in nature and a water droplet was stationary during this experiment unlike voluminous water under stirring during the dissolution test, it is clear that Sol, Kol, and HPC matrices containing GF behaved differently in water, which could shed light onto the observed slower GF dissolution from Sol matrix. Besides, the calculated wetting effectiveness factor (i.e., $\cos\theta_{ss}/\cos\theta_{w}$) for each polymer solution (i.e., Sol, Kol, and HPC) were 5, 38, and 27, respectively. The wetting effectiveness factor suggests that while the presence of each polymer enhanced the wettability of the hydrophobic drug significantly, a higher hydrophilicity and wettability enhancement was imparted by Kol in water followed by HPC, and then Sol. The greater wettability enhancement by Kol and HPC could result in the fast redispersion and release of drug nanoparticles observed in Figure 8.5 and associated immediate drug release in the dissolution testing. Despite the high supersaturating capability of the ASD, under the non-supersaturating condition/at low drug dose, the dissolution enhancement is perhaps affected more by the relative wettability/hydrophilicity, swelling–erosion, and size of the respective polymeric matrix.

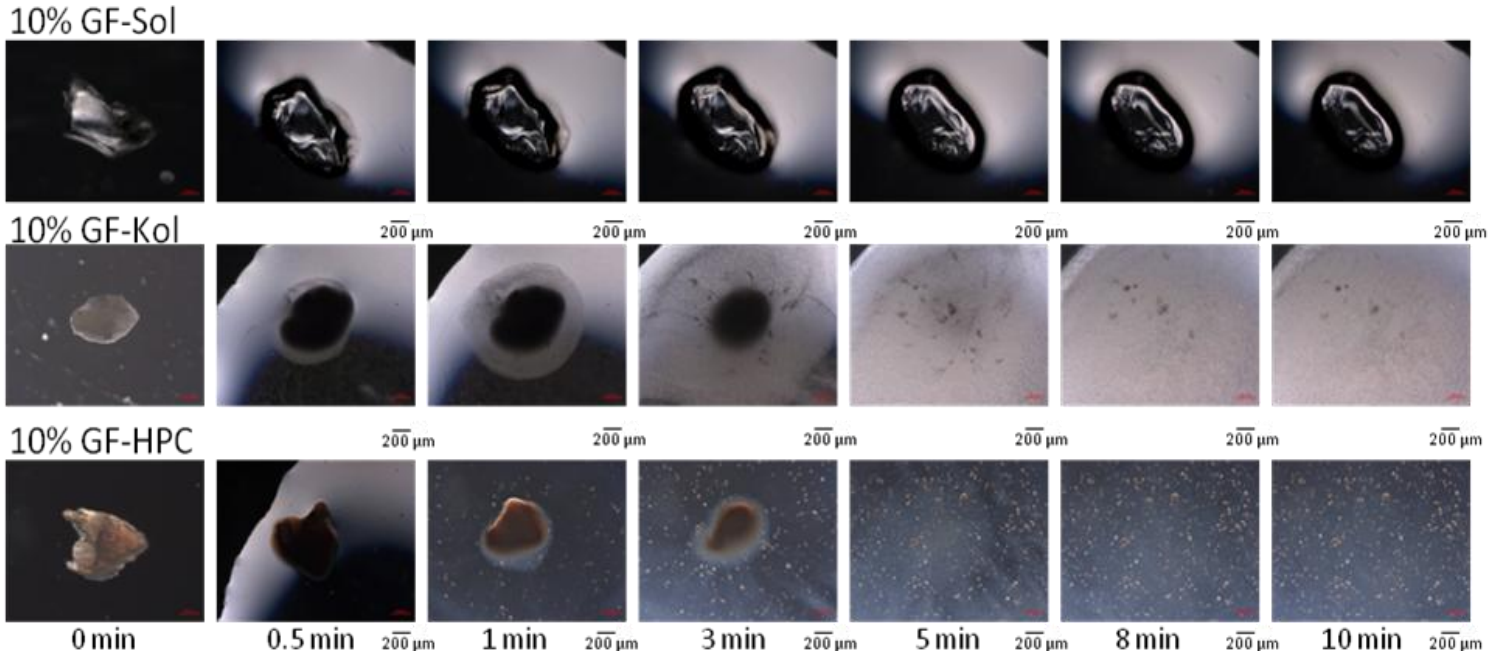

Figure 8.5 Digital microscope images showing the morphological changes of 10% GF-Sol (ASD), 10% GF-Kol (nanocomposite), and 10% GF-HPC (nanocomposite) particle in 3 µl deionized water.

8.2.5 Effect of Polymeric Matrix and Polymer Matrix Size at Supersaturating Condition

Additional dissolution testing was conducted with excess extrudate powder containing an equivalent of 100 mg GF. Figure 8.6 presents the dissolution performance under such supersaturating conditions. When a powder sample with 100 mg GF was used in the dissolution medium, the presence of polymer in the physical mixture led to drug supersaturation for all drug–polymer pairs, as compared to the as-received GF microparticles, which did not exhibit supersaturation (14.5 ± 0.3 mg/L at 210 min). Presence of Sol in the physical mixture resulted in a higher supersaturation extent than Kol, followed by HPC. Besides, the extent of supersaturation is also positively correlated with the polymer concentration in the physical mixture. For example, the physical mixture of 10% GF-Sol has less polymer than 2% GF-Sol in the physical mixture so that 2% GF-Sol physical mixture led to a higher extent of drug supersaturation than 10% GF-Sol physical mixture.

When dissolution was conducted on the extrudates, the nanocomposites containing GF nanocrystals supersaturated and dissolved faster than the as-received GF microparticles. Although nanocomposites also supersaturated, the extent of supersaturation and drug dissolution was much less than that of the ASDs, e.g., 98.8 ± 3.5 mg/L, 16.5 ± 0.4 mg/L, and 16.3 ± 0.5 mg/L for Sol, Kol, and HPC matrices, respectively, containing 10% drug theoretically with the matrix size of < 63 µm at 210 min. Hence, as expected from basic thermodynamic considerations and in line with previous literature (Zhang et al., 2013), for high drug dose, the amorphous form of the drug (Figures 8.6a and b) attained higher supersaturation and exhibited higher extent/amount of drug dissolution than the nanocrystalline form of the drug in the

nanocomposites (Figures 8.6c–f). Overall, the ASDs did indeed outperform drug nanocomposites in terms of the higher extent of drug dissolution when a high drug dose was used to allow for supersaturation in the bulk dissolution medium.

Under the supersaturating condition, smaller matrix size led to significantly faster dissolution for GF ASD in the matrix of Sol (Figure 8.6a and b). Also, it is very interesting that 10% GF-Sol dissolved faster than 10 GF-Sol when matrix size is < 63 μm. Above 425μm, 2% GF-Sol dissolved faster than 10% GF-Sol. This observation indicated an optimal polymer–matrix size combination. More polymer is needed to inhibit the drug recrystallization when the matrix size is large. On the other hand, for the nanocomposites considering the much lower extent of supersaturation, the matrix size impact does not seem to be significant (Figure 8.6c–f).

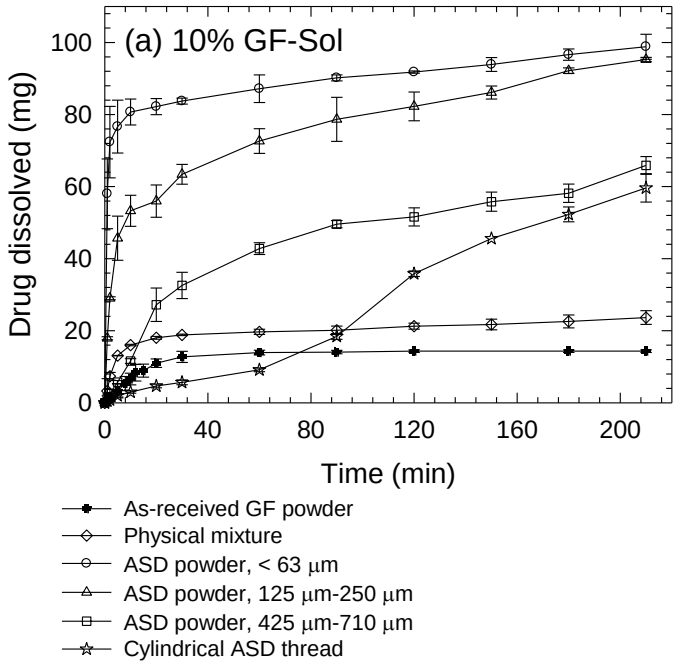

Figure 8.6 Evolution of GF dissolution from as-received GF microparticle powder, physical mixtures, and extrudates with various sizes of (a) 10% GF-Sol, (b) 2% GF-Sol, (c) 10% GF-Kol, (d) 2% GF-Kol, (e) 10% GF-HPC, and (f) 2% GF-HPC in a USP II apparatus. Sample size equivalent to 100 mg GF dose. (Continued)

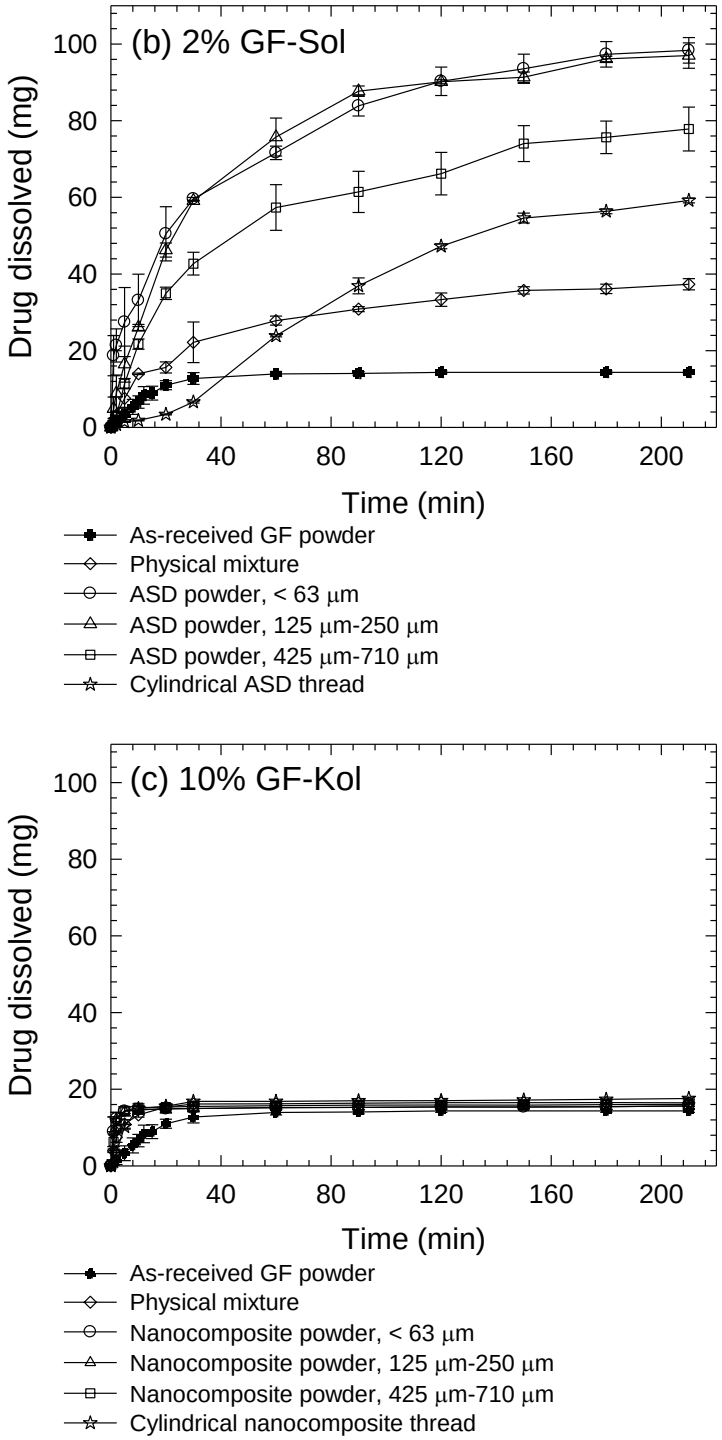

Figure 8.6 Evolution of GF dissolution from as-received GF microparticle powder, physical mixtures, and extrudates with various sizes of (a) 10% GF-Sol, (b) 2% GF-Sol, (c) 10% GF-Kol, (d) 2% GF-Kol, (e) 10% GF-HPC, and (f) 2% GF-HPC in a USP II apparatus. Sample size equivalent to 100 mg GF dose. (Continued)

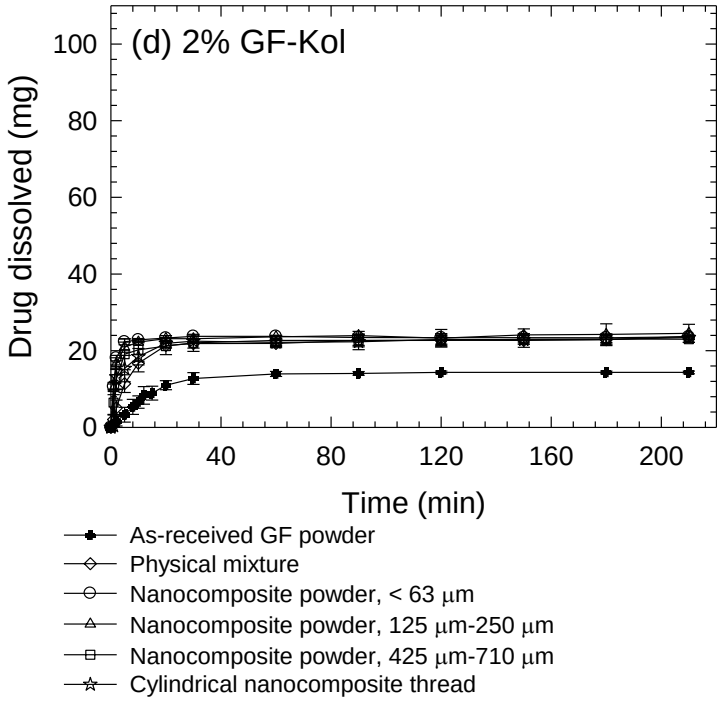

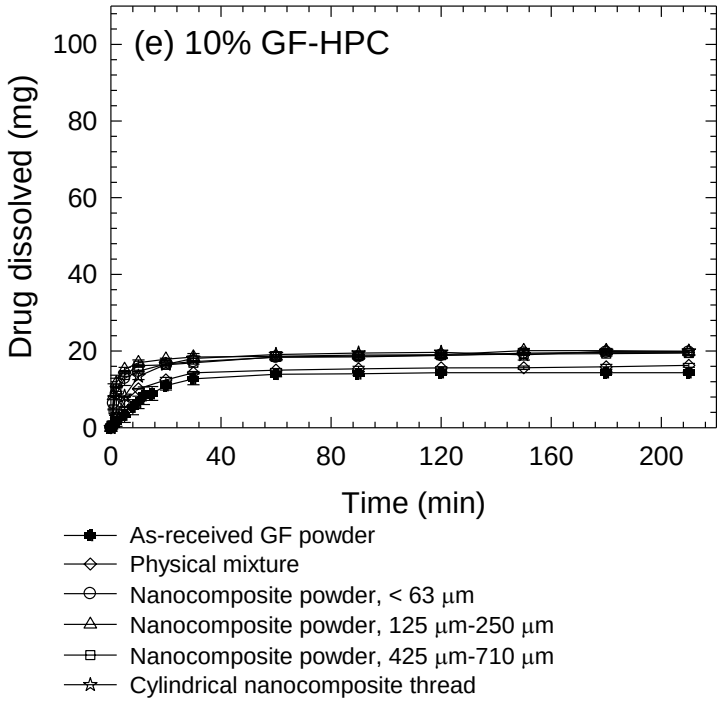

Figure 8.6 Evolution of GF dissolution from as-received GF microparticle powder, physical mixtures, and extrudates with various sizes of (a) 10% GF-Sol, (b) 2% GF-Sol, (c) 10% GF-Kol, (d) 2% GF-Kol, (e) 10% GF-HPC, and (f) 2% GF-HPC in a USP II apparatus. Sample size equivalent to 100 mg GF dose. (Continued)

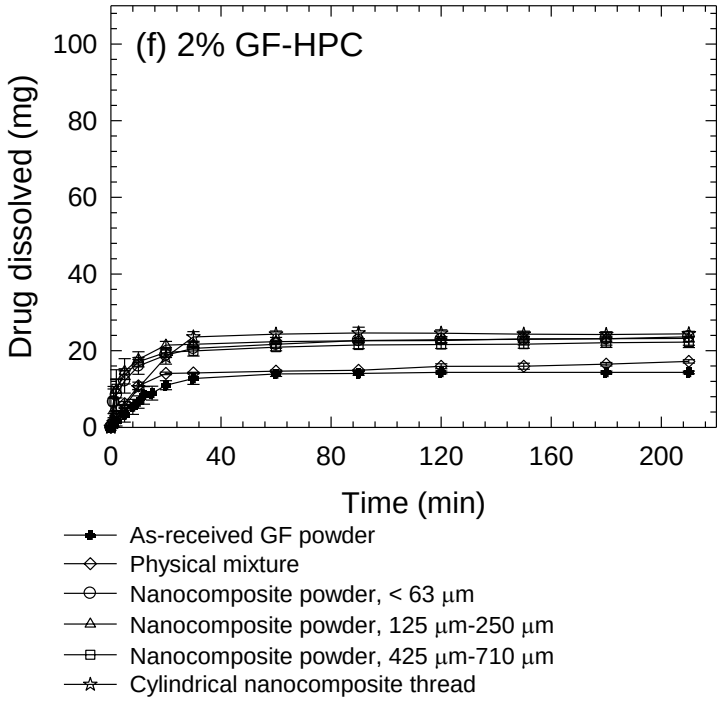

Figure 8.6 (Continued) Evolution of GF dissolution from as-received GF microparticle powder, physical mixtures, and extrudates with various sizes of (a) 10% GF-Sol, (b) 2% GF-Sol, (c) 10% GF-Kol, (d) 2% GF-Kol, (e) 10% GF-HPC, and (f) 2% GF-HPC in a USP II apparatus. Sample size equivalent to 100 mg GF dose.

8.3 Conclusions

The nanoextrusion process enabled the systemic investigation on the extrudate matrix size effect on the dissolution performance of griseofulvin (GF) nanocomposite, i.e., crystalline GF nanoparticles dispersed in the Kol/HPC matrices, and amorphous solid dispersion (ASD), i.e., amorphous GF molecularly dispersed within Sol, under both non-supersaturating and supersaturating conditions.

Under the non-supersaturating condition, nanocomposites dissolve faster than ASD when the matrix sizes are above 125 μm due to fast eroding/dissolving, hydrophilic matrix of Kol/HPC as compared with the slower drug release from the slowly eroding/dissolving Sol matrix. The drug ASDs outperformed the

nanocomposites in terms of the higher extent of drug dissolution under the supersaturation condition. The matrix size appears to play a major role in GF dissolution from ASD under both non-supersaturating and supersaturating conditions. The drug dissolution rate is negatively correlated with the matrix size. In the dissolution profiles of nanocomposites, the extrudate particle (polymeric matrix) size did not seem to have a significant impact under the non-supersaturating condition when the matrix size is below 250 μm. And the matrix size impact of nanocomposites is negligible considering their limited supersaturating capability. Formulations with more polymer dissolved slower, i.e., the drug in 10% GF-polymer always dissolved faster than 2% GF-polymer formulations, except when the matrix size is > 425 μm at the supersaturating condition for GF-Sol ASDs.

CHAPTER 9

CONCLUSIONS AND FUTURE WORK

9.1 Conclusions

In summary, this dissertation has developed a processing–formulation understanding of wet media milling process for fast–efficient production of drug nanoparticles in stable nanosuspension form, elucidated the impact of various classes dispersants on drug release rate and mechanisms during the redispersion–dissolution of nanocomposites prepared via dying of the drug nanosuspensions, and assessed the dissolution enhancement imparted by drug nanocomposites vs. ASDs prepared via drying of drug nanosuspensions by a novel nanoextrusion process.

The combination of cellulosic polymer and an anionic surfactant was proven to be a viable, general stabilization strategy for ensuring the physical stability of multiple wet-milled drug nanosuspensions, provided that the surfactant concentration is optimized to mitigate the Ostwald ripening. Further, with a well-stabilized suspension formulation, a microhydrodynamic rationale was developed for the selection of bead size in wet media milling process, which provides guidance on the wet media milling process design and optimization. Combining the knowledge obtained in both formulation and processing studies in drug nanosuspensions, wet stirred media milling process was intensified with the guidance of microhydrodynamic model for the fast production of sub-100 nm drug particles with reduced specific energy consumption and low bead wear.

The drug nanosuspensions were processed into nanocomposite microparticles/amorphous solid dispersions via various drying processes. Firstly, the drug nanosuspensions stabilized by polymer–surfactant was coated on Pharmatose® carriers via fluid bed coating process, from which an understanding was developed on the relationship between the physical stability of drug nanosuspensions, drug redispersion, and dissolution from the nanocomposite. It was found that good physical stability of a drug nanosuspension is a necessary condition for fast nanoparticle recovery and drug dissolution, but it was insufficient; dispersant concentration/type plays a critical role for fast drug release. For best drug dissolution performance from the nanocomposites, the presence of SDS is critical; a minimum concentration of the polymer as a film former is also required to prevent the formation of hard aggregates during drying. Fast drug dissolution from the nanocomposites was also attained by high drug-loaded, surfactant-free nanocomposites with a co-milled superdisintegrant–HPC prepared via spray drying. The drug release rate was found to correlate positively with the dispersant concentration and the swelling capacity of the superdisintegrant.

Finally, the dissolution profiles of nanoparticle-based formulations were also compared to those of the amorphous form of the same drug in ASDs prepared via the same nanoextrusion process for the first-time in literature. The findings imply that drug nanocomposites with fast eroding/dissolving, hydrophilic polymers like HPC/Kolliphor® could be competitive to drug ASDs with Soluplus® in enhancing the dissolution rate of low dose (e.g., highly potent) BCS Class II drugs. ASDs indeed outperform drug nanocomposites in terms of the higher extent of drug dissolution

when a high drug dose is used, generating high supersaturation in the bulk dissolution medium.

While this dissertation has established a platform approach (nanoextrusion) for a scientific comparison of drug nanocomposites vs. ASDs and the prerequisite processing–materials knowledge and methodology needed for such scientific comparison, there are still various areas for further research and investigation, which are summarized below.

9.2 Future Work

9.2.1 Production of Nanocomposites and ASDs of Multiple Poorly Water-Soluble Drugs via Nanoextrusion Process

In current dissertation, a head-to-head comparison of the dissolution performance of nanocomposites vs. ASD of one drug, i.e., griseofulvin, was made possible by using the same nanoextrusion process as a platform technology followed by dry milling. To generalize the conclusions, multiple drugs with various polymers, having a wide range of polymer–drug miscibility, should be tested in terms of formation of drug nanocomposites vs. ASD via nanoextrusion process as well as their dissolution performance at both non-supersaturating and supersaturating conditions. In addition, for a given drug–polymer pair, the dissolution performance of the extrudates obtained from nanoextrusion must be compared to that of traditional hot melt extrusion (HME) process to assess whether nanoextrusion offers any significant advantages.

9.2.2 Production of Nanocomposites and ASDs via Spray Drying

Although the nanoextrusion process could produce both forms of the same drug, i.e., nanocomposites vs. ASDs, the production of each form of the drug largely depends on the selection of polymer and the drug–polymer miscibility. Thus, it is very difficult, if not impossible, for the nanoextrusion process to produce both nanocomposite and ASDs using the same polymer. Alternatively, spray drying is also a well-established process for the preparation of ASDs and nanocomposites. For example, when water-based drug nanosuspensions were fed to the spray dryer, as shown in Chapter 6, drug nanocomposites were produced, and as demonstrated in literature, when a drug–polymer solution is fed, ASDs can be produced. Thus, it would be promising to use spray dryer to produce both nanocomposites and ASDs of the same drug with identical formulation by changing the precursor material, i.e., drug nanosuspension vs. drug solution.

9.2.3 Develop an Understanding of the Drug–Polymer Interaction on the Formation of Drug Nanocomposites and ASDs

Both nanoextrusion and spray drier can be used to produce drug nanocomposites as well as ASDs. However, the mechanisms for these two processes are quite different. It would be of fundamental importance to understand the role of drug–polymer interaction on the formation of drug nanocomposites and ASDs; and how these interactions affect the formation of drug nanocomposites and ASDs via each process. Multiple characterization techniques, such as DSC, XRD, Raman spectroscopy, and FTIR analysis, can be used to gain insight into the thermodynamic properties of different physical forms of the drug, transformation of physical forms of the drug

upon processing, and drug–polymer interactions. This understanding can help the formulation scientist on the selection of polymer and processing on drug development.

9.2.4 Understanding of the Impact of Physico-chemical/mechanical Properties and Outlook in Wet stirred media Milling

Considering the lack of correlation between the physical stability and physico-chemical drug properties, future research on the stabilization of drug nanosuspensions will probably continue to evolve along two major directions: first is further fundamental research on elucidating the impact of physico-chemical drug properties (Choi et al., 2005; Lee et al., 2008; Lee et al., 2005) and second is development of complementary characterization methods that help to screen stabilizer(s) and determine their optimal concentrations in a streamlined fashion (Knieke et al., 2013; Verma et al., 2009).

To generalize the findings in Chapters 3 and 4 and develop an understanding of the impact of various drug properties such as mechanical strength, elastic properties, etc., multiple drugs should be studied, and the impact of bead size and type at different bead loading levels should be investigated. Moreover, a mixture of different bead sizes, which entails a modification of the microhydrodynamic model for analysis, and staged use of different bead sizes (coarser beads during initial milling followed by their replacement with smaller beads) could offer further process optimization potential and warrant future investigation.

Regarding the intensified WSMM process, one can fine-tune or optimize the parameters of the process so as to minimize any one or all of the following response variables: desired fineness for a given application, production cycle time, specific

energy consumption, and bead wear/product contamination. When such a full-fledged, multi-objective optimization study is carried out for a specific industrial application, either a high weighting for bead wear can be used to ensure low media contamination or a constraint on bead wear can be imposed per strict health authority requirements.

APPENDIX A

CALCULATIONS OF MICROHYDRODYNAMIC PARAMETERS

The mathematical expressions for the effective drag (dissipation) coefficient R_{diss} and the microhydrodynamic parameters can be found in Eskin et al. (2005b). They are reported here for the sake of completeness. Wylie et al. (2003) gives R_{diss} as

$$R_{\text{diss}} = R_{\text{diss0}}(c) + K(c)\, d_{\text{b}} \rho_{\text{L}} \theta^{1/2} / \mu_{\text{L}} \tag{A.1}$$

where ρ_{L} is the density of the equivalent liquid and K is a coefficient given by an empirical correlation of bead concentration c

$$K(c) = \left(0.096 + 0.142 c^{0.212}\right) / (1-c)^{4.454} \tag{A.2}$$

R_{diss0} in Eq. (A.1) is the dissipation coefficient taking into account squeezing in the equivalent liquid film between two approaching beads and is expressed as follows:

$$R_{\text{diss0}}(c) = k_1(c) - k_2(c) \ln \varepsilon_{\text{m}} \tag{A.3}$$

In Eq. (A.3), ε_{m} is the non-dimensional bead–bead gap thickness at which the lubrication force stops increasing and becomes a constant. According to Sangani et al. (1996), ε_{m} can be taken as 0.003. k_1 and k_2 in Eq. (A.3) are computed using

$$k_1(c) = 1 + 3\sqrt{c/2} + (135/64) c \ln c + 11.26 c (1 - 5.1c + 16.57c^2 - 21.77c^3) \tag{A.4}$$

$$k_2(c) = c\left(1 - 0.5c\right) / (1-c)^3 \tag{A.5}$$

Eqs. (A.1)–(A.5) were used in Eq. (3.4) of the main text to calculate the granular temperature θ. With θ known, all other microhydrodynamic parameters were calculated, as discussed in the main text and below, using the expressions derived by

Eskin et. al (2005b). The average maximum normal force F_b^n and the radius of the contact circle α_b during collision of two identical elastic beads were calculated from

$$F_b^n = 1.96\left(\frac{Y_b}{1-\eta_b^2}\right)^{2/5}\rho_b^{3/5}R_b^2\theta^{3/5} \tag{A.6}$$

$$\alpha_b = \left[\frac{3}{4}\frac{\left(1-\eta_b^2\right)}{Y_b}R_b F_b^n\right]^{1/3} \tag{A.7}$$

where Y_b, and η_b are the Young modulus and Poisson's ratio of the bead material, i.e., yttrium stabilized zirconia, and were taken from the literature as 200 GPa and 0.2, respectively (Ashby and Cebon, 1993; Srikar et al., 2004); R_b is the bead radius and was taken as half of the measured median size d_b. The probability p of a single drug particle with radius R_p being caught between beads was estimated as the ratio of the volume containing the caught particles to the volume of milled drug suspension falling on a pair of the milling beads and is expressed as

$$p = 0.97\frac{c}{1-c}\left[\frac{\rho_b\left(1-\eta_b^2\right)}{Y_b}\right]^{2/5}\theta^{2/5}\frac{R_p}{R_b} \tag{A.8}$$

APPENDIX B

A MICROHYDRODYNAMIC RATIONALE FOR SELECTION OF BEAD SIZE IN PREPARATION OF DRUG NANOSUSPENSIONS VIA WET STIRRED MEDIA MILLING

The supplementary materials of Chapter 3 are shown in this section.

Table B.1 The Time It Takes Drug Median Size d_{50} to Reach 0.5 µm (t_{d50}) and d_{90} to Reach 1 µm (t_{d90}) and Characteristic Time Constant (τ_p) Fitted by the Empirical Model (Eq. (1)) to the Evolution of the Median Particle Size

Run No.	Stirrer Speed (rpm, m/s)	Bead Size (µm)	Characteristic Milling Times[a]		Parameters of the Empirical Model Fit		
			t_{d50} (min)	t_{d90} (min)	d_{lim} (µm)	τ_p (min)	R^2
1	1000, 3.67	200	129.1	242.8	0.256	33.4	0.970
2	1000, 3.67	400	60.2	100.3	0.324	12.7	0.955
3	1000, 3.67	800	107.1	185.8	0.465	16.9	0.904
4	1000, 3.67	1500	237.4	–[b]	0.878	20.1	0.870
5	1600, 5.86	100	41.9	105.9	0.220	11.0	0.986
6	1600, 5.86	200	21.0	27.3	0.187	5.9	0.990
7	1600, 5.86	400	23.5	42.3	0.214	8.0	0.945
8	1600, 5.86	800	43.6	60.2	0.278	11.5	0.945
9	1600, 5.86	1500	92.8	166.5	0.391	18.4	0.926
10	2800, 10.3	100	3.9	7.2	0.151	1.0	0.961
11	2800, 10.3	200	6.0	9.4	0.173	1.5	0.982
12	2800, 10.3	400	7.1	10.3	0.171	3.7	0.985
13	2800, 10.3	800	19.4	27.9	0.213	6.8	0.958
14	4000, 14.7	50	1.5	3.0	0.144	0.4	0.886
15	4000, 14.7	100	1.7	3.5	0.142	0.9	0.949
16	4000, 14.7	200	2.7	4.2	0.150	1.4	0.987
17	4000, 14.7	400	4.0	7.7	0.163	2.1	0.986
18	4000, 14.7	800	13.4	22.2	0.173	5.7	0.979

[a]Calculated by Hermite interpolation. [b]d_{90} = 1 µm was not reached during 256 min milling in Run 4.

Table B.2 Power Applied per Unit Volume of Slurry P_w, Apparent Shear Viscosity μ_L and Density ρ_L of the Milled Drug Suspensions, and All Microhydrodynamic Parameters (θ, u_b, ν, σ_b^{max}, a, and F) Calculated for Runs 1–18

Run No.	Stirrer Speed (rpm, m/s)	Bead Size (μm)	P_w (W/m^3)	μ_L (mPa·s)	ρ_L (kg/m^3)	θ (m^2/s^2)	u_b (m/s)	ν (KHz)	σ_b^{max} (GPa)	a (mHz)	F (m$^{0.6}$/s$^{2.6}$)
1	1000, 3.67	200	6.25×10^{4}	13.3	1020	7.70×10^{-4}	4.43×10^{-2}	2.73	1.12	7.47	1.43×10^{5}
2	1000, 3.67	400	8.33×10^{4}	13.3	1020	3.18×10^{-3}	8.99×10^{-2}	2.77	1.48	6.69	2.26×10^{5}
3	1000, 3.67	800	9.38×10^{4}	13.6	1020	7.75×10^{-3}	1.40×10^{-1}	2.33	1.77	4.33	2.09×10^{5}
4	1000, 3.67	1500	1.15×10^{5}	13.6	1030	1.64×10^{-2}	2.05×10^{-1}	1.86	2.06	2.55	1.66×10^{5}
5	1600, 5.86	100	8.33×10^{4}	10.5	1030	4.70×10^{-4}	3.46×10^{-2}	3.62	1.01	13.8	2.17×10^{5}
6	1600, 5.86	200	1.00×10^{5}	7.00	1030	1.96×10^{-3}	7.06×10^{-2}	4.35	1.34	17.3	4.82×10^{5}
7	1600, 5.86	400	1.04×10^{5}	8.9	1030	4.73×10^{-3}	1.10×10^{-1}	3.39	1.60	9.58	3.80×10^{5}
8	1600, 5.86	800	1.15×10^{5}	10.7	1020	9.75×10^{-3}	1.58×10^{-1}	2.62	1.85	5.33	2.82×10^{5}
9	1600, 5.86	1500	1.25×10^{5}	11.2	1020	1.81×10^{-2}	2.15×10^{-1}	1.95	2.10	2.78	1.89×10^{5}
10	2800, 10.3	100	1.46×10^{5}	5.3	1030	1.42×10^{-3}	6.02×10^{-2}	6.31	1.26	37.5	9.19×10^{5}
11	2800, 10.3	200	1.56×10^{5}	5.6	1020	3.32×10^{-3}	9.19×10^{-2}	5.67	1.49	27.8	9.58×10^{5}
12	2800, 10.3	400	2.13×10^{5}	6.1	1030	9.56×10^{-3}	1.56×10^{-1}	4.81	1.85	18.0	9.47×10^{5}
13	2800, 10.3	800	2.19×10^{5}	6.6	1020	1.74×10^{-2}	2.10×10^{-1}	3.49	2.08	8.95	5.97×10^{5}
14	4000, 14.7	50	4.79×10^{5}	4.9	1030	9.10×10^{-4}	4.81×10^{-2}	11.8	1.15	136	2.79×10^{6}
15	4000, 14.7	100	5.83×10^{5}	4.5	1030	5.45×10^{-3}	1.18×10^{-1}	12.3	1.65	125	5.26×10^{6}
16	4000, 14.7	200	6.15×10^{5}	4.5	1030	1.12×10^{-2}	1.69×10^{-1}	10.4	1.91	83.3	4.67×10^{6}
17	4000, 14.7	400	6.56×10^{5}	4.7	1030	2.34×10^{-2}	2.44×10^{-1}	7.52	2.21	40.3	3.03×10^{6}
18	4000, 14.7	800	6.77×10^{5}	5.3	1030	3.93×10^{-2}	3.16×10^{-1}	5.26	2.45	18.7	1.73×10^{6}

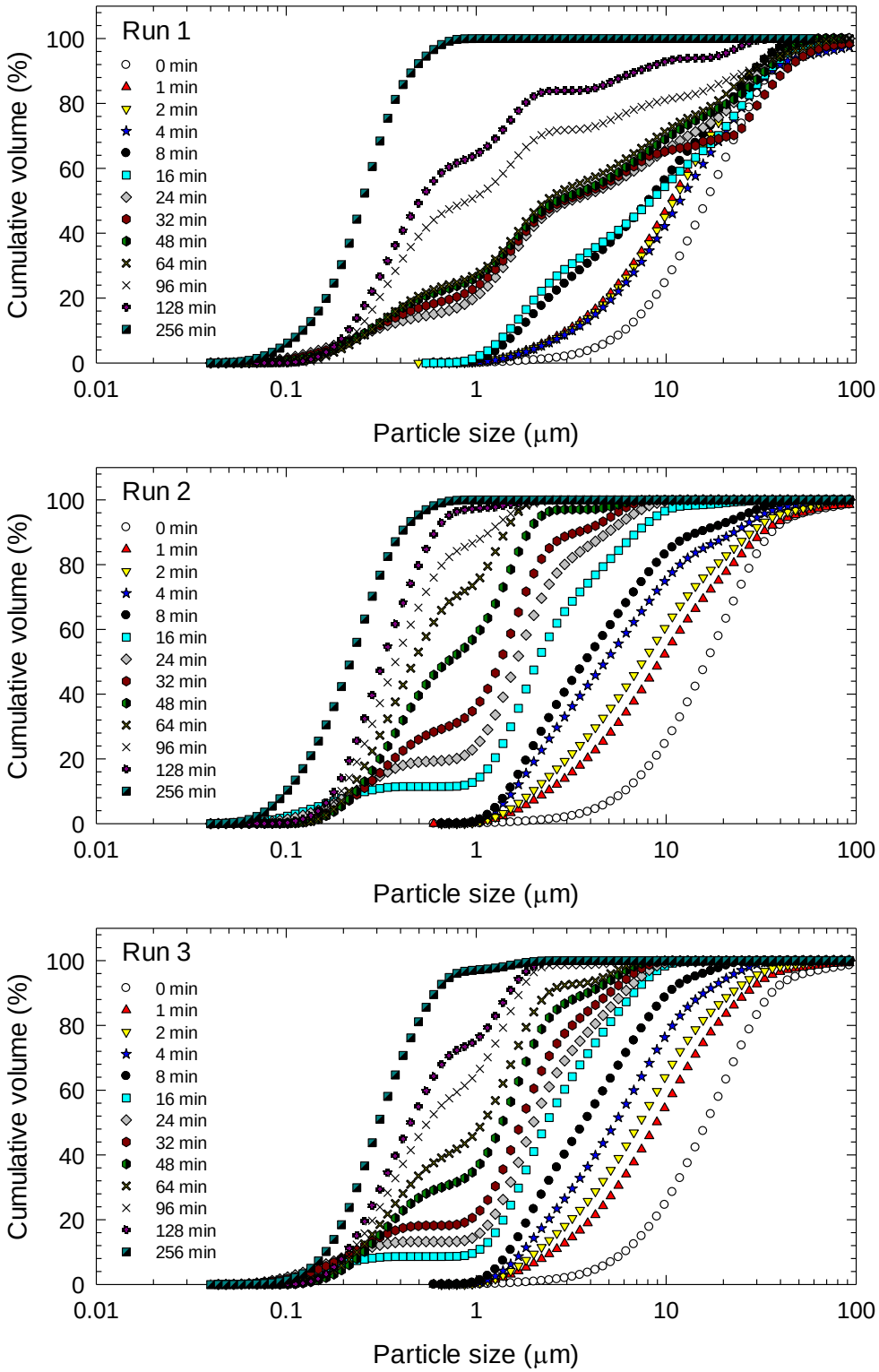

Figure B.1 Time-wise evolution of particle size distribution of griseofulvin during wet stirred media milling with various bead sizes–stirrer speeds (Runs 1–18). Each particle size distribution corresponds to an average of four (n = 4) laser diffraction measurements. (Continued)

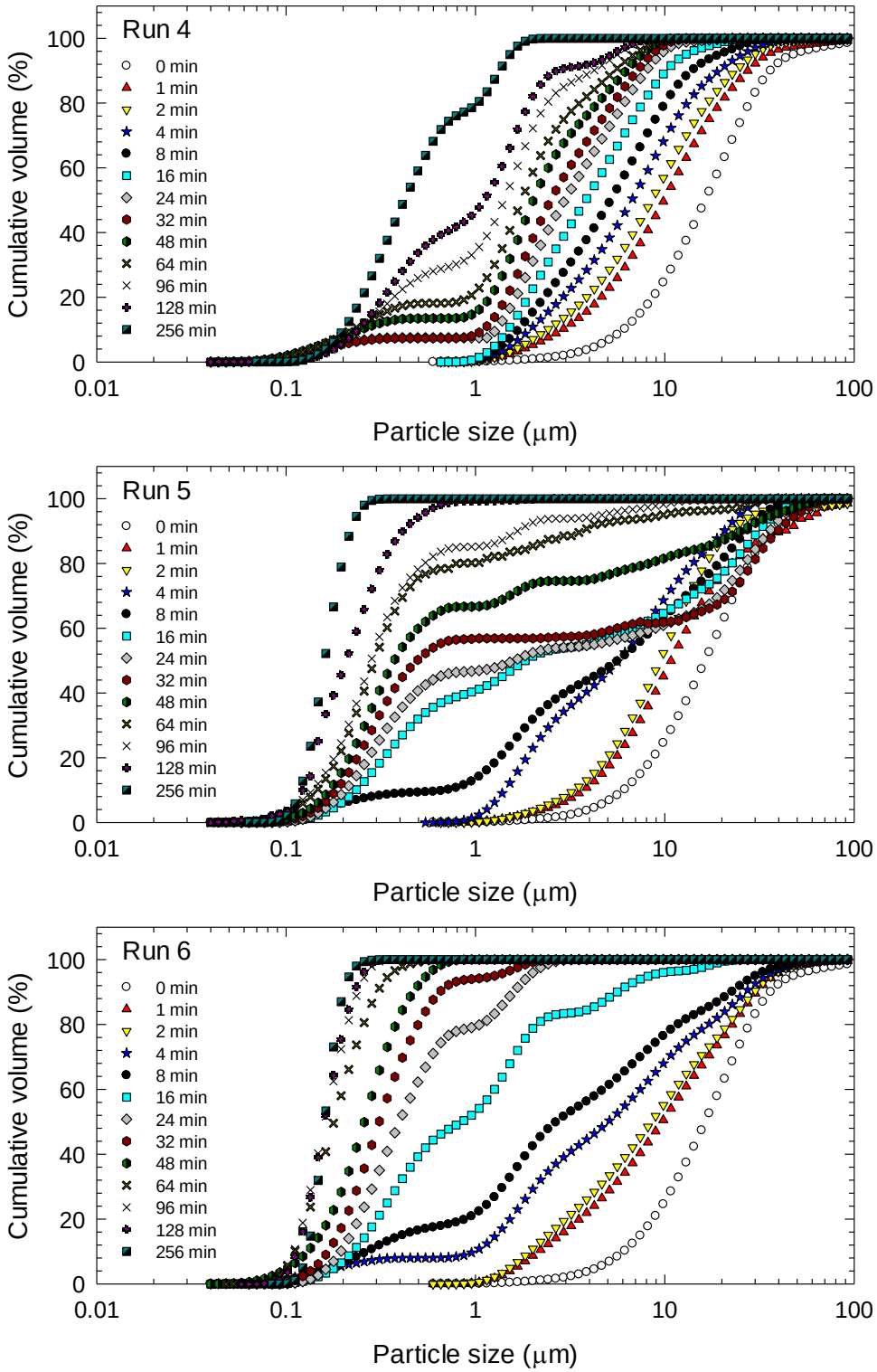

Figure B.1 Time-wise evolution of particle size distribution of griseofulvin during wet stirred media milling with various bead sizes–stirrer speeds (Runs 1–18). Each particle size distribution corresponds to an average of four (n = 4) laser diffraction measurements. (Continued)

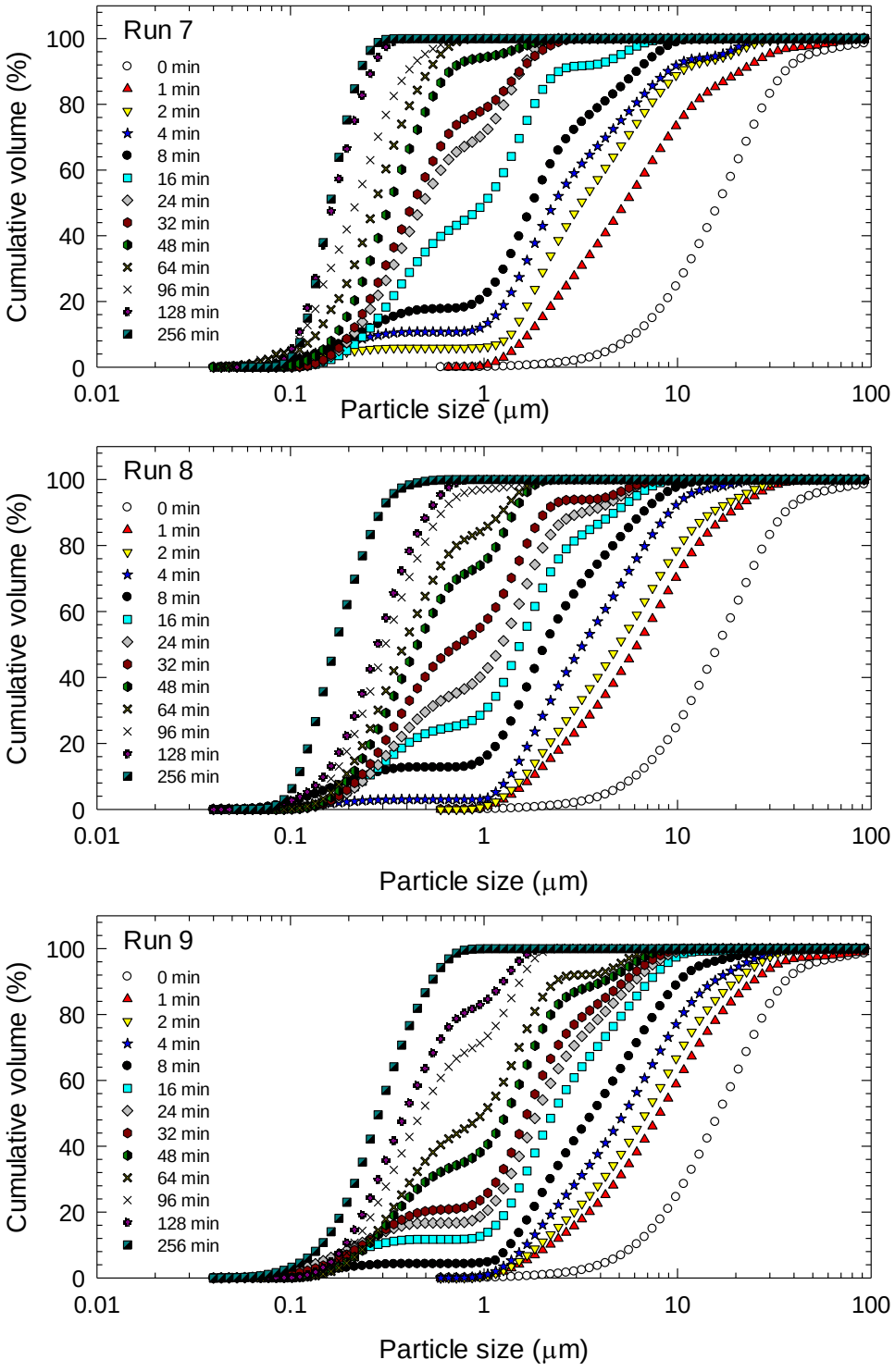

Figure B.1 Time-wise evolution of particle size distribution of griseofulvin during wet stirred media milling with various bead sizes–stirrer speeds (Runs 1–18). Each particle size distribution corresponds to an average of four (n = 4) laser diffraction measurements. (Continued)

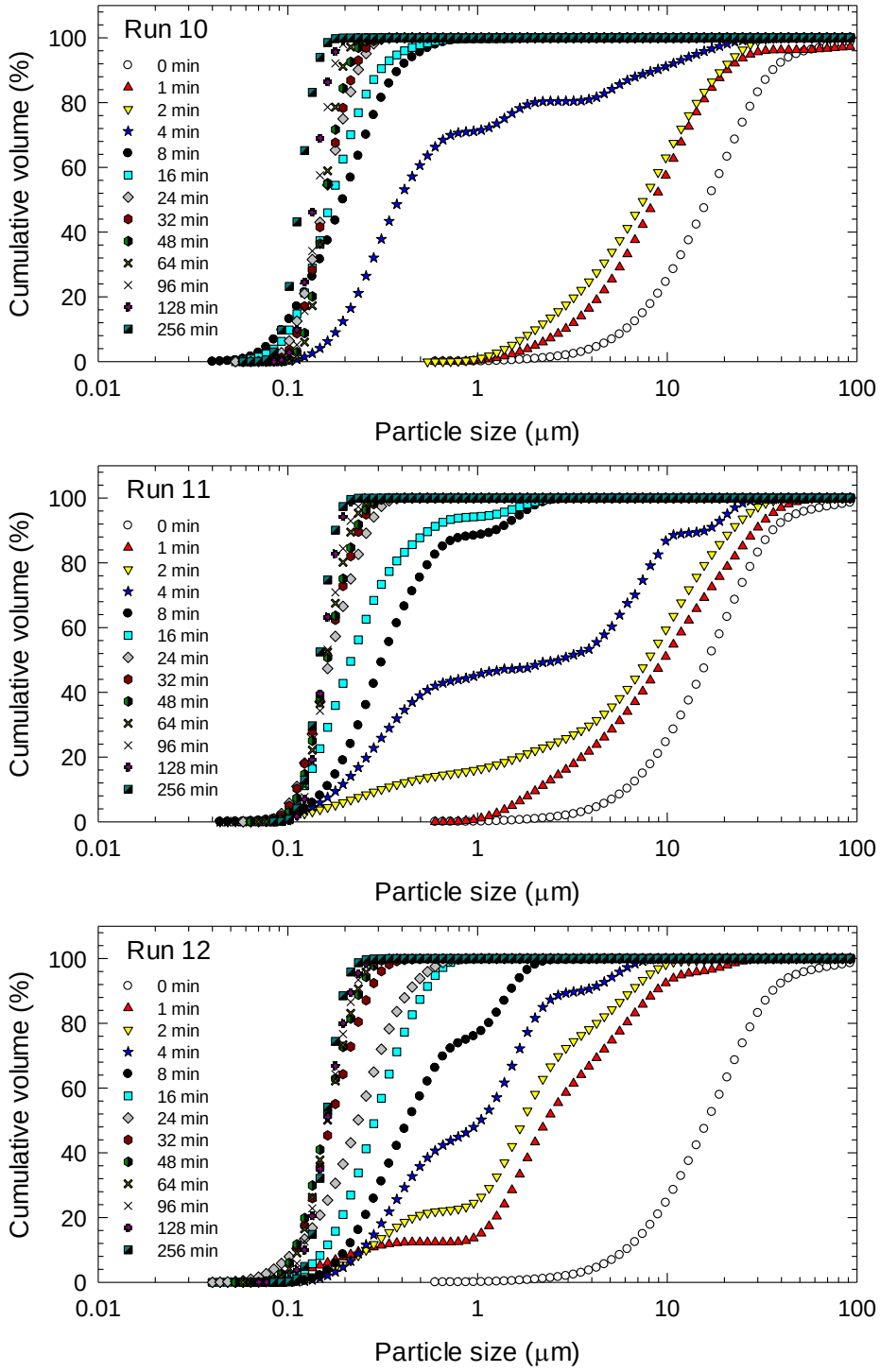

Figure B.1 Time-wise evolution of particle size distribution of griseofulvin during wet stirred media milling with various bead sizes–stirrer speeds (Runs 1–18). Each particle size distribution corresponds to an average of four (n = 4) laser diffraction measurements. (Continued)

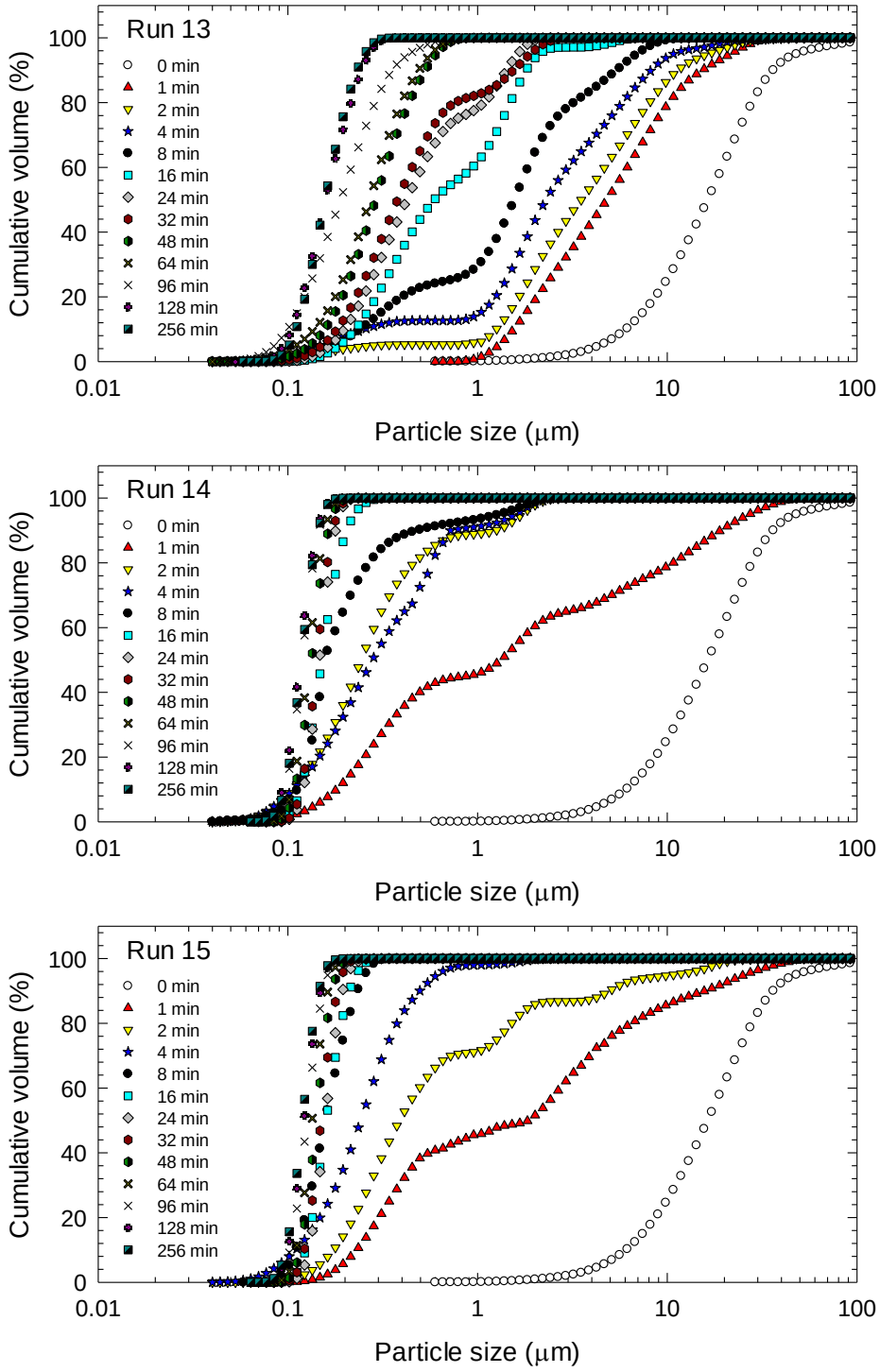

Figure B.1 Time-wise evolution of particle size distribution of griseofulvin during wet stirred media milling with various bead sizes–stirrer speeds (Runs 1–18). Each particle size distribution corresponds to an average of four (n = 4) laser diffraction measurements. (Continued)

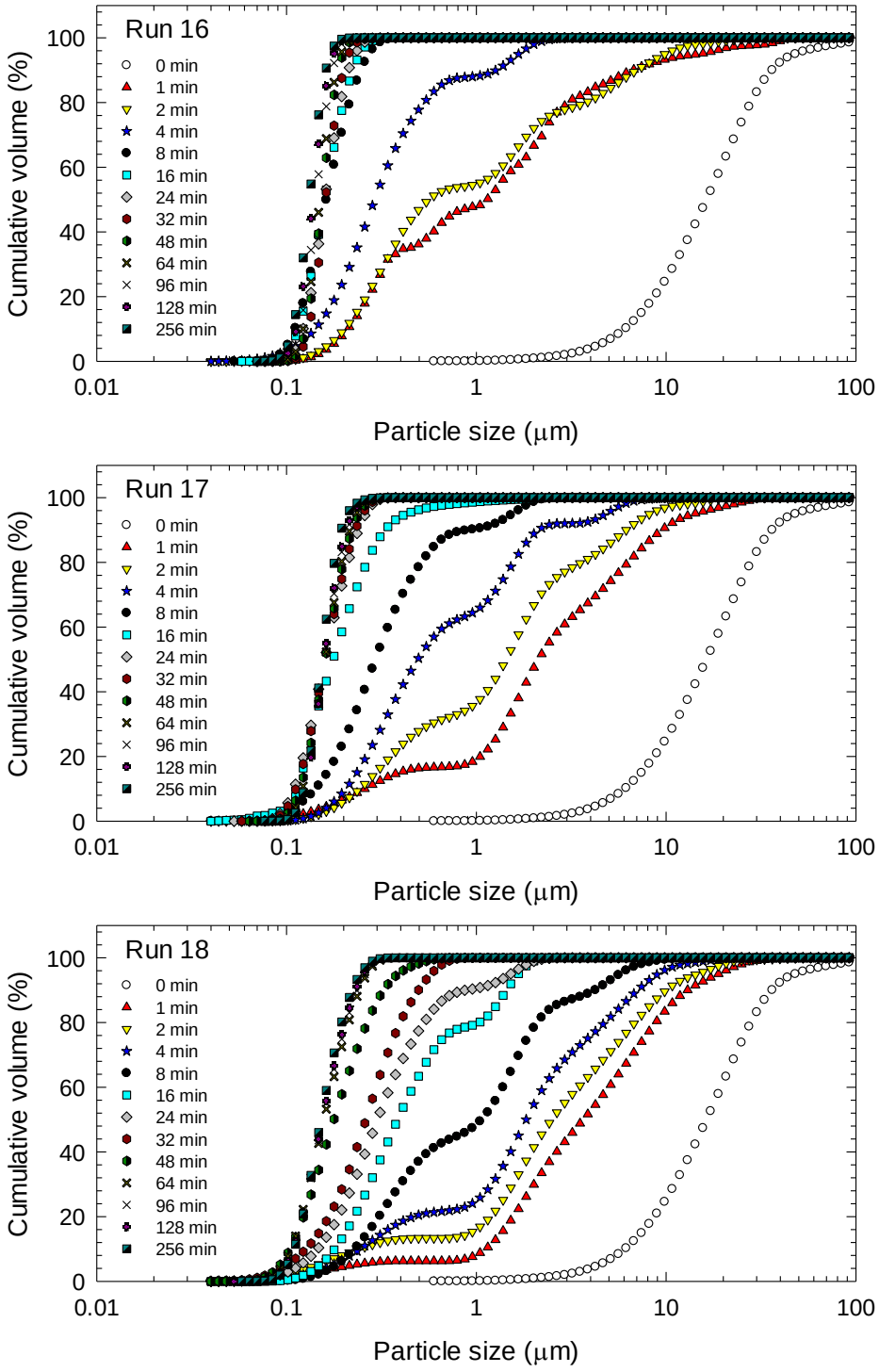

Figure B.1 (Continued) Time-wise evolution of particle size distribution of griseofulvin during wet stirred media milling with various bead sizes–stirrer speeds (Runs 1–18). Each particle size distribution corresponds to an average of four (n = 4) laser diffraction measurements.

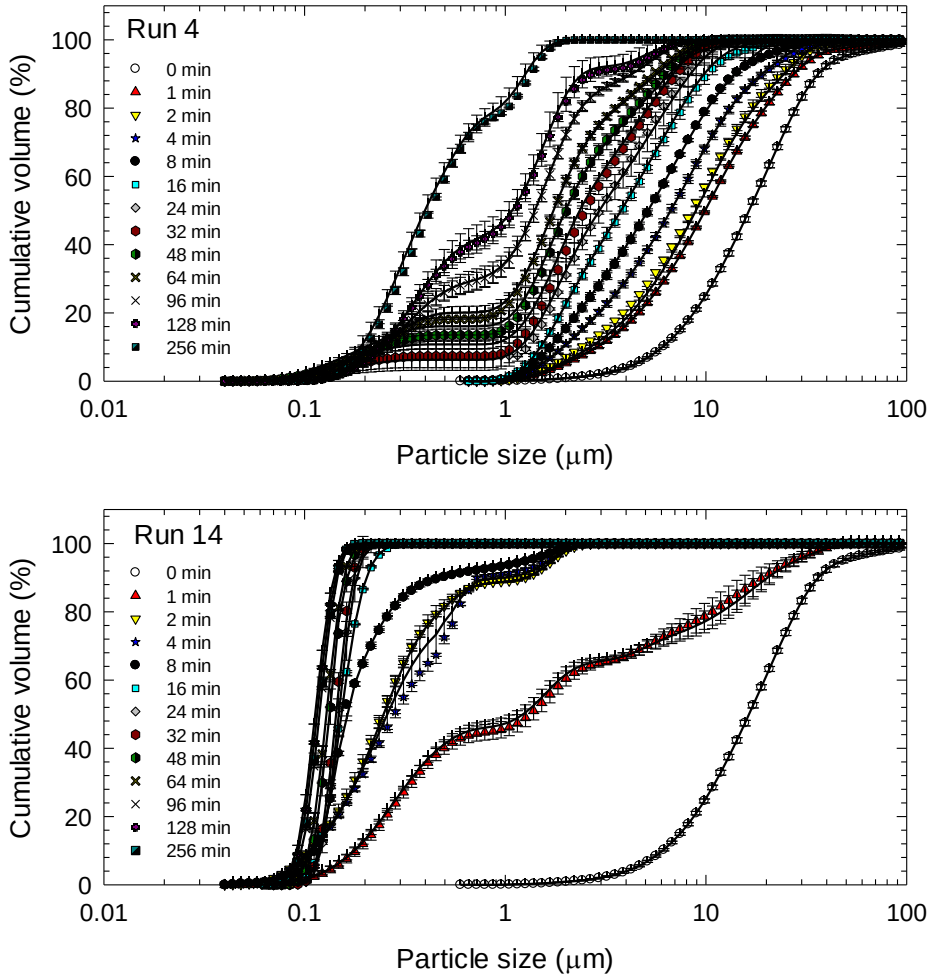

Figure B.2 Time-wise evolution of particle size distribution of griseofulvin during wet stirred media milling in Run 4 (the slowest, least intense breakage among all runs) and Run 14 (fastest, most intense breakage among all runs). Markers represent the experimental data in the original runs, while solid lines represent the experimental data in the repeated runs. Each particle size distribution corresponds to an average of four (n = 4) laser diffraction measurements.

APPENDIX C

ENHANCED DISSOLUTION OF ITRACONAZOLE FROM HIGH DRUG-LOADED SURFACTANT-FREE NANOCOMPOSITE MICROPARTICLES

C.1 Details of the Characterization Methods used for Liquid Penetration Study

Penetration of a liquid into a packed powder bed of a drug inside a cylindrical column allows for measurement of the drug powder wettability, based on the Washburn method (Hołownia et al., 2008; Washburn, 1921). In this study, liquids and powder are deionized water/stabilizer solutions (HPC, SDS, HPC–SDS/Mannitol/Sucrose) and itraconazole (ITZ), respectively. These formulations were selected corresponding to the precursor suspension formulations of F1–3, F6, F9, F10, and F17 in the absence of drug. The apparent shear viscosity and surface tension of the solutions were measured using R/S Plus Rheometer (Brookfield Engineering, Middleboro, MA, USA) and Attension Sigma 700 (Biolin Scientific, Linthicum, MD, USA), respectively; then, the drug wettability was quantified via a wetting effectiveness factor using the modified Washburn equation.

C.1.1 Surface Tension of the Solutions

The surface tension of deionized water and the aforementioned stabilizer solutions was measured using Attension Sigma 700 (Biolin Scientific, Linthicum, MD, USA) and reported in Table C2. The Attention software calculates surface tension from force measurements of the interaction of a probe (Wilhelmy plate) at the boundary between air and a liquid, i.e., the deionized water or the stabilizer solutions.

C.1.2 Liquid Penetration Study

Attension Sigma 700 set-up (Biolin Scientific, Linthicum, MD, USA) was used to study the penetration of water/aforementioned stabilizer solutions into a packed powder bed of drug (ITZ) particles inside a cylindrical column and determine the drug powder wettability, based on the Washburn method. The assembly consists of a sample holder in the form of a cylindrical metallic tube with small holes at the bottom as well as a hook at the top of the cover equipped with screw threads. About 0.8 g of ITZ powder was packed uniformly into the tube before each measurement. A filter paper was placed at the perforated end of the sample holder to support the drug powder sample. A petri dish containing deionized water/stabilizer solution was placed below the perforated end of the holder on the mechanical platform.

Upon contact of the sample holder with deionized water/stabilizer solution, the liquid penetrated into the drug powder bed, while Attension Sigma 700 recorded the mass of liquid penetrated into the drug powder bed as a function of time. The contact angle for the deionized water/stabilizer solution and the drug can be determined using the modified Washburn equation, which provides a relationship between liquid penetration rate and contact angle θ, i.e., $T = (\frac{\eta}{C\rho^2\gamma\cos\theta})M^2$, where T, M, η, ρ, and γ are time after contact, mass of the liquid penetrated into the drug powder bed, viscosity of the liquid, density of the liquid, and surface tension of the liquid, respectively. C is a characteristic parameter of the powder sample (ITZ powder in the current study), which could have been determined independently using a completely wetting liquid such as hexane, heptane, etc. Since the same drug powder (ITZ) was used as the powder sample and C depends only on powder packing, C

remained invariant for different stabilizer solutions and deionized water studied. This allows us to calculate the ratio of cosθss/cosθw as a wetting effectiveness factor, in which θ_{ss} is the contact angle between ITZ and the stabilizer solution and θw is the contact angle between ITZ and deionized water. The wettability enhancement upon the use of different stabilizers (polymers/surfactant) on the wetting of drug particles can be assessed by using this ratio, taking the wettability by water as a basis for comparison. The slope of the modified Washburn equation, i.e., $\frac{\eta}{C\rho^2\gamma\cos\theta}$, was obtained by fitting the linear region of liquid penetration curve (i.e., from T = 120 to 600 s). All the values of R^2 are above 0.99. Using the slope for different stabilizer solutions and water, $\cos\theta_{ss}/\cos\theta_w$ was calculated. The viscosity, surface tension, and the calculated wetting effectiveness factor are reported in Table C2.

C.2 Dissolution Profile Comparison

Dissolution profiles of F2, F4–F17 were compared to F1 and F3, respectively, and those with 4.5% total dispersants (F5, F8, F12, F14, and F16) were compared to F17, using difference ($f1$) and similarity ($f2$) factors (Boateng et al., 2009; Costa and Lobo, 2001). Generally, $f1$ values up to 15 (0–15) and $f2$ values greater than 50 (50–100) ensure similarity/sameness/equivalence of the two profiles. When $f1$ is greater than 15 or $f2$ is smaller than 50, the dissolution profiles were regarded as statistically different.

Table C.1 Volume-based Particle Sizes of the ITZ Precursor Suspensions (after Milling/Addition of Dispersants) and after 7-day Storage

Formula ID	Formulation (% w/w)[a]	After Milling/Addition of Dispersants (μm)						After 7-day Storage (μm)					
		d_{10}	SD	d_{50}	SD	d_{90}	SD	d_{10}	SD	d_{50}	SD	d_{90}	SD
F1	2.5% HPC	0.171	0.003	0.289	0.003	1.543	0.003	0.195	0.008	4.134	3.072	61.62	11.23
F2	0.2% SDS	4.322	0.212	10.09	0.712	21.97	0.581	4.887	0.193	11.69	0.858	24.22	1.665
F3	2.5% HPC, 0.2% SDS	0.116	0.001	0.168	0.001	0.242	0.000	0.119	0.003	0.169	0.002	0.242	0.001
F4	2.5% HPC, 1% Mannitol[b]	0.155	0.004	0.300	0.010	1.346	0.167	0.294	0.019	0.788	0.615	2.345	1.064
F5	2.5% HPC, 2% Mannitol[b]	0.195	0.005	0.331	0.006	1.628	0.055	0.188	0.005	0.679	0.077	2.190	0.032
F6	2.5% HPC, 4% Mannitol[b]	0.160	0.002	0.304	0.007	1.494	0.164	0.159	0.005	0.294	0.004	1.267	0.049
F7	2.5% HPC, 1% Sucrose[b]	0.187	0.002	0.311	0.003	1.544	0.008	0.161	0.013	0.275	0.003	1.711	0.001
F8	2.5% HPC, 2% Sucrose[b]	0.148	0.004	0.290	0.006	1.256	0.014	0.164	0.013	0.288	0.009	0.968	0.272
F9	2.5% HPC, 4% Sucrose[b]	0.180	0.004	0.307	0.004	1.585	1.555	0.173	0.003	0.325	0.037	2.457	0.402
F10	6.5% HPC	0.127	0.004	0.194	0.008	0.305	0.024	0.127	0.004	0.183	0.037	0.316	0.016
F11	2.5% HPC, 1% SSG[c]	0.189	0.001	0.342	0.004	28.26	0.361	0.195	0.007	1.082	0.868	23.00	6.121
F12	2.5% HPC, 2% SSG[c]	0.211	0.005	0.430	0.015	42.40	1.913	0.206	0.003	1.607	1.267	59.50	13.91
F13	2.5% HPC, 1% CP[c]	0.227	0.006	0.840	0.088	34.61	1.917	0.264	0.014	4.810	1.107	88.60	4.095
F14	2.5% HPC, 2% CP[c]	0.169	0.003	0.353	0.009	36.94	0.171	0.195	0.004	2.527	0.226	80.87	4.522
F15	2.5% HPC, 1% CCS[c]	0.177	0.002	0.477	0.042	44.38	4.651	0.192	0.003	0.511	0.055	58.63	4.375
F16	2.5% HPC, 2% CCS[c]	0.229	0.013	0.840	1.364	61.23	4.084	0.148	7.637	0.400	3.827	79.98	7.483
F17	4.5% HPC	0.130	0.001	0.210	0.002	0.346	0.006	0.111	0.040	0.236	0.003	0.421	0.008

[a]Drug loading in all suspensions is 10%. % w/w is with respect to the weight of deionized water, 200 g.
[b]Added to the suspension after milling.
[c]Co-milled along with ITZ for 15 min.

Table C.2 Area-based Particle Size of the ITZ Precursor Suspensions (after Milling/Addition of Dispersants) and after 7-day Storage

Formula ID	Formulation (% w/w)[a]	After Milling/Addition of Dispersants (μm)						After 7-day Storage (μm)					
		d_{10}	SD	d_{50}	SD	d_{90}	SD	d_{10}	SD	d_{50}	SD	d_{90}	SD
F1	2.5% HPC	0.151	0.004	0.232	0.003	0.420	0.008	0.137	0.003	0.225	0.002	0.431	0.003
F2	0.2% SDS	3.044	0.059	6.640	0.379	21.97	0.581	3.341	0.020	7.580	0.336	17.51	1.240
F3	2.5% HPC, 0.2% SDS	0.109	0.001	0.154	0.001	0.226	0.000	0.112	0.004	0.156	0.002	0.227	0.001
F4	2.5% HPC, 1% Mannitol[b]	0.126	0.004	0.216	0.004	0.454	0.022	0.139	0.008	0.246	0.009	1.058	0.559
F5	2.5% HPC, 2% Mannitol[b]	0.154	0.004	0.230	0.002	0.414	0.009	0.140	0.005	0.227	0.004	0.407	0.003
F6	2.5% HPC, 4% Mannitol[b]	0.131	0.003	0.220	0.003	0.452	0.024	0.132	0.006	0.222	0.006	0.436	0.005
F7	2.5% HPC, 1% Sucrose[b]	0.153	0.011	0.232	0.010	0.395	0.027	0.134	0.005	0.221	0.006	0.398	0.011
F8	2.5% HPC, 2% Sucrose[b]	0.128	0.021	0.214	0.015	0.433	0.012	0.141	0.017	0.225	0.012	0.438	0.033
F9	2.5% HPC, 4% Sucrose[b]	0.140	0.001	0.229	0.001	0.422	0.002	0.144	0.014	0.231	0.007	0.420	0.010
F10	6.5% HPC	0.117	0.004	0.172	0.006	0.271	0.015	0.117	0.004	0.174	0.005	0.282	0.011
F11	2.5% HPC, 1% SSG[c]	0.155	0.002	0.242	0.002	0.418	0.003	0.195	0.007	0.244	0.001	0.407	0.001
F12	2.5% HPC, 2% SSG[c]	0.171	0.002	0.257	0.002	0.421	0.005	0.156	0.009	0.242	0.007	0.388	0.014
F13	2.5% HPC, 1% CP[c]	0.105	0.004	0.183	0.052	0.470	0.015	0.140	0.006	0.237	0.007	0.453	0.013
F14	2.5% HPC, 2% CP[c]	0.133	0.004	0.222	0.002	0.409	0.004	0.140	0.006	0.237	0.007	0.453	0.013
F15	2.5% HPC, 1% CCS[c]	0.133	0.002	0.221	0.001	0.413	0.002	0.079	0.002	0.161	0.004	0.426	0.019
F16	2.5% HPC, 2% CCS[c]	0.133	0.005	0.231	0.004	0.454	0.008	0.106	0.015	0.211	0.013	0.449	0.012
F17	4.5% HPC	0.118	0.001	0.181	0.001	0.299	0.002	0.092	0.040	0.190	0.015	0.328	0.017

[a]Drug loading in all suspensions is 10%. % w/w is with respect to the weight of deionized water, 200 g.
[b]Added to the suspension after milling.
[c] Co-milled along with ITZ for 15 min.

Table C.3 Difference (f_1) and Similarity (f_2) Factors for Dissolution Profiles of ITZ Nanocomposites with Various Dispersants (F4–F17) as Compared with that of F1. F1 Formulation Has 10% ITZ–2.5% HPC in the Precursor Suspension

Difference and Similarity factors	Formula ID															
	F2*	**F3**	**F4***	**F5**	**F6**	**F7***	**F8***	**F9**	**F10**	**F11**	**F12**	**F13**	**F14**	**F15**	**F16**	**F17**
f_1	11.7	412.6	5.1	49.0	183.7	7.7	15.0	161.7	247.0	215.9	345.4	100.9	158.5	165.7	211.0	247.0
f_2	58.4	13.2	68.0	44.8	18.3	64.1	59.5	20.7	16.1	17.1	13.7	29.7	20.9	20.1	17.8	16.1

*These formulations have a statistical similarity comparing to F1.

Table C.4 Difference (f_1) and Similarity (f_2) Factors for Dissolution Profiles of ITZ Nanocomposites with Various Dispersants (F4–F17) as Compared with that of F3. F3 Formulation has 10% ITZ–2.5% HPC–0.2% SDS in the Precursor Suspension

Difference and Similarity Factors	**Formula ID**															
	F1	**F2**	**F4**	**F5**	**F6**	**F7**	**F8**	**F9**	**F10**	**F11**	**F12***	**F13**	**F14**	**F15**	**F16**	**F17***
f_1	80.5	87.0	84.7	73.5	34.9	84.8	81.9	43.7	37.8	37.3	7.2	63.3	47.2	44.6	37.2	6.0
f_2	13.2	11.7	12.3	15.4	31.4	12.3	12.8	26.9	29.9	30.7	62.3	18.8	25.2	26.1	30.6	63.0

*These formulations have a statistical similarity comparing to F3.

Table C.5 Difference (f_1) and Similarity (f_2) Factors for Dissolution Profiles of ITZ Nanocomposites with 2% Various Dispersants (F5, F8, F12, F14, F16) as Compared with That of F17. F17 Formulation Has 10% ITZ–4.5% HPC in the Precursor Suspension

Difference and Similarity Factors	Formula ID				
	F5	**F8**	**F12***	**F14**	**F16**
f_1	68.0	78.2	7.2	28.3	37.0
f_2	16.6	13.4	61.0	36.0	30.0

*This formulation has a statistical similarity comparing to F17.

APPENDIX D

A COMPARATIVE ASSESSMENT OF NANOCOMPOSITES VS. AMORPHOUS SOLID DISPERSIONS PREPARED VIA NANOEXTRUSION FOR DRUG DISSOLUTION ENHANCEMENT

D.1 Details of the Characterization Methods used for Drug Wettability Measurements

Penetration of a liquid into a packed powder bed of a drug inside a cylindrical column allows for measurement of the drug powder wettability, based on the Washburn method (Wahsburn, 1921; Hołownia et al. 2008). In the current study, liquids and powder are aqueous stabilizer solutions of HPC/Soluplus® with SDS and GF, respectively. Both solutions had 10% polymer and 0.002% SDS. All percentages are w/w with respective to deionized water. These concentrations were selected so that the viscosity can be accurately measured in our viscometer set-up, and the polymer-to-surfactant concentration ratio was kept the same as in F2/F4 extrudate formulations. The apparent shear viscosity and surface tension of the solutions were measured using R/S Plus Rheometer (Brookfield Engineering, Middleboro, MA, USA) and Attension Sigma 700 (Biolin Scientific, Linthicum, MD, USA) respectively, as described below; then, the drug wettability was quantified via a wetting effectiveness factor using the modified Washburn equation.

D.1.1 Apparent Shear Viscosity of the Polymeric Solutions

The apparent shear viscosity of the above solutions was measured using an R/S Plus Rheometer (Brookfield Engineering, Middleboro, MA, USA) with a water jacket assembly Lauda Eco (Lauda-Brinkmann LP, Delran, NJ, USA). A coaxial cylinder

(CC40) was used to provide a controlled shear rate on the samples from 0 to 1000 1/s for 60 s. The temperature of the jacket was kept constant at 25 ± 0.5 °C. The raw data were analyzed using the Rheo 3000 software (Brookfield Engineering, Middleboro, MA, USA) of the equipment to obtain the apparent shear viscosity as a function of the shear rate. The viscosities at the lowest shear rate that are representative of the low shear rates in the liquid penetration experiments below were reported in Table D.1.

D.1.2 Surface Tension of the Solutions

The surface tension of deionized water and the aforementioned solutions was measured using Attension Sigma 700 (Biolin Scientific, Linthicum, MD, USA) and reported in Table D.1. The Attention software calculates surface tension from force measurements of the interaction of a probe (Wilhelmy plate) at the boundary between air and a liquid, i.e., the deionized water or the solution.

D.1.3 Drug Wettability with the Solutions

Attension Sigma 700 set-up (Biolin Scientific, Linthicum, MD, USA) was used to study the penetration of water/aforementioned polymeric solutions into a packed powder bed of drug (griseofulvin, GF) particles inside a cylindrical column and determine the drug powder wettability, based on the Washburn method. The assembly consists of a sample holder in the form of a cylindrical metallic tube with small holes at the bottom as well as a hook at the top of the cover equipped with screw threads. About 0.8 g of GF powder was packed uniformly into the tube before

each measurement. A filter paper was placed at the perforated end of the sample holder to support the drug powder sample. A petri dish containing deionized water/polymeric solution was placed below the perforated end of the holder on the mechanical platform.

Upon contact of the sample holder with deionized water/polymeric solution, the liquid penetrated into the drug powder bed, while Attension Sigma 700 recorded the mass of liquid penetrated into the drug powder bed as a function of time. The contact angle for the deionized water/solution and drug can be determined using the modified Washburn equation, which provides a relationship between liquid penetration rate and contact angle θ, i.e., $T = (\frac{\eta}{C\rho^2\gamma\cos\theta})M^2$, where T, M, η, ρ, and γ are time after contact, mass of the liquid penetrated into the drug powder bed, viscosity of the liquid, density of the liquid, and surface tension of the liquid, respectively. C is a characteristic parameter of the powder sample (GF powder in the current study), which could have been determined independently using a completely wetting liquid such as hexane, heptane, etc. Since the same drug powder (GF) was used as the powder sample and C depends only on powder packing, C remained invariant for different polymer–SDS solutions and deionized water studied. This allows us to calculate the ratio of $\cos\theta_{ss}/\cos\theta_w$ as a wetting effectiveness factor, in which θ_{ss} is the contact angle between GF and the polymer–SDS stabilizer solution and θ_w is the contact angle between GF and deionized water. The wettability enhancement upon the use of different stabilizers (polymers/surfactant) on the wetting of drug particles can be assessed by using this ratio, taking the wettability by water as a basis for comparison. The slope of the modified Washburn equation, i.e.,

$\frac{\eta}{C\rho^2\gamma\cos\theta}$, was obtained by fitting the linear region of liquid penetration curve (i.e., from T = 200 to 450 s). Using the slope for different stabilizer solutions and water, $\cos\theta_{ss}/\cos\theta_w$ was calculated. The viscosity, surface tension, and calculated wetting effectiveness factor are reported in Table D.1.

Table D.1 Wetting Effectiveness Factor Calculated for Various Stabilizer Solutions using the Modified Washburn Method

Formulation	$\frac{\eta}{C\rho^2\gamma\cos\theta}$ **(s/g^2)**	**R^2**	**η (cP)**	**ρ (g/ml)**	**γ (mN/m)**	**$\cos\theta_{ss}/\cos\theta_w$**
Water	1078	0.997	0.89	1	70.8	1
HPC SL–SDS	1281	1.000	93.1	1.1	40.4	127
Soluplus®–SDS	487	0.997	5.15	1.1	41.9	20

APPENDIX E

IMPACT OF PARTICLE (MATRIX) SIZE ON DISSOLUTION ENHANCEMENT FROM GRISEOFULVIN-LADEN EXTRUDATES PREPARED VIA NANOEXTRUSION

E.1 Details of the Characterization Methods used for Drug Wettability Measurements

Penetration of a liquid into a packed powder bed of a drug inside a cylindrical column allows for measurement of the drug powder wettability, based on the Washburn method (Wahsburn, 1921; Hołownia et al. 2008). In the current study, liquids and powder are aqueous stabilizer solutions of Soluplus®/Kolliphor®/HPC with SDS and GF, respectively. All solutions had 10% polymer. All percentages are w/w with respective to deionized water. These concentrations were selected so that the viscosity can be accurately measured in our viscometer set-up. The apparent shear viscosity and surface tension of the solutions were measured using R/S Plus Rheometer (Brookfield Engineering, Middleboro, MA, USA) and Attension Sigma 700 (Biolin Scientific, Linthicum, MD, USA) respectively, as described below; then, the drug wettability was quantified via a wetting effectiveness factor using the modified Washburn equation.

E.1.1 Apparent Shear Viscosity of the Polymeric Solutions

The apparent shear viscosity of the above solutions was measured using an R/S Plus Rheometer (Brookfield Engineering, Middleboro, MA, USA) with a water jacket assembly Lauda Eco (Lauda-Brinkmann LP, Delran, NJ, USA). A coaxial cylinder (CC40) was used to provide a controlled shear rate on the samples from 0 to 1000 1/s

for 60 s. The temperature of the jacket was kept constant at 25 ± 0.5 °C. The raw data were analyzed using the Rheo 3000 software (Brookfield Engineering, Middleboro, MA, USA) of the equipment to obtain the apparent shear viscosity as a function of the shear rate. The viscosities at the lowest shear rate that are representative of the low shear rates in the liquid penetration experiments below were reported in Table S1.

E.1.2 Surface Tension of the Solutions

The surface tension of deionized water and the aforementioned solutions was measured using Attension Sigma 700 (Biolin Scientific, Linthicum, MD, USA) and reported in Table S1. The Attention software calculates surface tension from force measurements of the interaction of a probe (Wilhelmy plate) at the boundary between air and a liquid, i.e., the deionized water or the solution.

E.1.3 Drug Wettability with the Solutions

Attension Sigma 700 set-up (Biolin Scientific, Linthicum, MD, USA) was used to study the penetration of water/aforementioned polymeric solutions into a packed powder bed of drug (griseofulvin, GF) particles inside a cylindrical column and determine the drug powder wettability, based on the Washburn method. The assembly consists of a sample holder in the form of a cylindrical metallic tube with small holes at the bottom as well as a hook at the top of the cover equipped with screw threads. About 0.8 g of GF powder was packed uniformly into the tube before each measurement. A filter paper was placed at the perforated end of the sample

holder to support the drug powder sample. A petri dish containing deionized water/polymeric solution was placed below the perforated end of the holder on the mechanical platform.

Upon contact of the sample holder with deionized water/polymeric solution, the liquid penetrated into the drug powder bed, while Attension Sigma 700 recorded the mass of liquid penetrated into the drug powder bed as a function of time. The contact angle for the deionized water/solution and drug can be determined using the modified Washburn equation, which provides a relationship between liquid penetration rate and contact angle θ, i.e., $T = (\frac{\eta}{C\rho^2\gamma\cos\theta})M^2$, where T, M, η, ρ, and γ are time after contact, mass of the liquid penetrated into the drug powder bed, viscosity of the liquid, density of the liquid, and surface tension of the liquid, respectively. C is a characteristic parameter of the powder sample (GF powder in the current study), which could have been determined independently using a completely wetting liquid such as hexane, heptane, etc. Since the same drug powder (GF) was used as the powder sample and C depends only on powder packing, C remained invariant for different polymer solutions and deionized water studied. This allows us to calculate the ratio of $\cos\theta_{ss}/\cos\theta_w$ as a wetting effectiveness factor, in which θ_{ss} is the contact angle between GF and the polymer–SDS stabilizer solution and θ_w is the contact angle between GF and deionized water. The wettability enhancement upon the use of different stabilizers (polymers/surfactant) on the wetting of drug particles can be assessed by using this ratio, taking the wettability by water as a basis for comparison. The slope of the modified Washburn equation, i.e., $\frac{\eta}{C\rho^2\gamma\cos\theta}$, was obtained by fitting the linear region of liquid penetration curve (i.e., from T = 100 to

300 s). Using the slope for different stabilizer solutions and water, $\cos\theta_{ss}/\cos\theta_{w}$ was calculated. The viscosity, surface tension, and calculated wetting effectiveness factor are reported in Table E1.

Table E.1 Wetting Effectiveness Factor Calculated for Various Stabilizer Solutions Using the Modified Washburn Method

Formulation	$\frac{\eta}{C\rho^2\gamma\cos\theta}$ **(s/g^2)**	**R^2**	***η* (cP)**	***ρ*** **(g/ml)**	***γ*** **(mN/m)**	**$\cos\theta_{ss}/\cos\theta_{w}$**
Water	1331	0.967	0.89	1	70.8	1
Soluplus®	2315	0.991	5.10	1.1	41.6	5
Kolliphor®	470	1.000	7.42	1.1	36.2	38
HPC	7150	0.979	93.9	1.1	41.9	27

REFERENCES

Adamson, A., Gast, A., 1997. Physical Chemical of Surfaces. New York, NY: John Wiley & Son, Inc..

Afolabi, A., Akinlabi, O., Bilgili, E., 2014. Impact of process parameters on the breakage kinetics of poorly water-soluble drugs during wet stirred media milling: A microhydrodynamic view. Eur. J. Pharm. Sci. 51, 75–86.

Ain-Ai, A., Gupta, P.K., 2008. Effect of arginine hydrochloride and hydroxypropyl cellulose as stabilizers on the physical stability of high drug loading nanosuspensions of a poorly soluble compound. Int. J. Pharm. 351, 282–288.

Allen, T., 2003. Powder sampling and particle size determination. Amsterdam, Netherlands: Elsevier.

Alonzo, D.E., Zhang, G.G., Zhou, D., Gao, Y., Taylor, L.S., 2010. Understanding the behavior of amorphous pharmaceutical systems during dissolution. Pharm. Res. 27, 608–618.

Azad, M., Afolabi, A., Bhakay, A., Leonardi, J., Davé, R., Bilgili, E., 2015a. Enhanced physical stabilization of fenofibrate nanosuspensions via wet co-milling with a superdisintegrant and an adsorbing polymer. Eur. J. Pharm. Biopharm. 94, 372–385.

Azad, M., Arteaga, C., Abdelmalek, B., Davé, R., Bilgili, E., 2015b. Spray drying of drug-swellable dispersant suspensions for preparation of fast-dissolving, high drug-loaded, surfactant-free nanocomposites. Drug Dev. Ind. Pharm. 41, 1617–1631.

Azad, M., Moreno, J., Bilgili, E., Davé, R., 2016. Fast dissolution of poorly water soluble drugs from fluidized bed coated nanocomposites: Impact of carrier size. Int. J. Pharm. 513, 319–331.

Azad, M.A., Afolabi, A., Patel, N., Davé, R., Bilgili, E., 2014b. Preparation of stable colloidal suspensions of superdisintegrants via wet stirred media milling. Particuology 14, 76–82.

Baert, L., van ‘t Klooster, G., Dries, W., François, M., Wouters, A., Basstanie, E., Iterbeke, K., Stappers, F., Stevens, P., Schueller, L., Van Remoortere, P., Kraus, G., Wigerinck, P., Rosier, J., 2009. Development of a long-acting injectable formulation with nanoparticles of rilpivirine (TMC278) for HIV treatment. Eur. J. Pharm. Biopharm. 72, 502–508.

Barthelmes, G., Pratsinis, S., Buggisch, H., 2003. Particle size distributions and viscosity of suspensions undergoing shear-induced coagulation and fragmentation. Chem. Eng. Sci. 58, 2893–2902.

Basa, S., Muniyappan, T., Karatgi, P., Prabhu, R., Pillai, R., 2008. Production and in vitro characterization of solid dosage form incorporating drug nanoparticles. Drug Dev. Ind. Pharm. 34, 1209–1218.

Baumgartner, R., Eitzlmayr, A., Matsko, N., Tetyczka, C., Khinast, J., Roblegg, E., 2014. Nano-extrusion: A promising tool for continuous manufacturing of solid nano-formulations. Int. J. Pharm. 477, 1–11.

Berglund, K.D., Przybycien, T.M., Tilton, R.D., 2003. Coadsorption of sodium dodecyl sulfate with hydrophobically modified nonionic cellulose polymers. 1. Role of polymer hydrophobic modification. Langmuir 19, 2705–2713.

Bernard, V.E., Sofie, V., A, M.J., Jan, V., Ludo, F., Jan, V.H., Guy, V.d.M., Patrick, A., 2008. Microcrystalline cellulose, a useful alternative for sucrose as a matrix former during freeze-drying of drug nanosuspensions – A case study with itraconazole. Eur. J. Pharm. Biopharm. 70, 590–596.

Bernhardt, C., Reinsch, E., Husemann, K., 1999. The influence of suspension properties on ultra-fine grinding in stirred ball mills. Powder Technol. 105, 357–361.

Bhakay, A., Azad, M., Bilgili, E., Dave, R., 2014a. Redispersible fast dissolving nanocomposite microparticles of poorly water-soluble drugs. Int. J. Pharm. 461, 367–379.

Bhakay, A., Azad, M., Vizzotti, E., Dave, R.N., Bilgili, E., 2014b. Enhanced recovery and dissolution of griseofulvin nanoparticles from surfactant-free nanocomposite microparticles incorporating wet-milled swellable dispersants. Drug Dev. Ind. Pharm. 40, 1509–1522.

Bhakay, A., Davé, R., Bilgili, E., 2013. Recovery of BCS Class II drugs during aqueous redispersion of core–shell type nanocomposite particles produced via fluidized bed coating. Powder Technol. 236, 221–234.

Bhakay, A., Merwade, M., Bilgili, E., Dave, R.N., 2011. Novel aspects of wet milling for the production of microsuspensions and nanosuspensions of poorly water-soluble drugs. Drug Dev. Ind. Pharm. 37, 963–976.

Bilgili, E., Afolabi, A., 2012. A combined microhydrodynamics–polymer adsorption analysis for elucidation of the roles of stabilizers in wet stirred media milling. Int. J. Pharm. 439, 193–206.

Bilgili, E., Capece, M., Afolabi, A., 2016a. Modeling of Milling Processes via DEM, PBM, and Microhydrodynamics, in: Pandey, P., Bharadwaj, R. (Eds.),

Predictive Modeling of Pharmaceutical Unit Operations, 1 ed. Amsterdam, Netherlands: Elsevier, pp. 159–203.

Bilgili, E., Dave, R., Bhakay, A., Azad, M., 2016b. Systems and methods for superdisintegrant-based composite particles for dispersion and dissolution of agents. US Patents: US 9452107 B2

Bilgili, E., Hamey, R., Scarlett, B., 2004. Production of pigment nanoparticles using a wet stirred mill with polymeric media. China Particuology 2, 93–100.

Bilgili, E., Hamey, R., Scarlett, B., 2006. Nano-milling of pigment agglomerates using a wet stirred media mill: Elucidation of the kinetics and breakage mechanisms. Chem. Eng. Sci. 61, 149–157.

Bilgili, E., Li, M., Afolabi, A., 2016c. Is the combination of cellulosic polymers and anionic surfactants a good strategy for ensuring physical stability of BCS Class II drug nanosuspensions? Pharm. Dev. Technol. 21, 499–510.

Bilgili, E., Rosen, L.A., Ko, J.S., Chen, A., Smith, E.J., Fliszar, K., Wong, G., 2011. Experimental study of fluidized bed co-granulation of two active pharmaceutical ingredients: an industrial scale-up perspective. Particul. Sci. Technol. 29, 285–309.

Bitterlich, A., Laabs, C., Krautstrunk, I., Dengler, M., Juhnke, M., Grandeury, A., Bunjes, H., Kwade, A., 2015. Process parameter dependent growth phenomena of naproxen nanosuspension manufactured by wet media milling. Eur. J. Pharm. Biopharm. 92, 171–179.

Boateng, J.S., Matthews, K.H., Auffret, A.D., Humphrey, M.J., Stevens, H.N., Eccleston, G.M., 2009. < i> In vitro</i> drug release studies of polymeric freeze-dried wafers and solvent-cast films using paracetamol as a model soluble drug. Int. J. Pharm. 378, 66–72.

Bonda, A.F., Rinaldi, M., Segale, L., Palugan, L., Cerea, M., Vecchio, C., Pattarino, F., 2016. Nanonized itraconazole powders for extemporary oral suspensions: role of formulation components studied by a mixture design. Eur. J. Pharm. Sci. 83, 175–183.

Bose, S., Schenck, D., Ghosh, I., Hollywood, A., Maulit, E., Ruegger, C., 2012. Application of spray granulation for conversion of a nanosuspension into a dry powder form. Eur. J. Pharm. Sci. 47, 35–43.

Branchey, M.H., Lee, J.H., Amin, R., Simpson, G.M., 1978. High-and low-potency neuroleptics in elderly psychiatric patients. Jama 239, 1860–1862.

Branham, M.L., Moyo, T., Govender, T., 2012. Preparation and solid-state characterization of ball milled saquinavir mesylate for solubility enhancement. Eur. J. Pharm. Biopharm. 80, 194–202.

Breitung-Faes, S., Kwade, A., 2008. Nano particle production in high-power-density mills. Chem. Eng. Res. Des. 86, 390–394.

Brough, C., Williams III, R.O., 2013. Amorphous solid dispersions and nano-crystal technologies for poorly water-soluble drug delivery. Int. J. Pharm. 453, 157–166.

Brouwers, J., Brewster, M.E., Augustijns, P., 2009. Supersaturating drug delivery systems: The answer to solubility ‐ limited oral bioavailability? J. Pharm. Sci. 98, 2549–2572.

Bruno, J.A., Doty, B.D., Gustow, E., Illig, K.J., Rajagopalan, N., Sarpotdar, P., 1996. Method of grinding pharmaceutical substances. US Patents: US005518187A.

Bujňáková, Z., Dutková, E., Baláž, M., Turianicová, E., Baláž, P., 2015. Stability studies of As4S4 nanosuspension prepared by wet milling in Poloxamer 407. Int. J. Pharm. 478, 187–192.

Cerdeira, A.M., Gander, B., Mazzotti, M., 2011. Role of milling parameters and particle stabilization on nanogrinding of drug substances of similar mechanical properties. Chem. Eng. Technol. 34, 1427–1438.

Cerdeira, A.M., Mazzotti, M., Gander, B., 2010. Miconazole nanosuspensions: influence of formulation variables on particle size reduction and physical stability. Int. J. Pharm. 396, 210–218.

Cerdeira, A.M., Mazzotti, M., Gander, B., 2013. Formulation and drying of miconazole and itraconazole nanosuspensions. Int. J. Pharm. 443, 209–220.

Chaubal, M.V., Popescu, C., 2008. Conversion of nanosuspensions into dry powders by spray drying: a case study. Pharm. Res. 25, 2302–2308.

Cheow, W.S., Ng, M.L.L., Kho, K., Hadinoto, K., 2011. Spray-freeze-drying production of thermally sensitive polymeric nanoparticle aggregates for inhaled drug delivery: Effect of freeze-drying adjuvants. Int. J. Pharm. 404, 289–300.

Chiou, W.L., Riegelman, S., 1970. Oral absorption of griseofulvin in dogs: Increased absorption viasolid dispersion in polyethylene glycol 6000. J. Pharm. Sci. 59, 937–942.

Cho, H., Waters, M., Hogg, R., 1996. Investigation of the grind limit in stirred-media milling. Int. J. Miner. Process. 44, 607–615.

Choi, J.-Y., Park, C.H., Lee, J., 2008. Effect of polymer molecular weight on nanocomminution of poorly soluble drug. Drug Deliv. 15, 347–353.

Choi, J.-Y., Yoo, J.Y., Kwak, H.-S., Uk Nam, B., Lee, J., 2005. Role of polymeric stabilizers for drug nanocrystal dispersions. Curr. Appl. Phys. 5, 472–474.

Choi, P., Kavassalis, T.A., Rudin, A., 1994. Estimation of Hansen solubility parameters for (hydroxyethyl) and (hydroxypropyl) cellulose through molecular simulation. Ind. Eng. Chem. Res. 33, 3154–3159.

Costa, P., Lobo, J.M.S., 2001. Modeling and comparison of dissolution profiles. Eur. J. Pharm. Sci. 13, 123–133.

Costa, P., Sousa Lobo, J.M., 2001. Modeling and comparison of dissolution profiles. Eur. J. Pharm. Sci. 13, 123–133.

Craig, D.Q., 2002. The mechanisms of drug release from solid dispersions in water-soluble polymers. Int. J. Pharm. 231, 131–144.

Dalvi, S.V., Dave, R.N., 2010. Analysis of nucleation kinetics of poorly water-soluble drugs in presence of ultrasound and hydroxypropyl methyl cellulose during antisolvent precipitation. Int. J. Pharm. 387, 172–179.

De Smet, L., Saerens, L., De Beer, T., Carleer, R., Adriaensens, P., Van Bocxlaer, J., Vervaet, C., Remon, J.P., 2014. Formulation of itraconazole nanococrystals and evaluation of their bioavailability in dogs. Eur. J. Pharm. Biopharm. 87, 107–113.

de Villiers, M.M., 1996. Influence of agglomeration of cohesive particles on the dissolution behaviour of furosemide powder. Int. J. Pharm. 136, 175–179.

de Waard, H., Hinrichs, W.L.J., Frijlink, H.W., 2008. A novel bottom–up process to produce drug nanocrystals: Controlled crystallization during freeze-drying. J. Controlled Release 128, 179–183.

Deng, Z., Xu, S., Li, S., 2008. Understanding a relaxation behavior in a nanoparticle suspension for drug delivery applications. Int. J. Pharm. 351, 236–243.

Eskin, D., Miller, M.J., 2008. A model of non-Newtonian slurry flow in a fracture. Powder Technol. 182, 313–322.

Eskin, D., Zhupanska, O., Hamey, R., Moudgil, B., Scarlett, B., 2005a. Microhydrodynamic analysis of nanogrinding in stirred media mills. AlChE J. 51, 1346–1358.

Eskin, D., Zhupanska, O., Hamey, R., Moudgil, B., Scarlett, B., 2005b. Microhydrodynamics of stirred media milling. Powder Technol. 156, 95–102.

Evertsson, H., Nilsson, S., 1997. Microviscosity in clusters of ethyl hydroxyethyl cellulose and sodium dodecyl sulfate formed in dilute aqueous solutions as

determined with fluorescence probe techniques. Macromolecules 30, 2377–2385.

Fakes, M.G., Vakkalagadda, B.J., Qian, F., Desikan, S., Gandhi, R.B., Lai, C., Hsieh, A., Franchini, M.K., Toale, H., Brown, J., 2009. Enhancement of oral bioavailability of an HIV-attachment inhibitor by nanosizing and amorphous formulation approaches. Int. J. Pharm. 370, 167–174.

Forster, A., Hempenstall, J., Rades, T., 2001. Characterization of glass solutions of poorly water-soluble drugs produced by melt extrusion with hydrophilic amorphous polymers. J. Pharm. Pharmacol. 53, 303–315.

Fule, R., Paithankar, V., Amin, P., 2016. Hot melt extrusion based solid solution approach: Exploring polymer comparison, physicochemical characterization and in-vivo evaluation. Int. J. Pharm. 499, 280–294.

Garg, A., Sachdeva, R., Kapoor, G., 2013. Comparison of crystalline and amorphous carriers to improve the dissolution profile of water insoluble drug itraconazole. Int. J. Pharm. Bio. Sci. 2013; 4 (1): 934–948.

George, M., Ghosh, I., 2013. Identifying the correlation between drug/stabilizer properties and critical quality attributes (CQAs) of nanosuspension formulation prepared by wet media milling technology. Eur. J. Pharm. Sci. 48, 142–152.

Ghebremeskel, A.N., Vemavarapu, C., Lodaya, M., 2006. Use of surfactants as plasticizers in preparing solid dispersions of poorly soluble API: stability testing of selected solid dispersions. Pharm. Res. 23, 1928–1936.

Ghosh, I., Bose, S., Vippagunta, R., Harmon, F., 2011. Nanosuspension for improving the bioavailability of a poorly soluble drug and screening of stabilizing agents to inhibit crystal growth. Int. J. Pharm. 409, 260–268.

Ghosh, I., Schenck, D., Bose, S., Liu, F., Motto, M., 2013. Identification of critical process parameters and its interplay with nanosuspension formulation prepared by top down media milling technology-A QbD perspective. Pharm. Dev. Technol. 18, 719–729.

Ghosh, I., Schenck, D., Bose, S., Ruegger, C., 2012. Optimization of formulation and process parameters for the production of nanosuspension by wet media milling technique: Effect of Vitamin E TPGS and nanocrystal particle size on oral absorption. Eur. J. Pharm. Sci. 47, 718–728.

Ghosh, S., Sharma, A., Talukder, G., 1992. Zirconium. Biol. Trace Elem. Res. 35, 247–271.

Gidaspow, D., 1994. Multiphase flow and fluidization: continuum and kinetic theory descriptions. Cambridge, MA: Academic Press.

Gogos, C.G., Liu, H., Wang, P., 2012. Laminar Dispersive and Distributive Mixing with Dissolution and Applications to Hot‐Melt Extrusion. Hot-Melt Extrusion: Pharmaceutical Applications, 261−284. New York, NY: Springer,

Goldberg, A.H., Gibaldi, M., Kanig, J.L., 1966. Increasing dissolution rates and gastrointestinal absorption of drugs via solid solutions and eutectic mixtures III: experimental evaluation of griseofulvin—succinic acid solid solution. J. Pharm. Sci. 55, 487–492.

Greenhalgh, D.J., Williams, A.C., Timmins, P., York, P., 1999. Solubility parameters as predictors of miscibility in solid dispersions. J. Pharm. Sci. 88, 1182–1190.

Gupta, R.B., Kompella, U.B., 2006. Nanoparticle technology for drug delivery. New York, NY: Taylor & Francis.

Hall, M., 2010. Encyclopedia of nanoscience and nanotechnology. Valencia, CA: American Scientific.

Hancock, B.C., Parks, M., 2000. What is the true solubility advantage for amorphous pharmaceuticals? Pharm. Res. 17, 397–404.

Hardung, H., Djuric, D., Ali, S., 2010. Combining HME & solubilization: Soluplus®—the solid solution. Drug Deliv. Technol. 10, 20–27.

Hecq, J., Deleers, M., Fanara, D., Vranckx, H., Amighi, K., 2005. Preparation and characterization of nanocrystals for solubility and dissolution rate enhancement of nifedipine. Int. J. Pharm. 299, 167–177.

Hennart, S., Domingues, M., Wildeboer, W., van Hee, P., Meesters, G., 2010. Study of the process of stirred ball milling of poorly water soluble organic products using factorial design. Powder Technol. 198, 56–60.

Hołownia, D., Kwiatkowska, I., Hupka, J., 2008. An investigation on wetting of porous materials. Physico. Probl. Min. 42, 251–262.

Hu, J., Ng, W.K., Dong, Y., Shen, S., Tan, R.B., 2011. Continuous and scalable process for water-redispersible nanoformulation of poorly aqueous soluble APIs by antisolvent precipitation and spray-drying. Int. J. Pharm. 404, 198–204.

Jagtap, Y., Bhujbal, R., Ranade, A., Ranpise, N., 2012. Effect of various polymers concentrations on physicochemical properties of floating microspheres. Indian J. Pharm. Sci. 74, 512.

Jelinek, L., sz. Kovats, E., 1994. True surface areas from nitrogen adsorption experiments. Langmuir 10, 4225–4231.

Juhnke, M., Märtin, D., John, E., 2012. Generation of wear during the production of drug nanosuspensions by wet media milling. Eur. J. Pharm. Biopharm. 81, 214–222.

Juluri, A., Popescu, C., Zhou, L., Murthy, R.N., Gowda, V.K., P, C.K., Pimparade, M.B., Repka, M.A., Murthy, S.N., 2016. Taste masking of griseofulvin and caffeine anhydrous using kleptose linecaps DE17 by hot melt extrusion. AAPS PharmSciTech 17, 99–105.

Jung, J.-Y., Yoo, S.D., Lee, S.-H., Kim, K.-H., Yoon, D.-S., Lee, K.-H., 1999. Enhanced solubility and dissolution rate of itraconazole by a solid dispersion technique. Int. J. Pharm. 187, 209–218.

Junghanns, J.-U.A., Müller, R.H., 2008. Nanocrystal technology, drug delivery and clinical applications. Int. J. Nanomedicine 3, 295.

Kagotani, R., Kinugawa, K., Nomura, M., Imanaka, H., Ishida, N., Imamura, K., 2013. Improving the physical stability of freeze-dried amorphous sugar matrices by compression at several hundreds MPa. J. Pharm. Sci. 102, 2187–2197.

Kasim, N.A., Whitehouse, M., Ramachandran, C., Bermejo, M., Lennernäs, H., Hussain, A.S., Junginger, H.E., Stavchansky, S.A., Midha, K.K., Shah, V.P., 2004. Molecular properties of WHO essential drugs and provisional biopharmaceutical classification. Mol. Pharm. 1, 85–96.

Kawatra, S.K., 2006. Advances in comminution. Society for Mining Metallurgy. Englewood, CO: Society for Mining Metallurgy.

Keck, C.M., Müller, R.H., 2006. Drug nanocrystals of poorly soluble drugs produced by high pressure homogenisation. Eur. J. Pharm. Biopharm. 62, 3–16.

Kesisoglou, F., Panmai, S., Wu, Y., 2007. Nanosizing—oral formulation development and biopharmaceutical evaluation. Adv. Drug Deliver. Rev. 59, 631–644.

Khinast, J., Baumgartner, R., Roblegg, E., 2013. Nano-extrusion: a one-step process for manufacturing of solid nanoparticle formulations directly from the liquid phase. AAPS PharmSciTech 14, 601–604.

Kho, K., Hadinoto, K., 2010. Effects of excipient formulation on the morphology and aqueous re-dispersibility of dry-powder silica nano-aggregates. Colloid. Surface. A 359, 71–81.

Kim, S., Lee, J., 2010. Effective polymeric dispersants for vacuum, convection and freeze drying of drug nanosuspensions. Int. J. Pharm. 397, 218–224.

Kipp, J.E., 2004. The role of solid nanoparticle technology in the parenteral delivery of poorly water-soluble drugs. Int. J. Pharm. 284, 109–122.

Kissa, E., 1999. Dispersions: characterization, testing, and measurement. Boca Raton, FL: CRC Press.

Knieke, C., Azad, M., Davé, R., Bilgili, E., 2013. A study of the physical stability of wet media-milled fenofibrate suspensions using dynamic equilibrium curves. Chem. Eng. Res. Des. 91, 1245–1258.

Knieke, C., Azad, M.A., To, D., Bilgili, E., Davé, R.N., 2015a. Sub-100 micron fast dissolving nanocomposite drug powders. Powder Technol. 271, 49–60.

Knieke, C., Sommer, M., Peukert, W., 2009. Identifying the apparent and true grinding limit. Powder Technol. 195, 25–30.

Knopp, M.M., Chourak, N., Khan, F., Wendelboe, J., Langguth, P., Rades, T., Holm, R., 2016a. Effect of polymer type and drug dose on the in vitro and in vivo behavior of amorphous solid dispersions. Eur. J. Pharm. Biopharm. 105, 106–114.

Knopp, M.M., Nguyen, J.H., Becker, C., Francke, N.M., Jørgensen, E.B., Holm, P., Holm, R., Mu, H., Rades, T., Langguth, P., 2016b. Influence of polymer molecular weight on in vitro dissolution behavior and in vivo performance of celecoxib:PVP amorphous solid dispersions. Eur. J. Pharm. Biopharm. 101, 145–151.

Kolter, K., Karl, M., Gryczke, A., Ludwigshafen am Rhein, B., 2012. Hot-melt extrusion with BASF pharma polymers: extrusion compendium. BASF.

Konnerth, C., Flach, F., Breitung-Faes, S., Damm, C., Schmidt, J., Kwade, A., Peukert, W., 2016. Impact of stressing conditions and polymer–surfactant interactions on product characteristics of organic nanoparticles produced by media milling. Powder Technol. 294, 71–79.

Konno, H., Handa, T., Alonzo, D.E., Taylor, L.S., 2008. Effect of polymer type on the dissolution profile of amorphous solid dispersions containing felodipine. Eur. J. Pharm. Biopharm. 70, 493–499.

Konno, H., Taylor, L.S., 2006. Influence of different polymers on the crystallization tendency of molecularly dispersed amorphous felodipine. J. Pharm. Sci. 95, 2692–2705.

Korsmeyer, R.W., Gurny, R., Doelker, E., Buri, P., Peppas, N.A., 1983. Mechanisms of solute release from porous hydrophilic polymers. Int. J. Pharm. 15, 25–35.

Korson, L., Drost-Hansen, W., Millero, F.J., 1969. Viscosity of water at various temperatures. J. Phys. Chem. 73, 34–39.

Krull, S.M., Ma, Z., Li, M., Davé, R.N., Bilgili, E., 2016. Preparation and characterization of fast dissolving pullulan films containing BCS class II drug nanoparticles for bioavailability enhancement. Drug Dev. Ind. Pharm. 42, 1073–1085.

Kumar, S., Burgess, D.J., 2014. Wet milling induced physical and chemical instabilities of naproxen nano-crystalline suspensions. Int. J. Pharm. 466, 223–232.

Kushner, L.M., Duncan, B.C., Hoffman, J.I., 1952. A viscometric study of the micelles of sodium dodecyl sulfate in dilute solutions. J. Res. Nati. Bur. Stan. 49, 85–90.

Kyerematen, S.O., Pudlas, M., Woehrle, G.H., 2014. A fast and reliable empirical approach for estimating solubility of crystalline drugs in polymers for hot melt extrusion formulations. J. Pharm. Sci. 103, 2847–2858.

Langham, Z.A., Booth, J., Hughes, L.P., Reynolds, G.K., Wren, S.A.C., 2012. Mechanistic insights into the dissolution of spray-dried amorphous solid dispersions. J. Pharm. Sci. 101, 2798–2810.

Law, M., Wald, N., Morris, J., Jordan, R., 2003. Value of low dose combination treatment with blood pressure lowering drugs: analysis of 354 randomised trials. Br. Med. J. 326, 1427.

Layre, A.M., Couvreur, P., Richard, J., Requier, D., Eddine Ghermani, N., Gref, R., 2006. Freeze-drying of composite core-shell nanoparticles. Drug Dev. Ind. Pharm. 32, 839–846.

Lebhardt, T., Roesler, S., Uusitalo, H.P., Kissel, T., 2011. Surfactant-free redispersible nanoparticles in fast-dissolving composite microcarriers for dry-powder inhalation. Eur. J. Pharm. Biopharm. 78, 90–96.

Lee, J., 2003. Drug nano‐ and microparticles processed into solid dosage forms: physical properties. J. Pharm. Sci. 92, 2057−2068.

Lee, J., Choi, J.Y., Park, C.H., 2008. Characteristics of polymers enabling nano-comminution of water-insoluble drugs. Int. J. Pharm. 355, 328–336.

Lee, J., Lee, S.-J., Choi, J.-Y., Yoo, J.Y., Ahn, C.-H., 2005. Amphiphilic amino acid copolymers as stabilizers for the preparation of nanocrystal dispersion. Eur. J. Pharm. Sci. 24, 441–449.

Li, M., Azad, M., Davé, R., Bilgili, E., 2016a. Nanomilling of drugs for bioavailability enhancement: A holistic formulation-process perspective. Pharmaceutics 8, 17.

Li, M., Gogos, C.G., Ioannidis, N., 2015a. Improving the API dissolution rate during pharmaceutical hot-melt extrusion I: Effect of the API particle size, and the co-rotating, twin-screw extruder screw configuration on the API dissolution rate. Int. J. Pharm. 478, 103–112.

Li, M., Ioannidis, N., Gogos, C., Bilgili, E., 2017. A comparative assessment of nanocomposites vs. amorphous solid dispersions prepared via nanoextrusion for drug dissolution enhancement. Eur. J. Pharm. Biopharm. 119, 68–80.

Li, M., Lopez, N., Bilgili, E., 2016b. A study of the impact of polymer–surfactant in drug nanoparticle coated pharmatose composites on dissolution performance. Adv. Powder Technol. 27, 1625–1636.

Li, M., Yaragudi, N., Afolabi, A., Dave, R., Bilgili, E., 2015b. Sub-100nm drug particle suspensions prepared via wet milling with low bead contamination through novel process intensification. Chem. Eng. Sci. 130, 207–220.

Li, M., Zhang, L., Davé, R.N., Bilgili, E., 2016d. An intensified vibratory milling process for enhancing the breakage kinetics during the preparation of drug nanosuspensions. AAPS PharmSciTech 17, 389–399.

Lipinski, C.A., 2002. Poor aqueous solubility: an industry wide problem in drug discovery. Am. Pharm. Rev. 5, 82–85.

Liu, P., Rong, X., Laru, J., van Veen, B., Kiesvaara, J., Hirvonen, J., Laaksonen, T., Peltonen, L., 2011. Nanosuspensions of poorly soluble drugs: preparation and development by wet milling. Int. J. Pharm. 411, 215–222.

Liu, X., Lu, M., Guo, Z., Huang, L., Feng, X., Wu, C., 2012. Improving the Chemical Stability of Amorphous Solid Dispersion with Cocrystal Technique by Hot Melt Extrusion. Pharm. Res. 29, 806–817.

Liversidge, G.G., Cundy, K.C., 1995. Particle size reduction for improvement of oral bioavailability of hydrophobic drugs: I. Absolute oral bioavailability of nanocrystalline danazol in beagle dogs. Int. J. Pharm. 125, 91–97.

Maniruzzaman, M., Rana, M., Boateng, J., Mitchell, J., Douroumis, D., 2013. Dissolution enhancement of poorly water–soluble APIs processed by hot-melt extrusion using hydrophilic polymers. Drug Dev. Ind. Pharm. 39, 218–227.

Margulis-Goshen, K., Magdassi, S., 2009. Formation of simvastatin nanoparticles from microemulsion. Nanomed Nanotech. Biol. Med. 5, 274–281.

Marsac, P.J., Li, T., Taylor, L.S., 2009. Estimation of drug–polymer miscibility and solubility in amorphous solid dispersions using experimentally determined interaction parameters. Pharm. Res. 26, 139–151.

Meng, X., Yang, D., Keyvan, G., Michniak-Kohn, B., Mitra, S., 2012. Synthesis and immobilization of micro-scale drug particles in presence of β-cyclodextrins. Colloid. Surface. B 92, 213–222.

Merisko-Liversidge, E., Liversidge, G.G., 2011. Nanosizing for oral and parenteral drug delivery: A perspective on formulating poorly-water soluble compounds using wet media milling technology. Adv. Drug Deliver. Rev. 63, 427–440.

Merisko-Liversidge, E.M., Liversidge, G.G., 2008. Drug nanoparticles: formulating poorly water-soluble compounds. Toxicol. Pathol. 36, 43–48.

Mishra, P.R., Shaal, L.A., Müller, R.H., Keck, C.M., 2009. Production and characterization of Hesperetin nanosuspensions for dermal delivery. Int. J. Pharm. 371, 182–189.

Mittal, G., Sahana, D.K., Bhardwaj, V., Ravi Kumar, M.N.V., 2007. Estradiol loaded PLGA nanoparticles for oral administration: Effect of polymer molecular weight and copolymer composition on release behavior in vitro and in vivo. J. Control. Release 119, 77–85.

Möckel, J.E., Lippold, B.C., 1993. Zero-Order Drug Release from Hydrocolloid Matrices. Pharm. Res. 10, 1066–1070.

Monteiro, A., Afolabi, A., Bilgili, E., 2013. Continuous production of drug nanoparticle suspensions via wet stirred media milling: a fresh look at the Rehbinder effect. Drug Dev. Ind. Pharm. 39, 266–283.

Moore, J.W., Flanner, H.H., 1996. Mathematical comparison of dissolution profiles. Pharm. Technol. 20, 64–74.

Möschwitzer, J., Müller, R.H., Hunter, R., Preedy, V., 2011. Nanocrystal formulations for improved delivery of poorly soluble drugs. Nanomed. Health Dis. 79–99.

Müller, R.H., Jacobs, C., Kayser, O., 2001. Nanosuspensions as particulate drug formulations in therapy: Rationale for development and what we can expect for the future. Adv. Drug Deliver. Rev. 47, 3–19.

Müller, R.H., Peters, K., 1998. Nanosuspensions for the formulation of poorly soluble drugs: I. Preparation by a size-reduction technique. Int. J. Pharm. 160, 229–237.

Napper, D.H., 1970. Colloid stability. Ind. Eng. Chem. Prod. R. D. 9, 467–477.

Newman, A., Knipp, G., Zografi, G., 2012. Assessing the performance of amorphous solid dispersions. J. Pharm. Sci. 101, 1355–1377.

Ng, J.D., Lorber, B., Witz, J., Théobald-Dietrich, A., Kern, D., Giegé, R., 1996. The crystallization of biological macromolecules from precipitates: evidence for Ostwald ripening. J. Cryst. Growth 168, 50–62.

Niwa, T., Miura, S., Danjo, K., 2011. Design of dry nanosuspension with highly spontaneous dispersible characteristics to develop solubilized formulation for poorly water-soluble drugs. Pharm. Res. 28, 2339–2349.

Noyes, A.A., Whitney, W.R., 1897. The rate of solution of solid substances in their own solutions. J. Am. Chem. Soc. 19, 930–934.

Omidian, H., Park, K., 2008. Swelling agents and devices in oral drug delivery. J. Drug Deliv. Sci. Tec. 18, 83–93.

Opoczky, L., Farnady, F., 1984. Fine grinding and states of equilibrium. Powder Technol. 39, 107–115.

Panmai, S., Deshpande, S., 2003. Development of nanoformulations: Selection of polymeric stabilizers based on adsorption isotherm, Amer. Chem. Soc.. U532–U533.

Paradkar, A., Ambike, A.A., Jadhav, B.K., Mahadik, K.R., 2004. Characterization of curcumin–PVP solid dispersion obtained by spray drying. Int. J. Pharm. 271, 281–286.

Park, J.-B., Kang, C.-Y., Kang, W.-S., Choi, H.-G., Han, H.-K., Lee, B.-J., 2013. New investigation of distribution imaging and content uniformity of very low dose drugs using hot-melt extrusion method. Int. J. Pharm. 458, 245–253.

Parmentier, J., Tan, E.H., Low, A., Möschwitzer, J.P., 2017. Downstream drug product processing of itraconazole nanosuspension: Factors influencing drug particle size and dissolution from nanosuspension-layered beads. Int. J. Pharm. 524, 443–453.

Peeters, J., Neeskens, P., Tollenaere, J.P., Van Remoortere, P., Brewster, M.E., 2002. Characterization of the interaction of 2‐hydroxypropyl‐β‐cyclodextrin with itraconazole at pH 2, 4, and 7. J. Pharm. Sci. 91, 1414−1422.

Peltonen, L., Hirvonen, J., 2010. Pharmaceutical nanocrystals by nanomilling: critical process parameters, particle fracturing and stabilization methods. J. Pharm. Pharmacol. 62, 1569–1579.

Peppas, N., 1985. Analysis of Fickian and non-Fickian drug release from polymers. Pharm. Acta Helv. 60, 110.

Perissutti, B., Newton, J.M., Podczeck, F., Rubessa, F., 2002. Preparation of extruded carbamazepine and PEG 4000 as a potential rapid release dosage form. Eur. J. Pharm. Biopharm. 53, 125–132.

Plakkot, S., de Matas, M., York, P., Saunders, M., Sulaiman, B., 2011. Comminution of ibuprofen to produce nano-particles for rapid dissolution. Int. J. Pharm. 415, 307–314.

Ploehn, H., Russel, W., 1990. Interactions between colloidal particles and soluble polymers. Adv. Chem. Eng. 15, 137–228.

Pudlas, M., Kyerematen, S.O., Williams, L.A.M., Kimber, J.A., van Lishaut, H., Kazarian, S.G., Woehrle, G.H., 2015. Analyzing the impact of different excipients on drug release behavior in hot-melt extrusion formulations using FTIR spectroscopic imaging. Eur. J. Pharm. Sci. 67, 21-31.

Qian, F., Huang, J., Hussain, M.A., 2010. Drug–polymer solubility and miscibility: Stability consideration and practical challenges in amorphous solid dispersion development. J. Pharm. Sci. 99, 2941–2947.

Quadir, A., Kolter, K., 2006. A Comparative Study of Current Superdisintegrants. Pharm. Technol. 30, s38–s42.

Rabinow, B.E., 2004. Nanosuspensions in drug delivery. Nat. Rev. Drug Discov. 3, 785–796.

Rao, V.M., Lin, M., Larive, C.K., Southard, M.Z., 1997. A mechanistic study of griseofulvin dissolution into surfactant solutions under laminar flow conditions. J. Pharm. Sci. 86, 1132–1137.

Rasenack, N., Hartenhauer, H., Müller, B.W., 2003. Microcrystals for dissolution rate enhancement of poorly water-soluble drugs. Int. J. Pharm. 254, 137–145.

Ritger, P.L., Peppas, N.A., 1987a. A simple equation for description of solute release I. Fickian and non-Fickian release from non-swellable devices in the form of slabs, spheres, cylinders or discs. J. Control. Release 5, 23–36.

Ritger, P.L., Peppas, N.A., 1987b. A simple equation for description of solute release II. Fickian and anomalous release from swellable devices. J. Control. Release 5, 37–42.

Rowe, R., 1986. The effect of the molecular weight of ethyl cellulose on the drug release properties of mixed films of ethyl cellulose and hydroxypropylmethylcellulose. Int. J. Pharm. 29, 37–41.

Ryde, N.P., Ruddy, S.B., 2002. Solid dose nanoparticulate compositions comprising a synergistic combination of a polymeric surface stabilizer and dioctyl sodium sulfosuccinate. US Patents: US 09/666,539.

Sadler III, L.Y., Stanley, D.A., Brooks, D.R., 1975. Attrition mill operating characteristics. Powder Technol. 12, 19–28.

Sahoo, L., 2012. Studies on Effect of Process Parameters on Particle Growth in a Fluidized Bed Granulator. Thesis. National Institute of Technology, Rourkela.

Salazar, J., Müller, R.H., Möschwitzer, J.P., 2014. Combinative particle size reduction technologies for the production of drug nanocrystals. J. Pharm. 2014, 1–14.

Sarnes, A., Kovalainen, M., Häkkinen, M.R., Laaksonen, T., Laru, J., Kiesvaara, J., Ilkka, J., Oksala, O., Rönkkö, S., Järvinen, K., Hirvonen, J., Peltonen, L., 2014. Nanocrystal-based per-oral itraconazole delivery: Superior in vitro dissolution enhancement versus Sporanox® is not realized in in vivo drug absorption. J. Control. Release 180, 109–116.

Schersch, K., Betz, O., Garidel, P., Muehlau, S., Bassarab, S., Winter, G., 2010. Systematic investigation of the effect of lyophilizate collapse on pharmaceutically relevant proteins I: Stability after freeze-drying. J. Pharm. Sci. 99, 2256–2278.

Sepassi, S., Goodwin, D.J., Drake, A.F., Holland, S., Leonard, G., Martini, L., Lawrence, M.J., 2007. Effect of polymer molecular weight on the production of drug nanoparticles. J. Pharm. Sci. 96, 2655–2666.

Shah, D.A., Patel, M., Murdande, S.B., Dave, R.H., 2016. Influence of spray drying and dispersing agent on surface and dissolution properties of griseofulvin micro and nanocrystals. Drug Dev. Ind. Pharm., 1–9.

Shah, N.B., Sheth, B.B., 1976. Effect of polymers on dissolution from drug suspensions. J. Pharm. Sci. 65, 1618–1623.

Shah, S.R., Parikh, R.H., Chavda, J.R., Sheth, N.R., 2014. Glibenclamide nanocrystals for bioavailability enhancement: Formulation design, process optimization, and pharmacodynamic evaluation. J. Pharm. Innov. 9, 227–237.

Sharma, P., Denny, W.A., Garg, S., 2009. Effect of wet milling process on the solid state of indomethacin and simvastatin. Int. J. Pharm. 380, 40–48.

Shegokar, R., Müller, R.H., 2010. Nanocrystals: industrially feasible multifunctional formulation technology for poorly soluble actives. Int. J. Pharm. 399, 129–139.

Sievens-Figueroa, L., Bhakay, A., Jerez-Rozo, J.I., Pandya, N., Romañach, R.J., Michniak-Kohn, B., Iqbal, Z., Bilgili, E., Davé, R.N., 2012. Preparation and characterization of hydroxypropyl methyl cellulose films containing stable BCS Class II drug nanoparticles for pharmaceutical applications. Int. J. Pharm. 423, 496–508.

Singare, D.S., Marella, S., Gowthamrajan, K., Kulkarni, G.T., Vooturi, R., Rao, P.S., 2010. Optimization of formulation and process variable of nanosuspension: An industrial perspective. Int. J. Pharm. 402, 213–220.

Singh, S.K., Srinivasan, K., Gowthamarajan, K., Singare, D.S., Prakash, D., Gaikwad, N.B., 2011. Investigation of preparation parameters of nanosuspension by top-down media milling to improve the dissolution of poorly water-soluble glyburide. Eur. J. Pharm. Biopharm. 78, 441–446.

Sinha, B., Müller, R.H., Möschwitzer, J.P., 2013. Bottom-up approaches for preparing drug nanocrystals: formulations and factors affecting particle size. Int. J. Pharm. 453, 126–141.

Six, K., Verreck, G., Peeters, J., Brewster, M., Mooter, G.V.d., 2004. Increased physical stability and improved dissolution properties of itraconazole, a class II drug, by solid dispersions that combine fast- and slow-dissolving polymers. J. Pharm. Sci. 93, 124–131.

Sommer, M., Stenger, F., Peukert, W., Wagner, N.J., 2006. Agglomeration and breakage of nanoparticles in stirred media mills—a comparison of different methods and models. Chem. Eng. Sci. 61, 135–148.

Song, Y., Yang, X., Chen, X., Nie, H., Byrn, S., Lubach, J.W., 2015. Investigation of drug–excipient interactions in lapatinib amorphous solid dispersions using solid-state NMR spectroscopy. Mol. Pharm. 12, 857–866.

Stehr, N., 1984. Residence time distributions in a stirred ball mill and their effect on comminution. Chem. Eng. Process. 18, 73–83.

Stražišar, J., Runovc, F., 1996. Kinetics of comminution in micro-and sub-micrometer ranges. Int. J. Miner. Process. 44, 673–682.

Suzuki, M., Machida, M., Adachi, K., Otabe, K., Sugimoto, T., Hayashi, M., Awazu, S., 2000. Histopathological study of the effects of a single intratracheal instillation of surface active agents on lung in rats. J. Toxicol. Sci. 25, 49–55.

Tanaka, Y., Inkyo, M., Yumoto, R., Nagai, J., Takano, M., Nagata, S., 2012. Nanoparticulation of probucol, a poorly water-soluble drug, using a novel wet-milling process to improve in vitro dissolution and in vivo oral absorption. Drug Dev. Ind. Pharm. 38, 1015–1023.

Tatsumi, S., Murayama, Y., Hayakawa, H., Sano, M., 2009. Experimental study on the kinetics of granular gases under microgravity. J. Fluid Mech. 641, 521–539.

Thakral, S., Thakral, N.K., 2013. Prediction of drug–polymer miscibility through the use of solubility parameter based flory–huggins interaction parameter and the

experimental validation: PEG as model polymer. J. Pharm. Sci. 102, 2254–2263.

Trotta, M., Gallarate, M., Carlotti, M.E., Morel, S., 2003. Preparation of griseofulvin nanoparticles from water-dilutable microemulsions. Int. J. Pharm. 254, 235–242.

Tuomela, A., Laaksonen, T., Laru, J., Antikainen, O., Kiesvaara, J., Ilkka, J., Oksala, O., Rönkkö, S., Järvinen, K., Hirvonen, J., Peltonen, L., 2015. Solid formulations by a nanocrystal approach: Critical process parameters regarding scale-ability of nanocrystals for tableting applications. Int. J. Pharm. 485, 77–86.

Van Eerdenbrugh, B., Froyen, L., Martens, J., Blaton, N., Augustijns, P., Brewster, M., Van den Mooter, G., 2007. Characterization of physico-chemical properties and pharmaceutical performance of sucrose co-freeze–dried solid nanoparticulate powders of the anti-HIV agent loviride prepared by media milling. Int. J. Pharm. 338, 198–206.

Van Eerdenbrugh, B., Froyen, L., Van Humbeeck, J., Martens, J.A., Augustijns, P., Van den Mooter, G., 2008a. Drying of crystalline drug nanosuspensions—the importance of surface hydrophobicity on dissolution behavior upon redispersion. Eur. J. Pharm. Sci. 35, 127–135.

Van Eerdenbrugh, B., Raina, S., Hsieh, Y.-L., Augustijns, P., Taylor, L., 2014. Classification of the Crystallization Behavior of Amorphous Active Pharmaceutical Ingredients in Aqueous Environments. Pharm. Res. 31, 969–982.

Van Eerdenbrugh, B., Van den Mooter, G., Augustijns, P., 2008b. Top-down production of drug nanocrystals: nanosuspension stabilization, miniaturization and transformation into solid products. Int. J. Pharm. 364, 64–75.

Van Eerdenbrugh, B., Vermant, J., Martens, J.A., Froyen, L., Van Humbeeck, J., Augustijns, P., Van den Mooter, G., 2009. A screening study of surface stabilization during the production of drug nanocrystals. J. Pharm. Sci. 98, 2091–2103.

Varinot, C., Berthiaux, H., Dodds, J., 1999. Prediction of the product size distribution in associations of stirred bead mills. Powder Technol. 105, 228–236.

Venkatesh, G.M., Barnett, M.E., Owusu-Fordjour, C., Galop, M., 2001. Detection of low levels of the amorphous phase in crystalline pharmaceutical materials by thermally stimulated current spectrometry. Pharm. Res. 18, 98–103.

Verheezen, J.J.A.M., van der Voort Maarschalk, K., Faassen, F., Vromans, H., 2004. Milling of agglomerates in an impact mill. Int. J. Pharm. 278, 165–172.

Verma, S., Huey, B.D., Burgess, D.J., 2009. Scanning probe microscopy method for nanosuspension stabilizer selection. Langmuir 25, 12481–12487.

Verma, S., Kumar, S., Gokhale, R., Burgess, D.J., 2011. Physical stability of nanosuspensions: investigation of the role of stabilizers on Ostwald ripening. Int. J. Pharm. 406, 145–152.

Wang, Y., Kho, K., Cheow, W.S., Hadinoto, K., 2012. A comparison between spray drying and spray freeze drying for dry powder inhaler formulation of drug-loaded lipid–polymer hybrid nanoparticles. Int. J. Pharm. 424, 98–106.

Washburn, E.W., 1921. The dynamics of capillary flow. Phys. Rev. 17, 273.

Winnik, F.M., Winnik, M.A., 1990. The Interaction of sodium dodecylsulfate with (hydroxypropyl) cellulose. Polym. J. 22, 482–488.

Wu, L., Zhang, J., Watanabe, W., 2011. Physical and chemical stability of drug nanoparticles. Adv. Drug Deliver. Rev. 63, 456–469.

Wu, W., Nancollas, G.H., 1998. A New Understanding of the Relationship Between Solubility and Particle Size. J. Solution Chem. 27, 521–531.

Xiong, R., Lu, W., Li, J., Wang, P., Xu, R., Chen, T., 2008. Preparation and characterization of intravenously injectable nimodipine nanosuspension. Int. J. Pharm. 350, 338–343.

Yalkowsky, S.H., 1981. Techniques of solubilization of drugs. New York, NY: Marcel Dekker.

Yang, W., Johnston, K.P., Williams Iii, R.O., 2010. Comparison of bioavailability of amorphous versus crystalline itraconazole nanoparticles via pulmonary administration in rats. Eur. J. Pharm. Biopharm. 75, 33–41.

Yao, Q., Tao, X., Tian, B., Tang, Y., Shao, Y., Kou, L., Gou, J., Li, X., Yin, T., Tang, X., 2014. Improved oral bioavailability of core–shell structured beads by redispersion of the shell-forming nanoparticles: Preparation, characterization and in vivo studies. Colloid. Surface. B 113, 92–100.

Ye, X., Patil, H., Feng, X., Tiwari, R.V., Lu, J., Gryczke, A., Kolter, K., Langley, N., Majumdar, S., Neupane, D., 2015. Conjugation of hot-melt extrusion with high-pressure homogenization: a novel method of continuously preparing nanocrystal solid dispersions. AAPS PharmSciTech 17, 78–88.

Zhang, K., Yu, H., Luo, Q., Yang, S., Lin, X., Zhang, Y., Tian, B., Tang, X., 2013. Increased dissolution and oral absorption of itraconazole/Soluplus extrudate compared with itraconazole nanosuspension. Eur. J. Pharm. Biopharm. 85, 1285–1292.

Zheng, W., Jain, A., Papoutsakis, D., Dannenfelser, R.-M., Panicucci, R., Garad, S., 2012. Selection of oral bioavailability enhancing formulations during drug discovery. Drug Dev. Ind. Pharm. 38, 235–247.

Zhu, W., Romanski, F.S., Dalvi, S.V., Dave, R.N., Silvina Tomassone, M., 2012. Atomistic simulations of aqueous griseofulvin crystals in the presence of individual and multiple additives. Chem. Eng. Sci. 73, 218–230.